THE UNIVERSITY OF HULL

New pre-catalysts derived from calixarenes: synthesis, structural and polymerization studies.

Being a thesis submitted for the degree of Doctor of Philosophy at the University of Hull
Supervised by: Professor Carl Redshaw

By
Tian Xing

June-2021

Abstract

In this thesis, a series of V, Ti, Li and Pb compounds have been synthesized and fully characterized. The catalytic performance of these pre-catalysts towards different polymerization reactions, including ring opening polymerization (ROP) of cyclic esters, ethylene polymerization and co-polymerization of propylene oxide and CO_2 are studied.

Chapter 1 presents the history and research achievements of both calixarene and metallocalixarene compounds, with particular reference to polymerization reactions catalyzed by such coordination complexes, including ethylene polymerization, ring opening polymerization of cyclic esters and co-polymerization of propylene oxide and CO_2.

In **Chapter 2**, reactions of larger calix[*n*]arenes with vanadium precursors are studied. In particular, the reaction of Na[VO(*t*BuO)$_4$] (generated *in-situ* from $VOCl_3$ and NaO*t*Bu) with *p-tert*-butyltetrahomodioxacalix[6]areneH_6 ($L^{O6}H_6$) afforded, after work-up (in MeCN), the mixed-metal complex $[(VO)_2(\mu\text{-}O)Na_2(L^{O6})(MeCN)_4]\cdot 5(MeCN)$ (**1**·5MeCN), whilst the oxo complex $\{[VO]_4L^{O6}\}$ (**2**·6MeCN) was isolated via the use of [VO(O*n*Pr)$_3$]. Reaction of $L^{O6}H_6$ with [V(N*p*-$CH_3C_6H_4$)(O*t*Bu)$_3$] afforded the complex $\{[V(N\textit{p}\text{-}CH_3C_6H_4)]_2L^{O6}\}$ (**3**·7MeCN·0.5CH_2Cl_2). Use of similar methodology afforded the imido complexes $\{[V(N\textit{p}\text{-}RC_6H_4)]_2L^{O6}\}$ (R = OMe (**4**); CF_3 (**5**); Cl (**6**); F (**7**)); on one occasion, reaction of [V(N*p*-$CH_3C_6H_4$)(OEt)$_3$] with $L^{O6}H_6$ afforded the product $[VO(L^{6O'})]_2\cdot 4MeCN$ (**8**·4MeCN) ($L^{6O'}$ = 2-(*p*-CH_3-C_6H_4NCH)-4-*t*Bu-C_6H_2O-6-CH_2)-4-*t*BuC_6H_2OH) in which L^{O6} has been cleaved. For comparative catalytic ring opening polymerization (ROP) studies, the known complexes $[VOL^3]$ (L^3H_3 = oxacalix[3]arene) (**I**), $[V(N\textit{p}\text{-}CH_3\text{-}C_6H_4)L^3]_2$ (**II**), $[Li(MeCN)_4][V_2(O)_2Li(MeCN)(L^6H_2)_2]$ (L^6H_6 = *p-tert*-butylcalix[6]areneH_6) (**III**) and $[(VO)_2L^8H]$ (L^8H_8 = *p-tert*-butylcalix[8]areneH_8) (**IV**) have also been prepared. ROP studies, with or with or without external alcohol present, indicated that complexes **1** to **8** exhibited moderate to good conversions for ε-Cl, δ-VL and the co-polymerization thereof. Within the imido series, a positive influence was observed when electron withdrawing substituents were present. These systems afforded relatively low molecular weight products and were also inactive toward the ROP of *rac*-lactide. In the case of ethylene

polymerization, complexes **3**, **5** and **7** exhibited highest activity when screened in the presence of dimethylaluminium chloride/ethyltrichloroacetate; the activity of **4** was much lower. The products were highly linear polyethylene with M_w in the range 74-120x10^3 Da. In **Chapter 3**, a number of metallocalix[*n*]arenes, where n = 4, 6, or 8, of titanium and vanadium have been screened for their ability to act as catalysts for the co-polymerization of propylene oxide and CO_2 to form cyclic/polycarbonates. The vanadium-containing catalysts, namely [VO(L^4Me)] (**V**), [(VO_2)L^8H_6] (**VI**), [Na(NCMe)$_6$]$_2$[(Na(VO)$_4L^8$)(Na(NCMe))$_3$]$_2$ (**VII**), [VO(μ-OH)$L^{4S/}H_2$]$_2$·6CH_2Cl_2 (**9′**), [(VO)$_2$(μ-O)Na$_2$(L^{O6})(MeCN)$_4$] (**1**), {[V(N*p*-$CH_3C_6H_4$)]$_2L^{O6}$} (**3**) and [V(N*p*-RC_6H_4)Cl_3] (R = Cl (**VIII**), OMe (**IX**), CF_3 (**X**)), where L^4H_4 = p-*tert*-butylcalix[4]areneH_4, L^8H_8 = p-*tert*-butylcalix[8]areneH_8, $L^{4S}H_4$ = p-*tert*-butylthiacalix[4]areneH_4, performed poorly, affording, in the majority of cases, TONs less than 1 at 90 °C over 6 h. In the case of the titanocalix[8]arenes, {($TiX)_2$[TiX(NCMe)]$_2$(μ$_3$-O)$_2$(L^8)} (X = Cl (**10**), Br (**XI**), I (**XII**)), which all adopt a similar ladder-type structure, the activity under the same conditions is somewhat higher (TONs > 6) and follows the trend Cl > Br > I; by comparison the non-calixarene species [$TiCl_4$(THF)$_2$] (**XIII**) was virtually inactive. The molecular structures of the complexes [$HNEt_3$]$_2$[VO(μ-O)$L^{4S}H_2$]$_2$·3CH_2Cl_2 (**9**·3CH_2Cl_2), [VO(μ-OH)$L^{4S/}H_2$]$_2$·6CH_2Cl_2 (**9′**) (where $L^{4S/}H_2$ is a partially oxidized form of $L^{4S}H_4$) and {($TiCl)_2$[TiCl(NCMe)]$_2$(μ$_3$-O)$_2$(L^8)}·6.5MeCN (**10**·6.5MeCN) are reported.

In **Chapter 4**, the coordination chemistry of azacalix[*n*]arenes is studied focusing on reactions with titanium precursors. Reaction of excess [Ti(O*i*Pr)$_4$] with $L^{6O}H_6$ afforded, after work-up (MeCN), the complex [Ti_2(O*i*Pr)$_2$(MeCN)L^{6O}]·3.5MeCN (**11**·3.5MeCN), whilst the oxo complex [Ti_4O_4(L^{6O})$_2$]·MeCN (**12**·MeCN) was isolated via a fortuitous synthesis involving the use of two equivalents of [Ti(O*i*Pr)$_4$]. Reactions of *p*-methyl-dimethyldiazacalix[6]areneH_6 ($L^{6N}H_6$) with [TiF_4] (four equivalents), [$TiCl_4$(THF)$_2$] (two equivalents) or [$TiBr_4$] (>four equivalents) resulted in the titanium-based azacalix[*n*]arene complexes [$Ti_4F_{14}L^{6N}H_2$(H)$_2$]·2.5MeCN (**13**·2.5MeCN), [Ti_2X_4(H_2O)$_2$O$L^{6N}H_2$(H)$_2$] (X = Cl (**14**·5MeCN), Br (**15**·4.5MeCN) and [$Ti_4Br_{12}L^{6N}$(H)$_2$(MeCN)$_6$]·7MeCN (**16**·7MeCN), respectively. Reaction of four equivalents of [TiF_4] with L^3H_4 ($L^{4N}H_4$ = *p*-methyl-dimethyldiazacalix[4]areneH_4) afforded the product [Ti_2F_2(μ-F)$_3L^{4N}$(H)$_2$(SiF_5)]·2MeCN

(**17**·2MeCN). These complexes have been screened for their potential to act as pre-catalysts in the ring opening polymerization (ROP) of *ε*-caprolactone (*ε*-CL), *δ*-valerolactone (*δ*-VL) and *rac*-lactide (*r*-LA). Generally, the titanium complexes bearing oxacalixarene exhibited better activities than the azacalixarene-based pre-catalysts. For *ε*-CL, *δ*-VL and *r*-LA, moderate activity at 130 °C over 24 h was observed for **11**-**16**. In the case of the co-polymerization of *ε*-CL with *r*-LA, **11**-**16** afforded reasonable conversions and high molecular weight polymers; **17** exhibited lower catalytic performance due to low solubility. None of the complexes proved to be active in the polymerization of *ω*-pentadecalactone (*ω*-PDL) under the conditions employed herein.

In **Chapter 5**, a variety of lithiated calix[*n*]arenes, where n = 6 or 8, have been isolated, structurally characterized and screened for their ability to act as catalysts for the ring opening polymerization (ROP) of the cyclic esters *ε*-caprolactone (ε-CL), *δ*-valerolactone (δ-VL) and *r*-lactide (*r*-LA). In particular, interaction of L^6H_6 with LiO*t*Bu in THF afforded $[Li_{14}(L^6H)_2(CO_3)_2(THF)_6(OH_2)_6]$·14THF (**18**·14THF), whilst L^8H_8 afforded $[Li_{10}(L^8)(OH)_2(THF)_8]$·7THF (**19**·7THF). Similar use of de-butylated calix[8]areneH_8 (deBuL^8H_8) led to an elongated dimer $[Li_{18}(deBuL^8)_2(OtBu)_2(THF)_{14}]$·4THF (**20**·4THF). Interaction of L^8H_8 with LiOH·H_2O afforded $[Li_4(L^8H_4)(OH_2)_4(THF)_6]$·5.5THF (**21**·5.5THF), whilst addition of Me_3Al to the solution generated from L^8H_8 and LiO*t*Bu led to the isolation of $[(AlMe_2)_2Li_{20}(L^8H_2)_2(OH_2)_4(O^{2-})_4(OH)_2(NCMe)_{12}]$·10MeCN (**22**·10MeCN). These complexes have been screened for their potential to act as pre-catalysts in the ring opening polymerization (ROP) of ε-CL, δ-VL and *r*-LA. For ε-CL, δ-VL and *r*-LA, moderate activity for ROP at 130 °C over 8 h was observed for **18**-**21**. In the case of ROP using the mixed-metal (Li/Al) system **22**, better conversions and high molecular weight polymers were achieved. None of the complexes proved to be active in the ROP of ω-pentadecalactone (ω-PDL) under the conditions employed herein.

In **Chapter 6**, the lead coordination chemistry of large calix[*n*]arenes is studied. Reaction of $[LiPb(OiPr)_3]_2$ (generated *in-situ* from $Pb(OiPr)_2$ and LiO*i*Pr) with either L^4H_4 or L^6H_6 resulted in the heterometallic lithium/lead complexes $[Pb_4Li_2(L^4)_4H_6(MeCN)_3]$·4.5MeCN (**23**·4.5MeCN) and $[Pb_8Li_{10}Cl_2(L^6)_4(H)_8(O)_4(H_2O)_2(MeCN)_4]$·14MeCN (**24**·14MeCN), respectively. Reaction of five equivalents of $[Pb(OiPr)_2]$ with $L^{6O}H_6$ afforded

$[Pb_{13}(L^{6O})_3O_4(i\text{PrOH})]\cdot 11\text{MeCN}$ (**25**·11MeCN). Reaction of L^8H_8 with $[Pb(O\textit{t}Bu)_2]$ or $\{Pb[N(TMS)_2]\}$ (TMS = $SiMe_3$) afforded the products $[Pb_{12}(L^8)_2O_4]\cdot 8.7C_7H_8$ (**26**·$8.7C_7H_8$) or $[Pb_6(SiMe_3)_2(L^8)O_2Cl_2]$ (**27**), respectively. Reaction of $\{Pb[N(TMS)_2]\}$ (generated *in-situ* from $(Me_3Si)_2NH$, *n*BuLi and $PbCl_2$) with L^6H_6 afforded, after work-up (MeCN), the mixed-metal complex $[Pb_5Li(L^6)O_{2.5}Cl_{0.5}]\cdot 4.75\text{MeCN}$ (**28**·4.75MeCN). Complexes **23**-**27** have been screened for their potential to act as pre-catalysts in the ring opening polymerization (ROP) of *ε*-caprolactone (*ε*-CL) and *δ*-valerolactone (*δ*-VL) and the copolymerization thereof. Generally, the lithiated complexes **23** and **24** exhibited better activities than the other pre-catalysts screened herein. For *ε*-CL and *δ*-VL, moderate activity at 130 °C over 24 h was observed for **23**-**27**. In the case of the co-polymerization of *ε*-CL with *δ*-VL, **23**-**27** afforded reasonable conversions and high molecular weight polymers. The catalysts **23-27** also be proved to be active in the ROP of the *rac*-lactide (*r*-LA), the activity trend was found to be **24** >**23** >**25** >**26** ≈ **27**.

Chapter 7 presents the experimental section.

Chapter 8 Appendix.

Abbreviations

Å = angstrom

Ar = aryl

MeCN = acetonitrile

br = broad

*t*Bu = *tert*-butyl

PPNCl = bis(triphenylphosphine)iminiumchloride

L^4H_4 = *p-tert*-butylcalix[4]areneH_4

L^8H_8 = *p-tert*-butylcalix[8]areneH_8

$L^{4S}H_4$ = *p-tert*-butylthiacalix[4]areneH_4

$L^{6O}H_6$ = *p-tert*-butyltetrahomodioxacalix[6]areneH_6

δ = chemical shift

J = coupling constant

ε-CL = *ε*-caprolactone

^oC = degree Celsius

d = doublet

deBuL^8H_8 = de-butylated calix[8]areneH_8

$L^{6N}H_6$ = *p*-methyl-dimethyldiazacalix[6]areneH_6

$L^{4N}H_4$ = *p*-methyl-dimethyldiazacalix[4]areneH_4

ESI = electrospray ionization

ETA = ethyltrichloroacetate

GPC = gel permeation chromatography

h = hour

IR = infra-red

S_B = integral area measured by GC

m = medium

MS = mass spectrometry

MALDI = matrix-assisted laser desorption ionization

MAO = methylaluminoxane

Min = minute

Me = methyl

OMe = methoxide

NMR = nuclear magnetic resonance

M_n = number average molecular weight

L^3H_3 = oxacalix[3]arene

O*i*Pr = *iso*-propoxide

O*n*Pr = *n*-propoxide

O*t*Bu = *tert*-butoxide

PDI = polydispersity index

*i*Pr = *iso*-propyl

*n*Pr = *n*-propyl

ppm = parts per million

PCL = polycaprolactone

PVL = polyvalerolactone

PLA = polylactide

ROP = ring opening polymerization

s = singlet

s = strong

P_r = syndiotactic bias

t = triplet

TEA = triethylamine

THF = tetrahydrofuran

TMS = trimethylsilyl

TEA = triethylaluminium

δ-VL = δ-valerolactone

M_w = weight average molecular weight

Contents

Acknowledgements

Firstly, I would like to express my thanks to my principal supervisor, Professor Carl Redshaw, for giving this opportunity to do a PhD in UK. During the past four years, he not only gives assistance, encouragement and scientific suggestion but also provided excellent research resources in this study.

I also would like to say thank you to my second supervisors, Dr. Timothy J. Prior for the great help with X-ray crystallography and analysis. Then, I am thankful for all the academic staff of the chemistry department, who helped me a lot through my research.

Furthermore, I would like to thank my colleagues and friends, Kuiyuan Wang, Xin Zhang, Abdullah Fahad A. Alshamrani, Orlando Santoro and Dr. Fei Cheng for you've all been a joy to work with and made my time in the group the most fun possible.

Special thanks to China Scholarship Council for the economic supporting for my life and research. Without the help from my country, it would be impossible to undertake my PhD in the UK.

On a personal note, thanks should go to my parents, thanks for making the effort to learn about what I've been researching and always giving me encouragement. Lastly, I would like to say thank you to my wife-to-be, Jingjing Xu for all the support and understanding.

Chapter 1

General Introduction

1. Calixarene and metallocalixarenes compounds

1.1 History of calixarenes

A calixarene is a cyclic oligomer consisting of phenol units, which connected at the *ortho* position of the phenolic hydroxyl group by, mostly commonly, a methylene bridge. In the early 1940s, A. Zinke, an Austrian chemist, firstly studied the reaction of formaldehyde with p-*tert*-butylphenol to synthesize a high melting point crystalline compound.[1] In 1970s, American chemist C. David Gutsche firstly used the name "calixarene", which including "calix" (the name for a Greek chalice) and "arene" for the aryl groups in the macrocycle (Figure 1-1).[2] Based on the number of phenol units, the afforded compound was named calix[*n*]arene (n = the number of phenol units). Among these compounds, calix[4]arenes, calix[6]arenes, and calix[8]arenes have obtained a considerable amount of interest in the supramolecular chemistry, and have found applications for a range of areas; even numbered calix[*n*]arenes are the easiest to make/isolate.[3] With the development of calixarene synthesise procedure, a range of new larger sized calix[*n*]arenes have been synthesized, for example Guillaud *et. al*. have developed an optimized synthetic procedure to synthesis calix[7-20]arenes.[4] Furthermore, calix[*n*]arenes are conformationally mobile, based on the different number n of phenol groups, the calixarene conformation number X=2n/2. For example, the calix[4]arenes can possess the cone, partial cone, 1,3-alternate, and 1,2-alternate conformations (Figure 1-2).[5]

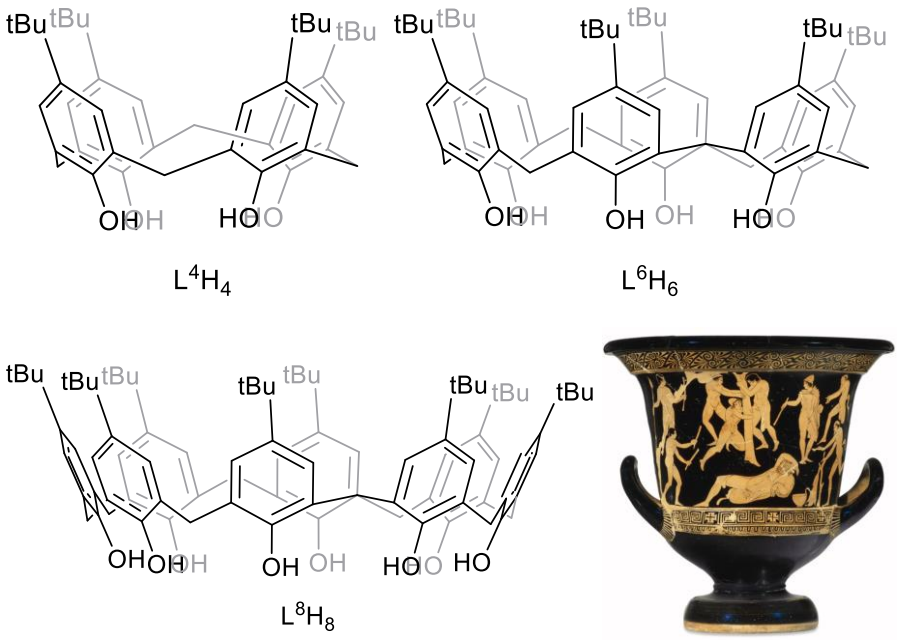

Figure 1-1. Calix[*n*]arenes (n = 4, 6 and 8) and a crater.

As organic supramolecular hosts, calixarenes have been described as a third generation of supramolecular hosts after cyclodextrins and crown ethers. Compared with cyclodextrins and crown ethers, calixarenes have the following specialties: (1) The bowl shape formation of calixarene lead to macrocycle cavity, which can be modified by size of cone; (2) The wide rim (hydrocarbon group) and the narrow rim (hydroxyl group) can be chemically modified to selectively complex a variety of metal ions; (3) calixarenes with ions or neutral molecules can easily form host-guest inclusion complexes; (4) Calixarenes have good thermal and chemical stability, some derivatives have good solubility; (5) Most of the calixarenes and their derivatives can be easily prepared and there are many kinds of calixarenes available commercially; (6) Calixarenes are stable in air, so they do not require preventive measures to exclude oxygen or water during synthesis and storage.[5]

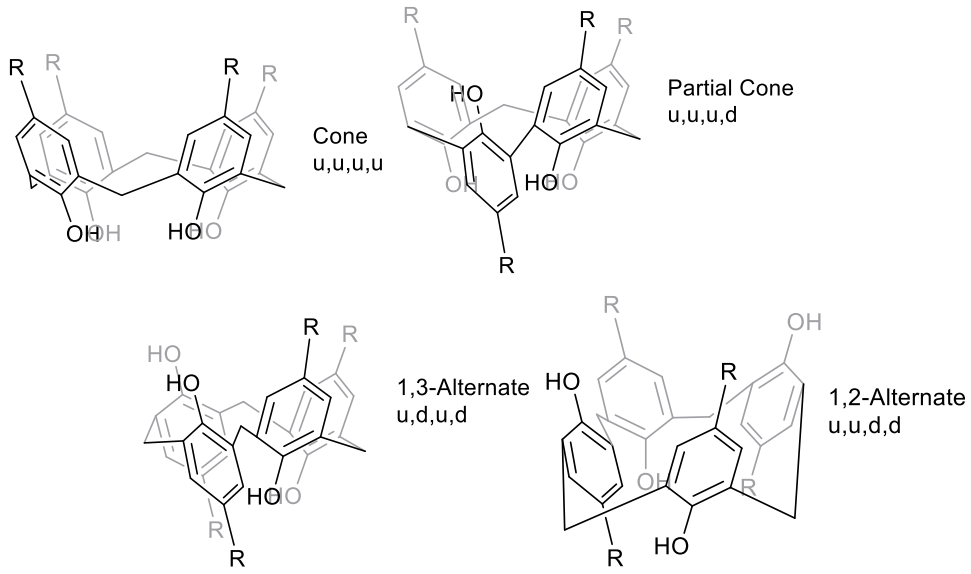

Figure 1-2. Different calix[4]arene conformations.

1.2 Development of calixarene synthesis

Since the 1950s, calixarenes have attracted great interest as a versatile class of macrocyclic host to synthesize complexes with lots of metal ions, inorganic anions and small organic molecules. In the meantime, a series of synthetic methods for calixarene chemistry have been developed. In 1958, Hayes and Hunter firstly reported the multi-step synthesis procedure for *p-methyl*-calix[4]arene, which introduced a bromine atom as the protecting group at the *ortho*-position during the first step of the synthesis under alkaline conditions.[6] The afforded mixture was then treated with HCl and a large excess of p-Cresol, and then heated at 70 ℃ for 18 h. Then, hydrogenolysis was used to remove the halogen atom and followed by the cyclisation under high dilution to afford the tetramer (Figure 1-3). However, this multi-step method takes a very long time to synthesis the calixarene and the overall yield is relatively low (0.5-11%).

Böhmer *et al*. did further work on the multi-step calixarene synthesis procedure by

developing convergent pathways to decrease the number of synthetic steps.[7] The corresponding linear phenol fragments were used to do the condensation reaction. For example, the synthesis of a calix[4]arene via a "3 + 1" convergent protocol employed a linear trimer and a 2,6-bis-halomethyl phenol to afford the target calixarene compound. Based on the "3 + 1" approach, more synthetic methods have been developed including "2+2", "2×1+2×1", "2+2×1", "4×1" procedures. The choice of synthesis depends on the ease of synthesis of the corresponding fragments (Figure 1-4).

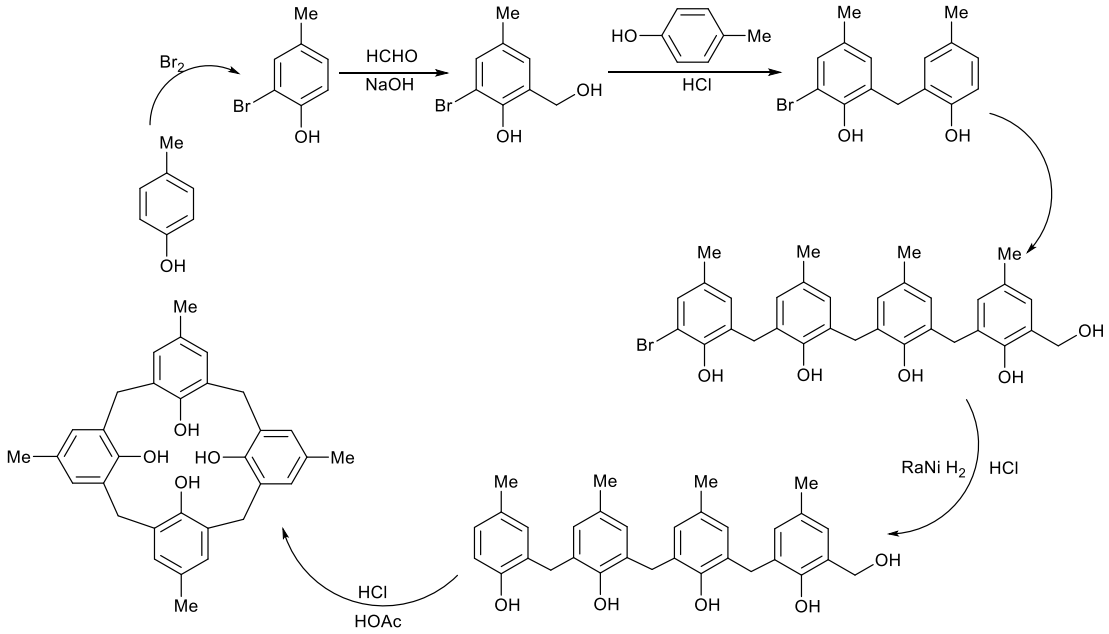

Figure 1-3. The multi-step synthesis procedure for p-methylcalix[4]arene.

Nowadays, the most common method employs the so-called "one-step synthetic procedure", whereby heating a mixture of *para-t*-butylphenol and formaldehyde under alkaline conditions affords the calixarene (Figure 1-5). By varying either the temperature or amount of base used in the preparation, calix[4, 6 and 8]arene (bridged by -CH_2- spacers) can be afforded.[8] Compared with the synthesis of tetrameric, hexameric, and octameric

phenolic ring systems, calix[*n*]arene with an odd number of phenolic residues are only accessible in low yield.

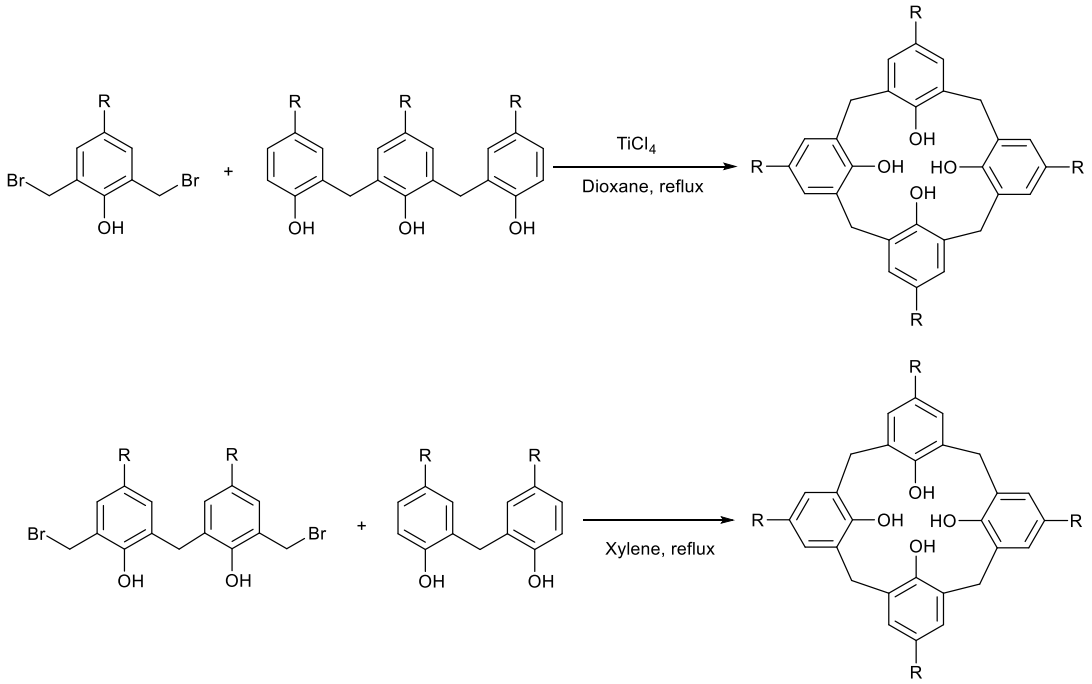

Figure 1-4. The "3+1" and "2+2" synthesis procedures for calix[4]arene.

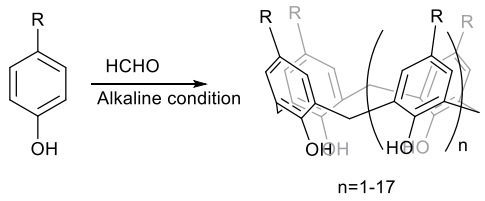

Figure 1-5. The one-step synthetic procedure for calixarenes.

1.3 Synthesis of heterocalixarenes

There is no doubt that the advent of heterocalixarenes has brought new horizons for supramolecular chemistry. During the past decades, the synthetic preparation method of heterocalixarenes has been developed to allow to change the calixarene bridging group from methylene (–CH_2–) to dimethyleneoxa (-CH_2OCH_2-), thia (-S-), and aza [-$CH_2N(R)CH_2$-] group[9] and these additional donors can provide extra binding sites.[10] The

design and synthesis of novel and heterocalixarenes has become a new direction of supramolecular chemistry.

1.3.1 Oxacalixarenes

Oxacalixarenes are a class of calixarene derivative which use -CH_2OCH_2- as the bridges either partly or completely replacing -CH_2- bridges between the phenol units. Like normal calix[*n*]arenes, oxacalixarenes have also received considerable attention because of their remarkable ionophoric receptor properties.[11-16]

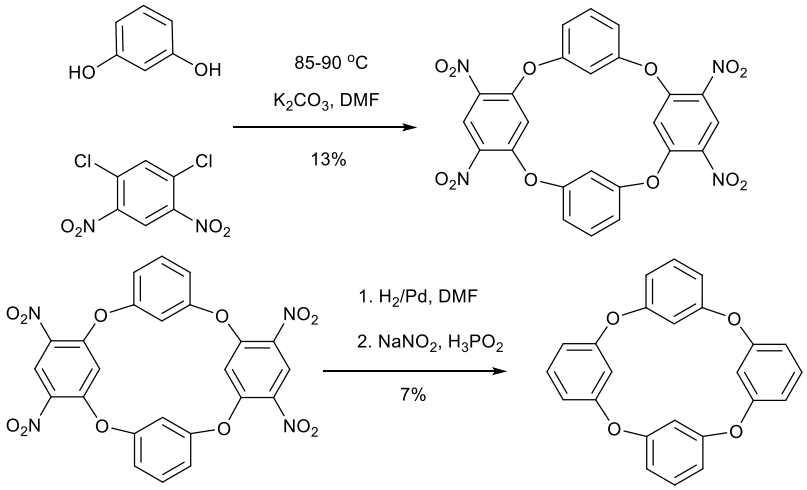

Figure 1-6. The first synthetic procedure for oxacalixarene tetramer.[11,14]

Back in the 1960s, N. Sommer and H. A. Staab firstly synthesized an oxacalixarene by using *m*-dihydroxybenzene and 1,3-dichloro-4,6-dinitrobenzene, however, the yields of the afforded compounds were extremely low (7-13%, Figure 1-6). Without more efficient synthetic technology, oxacalixarenes did not receive much attention from organic chemists for the next forty years, until when in 1974, Lehmann[12] reported a new method by using 1,5-difluoro-2,4-dinitrobenzene and resorcinols to synthesis oxacalix[4]arenes; the product were purified via precipitation in 23-77% yield. In the meanwhile, based on Lehmann's work, Gilbert[13] used a modified reaction and isolation conditions to produce

oxacalix[4]arene (Figure 1-7) in much better yields (60-95%). This simple and effective synthetic strategy still pervades to the current day.[14]

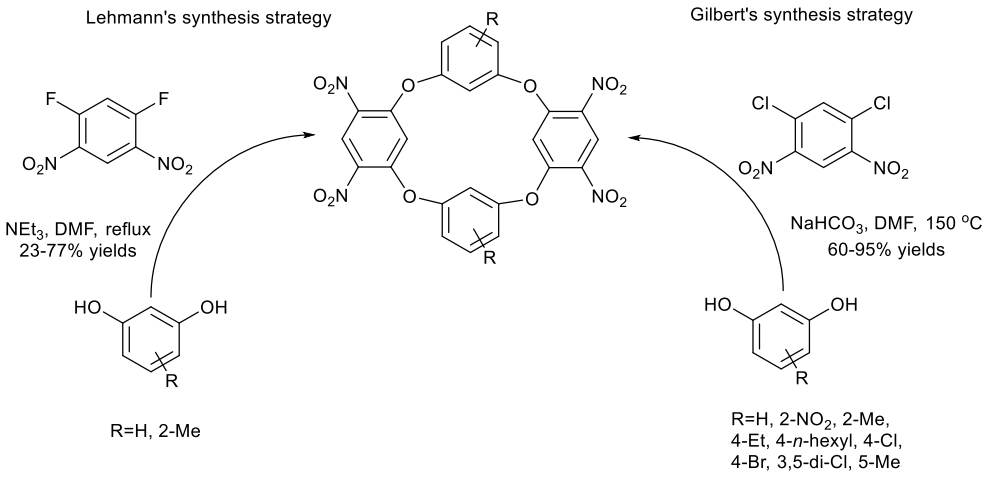

Figure 1-7. The two different synthetic methods for oxacalix[4]arene.

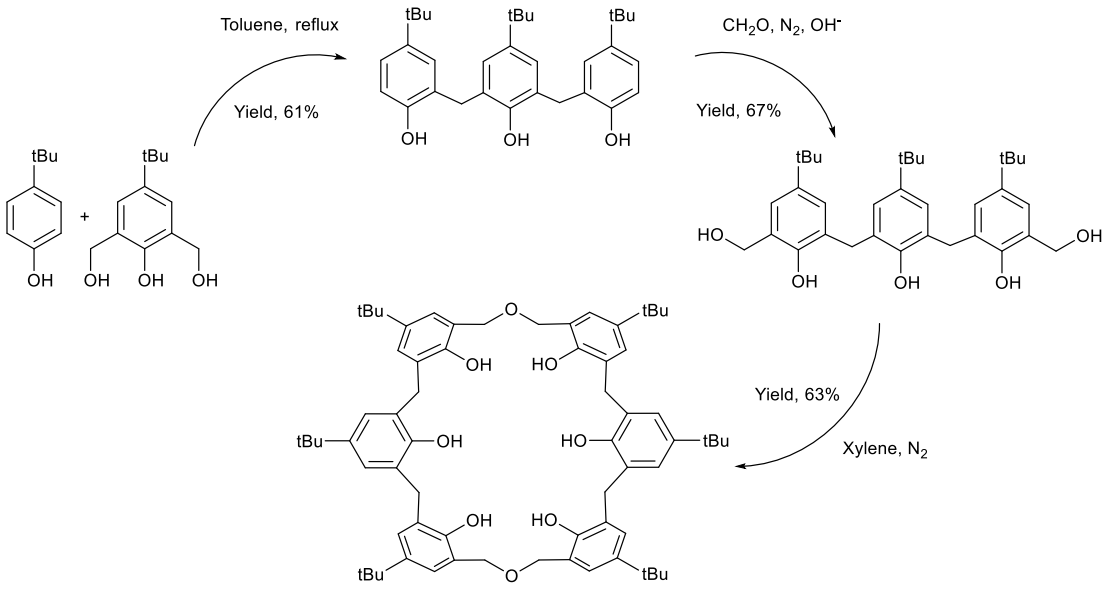

Figure 1-8. The synthetic method for *p-tert*-butyltetrahomodioxacalix[6]areneH_6

On the other hand, in 1983, Balram Dhawan and C. David Gutsche[15] reported a new method using aqueous formaldehyde with p-*tert*-butylphenol in an alkaline environment to prepare oxacalixarenes. Furthermore, Masci *et al*.[16] reported a new preparation method to

synthesize homooxacalixarenes through thermal dehydration of a bishydroxymethylated triphenol under a relatively mild conditions and the structure of p-*tert*-butylhexahomomtrioxacalix[*n*]arene (n=3, 4, 6 and 9) macrocycles was reported. For example, the synthetic method for p-*tert*-butylhexahomomtrioxacalix[6]arene is shown in Figure 1-8. The afforded macrocycle (Figure 1-9) was afforded in moderate to high yield (60~68%) under heating in xylene. Based on the current results, the thermal dehydration of bishydroxymethylated phenols is an alternative efficient way to prepare homooxacalixarenes.

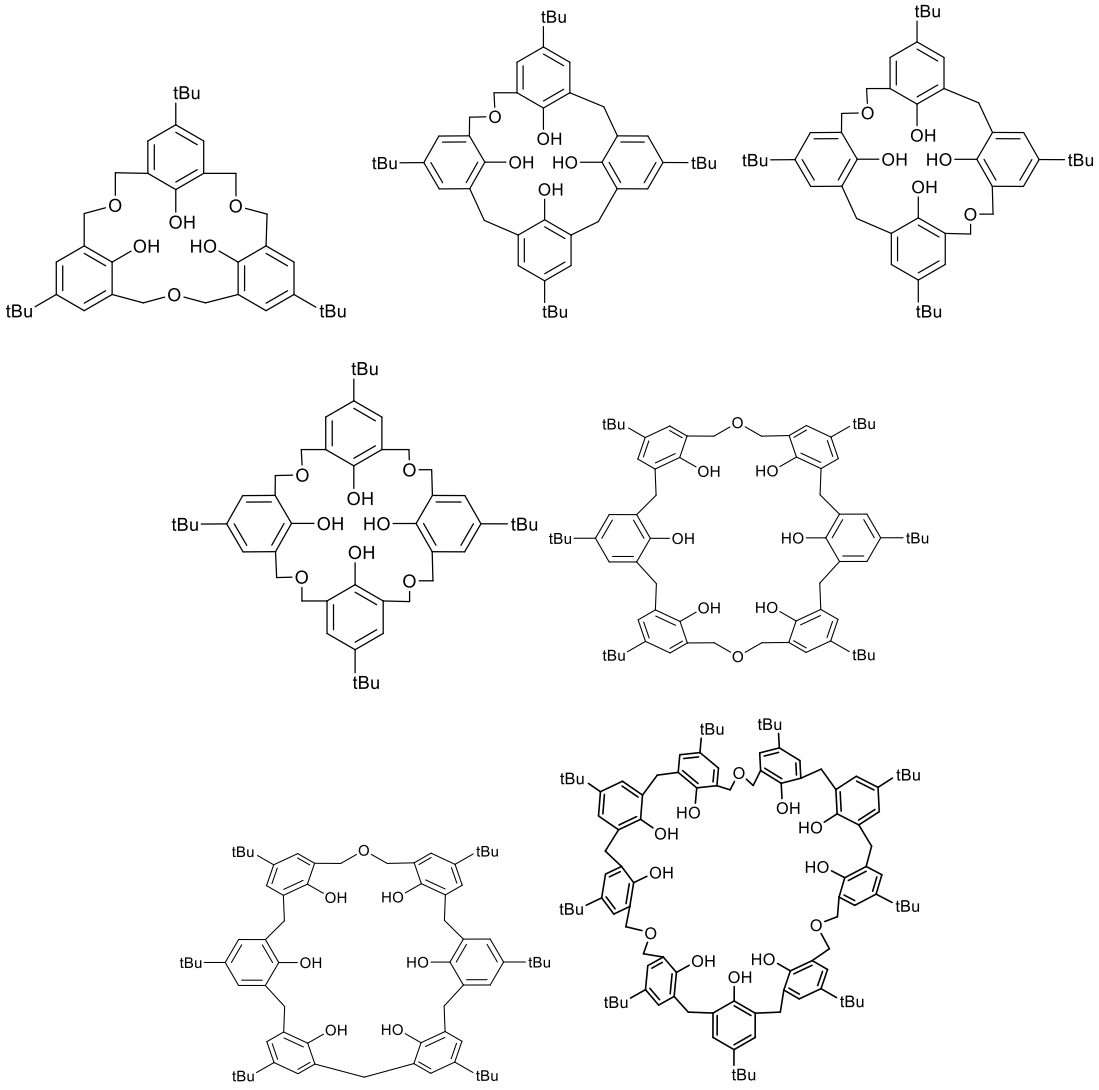

Figure 1-9. Structures of oxacalix[*n*]arenes (n=3, 4, 6 and 9).

1.3.2 Azacalixarenes

The first synthesis of an azacalixarene can be dated back to 1963[17], and unlike oxacalixarenes, the nitrogen atom in the calixarene bridge can possess an additional group, which makes the azacalixarene more amenable to functionalization. More importantly, the strong hydrogen bonding capability of the NH group means that azacalixarenes can be more easily self-assembled to form supramolecular structures, and this has laid a solid foundation for its application in supramolecular chemistry. After the synthesis of azacalixarenes in 1960s, Tanaka[18] used the Ullmann coupling reaction to prepare a series of *N*-methyl substituted azacalix[4]arenes (Figure 1-10). Based on the Ullmann catalyzed aromatic amination reaction, Tamura[19] also synthesized methyl substituted azacalix[4]arenes from anilines and dibromobenzene derivatives. Through this study, the author also confirmed that the afforded compounds possess a 1,3-alternating conformation by single crystal X-ray diffraction.

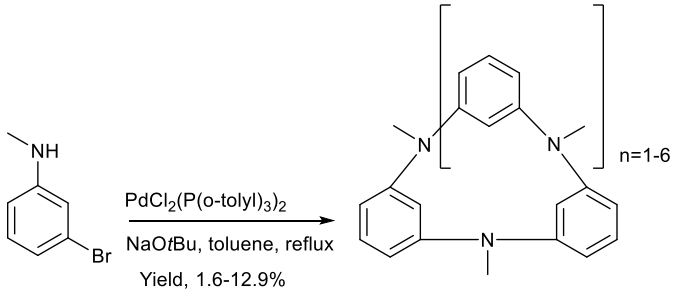

Figure 1-10. The Ullmann coupling reaction to prepare azacalixarenes.

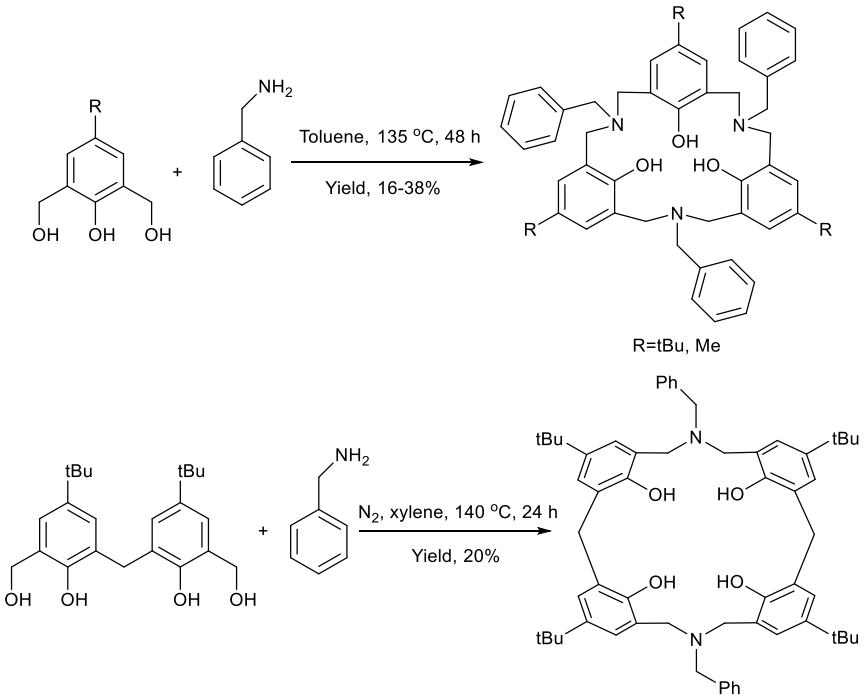

Figure 1-11. The one-step synthetic method for hexahomotriazacalix[3]arene and homoazacalix[4]arene.

Furthermore, in 1992, Takemura's group firstly reported a new cyclization method leading to a one-step synthesis of hexahomotriazacalix[*n*]arenes (n = 3, 4 and 6) by using bis(hydroxymethyl)phenols and benzylamine. For example, the hexahomotriazacalix[3]arene and homoazacalix[4] arene synthetic procedures are shown in Figure 1-11. The obtained azacalixarenes have a symmetrical structure along the N···N' axis or the N···CH_2 axis.[20] Based on their former work, they further developed a different procedure by using the phenol oligomers and the benzoxazine derivatives of phenols (Figure 1-12) to produce azacalixarene in satisfactory yields.[21] The afforded azacalixarene compounds are shown in Figure 1-13.

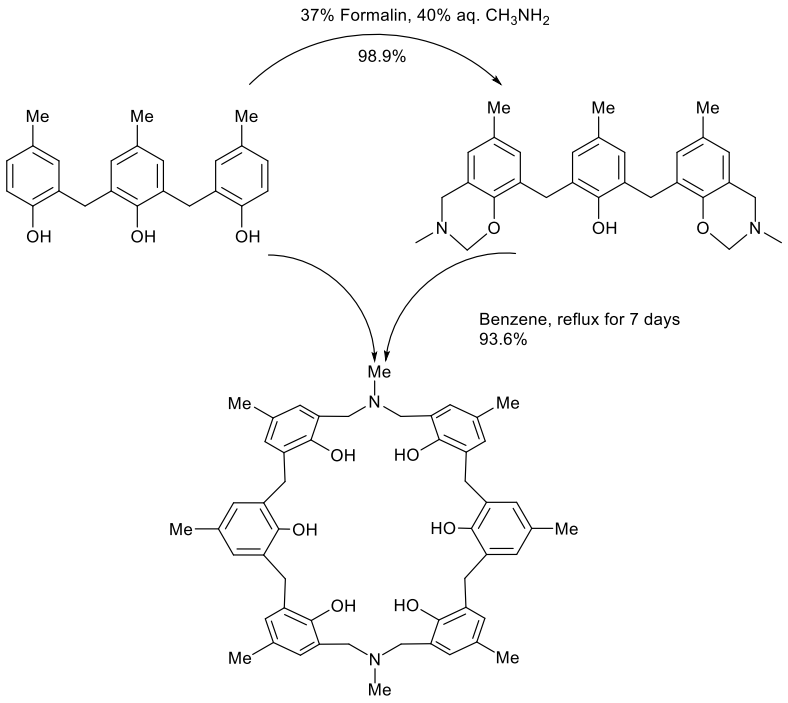

Figure 1-12. The synthetic procedure for azacalix[6]arene by using benzoxazine derivatives of phenols and the phenol trimer.

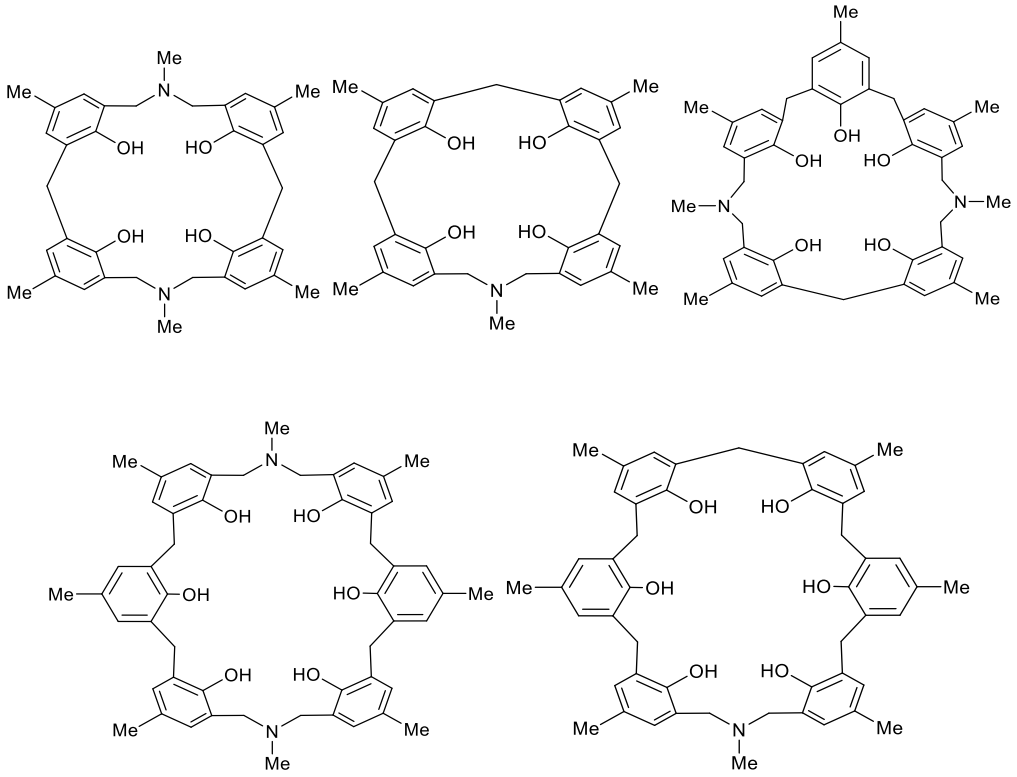

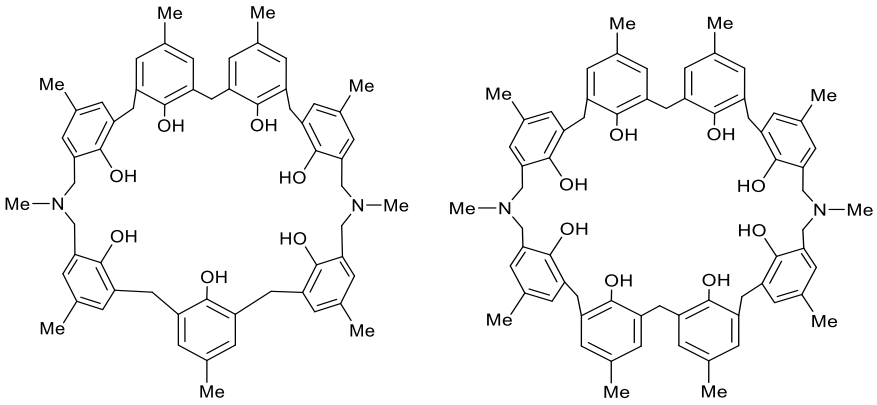

Figure 1-13. Structures of azacalix[*n*]arenes (n = 4, 5, 6, 7 and 8).

1.3.3 Thiacalixarenes

Sulfur is an element in the same main group as oxygen, which has relatively similar chemical properties, however thiacalixarenes were synthesized before oxacalixarenes and have been widely utilized. Sone *et al*. firstly reported a synthesis procedure by using p-*tert*-butylphenol with sulfur and the afforded p-*tert*-butylthiacalix[4]arenes are more structurally flexible with the increasing the number of the sulfur bridges.[22] Based on this research, Miyano[23] optimized the reaction conditions and developed a new one-step synthetic method by heating p-*tert*-butylphenol and sulfur in tetraethylene glycol dimethyl under alkaline conditions which afforded a 54% yield of *p-tert*-butylthiacalix[4]arene (Figure 1-14).

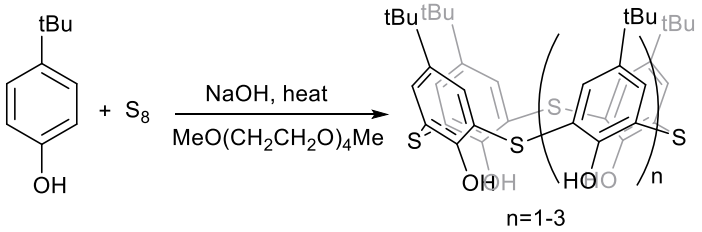

Figure 1-14. Facile synthetic method for p-*tert*-butylthiacalix[*n*]arene (n = 4, 6 and 5).

Within the calixarene family, by comparison with azacalixarenes and oxacalixarenes, thiacalixarenes have captured the attention of researchers given their potential superior applications in industrial and academic fields.[24] Due to the presence of the bridging sulfur atom, thiacalixarenes and derivatives can possess unique properties and functions for selective binding to the metal ions. Based on this feature, a series of supramolecular metal complexes have been developed, which have been applied to wide ranging applications such as oxidative catalysis, self-assembled metal cluster/cage formation and energy-transfer luminescence for probes.[25] It is clear that the research on thiacalixarenes is far from finished, and much chemistry remains to be discovered.

1.4. Metallocalixarene compounds

Calixarene coordination chemistry started from 1980s, and over the past decades, a number of new metallocalixarenes have been reported.[10] Therefore, metallocalixarenes have obtained a range of attentions in the catalysis field, and have found applications for different areas.[15] For example, calix[*n*]arenes are able to bind with a variety of metal ions and can be utilized as components of catalysts in different transformations. Figure 1-15 shows the different reaction types catalyzed by metallocalixarene complexes.[10] Previous research has also shown that metallocalixarenes can be applied in a number of areas, including as metal-based anti-cancer agents, for CO_2 storage, in medical diagnostics, as fluorescent probes, as phase-transfer agents, in polymerization catalysis, in separation chemistry and in nanochemistry.[10,26] Furthermore, the chemical modification of both the upper and lower rims offers more possibilities to synthesize calixarene-based anion receptors.

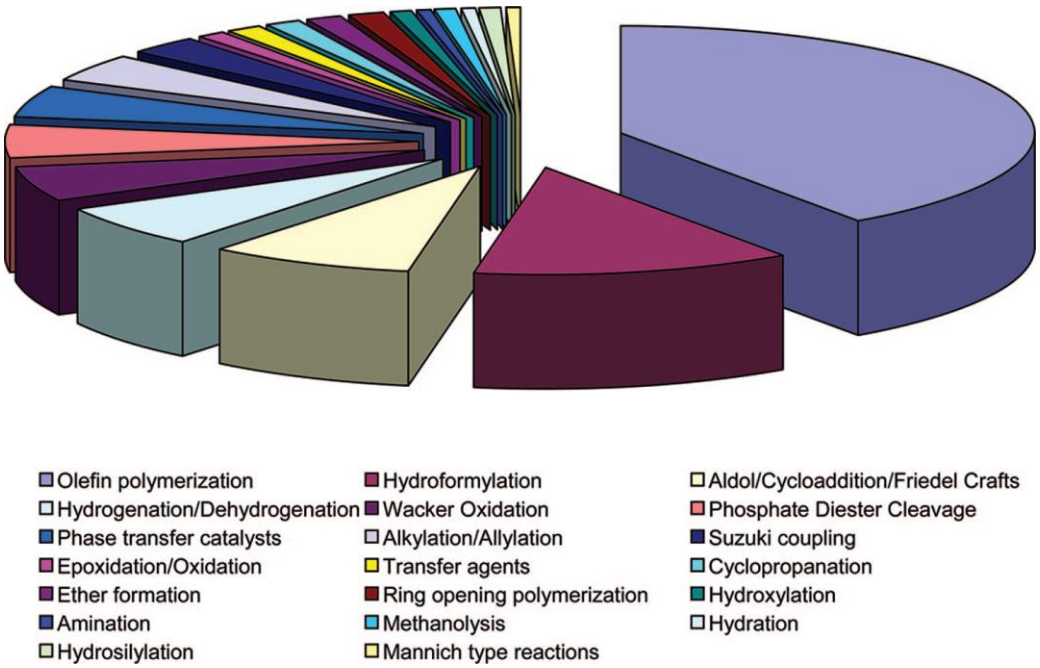

Figure 1-15. Different reaction types catalyzed by metallocalixarene complexes until 2008.[10]

1.4.1 Alkali metal complexes bearing calixarene ligands

For alkali metal calixarene compounds, numerous works on the complexation of alkali metal based on calixarene ligands have been reported.[27]

For lithium calixarene complex, Havlas *et al*.[28] reported the early work on synthesis procedure for lithium calix[n]arenes complexes by using *p-tert*-butylcalix[4]arene and lithium amide. Furthermore, for larger calixarene, Hanna *et al*. employed and structurally characterized lithiated compounds prepared from calix[*n*]arenes (n = 4 and 8) via the use of LiO*t*Bu or $LiOSiMe_3$.[29] In recent studies, Hanna *et al*. reported a range of lithiated calix[5]arene complexes, which were synthesized by employing different lithiated reagents (LiOH, *n*BuLi and LiH) with the parent calix[5]arene. Also, Redshaw *et al*. recently synthesized and structurally characterized numerous new lithiated calix[3 and 4]arene compounds, which used calixarenes containing different bridging groups (–CH_2–, –S–, –

SO–, $–SO_2–$ or $–CH_2OCH_2–$). These were accessed by interaction of the respective calixarene with a series of lithium starting materials (Li*O*t*Bu*, LiOH or *n*BuLi) and the afforded complexes proved to be active for the ring opening homo-/co-polymerization of a number of cyclic esters (*ε*-caprolactone, *δ*-valerolactone and *rac*-lactide).[30]

Hanna and Thuéry[29, 31] reported a systematic synthetic procedure for accessing alkali metal calixarene complexes by using M_2CO_3 or M*O*t*Bu* precursors (M = Li, Na, K, Rb and Cs), and the resulting complexes were structurally characterized. (Figure 1-16) Hanna *et al*.[29] also described a new theory, which suggested that the conformations of alkali metal complexes can systematically be divided into four structural types, namely *endo*/*exo*-polymers, polymers of dimers, discrete dimers and discrete monomers, whilst the stability of alkali metallocalixarenes is highly dependent on the ring size of the calixarene.

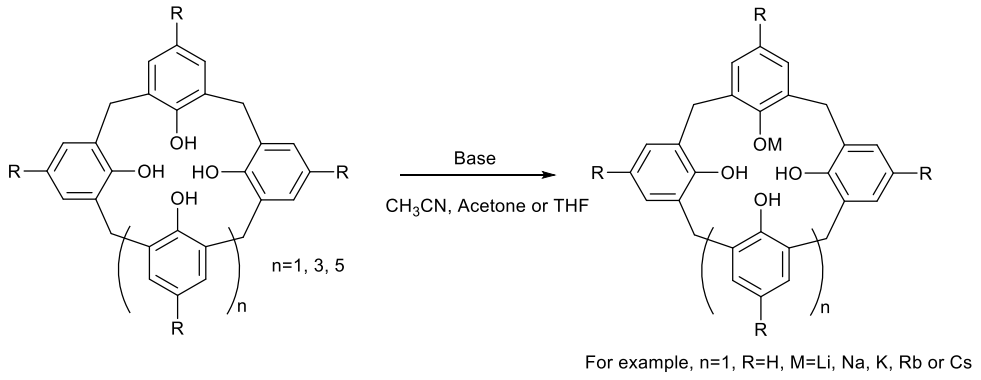

Figure 1-16. Synthesis of alkali metal containing calixarenes reported by Hanna *et al*.[29]

1.4.2 Transition metal complexes bearing calixarene ligands.

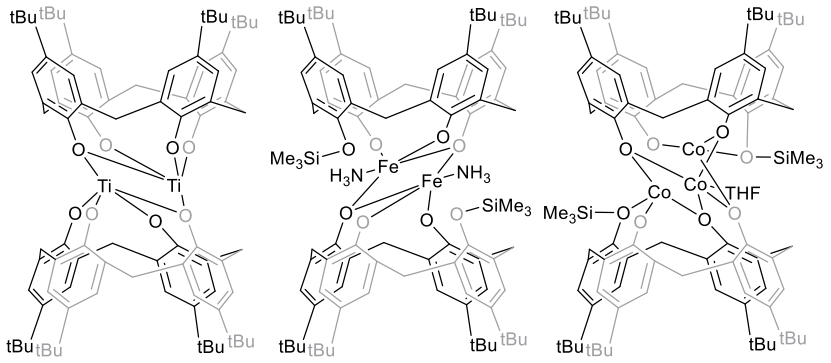

Figure 1-17. Ti (IV), Fe (III) and Co (II) metallocalixarenes complexes bearing p-*tert*-butylcalix[4]arene derived ligation.[32]

For transition metal calixarene compounds, the early work mainly focused on metallocalixarenes containing Ti, Fe and Co, (Figure 1-17) which were synthesized by using metal amide precursors (for example, $Ti(NMe_2)_4$, $Fe[N(SiMe_3)_2]_3$ or $Co[N(SiMe_3)_2]_2$).[32] Furthermore, Taoufik[33] *et al*. extended the studies for titanium metallocalixarenes compounds by varying the 1,3-dialkyloxy group to methyl, ethyl, *n*-propyl and *i*-butyl and the resulting complexes were investigated for their catalytic performance in ethylene as well as cyclic ester polymerization (Figure 1-18). Subsequently, Redshaw *et al*.[34] reported titanocalixarenes derived from the interaction of tetrahalides $[TiX_4]$ (X = Cl, Br, F, I) with larger p-*tert*-butylcalix[*n*]arenes (n=6, 8). The afforded complexes not only exhibited intriguing molecular structures, but also achieved reasonable conversions for ring opening polymerization of cyclic ester (Figure 1-19).

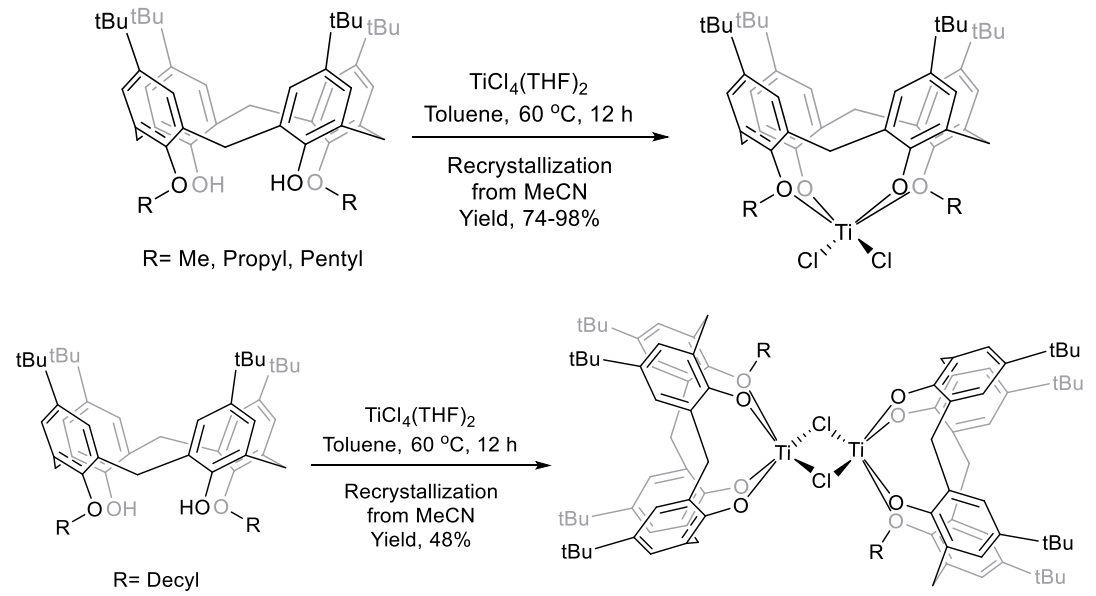

Figure 1-18. Synthesis of titanocalix[4]arenes complexes.[33]

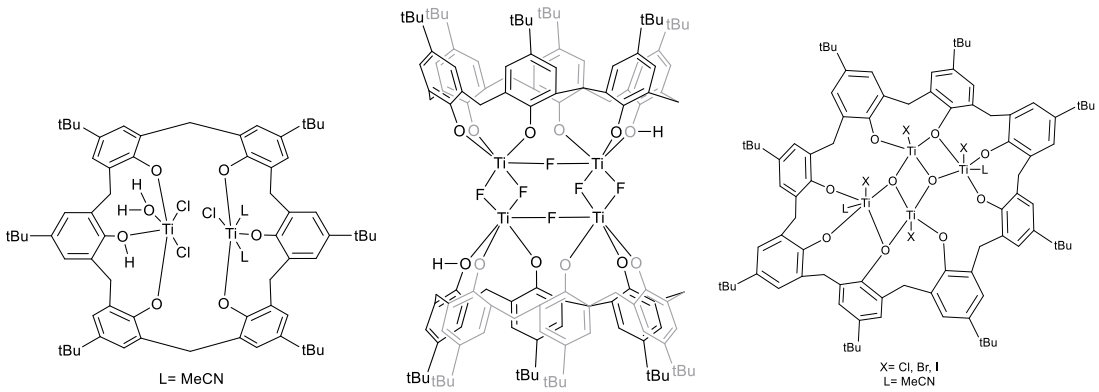

Figure 1-19. Titanocalixarenes complexes based on larger calix[*n*]arene (n = 6, 8) frameworks.

Moreover, vanadium metallocalixarene compounds have been reported by the groups of Redshaw and Limberg.[35] The catalytic performance of the afforded vanadium complexes for ethylene and ε-caprolactone polymerization were also investigated (Figure 1-20). However, compared with the vanadium coordination system associated with calix[4]arene system, there is a lack of such studies on larger calix[*n*]arenes (n=6, 8). Subsequently, Redshaw *et al*.[36] reported a range of procedures as well as molecular structures for both oxo- and imido vanadium metallocalix[*n*]arenes for n = 4, 6 and 8 (Figure 1-21).

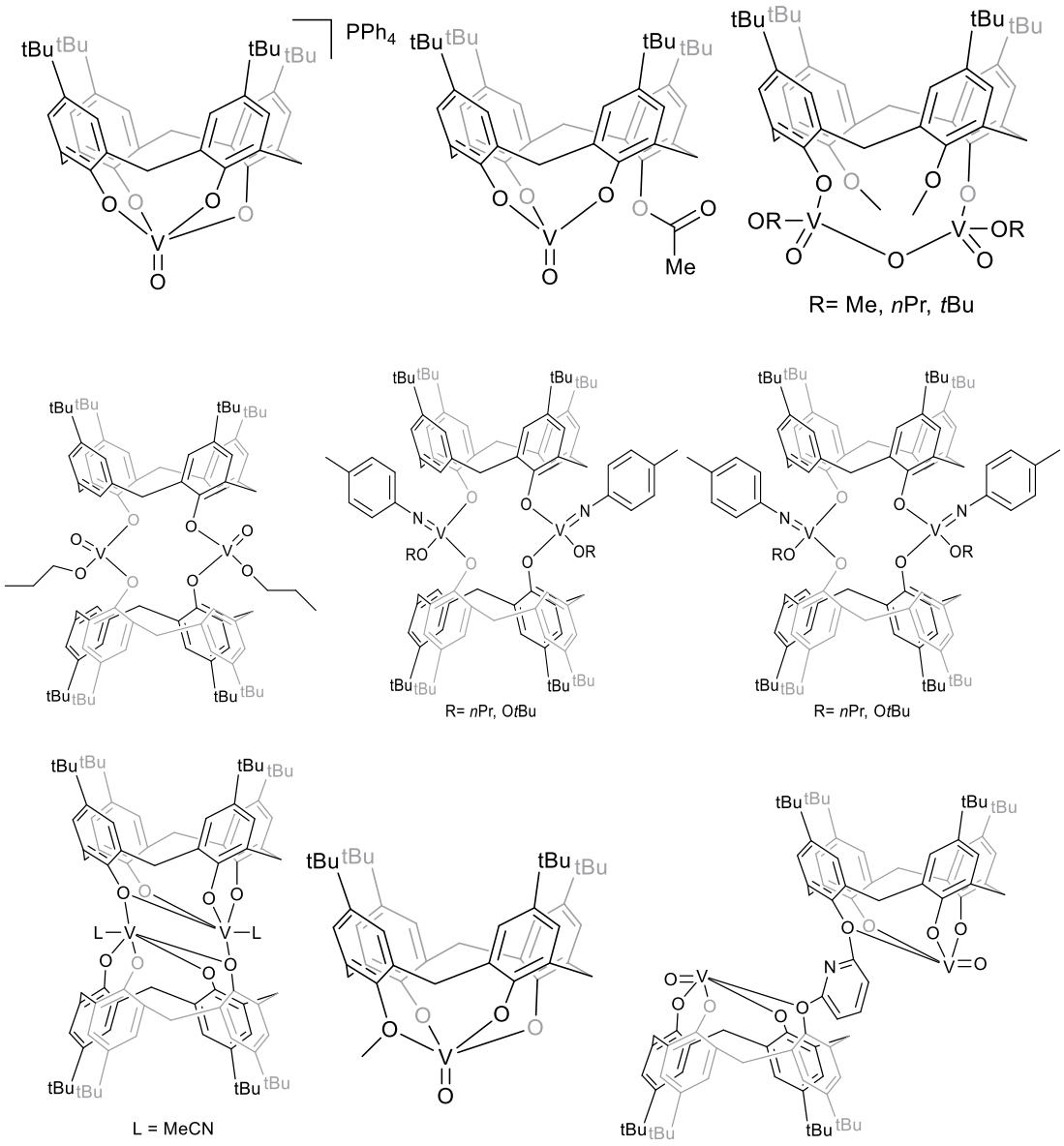

Figure 1-20. Vanadium-based metallocalix[4]arene compounds.[35]

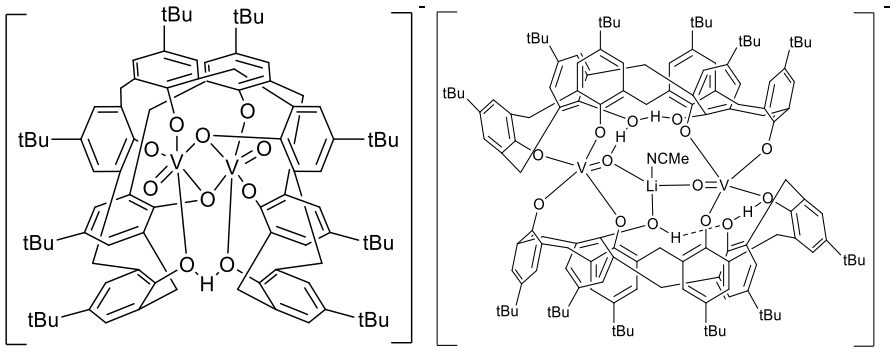

Figure 1-21. Vanadium-based metallocalix[*n*]arene (n = 6, 8) compounds.[36]

The other group V metals, niobium and tantalum have also been utilized to synthesize metallocalixarenes based on p-*tert*-butylcalix[*n*]arenes (n = 4, 6, 8). Redshaw *et al*.[37] found that the complexes resulting from p-*tert*-butylcalix[*n*]arene (n = 4, 6, 8) with $NbCl_5$/$TaCl_5$ exhibited an isostructural molecular conformation, but their performance as pre-catalysts for ethylene polymerization was poor.

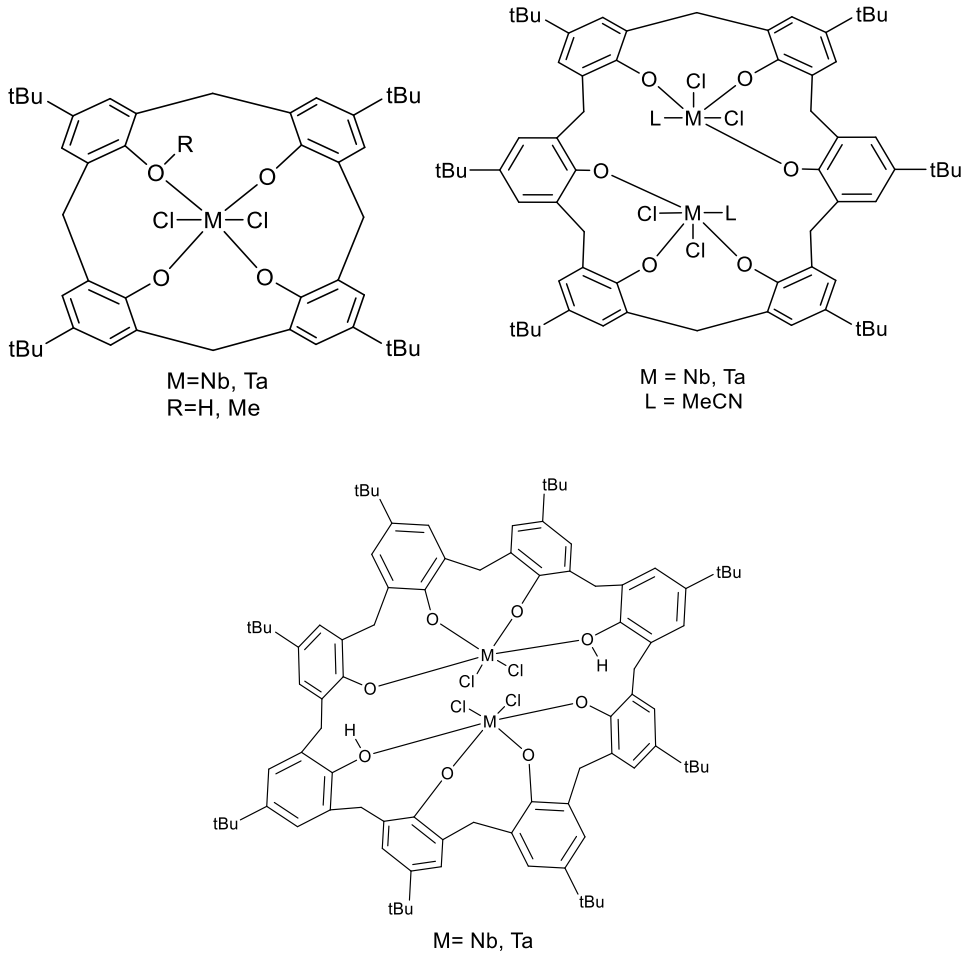

Figure 1-22. Niobium and tantalum metallocalixarenes.[37]

The use of calixarene has been further extended to the group VI metals. Kim *et al*.[38] investigated both dinuclear or mononuclear chromium(III) complexes, for which ethylene polymerization screening showed reasonable activities with triethylaluminium (TEA) as cocatalyst. Meanwhile, a range of tungstocalix[*n*]arene (n= 4, 6, 8) systems have been

prepared and structurally characterized, and their potential as pre-catalysts for the ROP of cyclic esters investigated, which showed superior activites for polyester synthesis.[39] The molecular structures of typical chromium and tungsten complexes bearing calixarene ligands are shown in Figure 1-23.

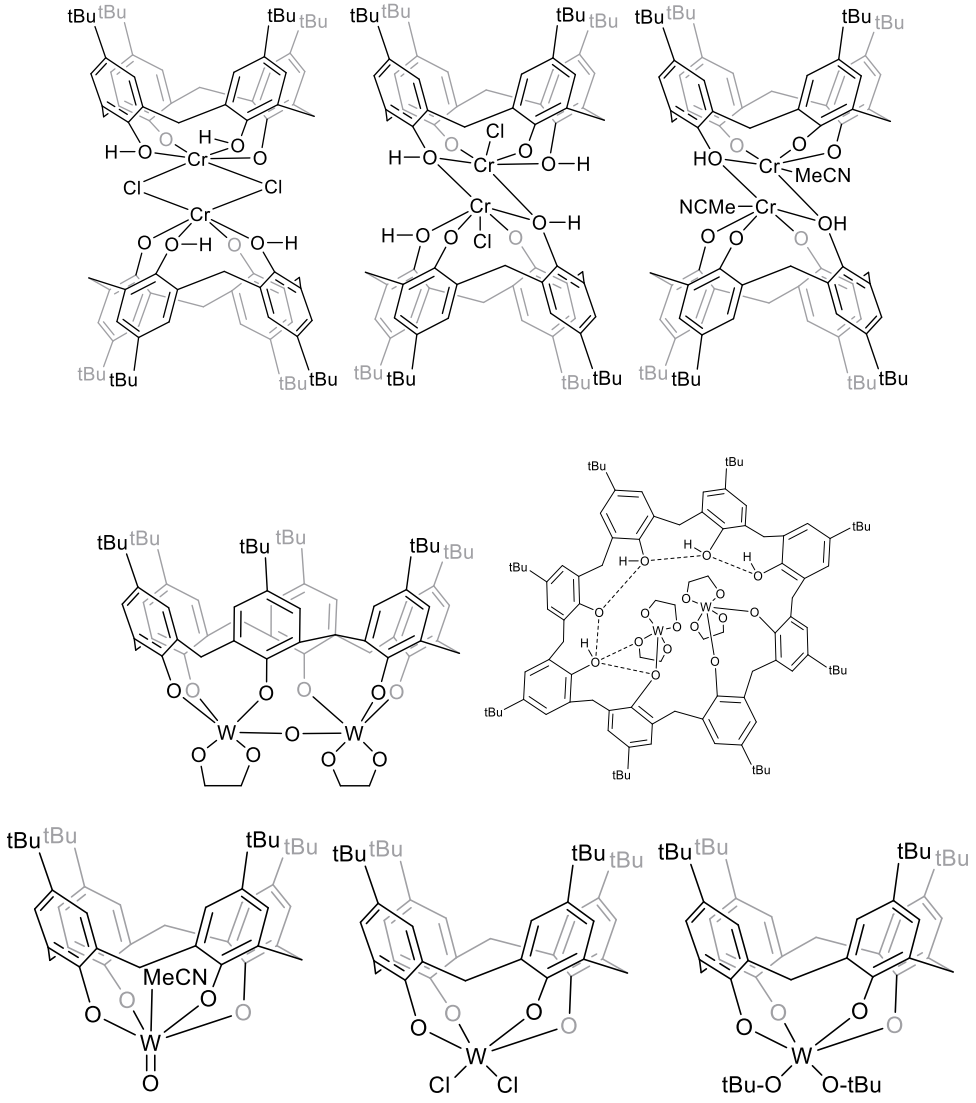

Figure 1-23. The molecular structures of typical chromium and tungsten complexes bearing calixarene ligands.

1.4.3 Metal complex derived from heterocalixarenes

Complexes derived from heterocalixarenes have shown not only favorable conformational flexibility but also great potential in a variety of catalytic applications.[10] However, coordination chemistry studies involving thia (–S–), sulfinyl (–SO–), sulfonyl ($–SO_2–$), dimethyleneoxa ($-CH_2OCH_2-$)-bridged containing metallocalixarenes have received limited attention compared to calix[4]arenes. Furthermore, azacalix[*n*]arenes are a new family of macrocycles in which the bridging methylene ($–CH_2–$) bridge has been replaced by an -NR- group, and such systems have received even less attention.

Previously reported work includes the reaction of p-*tert*-butylthiacalix[4]areneH_4 with 2 equivalents of $TiCl_4$ which produced two dinuclear titanium(IV) complexes (Figure 1-24), which showed good performance for Mukaiyama–aldol reaction catalysis.[40] Redshaw and Limberg *et al*.[30, 35(c)] have prepared and structurally characterized a range of lithium and vanadium complexes derived from thiacalixarenes, the structures are shown in Figure 1-24. However, compared with thiacalixarene, there is a lack of coordination chemistry research involving oxacalixarenes and azacalixarenes. Redshaw *et al*. reported a vanadium oxacalixarene system based on oxo- or imidovanadium centers and supported by the hexahomotrioxacalix[3]arene ligand.[35(a)] Moreover, Redshaw extended the former study to lithium, niobium- and tantalum-based complexes bearing hexahomotrioxacalix[3]arenes and reported the synthesis, characterization and ethylene or cyclic ester polymerization behavior.[30, 37] Furthermore, Redshaw *et al*. reported ethyleneglycol tungsten complexes of the larger p-*tert*-butyltetrahomodioxacalix[6]areneH_6 via reaction with [W(1,2-ethanediolato)$_3$].[39(a)] The coordination chemistry of azacalixarenes is also scant. Thuéry *et*

al. synthesized a range of UO_2^{2+}, Nd^{3+}, and Yb^{3+} complexes derived from azacalixarenes and the afforded compounds were suitable for crystallographic characterization.[41] The molecular structures of typical complexes bearing oxacalixarene and azacalixarene ligand are shown in Figure 1-25.

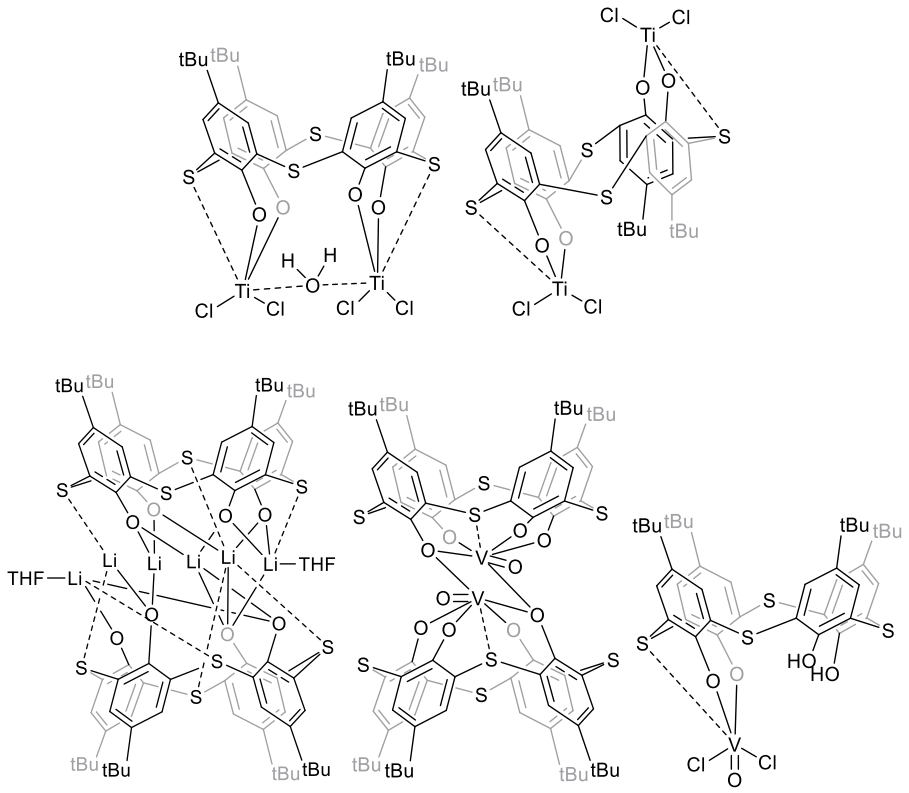

Figure 1-24. Molecular structures of typical complexes derived from thiacalix[4]arene.

Research has indicated that catalytic performance can be increased if the -CH_2- bridges are changed to potentially more reactive heteroatom-containing bridges.[10] Given this, the coordination systems based on heterocalixarenes ligands may lead a new catalytic system to rival the traditional metallocene technology.

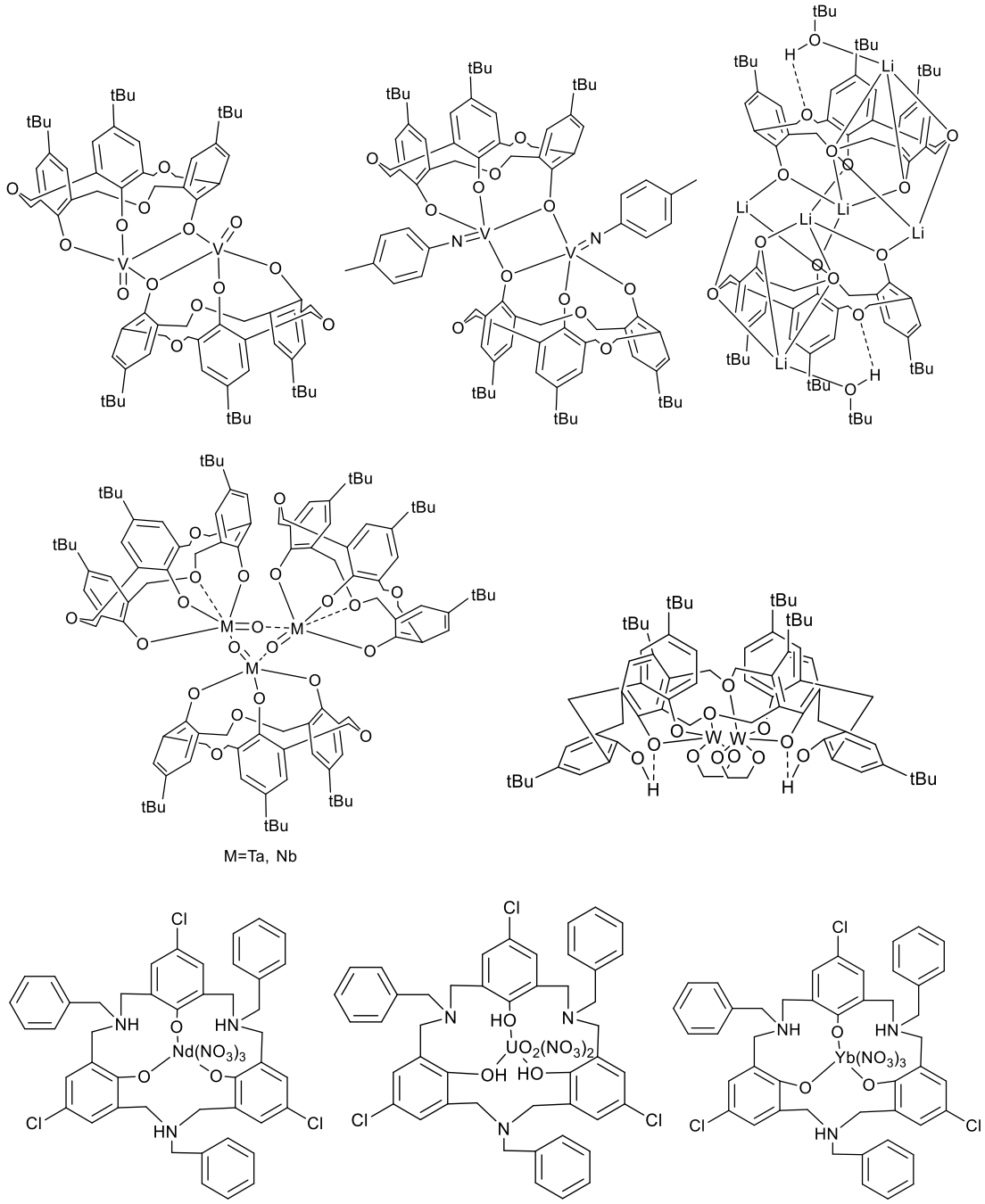

Figure 1-25. Molecular structures of typical complexes derived from oxacalixarenes and azacalixarenes.

2. Polymerization catalyzed by coordination compounds

In the 1950s, coordination polymerization, a new class of catalysis, emerged with the development of Ziegler–Natta catalysts, which are based on tetrachlorotitanium and an

organoaluminium co-catalyst. Ziegler–Natta catalysts exhibited superior activities for the synthesis of polyethylene or polypropene.[42] Over the past decades, numerous new coordination catalysts have been developed for the polymerization of different substrates, including dehydrogenative coupling of silanes of dihydro- and trihydrosilanes to polysilanes, propylene oxide polymerization, olefin polymerization and ring opening polymerization of cyclic esters.[10]

2.1 Ethylene polymerization

Polyolefin materials represented by polyethylene and polypropylene are common materials which are indispensable to our society. Polyethylene is the largest species used as a general purpose plastic, and the annual rate of demand for polyethylene continues to grow, typically up by 6.3 % in the last decade.[43] Since the 1970s, much effort had been devoted to supported Ziegler-Natta catalysts for olefin polymerization. The Ziegler-Natta catalyst, named from the discoverers K. Ziegler and G. Natta, exhibits excellent activities for polyolefin synthesis.[42] Generally, the main components of Ziegler–Natta catalysts are a transition metal complex and an organoaluminium co-catalyst, e.g. $TiCl_4$ + $Al(Et)_3$, $TiCl_3$ + $Al(Et)_2Cl$ (Figure 1-26).

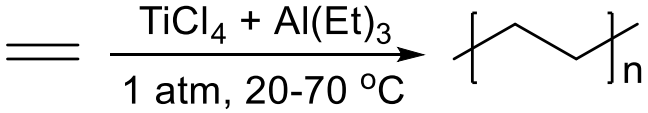

Figure 1-26. Ethylene polymerization catalyzed by the Ziegler-Natta catalytic system.

In 1980, Kaminksy *et al*. developed the metallocene catalytic system for olefin polymerization, which contained a group IV transition metal sandwich compound and with

methylaluminoxane (MAO) as co-catalyst.[44] Compared with the Ziegler-Natta catalytic system, the metallocene system is homogeneous and the catalyzed polymerization is able to afford purer and consistent polyolefin materials. Some of the typical metallocene catalysts are shown in Figure 1-27.

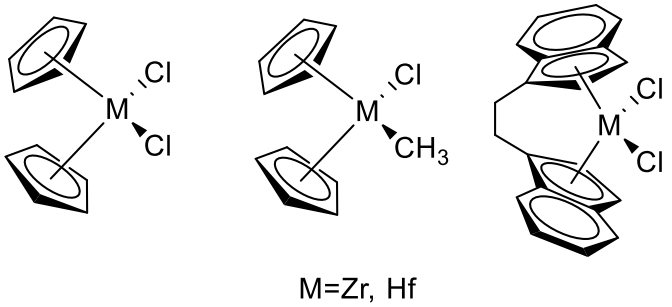

Figure 1-27. Typical metallocene pre-catalysts for olefin polymerization.

After the discovery of the metallocene catalytic system for olefin polymerization, McConville *et al*.[45] described titanium complexes with a bis(amide) ligand and their catalytic potential for olefin polymerization. Based on this work, a tremendous number of non-metallocene catalysts based on different ligands have been reported.[10, 46] Researchers found that ligand selection and modification for non-metallocene catalysts plays an important role in the catalytic performance and the control of dispersity or tacticity for the afforded polymer product.[46] Both metallocene catalyst and non-metallocene catalysts can follow a single site mechanism for olefin polymerization, and this means such systems can be controlled during the polymerization process. Despite the extensive research effort on metallocene catalysts and non-metallocene catalysts in recent decades, new progress on such catalytic systems can still be expected in the near future.

2.2 Ring opening polymerization of cyclic esters

Poly(ε-caprolactone) (PCL), poly(δ-valerolactone) (PVL) and polylactide (PLA) are

polymer plastics which possess biodegradability and biocompatibility. The raw materials to synthesize PCL, PVL and PLA can be obtained from corn, beets and other natural crops, and they eventually degrade into carbon dioxide and water. The raw materials of PCL, PVL and PLA are renewable resources while the traditional plastic was from petroleum, so there is less impact on the environment with these alternative polymers. There is now a big drive by industry to develop new "eco materials". In the 1930s, Carothers and coworkers[47] firstly synthesized PCL from ε-caprolactone via ring opening polymerization, and now the method of "Ring-opening Polymerization (ROP)" is an accepted way to prepare PCL, PVL and PLA (Figure 1-28). Currently, ring-opening polymerization has become a research hot topic, with emphasis on how to improve the mechanical properties of the polymer products and the synthesis of novel copolymers.

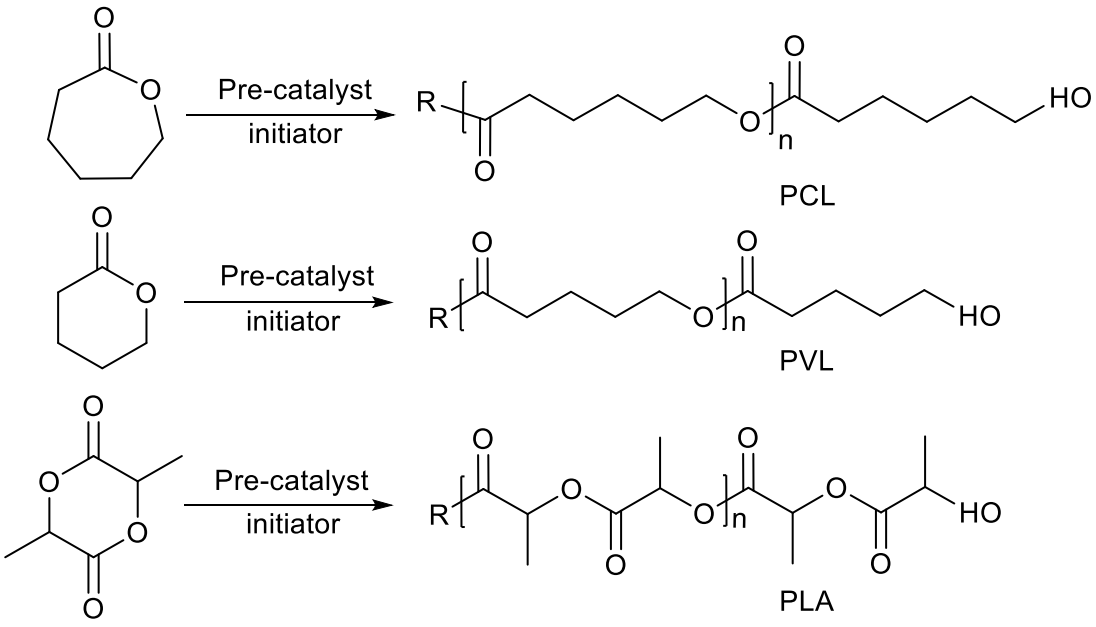

Figure 1-28. Ring opening polymerization of *rac*-lactide, ε-caprolactone and δ–valerolactone.

Furthermore, it is clear that the polylactone and polylactide polymer chains are terminated

by two functional groups, which are determined by the monomer, the catalyst or the initiator employed. The end group of the obtained polymer can be controlled via varying the catalyst and initiator, whilst also changing the properties of the polymer product.[48] Currently, use of an alcohol is the most common initiator for polymerization catalyzed by coordination complexes, which can link the metal center to create an alkoxide bond.

The ring opening polymerization catalyzed by coordination compounds normally follows the coordination-insertion mechanism.[49] For example, during the ring opening polymerization of ε-caprolactone, the monomer firstly coordinates to the metal center, and then the monomer will insert into the metal alkoxide bond via nucleophilic attack at the acyl-carbon atom, which will also lead to cleavage of the acyl-oxygen bond. After the ring opening of ε-caprolactone, the afforded polymer chain is linked to the metal by a coordination bond, which can help to continue the polymerization via insertion of another monomer into the metal alkoxide bond (Figure 1-29).

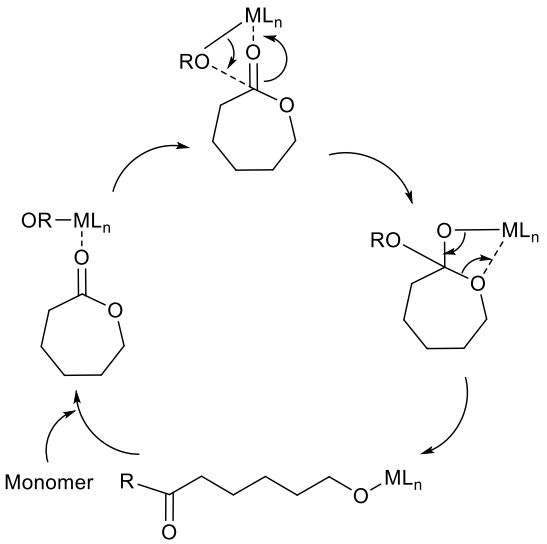

Figure 1-29. Proposed mechanism for the ring opening polymerization of ε-caprolactone.

2.3 Co-polymerization of propylene oxide and CO_2

Carbon dioxide is the main greenhouse gas, and is the most abundant resource for C1 chemicals. In 1969, Inoue *et al*. [50] firstly reported co-polymerization reaction of epoxides oxide and CO_2 by using a coordination compound. Over the past decades, using carbon dioxide and epoxide to produce biodegradable polycarbonate has become increasingly topical (Figure 1-30).[51] The current research situation highlights the main problems of carbon dioxide and epoxide copolymerization catalytic systems, which are low catalytic efficiency, high catalyst cost, harsh reaction conditions, low copolymer yield and complicated catalyst separation.

The generally accepted mechanism for the copolymerization of CO_2 and epoxides involves the alternate enchainment of CO_2 and the epoxide via insertion into either a metal alkoxide or carbonate bond (Figure 1-31). A growing polymer dissociates from an electron-rich metal center leading to the formation of cyclic carbonate and polycarbonates.

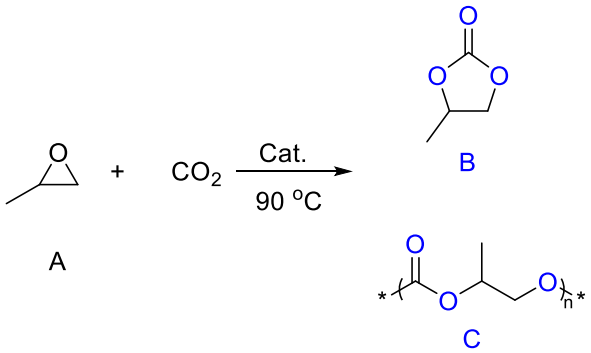

Figure 1-30. Co-polymerization reaction of propylene oxide and CO_2.

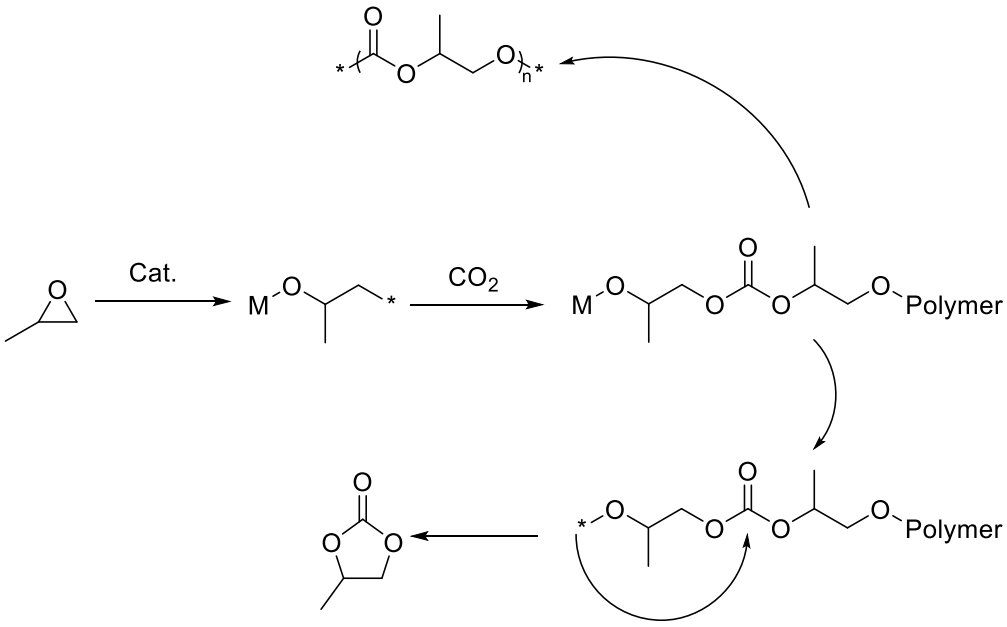

Figure 1-31. Proposed mechanism for the copolymerization of propylene oxide and CO_2.

2.4 Polymer characterization

Generally, each kind of polymer has its own structural characteristics, and there is a need to probe into their structure and find out their properties so as to understand this world of materials. Thereupon, we can have a clearer vision of how to synthesize polymeric materials, improve their performance and utilize them to a fuller extent.

2.4.1 ^{1}H and ^{13}C NMR spectroscopy

There are many analytical and spectroscopic methods used to study polymers, and nuclear magnetic resonance (NMR) is one of the most significant ways of analyzing the structure of a polymer material. ^{1}H and ^{13}C NMR spectroscopy are two kinds of common and useful methods for polymerization studies. They depend on different atoms in the process, and also have difference in the scope of application. ^{1}H NMR spectroscopy can be used to calculate the polymer conversion via assigning the characteristic group. Importantly, ^{1}H NMR spectroscopy plays an important role for analysis of polymer structure, for example

the branched chains and end groups of the molecular chain and isomers present can both be analyzed via ^{1}H NMR spectroscopy. Furthermore, ^{13}C NMR spectroscopy can also be used to determine the composition of a copolymer, and can also calculate the number-average sequence length for a polymer structure.

2.4.2 Homonuclear-decoupled NMR spectroscopy

For polylactide polymers, the stereo regularity of polymer molecular chains is an important parameter for polylactide conformation, which can be analyzed by homonuclear-decoupled ^{1}H NMR spectroscopy. For example, syndiotactic bias can be determined by 2D J-resolved ^{1}H NMR spectroscopy by investigating the methine area (5.13–5.20 ppm) of the spectrum. For *rac*-lactide, when *P*r = 0.5, the afforded PLA is an atactic polymer, and when *P*r = 0, an isotactic polymer.[52]

2.4.3 Gel Permeation Chromatography (GPC)

Gel permeation chromatography is a useful characterization technique for testing the molecular weight distribution of polymeric materials, and was invented by J. C. Moore in 1964.[53] The polymer sample is normally soluble in an organic solvent (e.g. THF or chloroform) and the afforded solution passes through a column of porous material to separate the polymers of different molecular weight. Based on the chromatographic separation theory, the detector of GPC will determinate elution volume to generate a chromatogram of polymer molecular weight distribution.

3. Thesis overview

This study focuses on the synthesis, structural and polymerization studies of a series of new pre-catalysts derived from calixarenes. A number of mono- or multi-nuclear pre-catalyst

systems have been synthesized and characterized, and their catalytic performance for polymerization has also been tested, including ring opening homo-/co-polymerization of ε-caprolactone, δ-valerolactone and *rac*-lactide, ethylene polymerization and co-polymerization of propylene oxide and CO_2.

In **Chapter 2**, the synthesis of oxo- and imidovanadium complexes derived from p-*tert*-butyltetrahomodioxacalix[6]areneH_6 are described, and the afforded compounds have been screened for their catalytic performance for ethylene polymerization and ring opening polymerization of ε-caprolactone and δ-valerolactone.

In the second study (**Chapter 3**), a range of transition metal (of groups IV and V) metallocalix[*n*]arenes have been synthesized and their catalytic ability for co-polymerization of propylene oxide and CO_2 investigated.

Chapter 4 mainly focuses on titanium complexes bearing oxa- and azacalix[4, 6]arenes. These complexes have been screened for their potential to act as pre-catalysts in the ring opening polymerization of ε-caprolactone (ε-CL), δ-valerolactone (δ-VL) and *rac*-lactide (*r*-LA).

Chapter 5 involves the synthesis of a range of lithiated calix[*n*]arenes (n = 6 or 8) bearing p-*tert*-butylcalix[6]areneH_6, *p-tert*-butylcalix[8]areneH_8 or de-butylated calix[8]areneH_8. The resulting pre-catalysts have all been screened for their catalytic performance for the ROP of ε-caprolactone (ε-CL), δ-valerolactone (δ-VL) and *rac*-lactide (*r*-LA).

The fifth piece of work (**Chapter 6)** mainly focuses on the synthesis of lead complexes derived from *p-tert*-butylcalix[4]areneH_4, *p-tert*-butyltetrahomodioxacalix[6]areneH_6, *p-tert*-butylcalix[6]areneH_6, or p-*tert*-butylcalix[8]areneH_8 ligands. These lead complexes

have been screened for their potential to act as pre-catalysts in the ring opening polymerization of ε-caprolactone (ε-CL), δ-valerolactone (δ-VL) and *rac*-lactide (*r*-LA).

Chapter 7 presents all the synthetic procedures, characterization data and polymerization methods used during this work.

3.1 Ligands used in this study

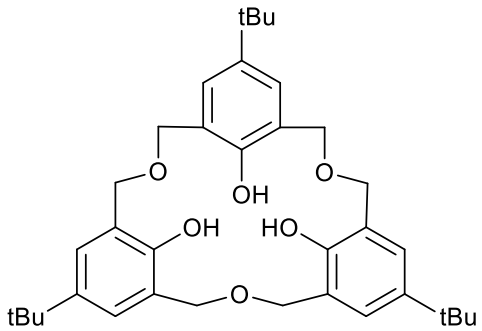

L^3H_3

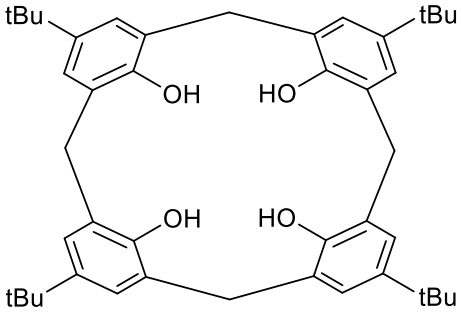

L^4H_4

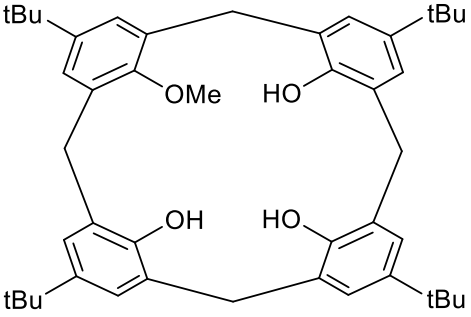

$L^4(Me)H_3$

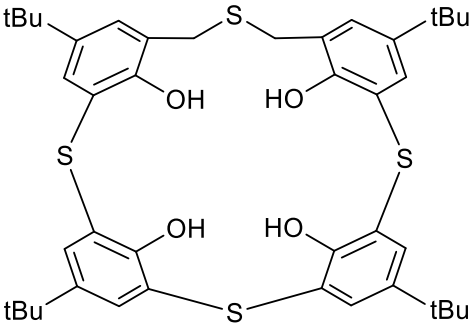

$L^{4S}H_4$

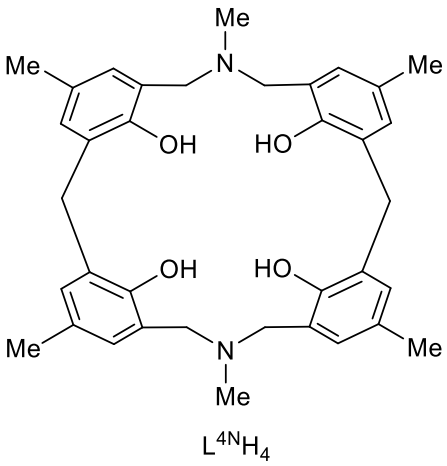

$L^{4N}H_4$

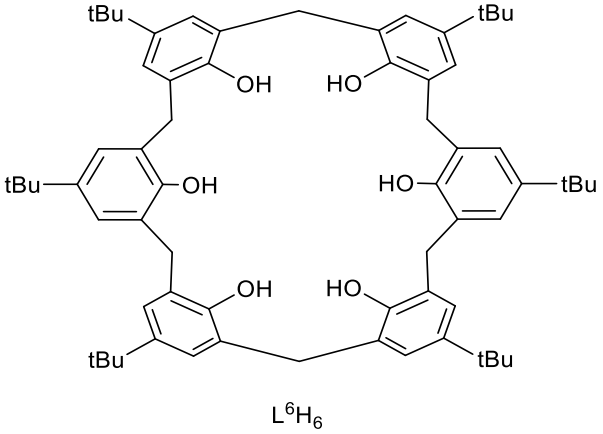

L^6H_6

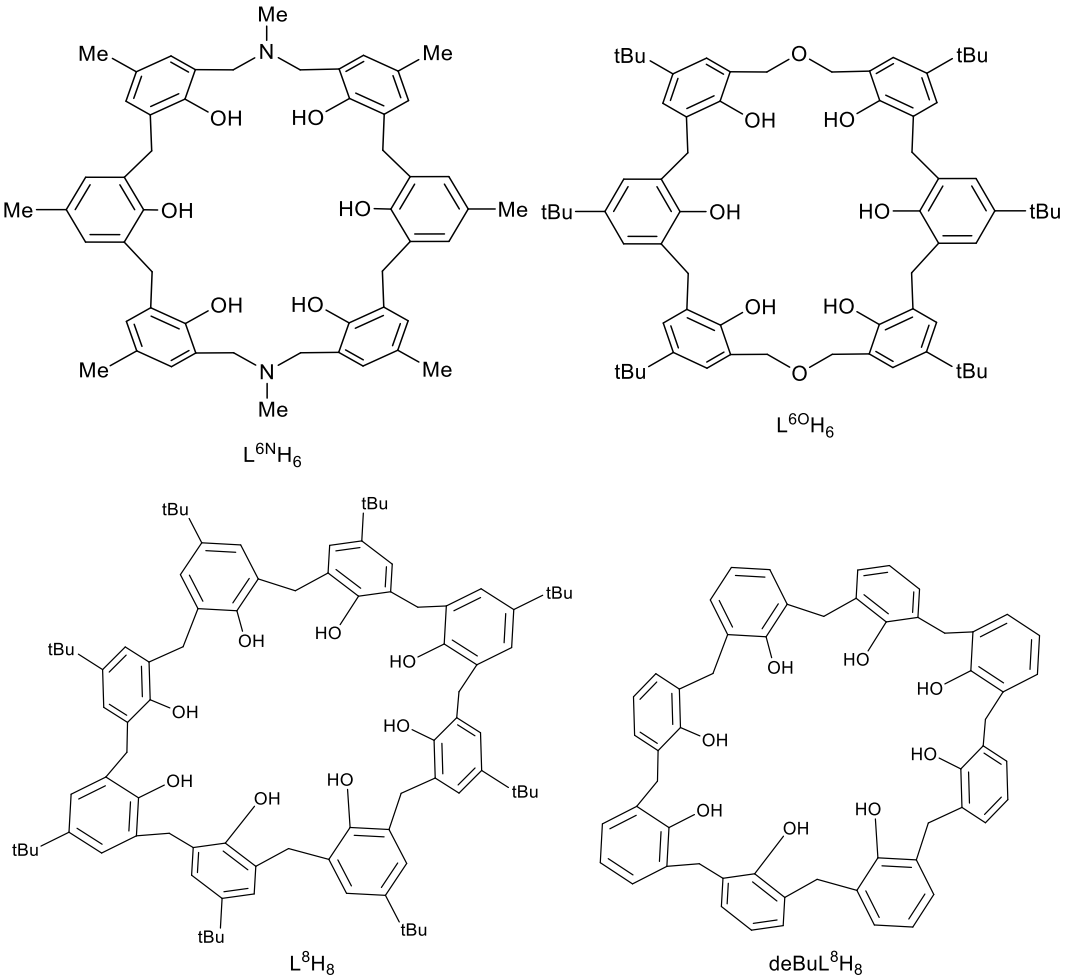

Figure 1-32. Ligands used in this study.

3.2 Complexes used in this study

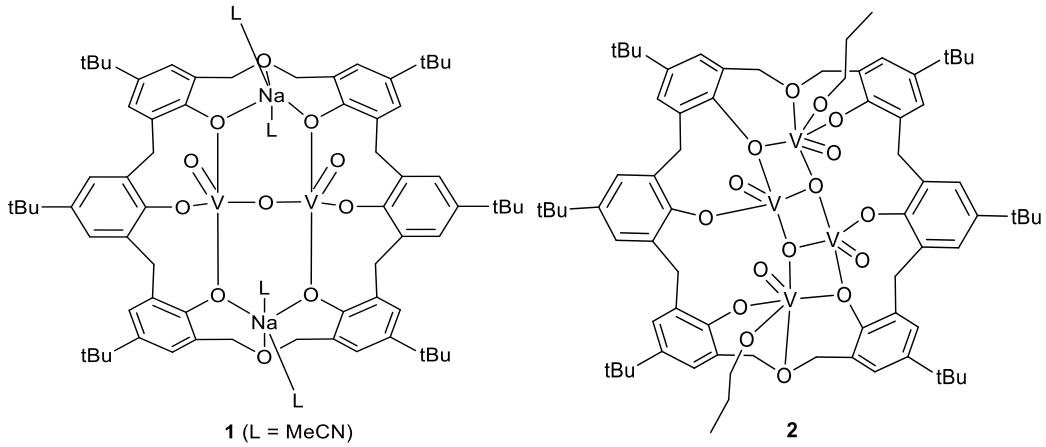

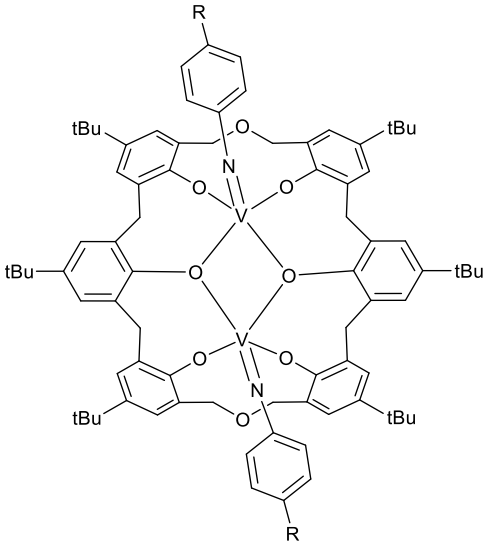

R=Me (**3**), OMe (**4**), CF_3 (**5**), Cl (**6**), F(**7**)

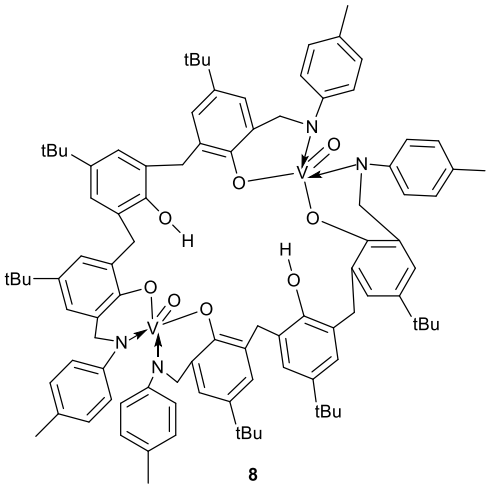

8

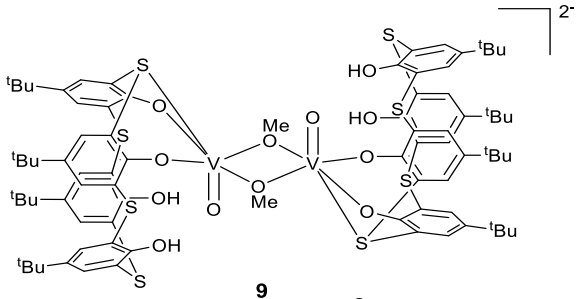

9

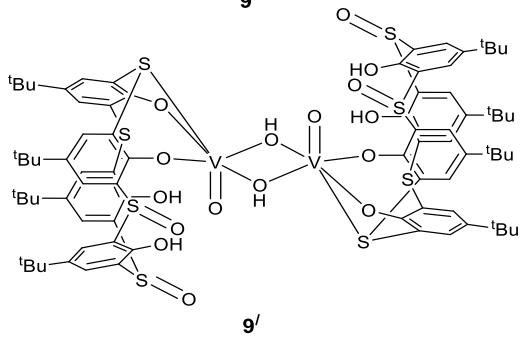

9′

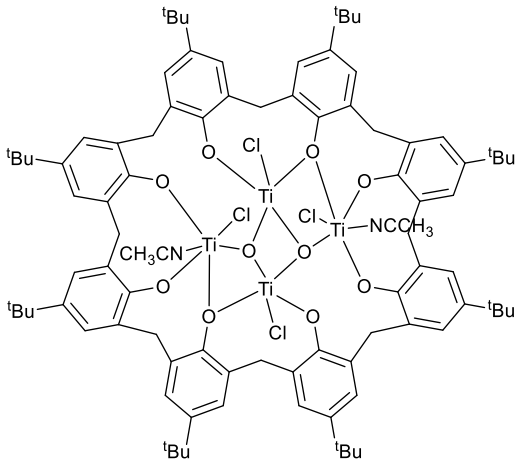

10

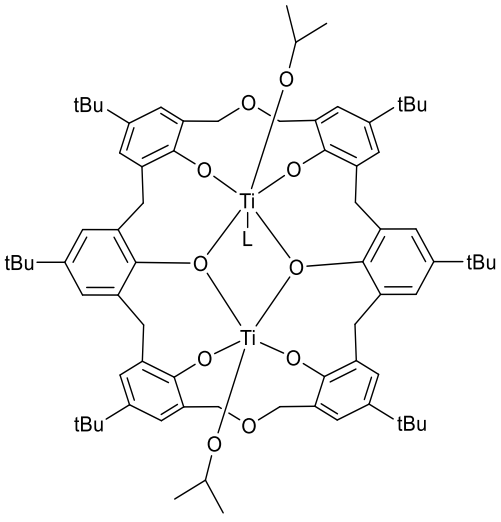

11 (L=MeCN)

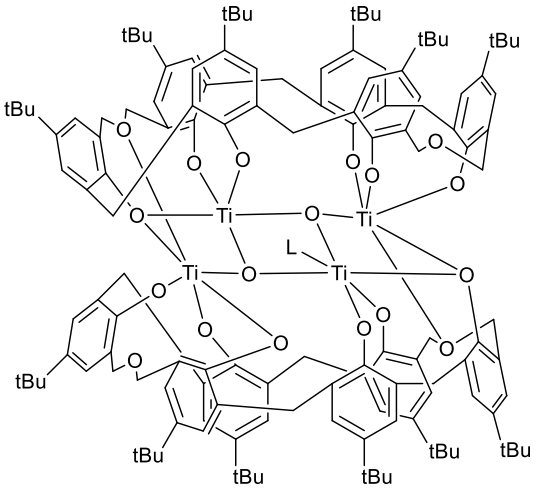

12 (L=H_2O)

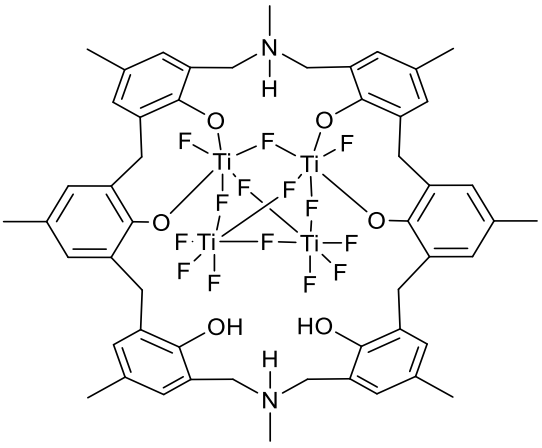

13

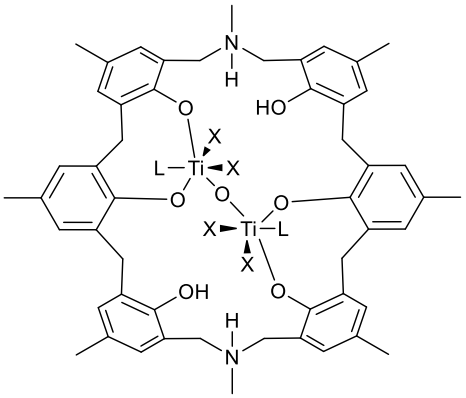

X=Cl
L=H_2O
14

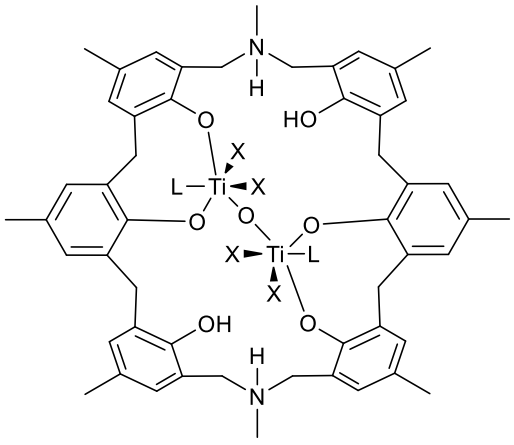

X=Br
L=H_2O
15

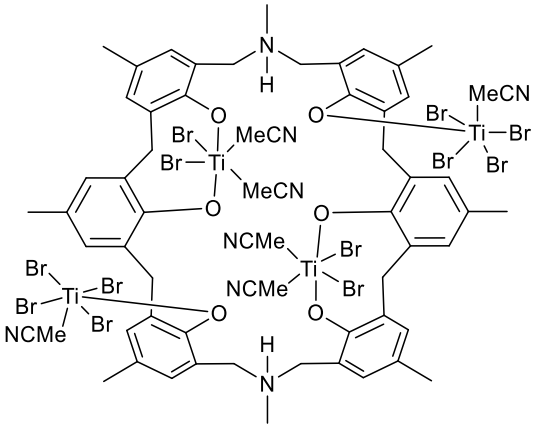

16

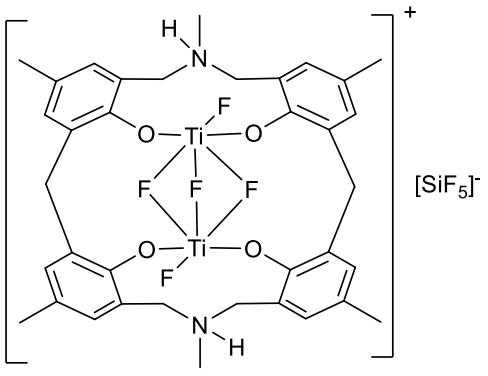

17

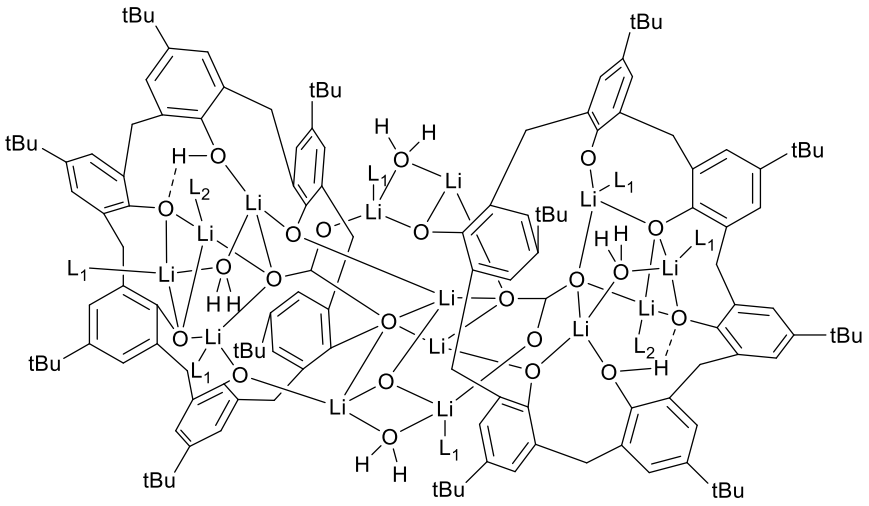

L_1=THF
L_2=H_2O

18

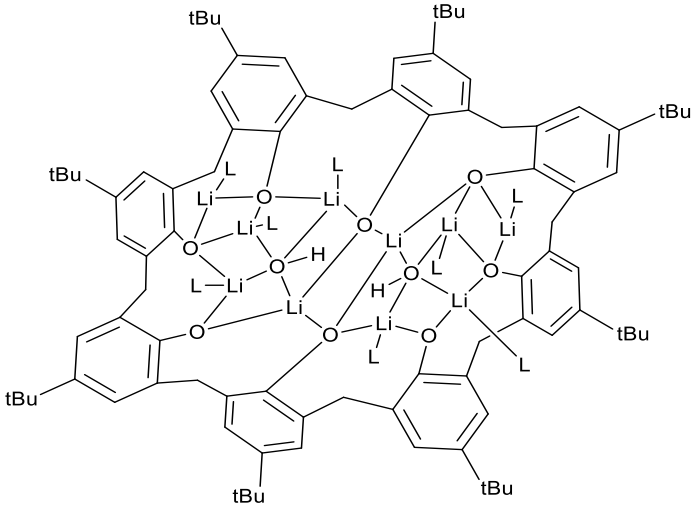

L=THF

19

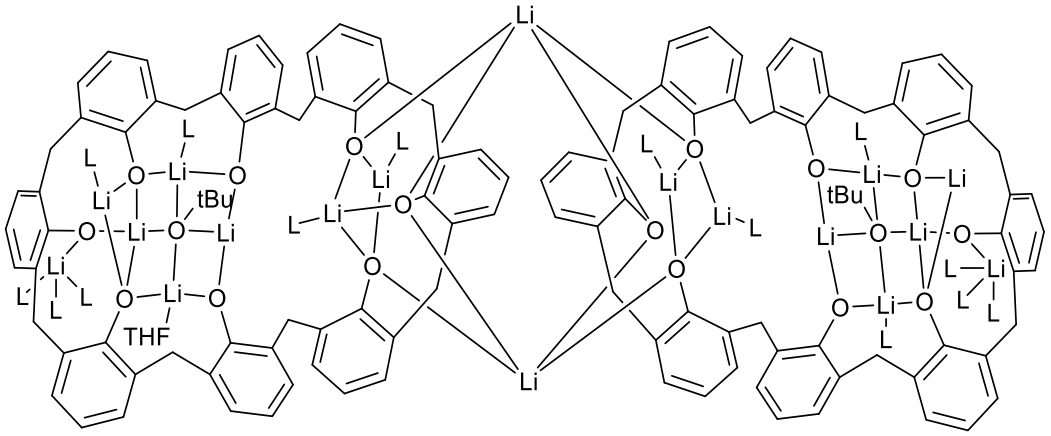

L=THF

20

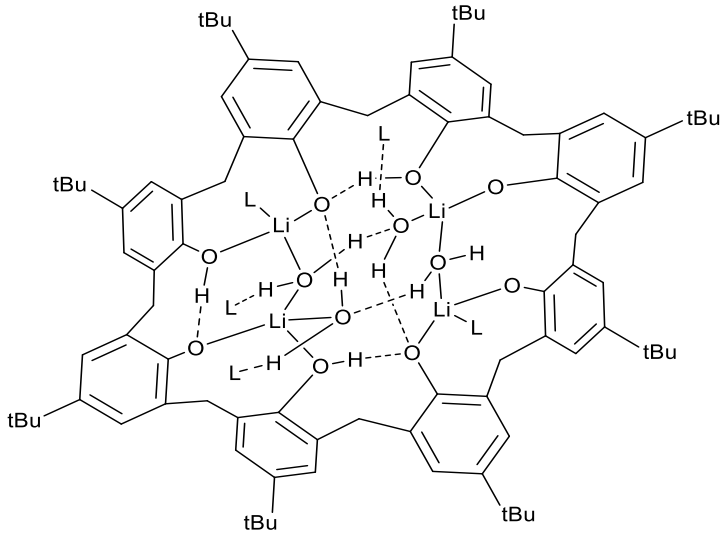

21

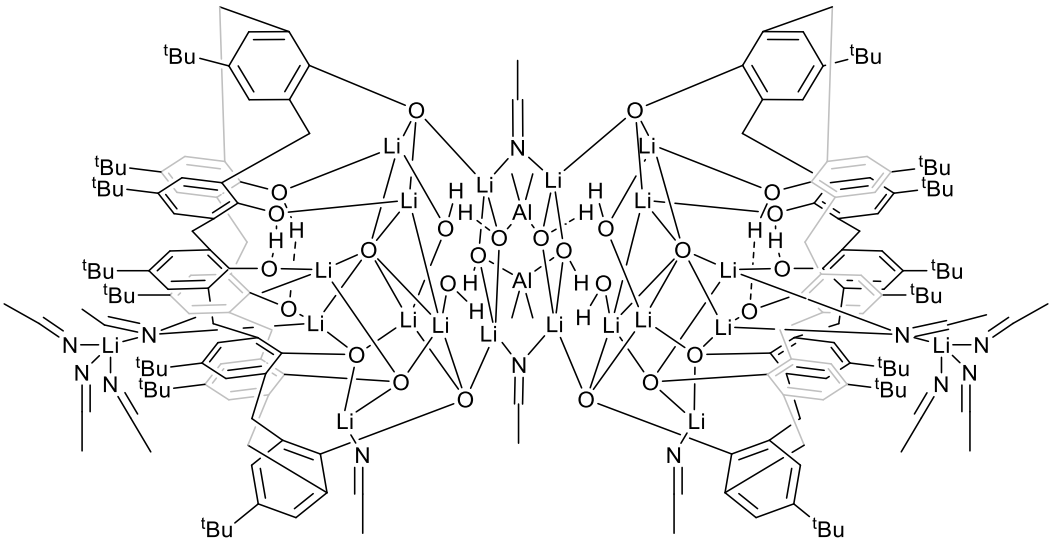

22

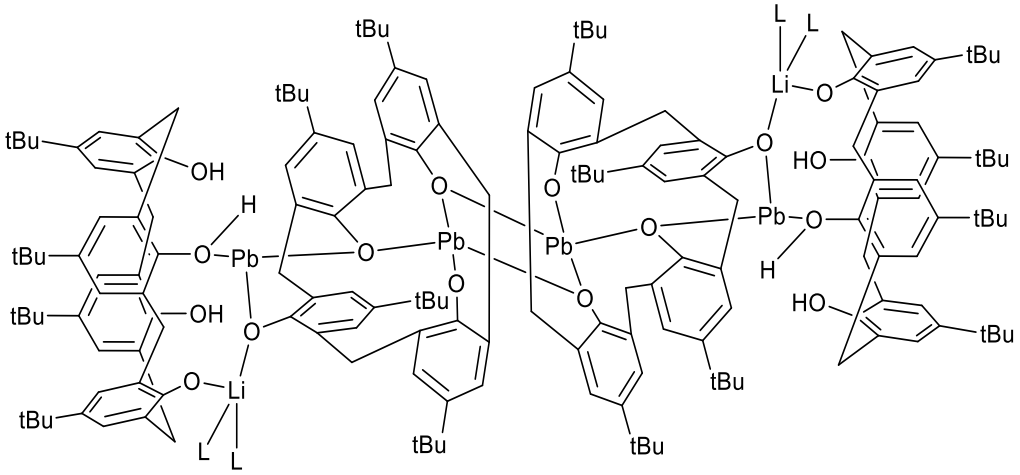

L=MeCN

23

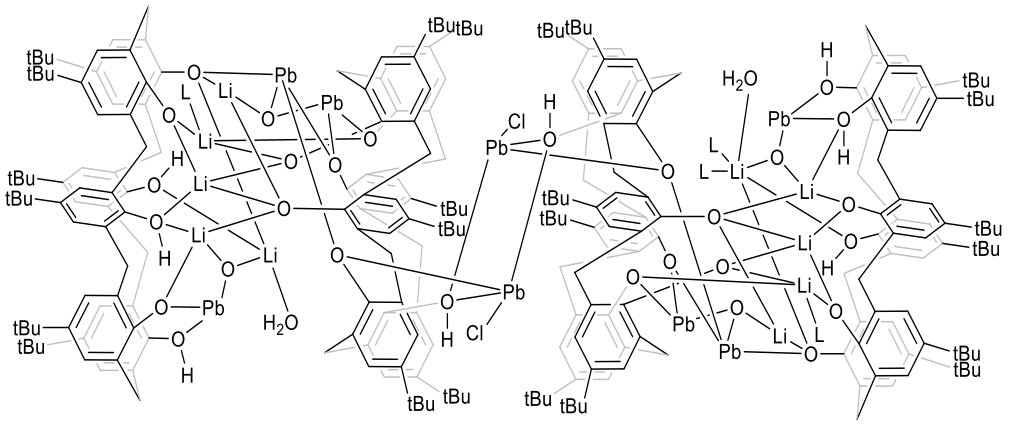

L=MeCN

24

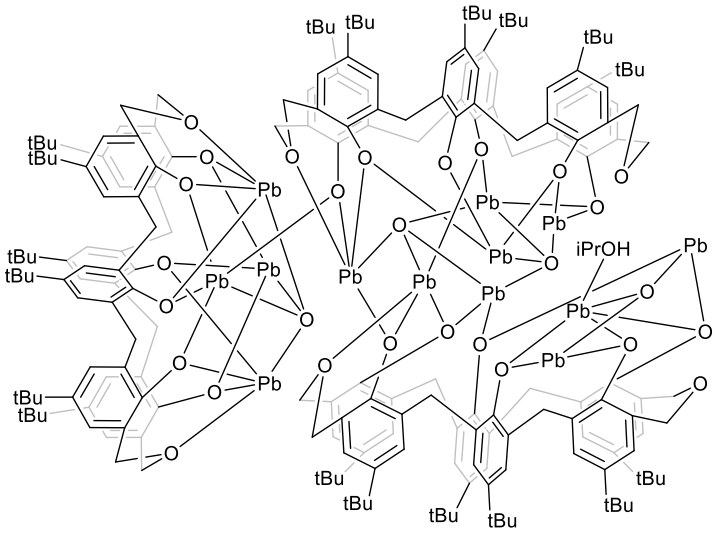

25

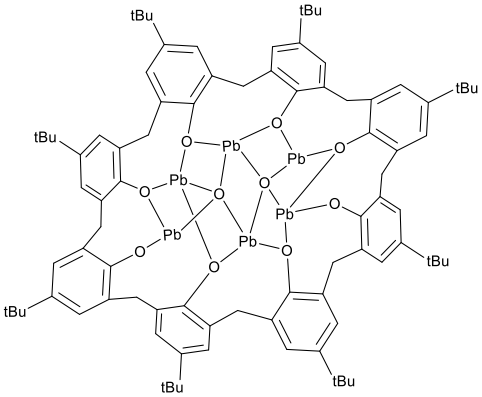

26

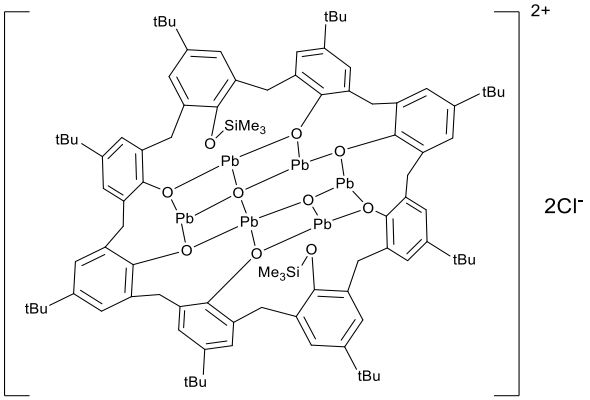

27

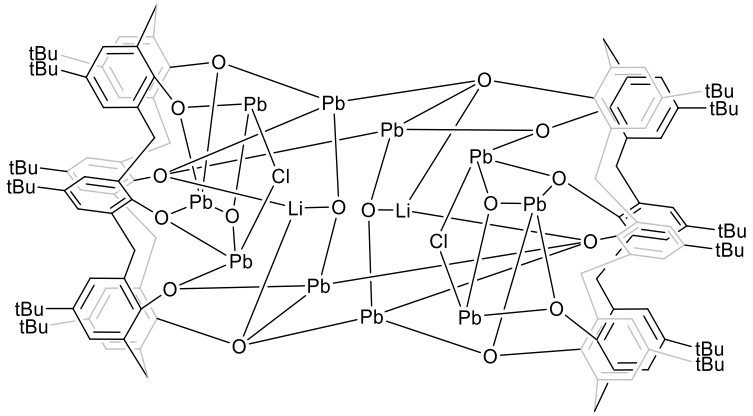

28

Figure 1-33. Complexes used in this study.

4. References

[1] (a) A. Zinke and E. Ziegler. *Chem Ber*, 1944, 77, 264-272; (b) J. Harrowfield, *Chem Commun*, 2013, 49, 16, 1578-1580; (c) P. M. S. Pulkkinen, J. Hassinen, R. H. A. Rasb and H. Tenhu, *RSC Adv.*, 2014, 4, 13453-13460. (d) P. Timmeman, W. Veiboom and D. N. Reithoudt, *Tetrahedron*, 1996, 52, 2663-2704.

[2] (a) C. D. Gutsche, B. Dhawan, K. H. No and R. Muthukrishnan, *J. Am. Chem. Soc*., 1981, 103, 3782-3792. (b) C. D. Gutsche, *Acc Chem Res*, 1983, 16, 161-170.

[3] Coordination Chemistry and Applications of Phenolic Calixarene–metal Complexes. Y. Li, K.-Q. Zhao, C. Redshaw, B. A. Martínez Ortega, A. Y. Nuñez, T. A. Hanna in Patai's Chemistry of Functional Groups, Wiley, 2014.

[4] (a) R Mlika, I. Dumazet, MGamoudi, RLamartine, H. Ben Ouada, N. Jaffrezic-Renault and G. Guillaud, *Anal. Chim. Acta*., 1997, 354, 283-289. (b) F. Vocanson, R. Lamartine, P. Lanteri, R. Longeray and J.Y. Gauvrit, *New J. Chem*. 1995, 19, 825-829. (c) D. R. Stewart and C. D. Gutsche, *J. Am. Chem. Soc*., 1999, 121, 4136-4146.

[5] D.M. Roundhill, *Compr. Coord. Chem. II*, 2004, 1, 485-490.

[6] B. T. Hayes and R. F. Hunter, *Chem. Ind*. 1956, 193.

[7] (a) V. Böhmer, P. Chhim and H. Kämmerer, *Makromol. Chem*. 1987, 180, 2503-2506. (b) V. Böhmer, F. Marschollek and I. Zetta, *J. Org. Chem*. 1987, 52, 3200-3205. (c) V. Böhmer, L. Merkel and U. Kunz, *J. Chem. Soc. Chem. Commun*. 1987, 896-897. (d) E. Paulus, V. Böhmer, H. Goldmann and W. Vogt, *J. Chem. Soc., Perkin Trans. 2*, 1987, 1609-1615.

[8] C. D. Gutsche, M. Iqbal and D. Stewart, *J. Org. Chem*., 1986, 51, 742-745.

[9] (a) K. Araki, N. Hashimoto and S. J. Shinkai, *Org. Chem*. 1993, 58, 5958-5963. (b) H. Matsumoto, S. Nishio, M. Takeshita and S. Shinkai, *Tetrahedron* 1995, 51, 4647–4654. (c) H. T. Sone, Y. Ohba, K. Moriya, H. Kumada and K. Ito, *Tetrahedron* 1997, 53, 10689–10698. (d) H. Kumagai, M. Hasegawa, S. Miyanari, Y. Sugawa, Y. Sato, T. Hori, S. Ueda, S. Kamiyama and S. Miyano, *Tetrahedron Lett*. 1997, 38, 3971–3972. (e) N. Shinmyozu, N. Shibakawa, K. Sugimoto, H. Sakane, H. Takemura, K. Sako and T. Inazu, *Synthesis*, 1993, 1257–1260. (f) H. Takemura, N. Shinmyozu, H. Miura, I. U. Khan and T. J. Inazu, *Inclusion Phenom*. 1994, 19, 193–206. (g) P. D. Hampton, W. D. Tong, S. Wu and E. N. J. Duesler, *Chem. Soc., Perkin Trans*. 1996, 1127–1130. (h) P. Chirakul, P. D. Hampton and E. N. Duesler, *Tetrahedron Lett*. 1998, 39, 5473–5476. (i) M. J. Grannas, B. F. Hoskins and R. Robson, *Inorg. Chem*. 1994, 33, 1071–1079. (j) C. Redshaw, L. Clowes, D. L. Hughes, M. R. J. Elsegood and T. Yamato, *Organometallics,* 2011*,* 30, 21, 5620-5624.

[10] D. M. Homden and C. Redshaw, *Chem. Rev.*, 2008, 108, 5086–5130.

[11] N. Sommer and H. A. Staab, *Tetrahedron Lett*., 1966, 7, 2837-2841.

[12] P. A. Lehmann, *Tetrahedron*. 1974, 30, 727–733.

[13] E. E. Gilbert, *J. Heterocycl. Chem*. 1974, 11, 899–904.

[14] R. Hudson, J. L. Katz, Oxacalixarenes. In: Neri P., Sessler J., Wang MX. (eds) Calixarenes and Beyond, Springer, 2016, 399-420.

[15] B. Dhawan and C. D. Gutsche, *J. Org. Chem*., 1983, 48, 1536-1539.

[16] B. Masci, *J. Org. Chem.* 2001, 66, 1497–1499.

[17] G. W. Smith, *Nature* 1963, 198, 879.

[18] A. Ito, Y. Ono and K. Tanaka, *J. Org. Chem.* 1999, 64, 8236-8241

[19] (a) H. Tsue, K. Ishibashi, H. Takahashi and R. Tamura, *Org. Lett*. 2005, 7, 2165–2168. (b) K. Ishibashi, H. Tsue, S. Tokita, K. Matsui, H. Takahashi, and R. Tamura, *Org. Lett*., 2006, 8, 5991–5994.

[20] (a) H. Takemura, *J. Inclusion Phenom. Macrocyclic Chem*., 2002, 42, 169–186. (b) H. Takemura, K. Tani, H. Miura, G. Wen, T. Shinmyozu and T. Inazu, *Supramol. Chem*., 1999, 11, 83–91. (c) H. Takemura, Y. Kozima and T. Inazu, *Tetrahedron Lett*. 1999, 40, 6431–6434. (d) H. Takemura, T. Shinmyozu and T. Inazu, *Coord. Chem. Rev*. 1996, 156, 183–200. (e) H. Takemura, T. Shinmyozu, H. Miura, I. U. Khan and T. Inazu, *J. Inclusion Phenom*. 1994, 19, 193–206. (f) I. U. Khan, H. Takemura, M. Suenaga, T. Shinmyozu and T. Inazu, *J. Org. Chem*. 1993, 58, 3158–3161. (g) H. Takemura, K. Yoshimura, I. U. Khan, T. Shinmyozu and T. Inazu, *Tetrahedron Lett*. 1992, 33, 5775–5778.

[21] H. Takemura, A. Takahashi, H. Suga, M. Fukuda and T. Iwanaga, *Eur. J. Org. Chem*., 2011, 3171–3177.

[22] T. Sone, Y. Ohba, K. Moriya, H. Kumada and K. Ito, *Tetrahedron*, 1997, 53, 10689–10698.

[23] H. Kumagai, M. Hasegawa, S. Miyanari, Y. Sugawa, Y. Sato, T. Hori, S. Ueda, H. Kamiyama and S. Miyano, *Tetrahedron Lett*., 1997, 38, 3971–3972.

[24] (a) N. Iki and S. Miyano, *J. Inclusion Phenom. Macrocyclic Chem*., 2001, 41, 99–105. (b) P. Lhoták, *Eur. J. Org. Chem*., 2004, 8, 1675–1692. (c) N. Morohashi, F. Narumi, N. Iki, T. Hattori and S. Miyano, *Chem. Rev*. 2006, 106, 5291–5316. (d) N. Iki, *J. Inclusion Phenom. Macrocyclic Chem*. 2009, 64, 1–13. (e) N. Iki, *Supramol. Chem*., 2011, 23, 160–168. (f) R. Kumar, Y. O. Lee, V. Bhalla, M. Kumar and J. S. Kim*, Chem. Soc. Rev*. 2014, 43, 4824–4870.

[25] N. Iki, Thiacalixarenes. In: Neri P., Sessler J., Wang MX. (eds) Calixarenes and Beyond. Springer, 2016, 335-362.

[26] Coordination Chemistry and Applications of Phenolic Calixarene–metal Complexes, Y. Li, K.-Q. Zhao, C. Redshaw, B. A. M. Ortega, A. Y. Nuñez and T. A. Hanna in Patai's Chemistry of Functional Groups, 2014, Wiley.

[27] (a) N. S. Venkataramanan, R. Sahara, H. Mizuseki and Y. Kawazoe, *J. Phys. Chem.*, 2008, 112C, 19676–19679. (b) H. Li, Y. Chen, D. Tian and Z. Gao, *J. Memb. Sci.*, 2008, 310, 431–437.

[28] H. Bock, A. John, C. Nather and Z. Havlas, *J. Am. Chem. Soc*., 1995, 117, 9367-9368.

[29] T. A. Hanna, L. Liu, A. M. Angeles-Boza , X. Kou , C. D. Gutsche , K. Ejsmont, W. H. Watson, L. N. Zakharov, C. D. Incarvito and A. L. Rheingold, *J. Am. Chem. Soc*., 2003, 125 , 6228-6238.

[30] O. Santoro, M. R. J. Elsegood, S. J. Teat, T. Yamato and C. Redshaw, *RSC Adv*., 2021, 11, 11304-11317.

[31] P. Thuery, Z. Asfari, J. Vicens, V. Lamare and J.-F. Dozol, *Polyhedron*, 2002, 21, 2497–2503.

[32] M. M. Olmstead, G. Sigel, H. Hope, X. Xu and P. P. Power, *J. Am. Chem. Soc*. 1985, 107, 8087–8091.

[33] (a) J. Espinas, U. Darbost, J. Pelletier, E. Jeanneau, C. Duchamp, F. Bayard, O. Boyron, J.-P. Broyer, J. Thivolle-Cazat, J.-M. Basset, M. Taoufik and I. Bonnamour, *Eur. J. Inorg. Chem.*, 2010, 1349–1359; (b) Z. Sun, Y. Zhao, O. Santoro, M. R. J. Elsegood, E. V. Bedwell, K. Zahra, A. Walton and C. Redshaw, *Catal. Sci. Technol*., 2020, 10, 1619-1639.

[34] O. Santoro, M. R. J. Elsegood, E. V. Bedwell, J. A. Pryce and C. Redshaw, *Dalton Trans*., 2020, 49, 11978-11996.

[35] (a) C. Redshaw, M. A. Rowan, L. Warford, D. M. Homden, A. Arbaoui, M. R. J. Elsegood, S. H. Dale, T. Yamato, C. P. Casas, S. Matsui and S. Matsuura, *Chem. Eur. J*., 2007, 13, 1090 – 1107. (b) L. Clowes, C. Redshaw, D. L. Hughes, *Inorg. Chem*., 2011, 50, 16, 7838–7845. (c) E. Hoppe and C. Limberg, *Chem. Eur. J*., 2007, 13, 7006 – 7016. (d) E. Hoppe, C. Limberg and B. Ziemer, *Inorg. Chem*., 2006, 45, 8308−8317. (e) E. Hoppe, C. Limberg, B. Ziemer and C. Mugge, *J. Mol. Catal. A: Chem*., 2006, 251, 34–40.

[36] C. Redshaw, M. Walton, K. Michiue, Y. Chao, A. Walton, P. Elo, V. Sumerin, C. Jiang and M. R. J. Elsegood, *Dalton Trans*., 2015, 44, 12292-12303.

[37] C. Redshaw, M. Rowan, D. M. Homden, M. R. J. Elsegood, T. Yamato and C. Pérez-Casas, *Chem. Eur. J.,* 2007, 13, 10129 – 10139.

[38] C. Z. Huang, J. Ahn, S. Kwon, J. Kim, J. Lee, Y. H. Han and H. Kim, *Appl. Catal. A*, 2004, 258, 173–181.

[39] (a) V. C. Gibson, C. Redshaw and M. R. J. Elsegood, *Chem. Commun*., 2002, 1200-1201. (b) Y. Li, K.-Q. Zhao, C. Feng, M. R. J. Elsegood, T. J. Prior, Xi. Sun and C. Redshaw, *Dalton Trans*., 2014, 43, 13612-13619. (c) Z. Sun, Y. Zhao, T J. Prior, M R. J. Elsegood, K. Wang, T. Xing and C. Redshaw, *Dalton Trans*., 2019, 48, 1454-1466.

[40] N. Morohashi, T. Hattori, K. Yokomakura, C. Kabuto and S. Miyano, *Tetrahedron Lett*. 2002, 43, 7769–7772.

[41] (a) P. Thuéry, M. Nierlich, J. Vicens and H. Takemura, *J. Chem. Soc. Dalton Trans*., 2000, 3, 279-283. (b) P. Thuéry, M. Nierlich, J. Vicens, B. Masci and H. Takemura, *Eur. J. Inorg. Chem*., 2001, 3, 637-643. (c) P. Thuéry, M. Nierlich, J. Vicens and H. Takemura, *Polyhedron*, 2000, 19, 2673-2678.

[42] (a) K. Soga and T. Shiono, *Prog. Polym. Sci*., 1997, 22, 1503-1546. (b) J. Huang and G. L. Rempel, *Prog. Polym. Sci*., 1995, 20, 459-526. (c) J. P. Claverie and F. Schaper, *MRS Bulletin*, 2013, 38, 213–218.

[43] Handbook of polyolefins. Synthesis and properties. C. Vasile, R. B. Seymour (eds.) Marcel Dekker Inc. New York, 1993, 1091.

[44] (a) W. Kaminsky, *J. Chem. Soc., Dalton Trans*., 1998, 9, 1413-1418. (b) H. Sinn, W. Kaminsky, H. J. Vollmer and R. Woldt, *Angew. Chem*., 1980, 92, 396-402. (c) W. Kaminsky, *Macromol, Chem. Phys*., 1996, 197, 3907-3945.

[45] (a) J. D. Scollard and D. H. McConville, *J. Am. Chem. Soc*., 1996, 118, 10008–10009. (b) J. D. Scollard, D. H. McConville, N. C. Payne and J. J. Vittal, *Macromolecules*, 1996, 29, 5241–5243.

[46] K. Nomura, W. Zhang, Olefin Polymerization with Non-metallocene Catalysts (Early

Transition Metals). In: Osakada K. (eds) Organometallic Reactions and Polymerization. Lecture Notes in Chemistry, vol 85. Springer, Berlin, Heidelberg, 2014.

[47] F. J. Van Natta, J. W. Hill and W. H. Carruthers, *J. Am. Chem. Soc*. 1934, 56, 455-459.

[48] C. K. Williams, *Chem. Soc. Rev*., 2007, 36, 1573-1580.

[49] (a) A. Löfgren, A.-C. Albertsson, P. Dubois, R. Jérôme and J. Macromol. *Sci. Rev. Macromol. Chem. Phys*., 1995, 35, 379-418. (b) D. Mecerreyes, R. Jérôme and P. Dubois, *Adv. Polym. Sci*., 1999, 147, 1-59.

[50] S. Inoue, H. Koinuma and T. Tsuruta, *Polym. Sci., Part B: Polym Lett*, 1969, 7, 287-292.

[51] (a) E. J. Beckman, *Science*, 1999, 283, 946–947. (b) G. W. Coates and D. R. Moore, *Angew. Chem. Int. Ed*., 2004, 43, 6618–6639. (c) M. R. Kember, A. Buchard and C. K. Williams, *Chem. Commun*., 2011, 47, 141–163.

[52] (a) C. Ludwig and M. R. Viant, *Phytochem. Anal*., 2010, 21, 22–32; (b) M. J. Walton, S. J. Lancaster and C. Redshaw, *ChemCatChem*, 2014, 6, 1892–1898.

[53] J. C. Moore, *J. Polym. Sci*., 1964, 2, 835-843.

Chapter 2

Vanadium pre-catalysts derived from oxacalix[6]arenes: structural studies and use in the ring opening homo-/co-polymerization of ε-caprolactone/δ-valerolactone and ethylene polymerization

1. Introduction

The recent COVID19 outbreak is a good illustration of our dependence on plastics, where there was widespread demand for the use of plastic-based facemasks.[1] In the meanwhile, the need for new environmentally friendly plastics has been highlighted by on-going global pollution issues, however traditional plastics, when used and disposed of correctly, still have a large part to play in society. Metal catalysts play a central role in the production of both petroleum-based plastics (α-olefin polymerization) and biodegradable polymers formed via the ring opening polymerization (ROP) of cyclic esters.[2] For these two processes, manipulation of the catalyst properties can be achieved by variation of the metal-bound groups, and this allows for control over both catalytic activity and polymer properties. More importantly, the catalytic metal centre should be cheap and non-toxic. Given this, a number of earth-abundant metals have been employed as the reactive metal centre in both polymerization processes.[1,3] Moreover, results using vanadium-based systems indicate this metal also has potential in this area,[4] and it is noteworthy that reports on the effect of imido ligand variation in vanadium-based systems have appeared for studies on oligo-/polymerization of ethylene, ethylene/propylene copolymerization and ethylene/cyclic olefin copolymerization.[5] The ligands in the pre-catalyst can take a number of forms, selected in-part for their ability to impose some stability to the catalytically active species. In α-olefin polymerization, an external alkylating co-catalyst is typically employed to form a metal-alkyl [M-R] species, whilst in ROP, the generation of metal alkoxide [M-OR] species is favoured. Calix[*n*]arenes, which are phenolic macrocycles, have shown potential in a variety of catalytic applications.[6] By variation of

n, the number of phenolic groups, calix[*n*]arenes can act as platforms for binding multiple metal centres.[7] Based on the previous work in our group, a series of vanadium-based calix[*n*]arene complexes were structurally identified, and by changing the calixarene bridging group from a methylene (-CH_2-) to a dimethyleneoxa group (-CH_2OCH_2-), vanadium complexes with superior catalytic performance for both α-olefin homo- and co-polymerization over related methylene-bridged systems were obtained.[8] These vanadium studies previously focused on oxacalix[3]arene derivatives, however larger oxacalix[*n*]arenes are known.[9] In the current study, my research work investigate the use of the p-*tert*-butyltetrahomodioxacalix[6]areneH_6-derived systems (Chart 2-1) in both the ROP of the cyclic esters ε-caprolactone and *δ*-valerolactone, and the copolymerization thereof, and for the polymerization of ethylene. Results are compared *versus* known vanadium catalysts bearing either p-*tert*-butylhexahomotrioxacalix[3]areneH_3 or p-*tert*-butylcalix[6 and 8]arene$H_{6,8}$-derived ligands (Chart 2-2).[7,8,10] It is obvious that poly(*ε*-caprolactone) (PCL), and poly(*δ*-valerolactone) (PVL) are favoured polymers given their biodegradability and the fact that they are considered as potential environmentally friendly commodity plastics.[11]

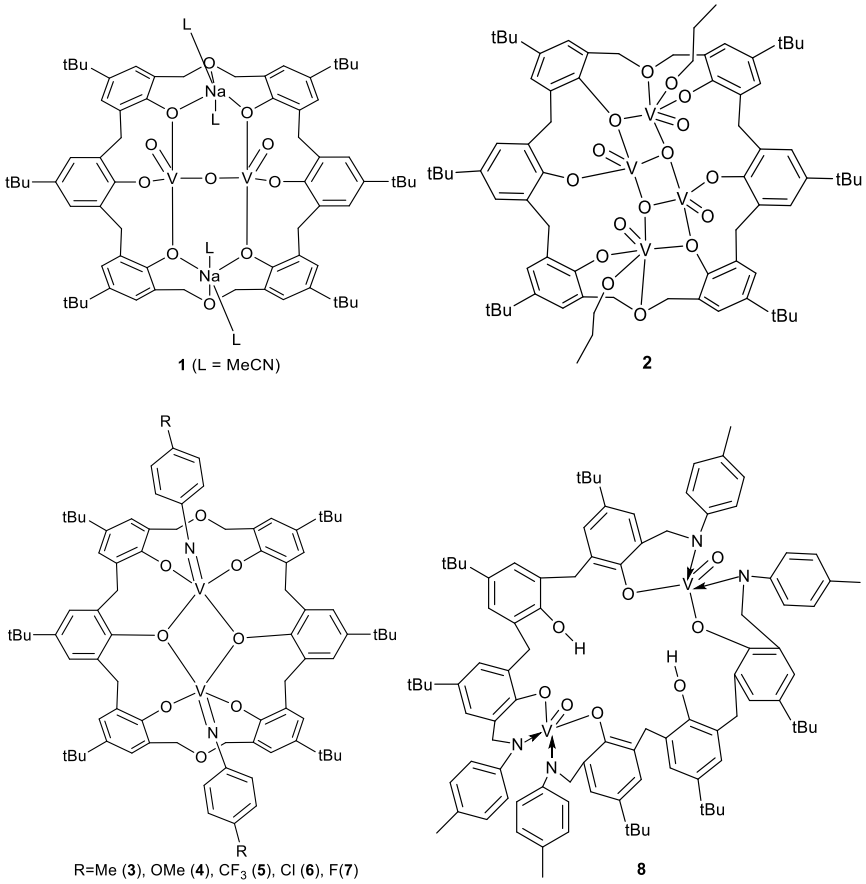

Chart 2-1. The pre-catalysts **1** – **8** prepared herein.

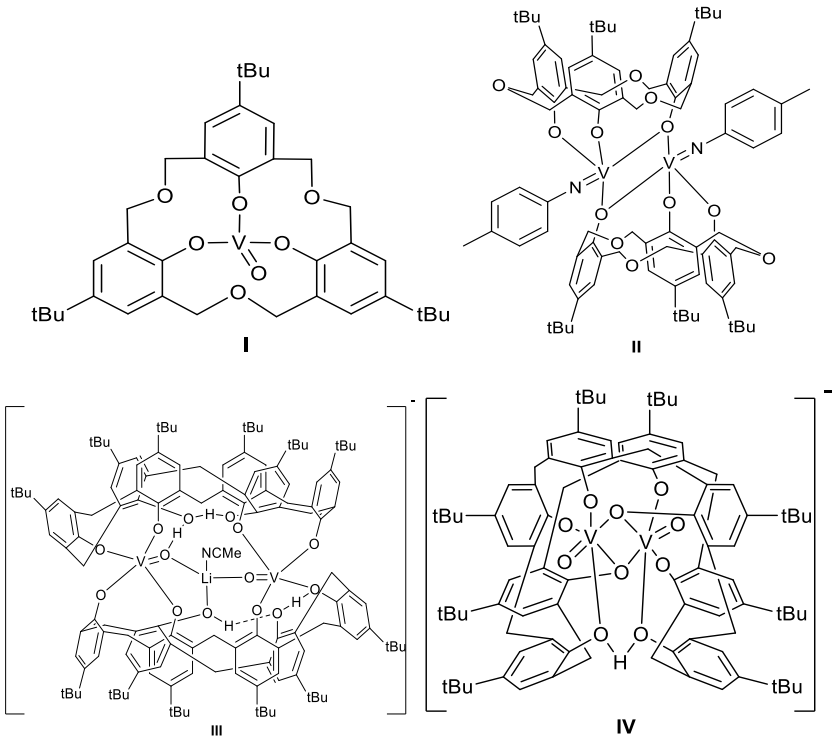

Chart 2-2. Known pre-catalysts **I** – **IV** used herein.[7,8,10]

2. Results and Discussion

2.1 Syntheses and solid-state structures

2.1.1 Oxo complexes

The heterobimetallic vanadium(V)/alkali metal reagent [NaVO(O*t*Bu)$_4$], was synthesised by an adaptation of a procedure described by Wilkinson and co-workers,[12] whereby [VOCl$_3$] and four equivalents of NaO*t*Bu were stirred in diethylether (or THF) at −78 °C for 12 h. *In-situ* reaction of this vanadyl salt (two equivalents) with p-*tert*-butyltetrahomodioxacalix[6]areneH$_6$, L^{6O}H$_6$ afforded, following work up (acetonitrile) and standing at 0 ºC, dark green blocks, which proved suitable for single crystal X-ray diffraction. The complex was found to be [(VO)$_2$(μ-O)Na$_2$(L^{6O})(MeCN)$_4$]·5(MeCN) (**1**·5MeCN), and the molecular structure of **1**·5MeCN is shown in Figure 2-1, with selected bond lengths and angles given in the caption. The complex contains two trigonal bipyramidal vanadyl centres, for which the V=O5 bond length is typical at 1.588(3) Å,[10] linked via near linear (171.8(2)^o) V–O11–V bonding. Each vanadium is further coordinated by three phenoxide oxygens of the oxacalix[6]arene, with longer bonding (*ca*. 1.95 Å) observed to each of the bridging calixarene oxygens (O2 and O8) which are also involved in bonding to a 5-coordinate sodium cation, with the latter (Na1 and Na2) each bonding to two of the phenoxide oxygens and the oxygen of the dimethyleneoxa bridge. Two acetonitrile ligands complete the bonding at each sodium centre.

Reaction of [VO(O*n*Pr)$_3$] (4 equivalents) with L^{6O}H$_6$ led, after work-up, to the blue complex {[VO]$_4$L^1}·6MeCN (**2**·6MeCN). The molecular structure is shown in Figure 2-2, with selected bond lengths and angles given in the caption. The calixarene binds four vanadyl

centres, the latter forming a 3-step V_4O_4 ladder. Such ladders have been observed previously in titanium calixarene chemistry.[13]

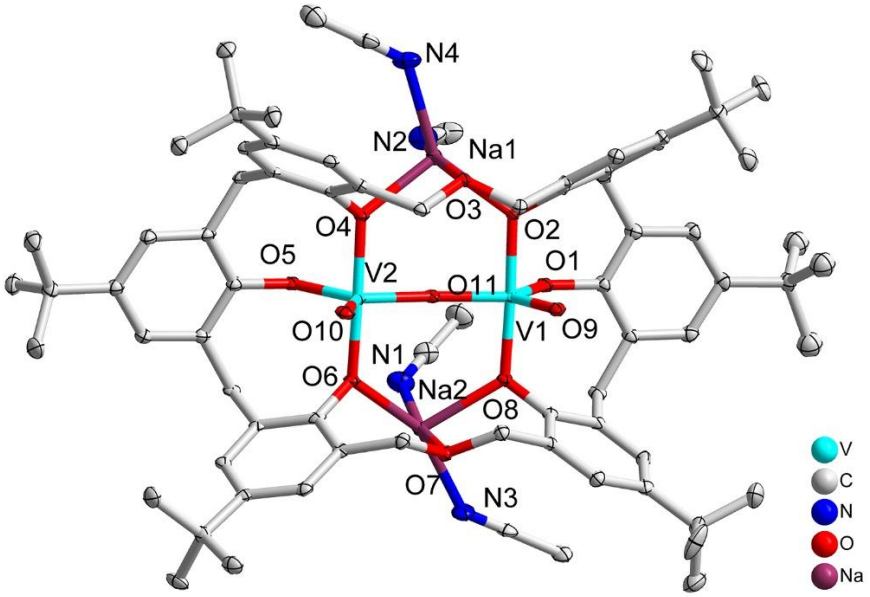

Figure 2-1. Molecular structure of $[(VO)_2(\mu\text{-}O)Na_2(L^{6O})(MeCN)_4]\cdot 5(MeCN)$ (**1**·5MeCN) (H atoms and free MeCN molecules are omitted for clarity). Selected bond lengths (Å) and angles (°): V1–O1 1.832(3), V1–O2 1.946(3), V1–O8 1.949(3), V1–O9 1.588(3), V1–O11 1.825(3), Na1–O2 2.231(3), Na1–O3 2.427(4), Na1–O4 2.232(4), Na1–N2 2.459(6), Na1–N4 2.396(5); O1–V1–O2 87.74(14), O1–V1–O9 112.40(16), O2– V1–O8 176.37(14), V1–O11–V2 171.8(2), O2–Na1–O4 107.28(13).

Two of the vanadyl centres (V1) are distorted octahedral and are bound by a long V – O2 bond (*ca*. 2.37 Å) involving the oxygen of the dimethyleneoxa bridge *trans* to the vanadyl group, two phenoxides (*ca*. 1.79 and 1.81 Å) and an *n*-propoxide (V1-O8 *ca*. 1.79 Å). The other vanadyl centre (V2) is tetragonal pyramid (the geometric parameter, $\tau = 0.18$ is closed to zero),[14] and is linked to V1 via a triply bridging oxygen O6.

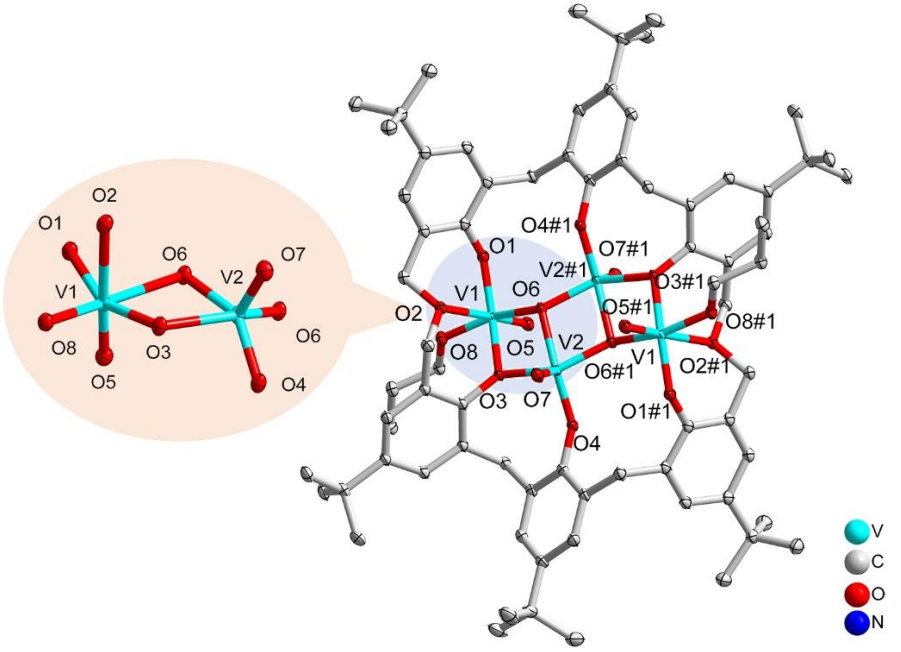

Figure 2-2. View of the molecular structure of {[VO]$_4$L^{6O}}·6MeCN (**2**·6MeCN) (H atoms and free MeCN molecules are omitted for clarity; Symmetry codes: #1: 1-x, 1-y, 1-z;). Selected bond lengths V1–O1 1.8128(14), V1–O2 2.3732(14), V1–O3 2.0152(13), V1–O5 1.5866(15), V1–O6 2.0667(14), V1–O8 1.7869(14), V2–O3 1.9977(13), V2–O4 1.7934(14) , V2–O6 1.9822(14), V2–O7 1.5830(15); O5–V1–O8 99.86(7), O5–V1–O1 100.97(7), O8–V1–O1 102.34(6), O5–V1–O3 101.19(7), O8–V1–O3 89.29(6), O1–V1–O3 152.74(6), O5–V1–O6 95.07(7), O8–V1–O6 157.22(6), O1–V1–O6 91.50(6), O3–V1–O6 70.89(5), O5–V1–O2 177.99(6), V2–O3–V1 107.25(6).

2.1.2 Imido complexes

Given that the oxo group is isoelectronic with the imido group,[15] and that the latter can provide a useful NMR handle and can also be varied to alter the electronics, and to a lesser degree the sterics of the system,[5] we also prepared a number of organoimido-containing vanadium complexes derived from L^{6O}H$_6$. The entry into this chemistry is via the organoimido tris-alkoxides of the type [V(NAr)(OR)$_3$] (R = *t*Bu, *i*Pr, *n*Pr or Et) which are readily available either via the use of [V(N*p*-RC$_6$H$_4$)Cl$_3$] and subsequent addition of KO*t*Bu,[16] or via the addition of ArNCO to [VO(OR)$_3$].[17] Both routes have been utilized herein.

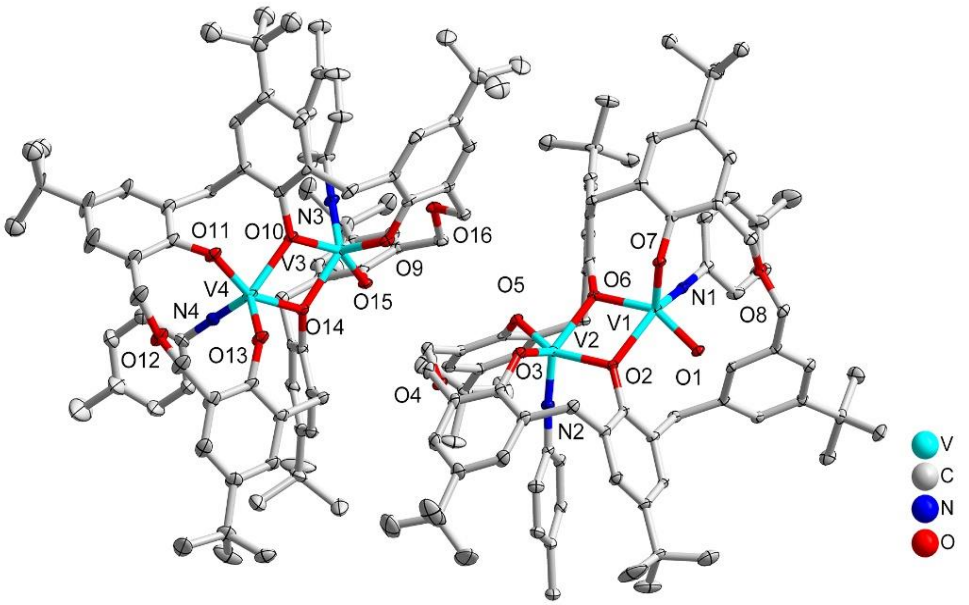

Figure 2-3. Molecular structure of $\{[V(Np\text{-}CH_3C_6H_4)]_2L^{6O}\}\cdot 7MeCN\cdot 0.5CH_2Cl_2$ (**3**$\cdot 7MeCN\cdot 0.5CH_2Cl_2$). (H atoms and CH_2Cl_2 molecules are omitted for clarity).

Interaction of $[V(Np\text{-}CH_3C_6H_4)(O\mathit{t}Bu)_3]$ with $L^{6O}H_6$ led, following work-up, to the isolation of the complex $\{[V(Np\text{-}CH_3C_6H_4)]_2L^{1}\}\cdot 7MeCN\cdot 0.5CH_2Cl_2$ (**3**$\cdot 7MeCN\cdot 0.5CH_2Cl_2$). Single crystals were grown from a saturated acetonitrile solution at ambient temperature and an X-ray structure determination revealed the structure shown in Figure 2-3; selected bond lengths and angles are given Table 2-1. Each vanadium adopts a distorted squared-based pyramidal geometry with the near-linear imido ligand at the tetragonal pyramid ($\tau = 0.11$),[14] and are linked via asymmetric aryloxide bridges (of the dioxacalix[6]arene).

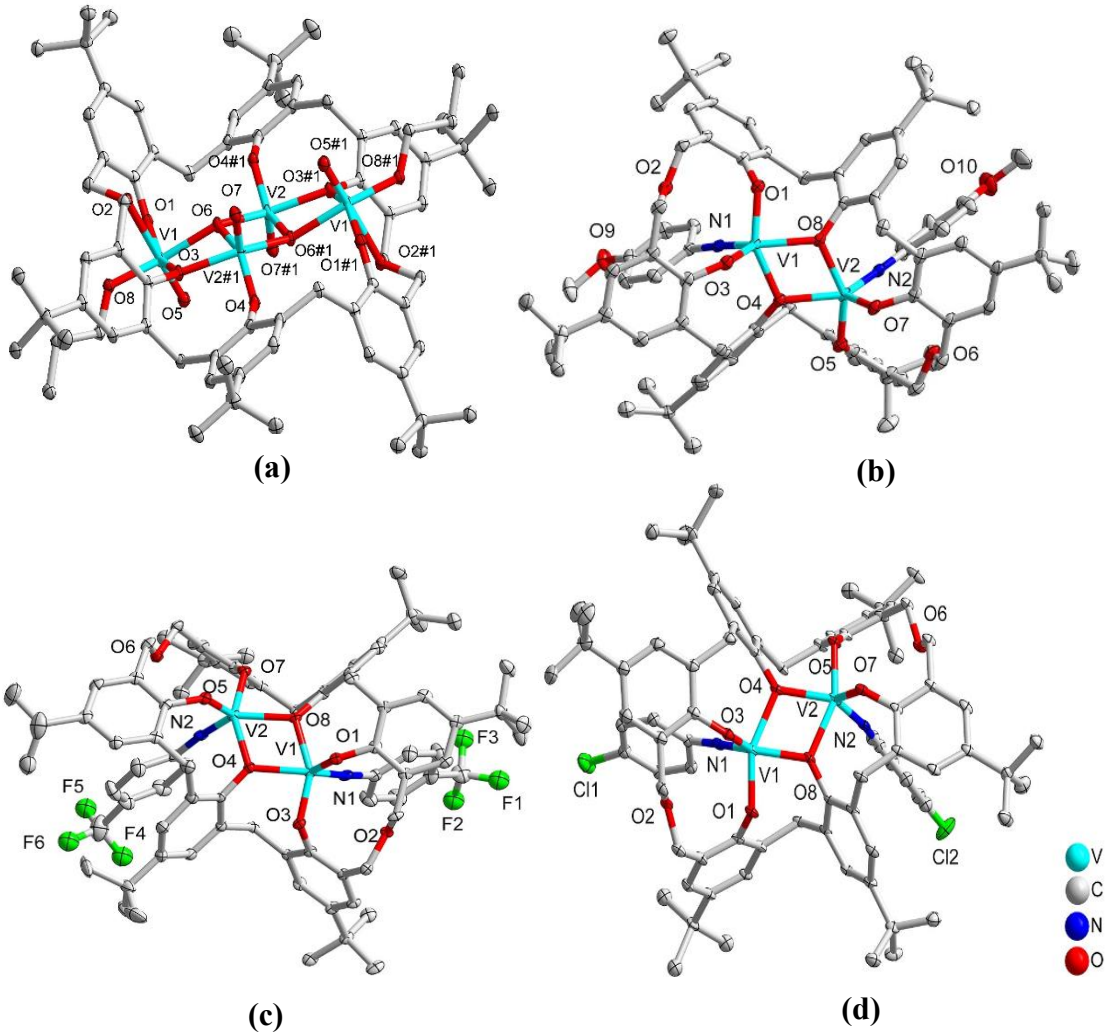

Figure 2-4. Molecular structures of (a) $[(VO)_4L^{6O}]$ (**2**) (b) $[V(N\textit{p}\text{-}(OMe)C_6H_4)]_2L^{6O}$ (**4**) (hydrogens and four MeCN molecules are omitted for clarity), (c) $[V(N\textit{p}\text{-}(CF_3)C_6H_4)]_2L^{6O}$ (**5**), (d) $[V(N\textit{p}\text{-}Cl\text{-}C_6H_4)]_2L^{6O}$ (**6**).

Replacement of the *para* methyl group by OMe (**4**), CF_3 (**5**), Cl (**6**) and F (**7**) led to the formation of the complexes **4** – **7** adopting the same general dimeric structure as observed for **3** (for synthetic details see the experimental section). The geometrical parameters (Table 2-1), show the similarity between these molecules and the *p*-tolyl analogue. The molecular structures of **4** – **6** are given in the Figure 2-4. As reported by Maatta *et al.*,[16] the ^{51}V NMR shifts are very sensitive to the nature of the *para* substituent in such imido complexes (Figure 2-5). In general, the trend observed

herein is as observed by Maatta, with the electron donating groups (e.g. *p*-OMe) at low field *versus* electron withdrawing groups (e.g. *p*-CF_3) at high field. The exception is the *p*-F derivative, which surprisingly is found at low field (-173.4 ppm) and we tentatively attribute this to its position in relation to the macrocycle conformation. Compared with V tolylimido complex, an additional contribution to different ^{51}V chemical shift of vanadium calixarene complex can be expected to result from calixarene framework.

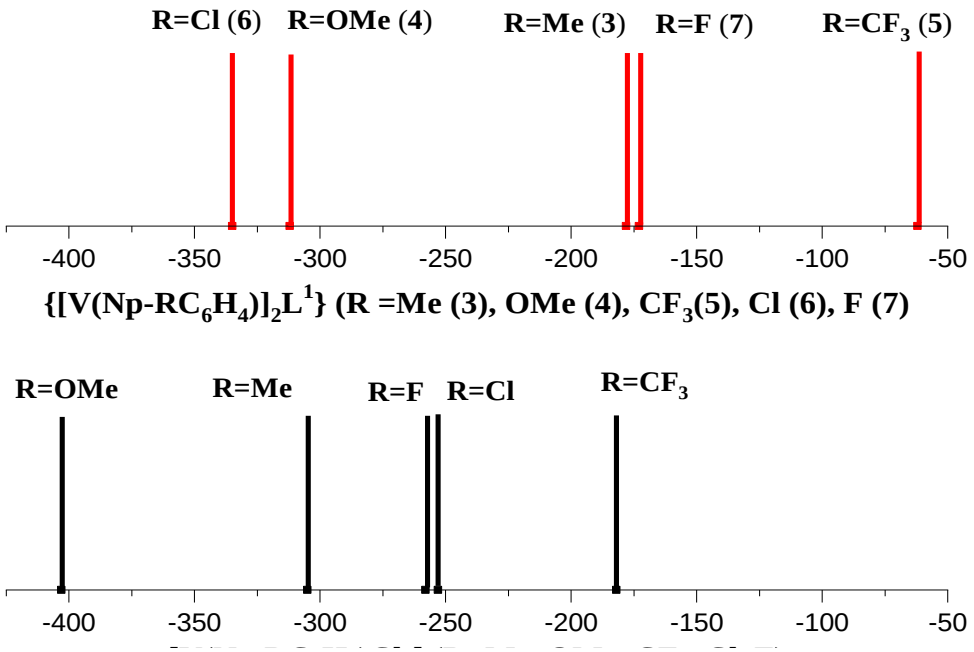

Figure 2-5. ^{51}V NMR chemical shifts for **3**–**7** and $[V(Np\text{-}RC_6H_4)Cl_3]$ (R = Me, OMe, CF_3, Cl, F).[16]

Table 2-1 Selected bond lengths (Å) and angles (°) for **3** – **6**.

bond	**3**·7MeCN·0.5CH_2Cl_2	**4**·4MeCN	**5**	**6**
V1–O1	1.837(3)	1.852(15)	1.786(4)	1.826(4)
V1–O2	2.095(3)	-	-	-
V1–O3	-	1.789(14)	1.815(4)	1.782(4)
V2–O4	-	2.068(15)	2.015(4)	2.010(4)
V2–O5	1.839(3)	1.841(16)	1.775(4)	1.836(4)

V2–O7	-	1.785(15)	1.818(4)	1.794(4)
V1–N1	1.652(3)	1.656(18)	1.645(5)	1.665(5)
V1–O6	2.016(3)	-	-	-
V1–O7	1.786(3)	-	-	-
V1–O1–C1	123.2(2)	123.00(12)	127.2(3)	122.7(4)
V1–O1–C58	129.3(2)	-	-	-
V1–O8–C58	-	128.44(12)	120.9(3)	127.4(3)
V1–O2–V2	108.34(11)	-	-	-
V1–O6–V2	110.10(11)	-	-	-
V2–O4–V1	-	108.68(7)	109.14(19)	108.7(2)
V1–O8–V2	-	109.05(7)	108.65(19)	108.5(2)
V1–N1–C70	173.7(3)	-	-	169.5(5)
V1–N1–C71	-	176.51(16)	175.9(5)	-
V2–N2–C81	-	178.53(17)	174.5(5)	-
V1–N2–C76A	-	-	-	174.0(4)

When the metal precursor employed was [V(Np-$CH_3C_6H_4$)$(OEt)_3$], reaction with $L^{6O}H_6$ led to the formation of small yellow prisms of [$VO(L^{6O'})]_2$·4MeCN (**8**·4MeCN) (($L^{6O'}$ = 2-(*p*-CH_3-C_6H_4NCH)-4-*t*Bu-C_6H_2O-6-CH_2)-4-*t*BuC_6H_2OH)). The molecular structure of **8**, as determined using synchrotron radiation, is shown in Figure 2-6, with selected bond lengths and angles given in the caption. The molecule sits on a centre of symmetry. Interestingly, the dioxacalix[6]arene has been split in two by a reaction of the bridging oxygens and the *p*-tolylimido groups. The result is a metallo-macrocycle containing two square-based pyramidal vanadyl centres. The vanadyl V=O4 bond length is typical at 1.5933(4) Å,[10] whilst the phenoxide bond lengths at 1.8891(15) and 1.9046(15) Å are comparable with those observed elsewhere in vanadyl calixarene chemistry.[7,10] The two uncoordinated phenolic OH groups are involved in H-bonding to vanadium-bound phenoxide groups. There are four solvent

molecules (MeCN) of crystallization per molecule, with two residing inside the metallo-macrocycle. We note that calixarene cleavage is rare, with previous reports involving cleavage of a methylene bridge under acidic conditions.[18]

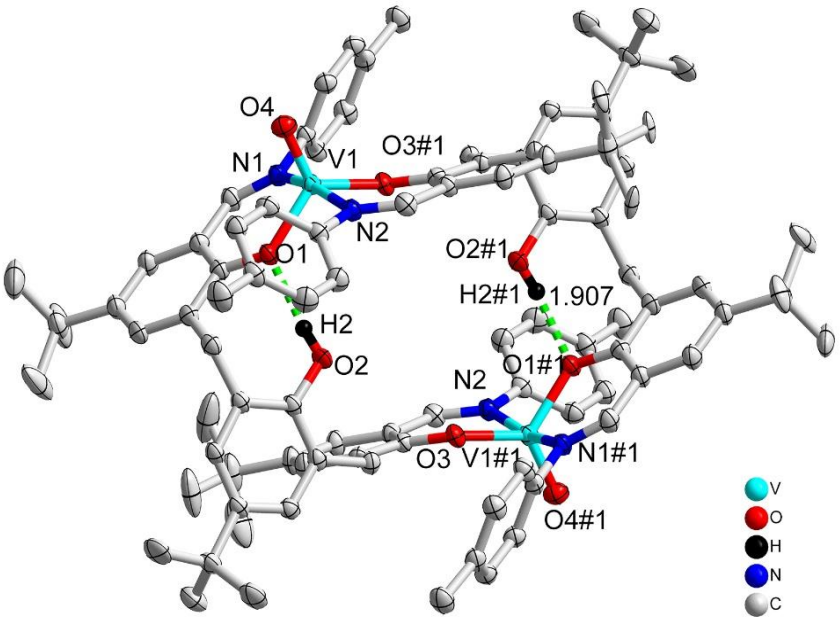

Figure 2-6. View of the molecular structure of $[VO(L^{6O'})]_2 \cdot 4MeCN$ (**8**·4MeCN) (H atoms and MeCN molecules are omitted for clarity) ($L^{6O'}$ = 2-(p-$CH_3C_6H_4NCH$)-4-*t*Bu-C_6H_2O-6-CH_2)-4-*t*BuC_6H_2OH). Selected bond lengths (Å) and angles (º): V1–O1 1.9046(15), V1–O3A 1.8891(15), V1–O4 1.5933(17), V1–N1 2.1192(18), V1–N2A 2.1118(19), V1–O1–C9 131.18(14), V1– O3–C31 131.67(13), V1–N1–C1 117.87(19), V1–N1–C(8) 124.00(15).

2.2 Ring opening polymerization studies

General: The performance of these complexes to act as catalysts for the ring opening polymerization (ROP) of ε-caprolactone (ε-CL) (Table 2-2), *δ*-valerolactone (*δ*-VL) (Table 2-3), both with and without one equivalent of benzyl alcohol (BnOH) per vanadium present, has been investigated.

Results in the absence of BnOH were less controlled but for completion are presented in the Tables 8-1 and 8-2, Chapter 8. The co-polymerization of *ε*-

caprolactone and δ-valerolactone (Table 2-4) has also been investigated. In each case, performances are compared against the known complexes **I** – **IV** (Chart 2-2).

2.2.1 ROP of ε-caprolactone (ε-CL)

Complexes **1**-**8** and **I**-**IV** were screened for their ability to polymerise ε-caprolactone and the results are collated in Table 2-2. The polymerization screening indicated that the best conditions were 500 equivalents of ε-caprolactone to vanadium at 130 ^{o}C. The activity of complex **1** increased with temperature and peaked at 500 equivalents of monomer. Complex **1** was also active at low catalyst loading leading to 82.5% conversion after 8 h for 1000 equivalents of monomer.

The observed activity of complex **1** surpassed that of the other complexes screened herein, and this was attributed to the additional presence of the sodium centres. All polymers obtained were of low polydispersity (PDI < 1.6), which suggested that these polymerizations occurred without significant side reactions. Interestingly, only low molecular weight polymers were obtained using these oxovanadium/imido vanadium systems.

The screening of complexes **1**–**8** and **I**-**IV** (Table 2-2) revealed that the vanadium-based L^{6O} or $L^{6O'}$-containing complexes namely **1**, **5**, **6** and **8** herein, exhibited higher activities than the known complexes **I**-**IV** under the conditions employed. After 24 h (Table 2-2, run 20-31), complexes **2**, **I**, **II**, **III** and **IV** afforded relatively lower conversions (<90%), whereas higher conversions (>90%) were reached using complexes **1**, **3**–**7**, **8**, under similar conditions. From a kinetic study (Figure 2-7(a)),

it was observed that the PCL polymerization rate followed the order: **1**>**8**>**II**>**I**>**III**≈**3**>**2**>**IV**. For complexes within the imido-alkoxide family, the kinetic results (Figure 2-7(b)) showed that the catalytic activity followed the order: **5** (CF_3) > **6** (Cl) > **7** (F) > **4** (OMe) > **3** (Me), which suggested that the presence of electron withdrawing *para* substituents favours higher activity. ^{1}H NMR spectra of the PCL indicated the presence of a BnO end group (e.g. Figure 2-8), which agrees with the MALDI-ToF mass spectra (e.g. Figure 2-9) and indicates that the polymerization proceeded via a coordination insertion mechanism. The observed molecular weights were lower than the calculated values, whilst the MALDI-ToF mass spectra were consistent with BnO end groups [M = n × 114.12 (CL) + 108.05 (BnOH) + 22.99 (Na^+)]. In the absence of BnOH, spectra (Figures 8-4 and 8-7, Chapter 8) indicated the products were catenulate with chains and cyclic polymers present. In the MALDI-ToF mass spectra, a part family of peaks consistent with the chain polymer (terminated by 2 OH) [M = 17 (OH)+ 1(H) + n × 114.14 (CL) + 22.99 (Na^+)] and the cyclic polymer [M=22.99 (Na^+) + n × 114.14 (CL)] were observed.

Table 2-2. ROP of ε-CL using **1** – **8** and **I - IV** in the presence of BnOH.

Run	Cat.	CL: V: BnOH	t/h	T/^{o}C	Conv^a (%)	$M_{n,GPC}\times10^{-3b}$	$M_w\times10^{-3b}$	$M_{n,Cal}\times10^{-3c}$	PDI^d
1	**1**	1000: 1: 1	8	130	82.5	10.22	17.21	94.26	1.68
2	**1**	500: 1: 1	8	130	89.2	11.89	16.48	51.01	1.39
3	**1**	250: 1 :1	8	130	87.9	4.59	6.49	25.19	1.41
4	**1**	100: 1: 1	8	130	86.3	2.34	3.01	9.96	1.28
5	**1**	500: 1: 1	8	100	44.9	5.99	7.49	25.73	1.24
6	**1**	500: 1: 1	8	80	25.1	1.42	1.76	14.43	1.26
7	**2**	500: 1: 1	8	130	34.1	4.98	5.98	19.57	1.20
8	**3**	500: 1: 1	8	130	39.2	5.26	6.31	22.48	1.19

9	**4**	500: 1: 1	8	130	41.2	5.89	6.72	23.62	1.14
10	**5**	500: 1: 1	8	130	59.2	9.05	13.76	33.89	1.52
11	**6**	500: 1: 1	8	130	46.6	6.54	8.05	26.70	1.24
12	**7**	500: 1: 1	8	130	43.1	6.40	7.33	24.70	1.16
13	**8**	500: 1: 1	8	130	71.4	9.87	12.59	40.85	1.27
14	**8**	500: 1: 1	8	100	49.7	6.92	7.92	28.47	1.14
15	**8**	500: 1: 1	8	80	-	-	-	-	-
16	**I**	500: 1: 1	8	130	32.8	4.63	5.33	18.82	1.15
17	**II**	500: 1: 1	8	130	44.5	6.13	8.26	25.50	1.34
18	**III**	500: 1: 1	8	130	32.5	4.62	6.78	18.65	1.47
19	**IV**	500: 1: 1	8	130	30.8	2.76	3.12	17.68	1.12
20	**1**	500: 1: 1	24	130	99.4	11.61	16.42	56.83	1.41
21	**2**	500: 1: 1	24	130	65.3	5.56	7.42	37.37	1.33
22	**3**	500: 1: 1	24	130	90.3	5.20	6.42	51.63	1.23
23	**4**	500: 1: 1	24	130	96.5	6.13	7.51	55.17	1.23
24	**5**	500: 1: 1	24	130	99.0	9.52	11.01	56.60	1.16
25	**6**	500: 1: 1	24	130	98.1	7.45	8.53	56.08	1.14
26	**7**	500: 1: 1	24	130	98.3	7.12	8.56	56.20	1.20
27	**8**	500: 1: 1	24	130	99.5	10.33	13.63	56.88	1.32
28	**I**	500: 1: 1	24	130	62.5	4.36	7.63	35.77	1.75
29	**II**	500: 1: 1	24	130	76.2	6.88	7.52	43.59	1.09
30	**III**	500: 1: 1	24	130	60.5	5.12	6.23	34.63	1.22
31	**IV**	500: 1: 1	24	130	58.3	3.20	4.13	33.37	1.29

[a] Determined by ^{1}H NMR spectroscopy. [b] Values corrected considering Mark–Houwink factor (0.56) from polystyrene standards in THF. [c] Calculated from ([monomer]$_0$/[V]) × conv (%) × monomer molecular weight (M_{CL}=114.14) + Molecular weight of BnOH. [d] From GPC. Solvent used in the ROP: toluene.

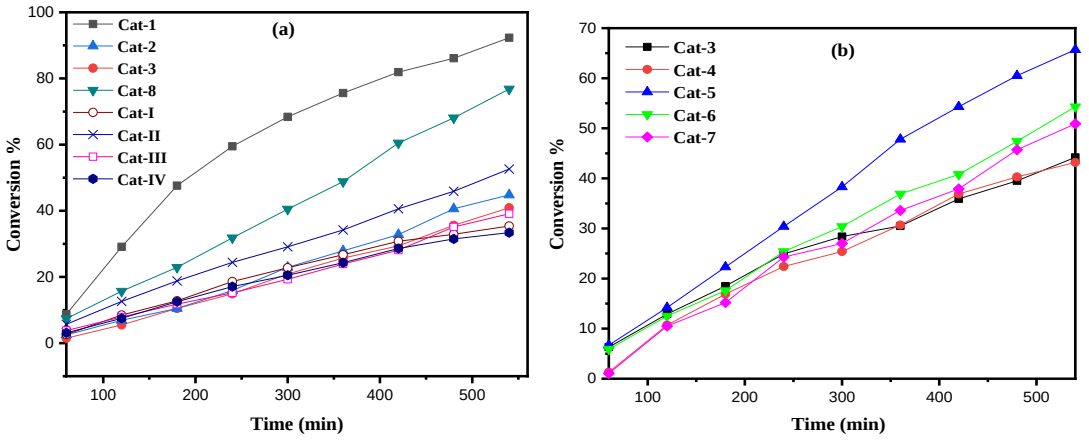

Figure 2-7. (a) Relationship between conversion and time for the polymerization of ε-CL by using complex **1-3**, **8**, and **I – IV;** (b) Relationship between conversion and time for the polymerization of ε-CL by using complexes **3-7**; Conditions: T=130 °C, $n_{Monomer}$: n_V:

BnOH=500: 1: 1.

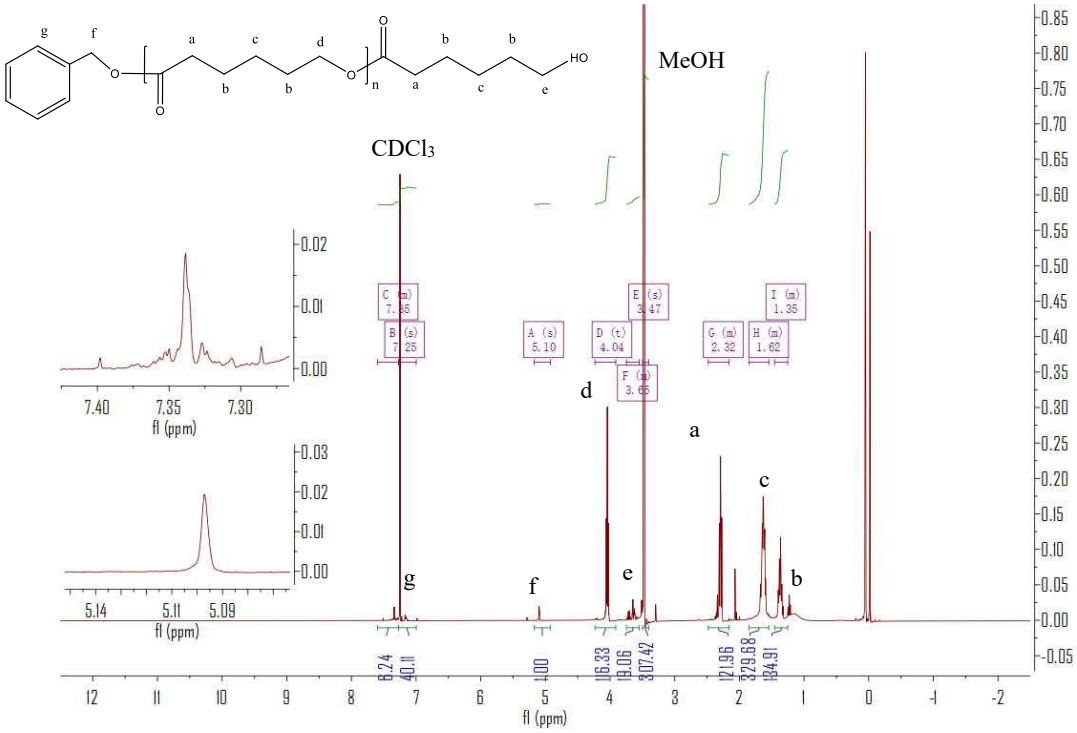

Figure 2-8. ^{1}H NMR spectrum ($CDCl_3$, 400 MHz, 298 K) of the PCL synthesized with **6**/BnOH (run 11, Table 2-2).

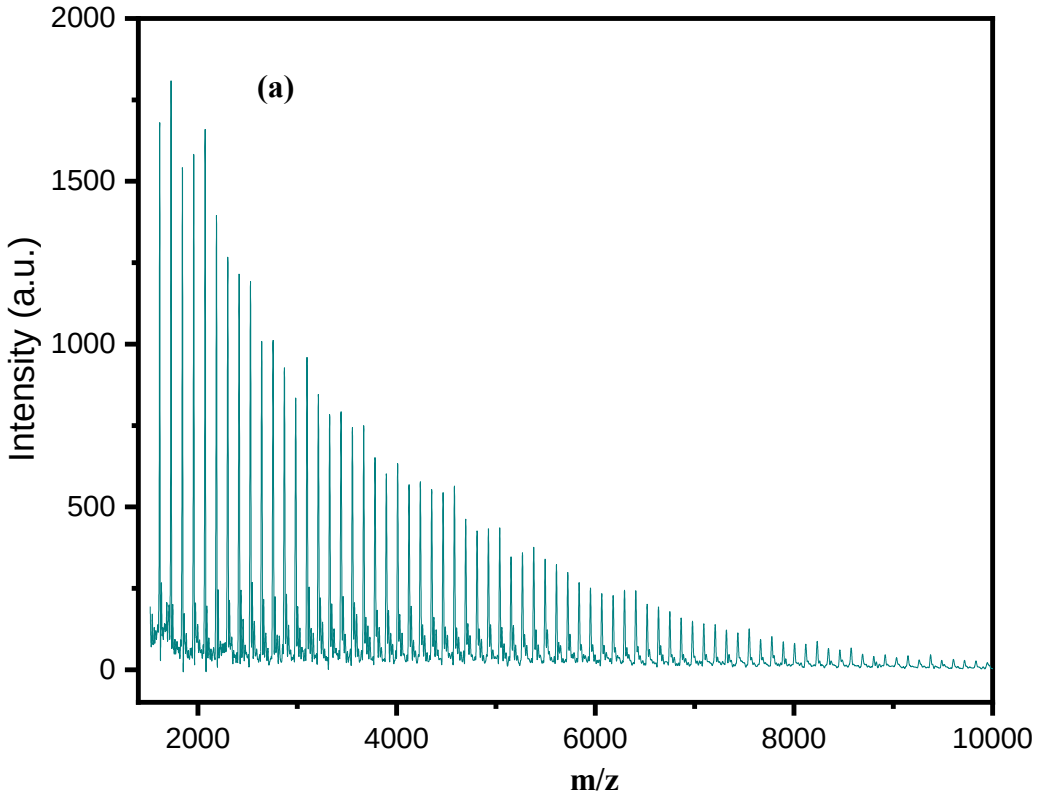

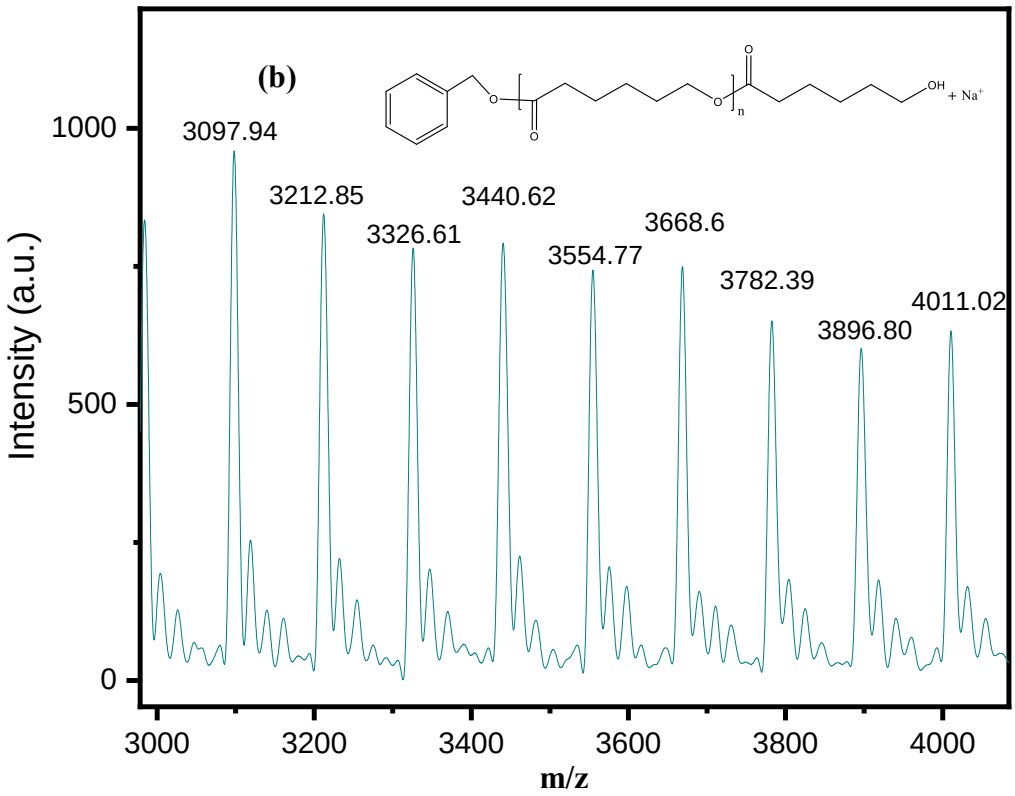

Figure 2-9. (a) Mass spectrum of PCL by using **5**/BnOH (run 10, Table 2-2) (0-10000 m/z); (b) Mass spectrum of PCL by using **5**/BnOH (run 10, Table 2-2) (3000-4000 m/z).

2.2.2 *δ*-valerolactone (*δ*-VL)

Table 2-3. ROP of *δ*-VL using **1** – **8** and **I – IV** in the presence of BnOH.

Run	Cat.	VL: V: BnOH	t/h	T/°C	Conv[a] (%)	$M_{n,GPC}\times10^{-3b}$	$M_w\times10^{-3b}$	$M_{n,Cal}\times10^{-3c}$	PDI[d]
1	**1**	1000: 1: 1	8	130	79.9	10.57	18.69	80.10	1.76
2	**1**	500: 1: 1	8	130	86.3	12.38	16.31	43.31	1.31
3	**1**	250: 1: 1	8	130	84.6	4.26	6.45	21.28	1.51
4	**1**	100: 1: 1	8	130	82.1	2.38	3.95	8.33	1.70
5	**1**	500: 1: 1	8	100	42.1	6.01	7.22	21.18	1.20
6	**1**	500: 1: 1	8	80	20.5	1.89	3.25	10.37	1.72
7	**2**	500: 1: 1	8	130	35.9	4.28	6.51	18.08	1.52
8	**3**	500: 1: 1	8	130	38.4	5.23	7.24	19.33	1.38
9	**4**	500: 1: 1	8	130	44.3	6.90	8.49	22.28	1.23
10	**5**	500: 1: 1	8	130	58.1	9.43	13.25	29.19	1.40
11	**6**	500: 1: 1	8	130	43.9	6.27	7.53	22.08	1.20
12	**7**	500: 1: 1	8	130	42.1	5.94	7.56	21.18	1.27
13	**8**	500: 1: 1	8	130	75.5	10.61	14.64	37.90	1.38
14	**I**	500: 1: 1	8	130	37.0	4.84	5.47	18.63	1.12
15	**II**	500: 1: 1	8	130	48.9	7.24	8.92	24.59	1.23

16	**III**	500: 1: 1	8	130	35.6	4.21	6.21	17.93	1.48
17	**IV**	500: 1: 1	8	130	34.5	3.42	4.51	17.38	1.32

[a] Determined by ^{1}H NMR spectroscopy. [b] Values corrected considering Mark–Houwink factor (0.57) from polystyrene standards in THF. [c] Calculated from ([monomer]$_0$/V) × conv (%) × monomer molecular weight (M_{VL}=100.16) + Molecular weight of BnOH. [d] From GPC. Solvent used in the ROP: toluene.

Complexes **1**–**8** and **I-IV** were also evaluated as catalysts in the presence of one equivalent of BnOH for the ROP of *δ*-VL (Table 2-3). Using compound **1**, the conditions of temperature and [V]: [*δ*-VL] were varied. Best observed results were achieved at 130 °C using [V]: [*δ*-VL] at 1: 500 over 8 h. As in the case of the ROP of *ε*-CL, kinetic studies (Figures 2-10) revealed that the catalytic activities followed the order: **1**>**8**>**II**>**I**>**III**≈**3**>**2**>**IV**, whilst the performance of the vanadium-based imido catalysts exhibited the order **5**>**6**≈**7**>**4**>**3**, which was again suggestive of a positive influence exerted by electron-withdrawing *para* substituents on the imido group. As for the ROP of *ε*-Cl, there was evidence of significant transesterification and nearly all observed M_n values were significantly lower than the calculated values. The MALDI-ToF mass spectra (Figure 2-11) exhibited a major family of peaks consistent with OBn end groups [M = 108.05 (BnOH) + n × 100.12 (VL) + 22.99 (Na^+)], and a minor family assigned to cyclic PVL. ^{1}H NMR spectra of the PVL also indicated the presence of a BnO end group (e.g. Figure 2-12). In the absence of BnOH, spectra (Figures 8-5 and 8-8, Chapter 8) again indicated the products were catenulate. The MALDI-ToF mass spectra exhibited the peaks consistent with the chain polymer (terminated by 2 OH) [M = 17 (OH)+ 1(H) + n × 100.12 (VL) + 22.99 (Na^+)] and cyclic polymer [M= 22.99 (Na^+) + n × 100.12 (VL)].

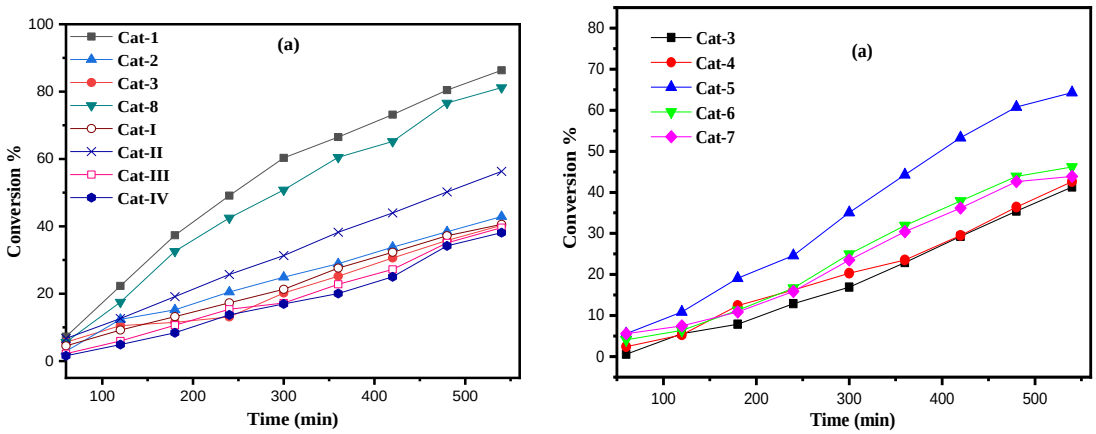

Figure 2-10. (a) Relationship between conversion and time for the polymerization of *δ*-VL by using **1-3**, **8**, and **I** – **IV**; (b): Relationship between conversion and time for the polymerization of *δ*-VL by using complexes **3-7**; Conditions: T = 130 °C, $n_{Monomer}$: n_V: BnOH = 500: 1: 1.

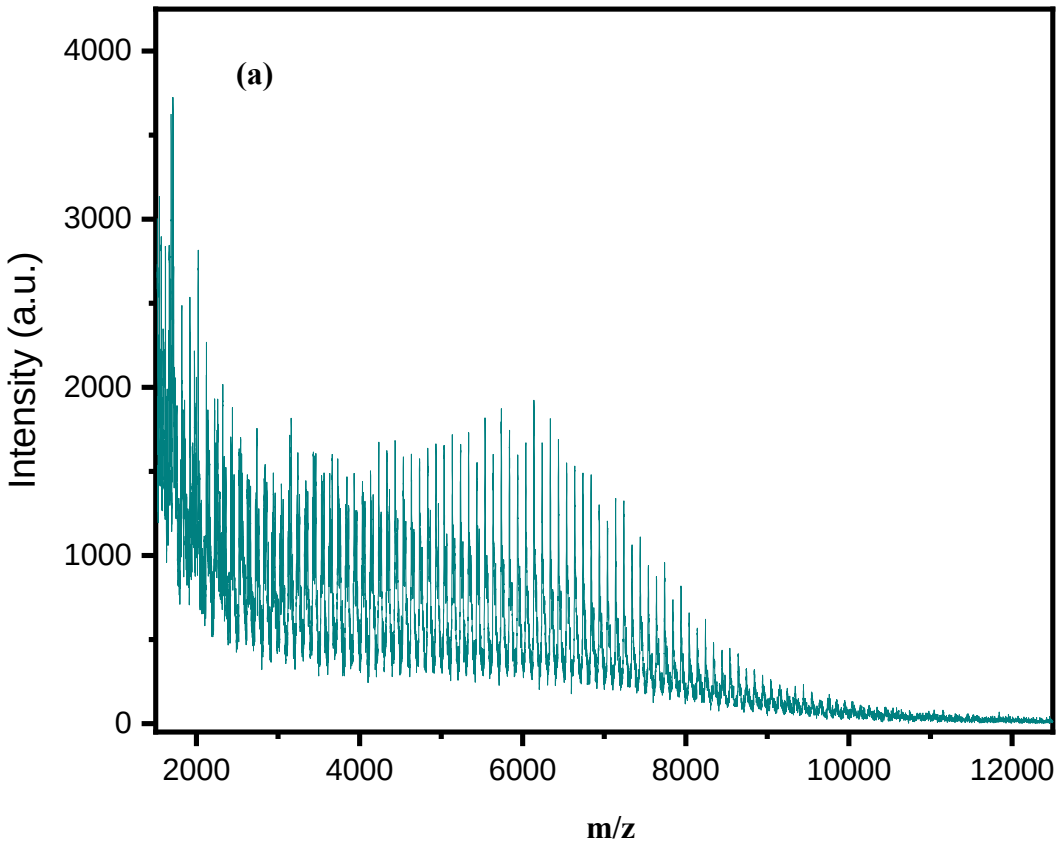

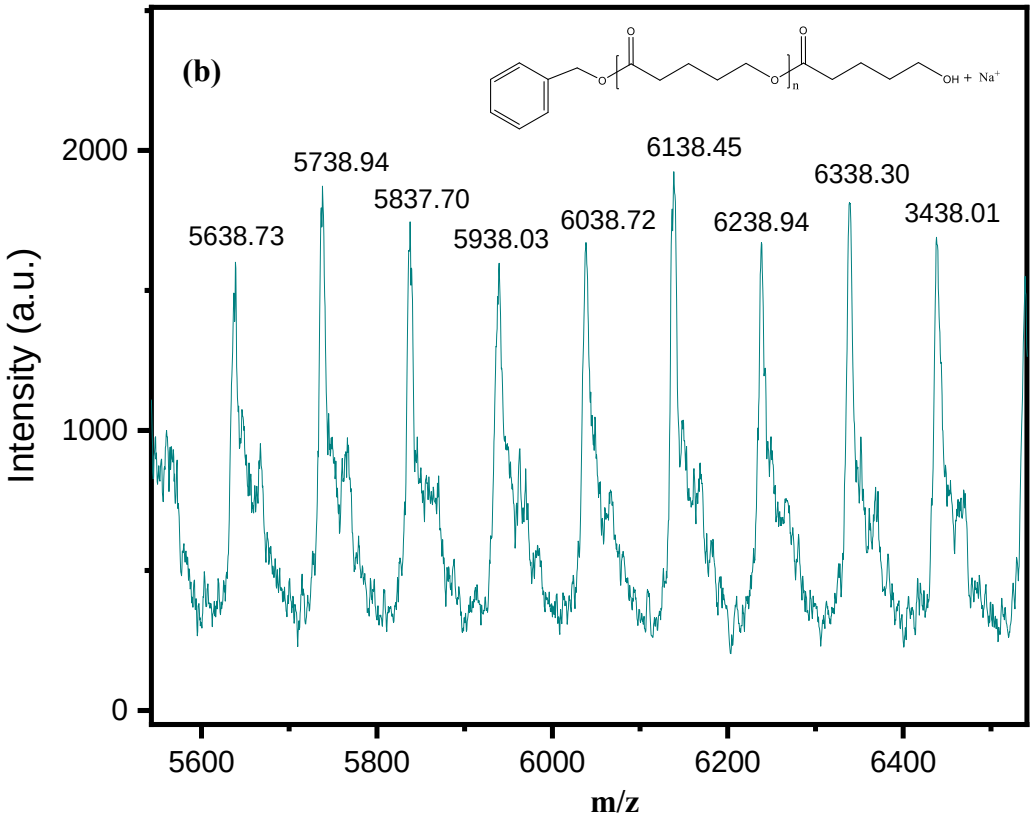

Figure 2-11. (a) Mass spectrum of PVL by using **7**/BnOH (run 12, Table 3) (0-12000 m/z); (b) Mass spectrum of PVL by using **7**/BnOH (run 12, Table 3) (5600-6400 m/z).

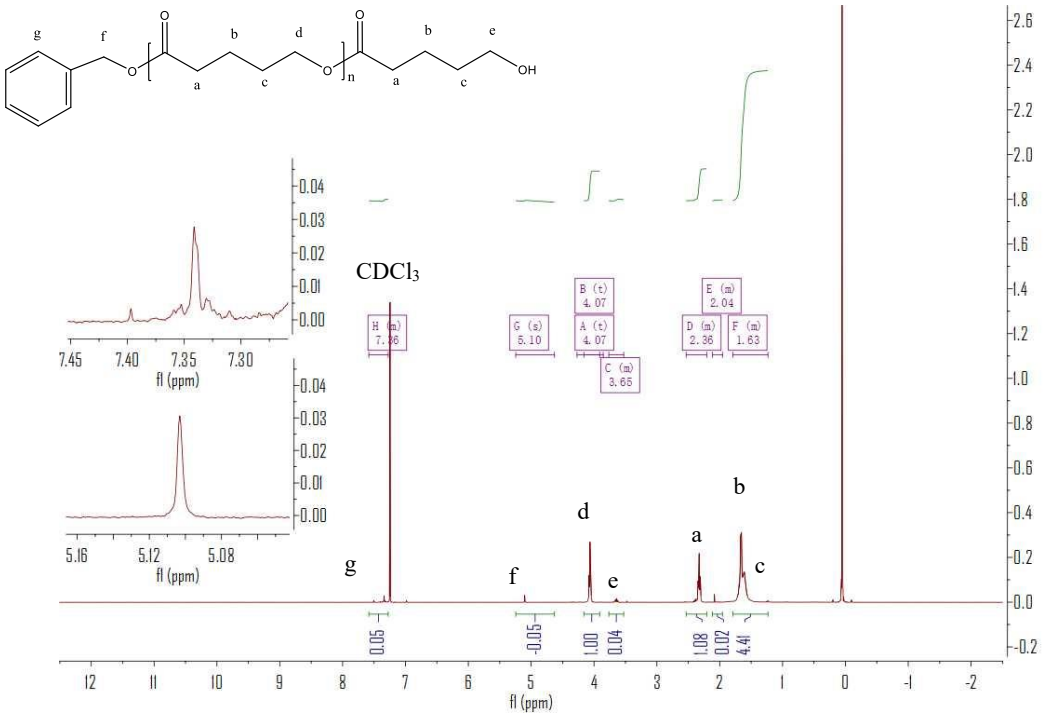

Figure 2-12. ^{1}H NMR spectrum ($CDCl_3$, 400 MHz, 298 K) of the PVL synthesized with **1**/BnOH (run 1, Table 2-3).

2.2.3 Kinetics study for ROP of ε-CL and δ-VL

The kinetic results are consistent with a zero-order dependence in monomer (Figure 2-7, 2-10). Whilst this kind of behaviour is uncommon, systems that behave in a similar manner have been reported.[19] The dependence of the M_n and molecular weight distribution on the monomer conversion in the reactions catalyzed by **1**, **3**, **8** with BnOH was also investigated (Figure 2-13). For the ROP of ε-CL, the polymer M_n was shown to increase linearly with the conversion, which suggested that the polymerization was well controlled (Figure 2-13, left)**.** A similar outcome was also observed in the reaction involving *δ*-VL (Figure 2-13, right).

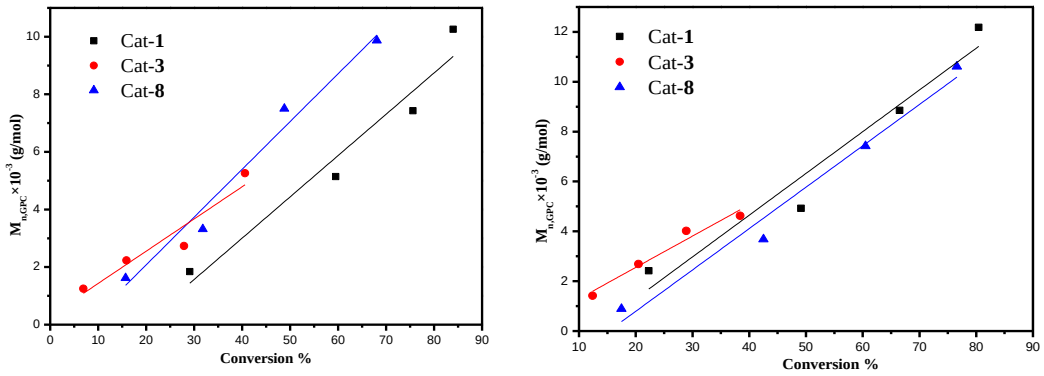

Figure 2-13. Left: M_n *vs*. monomer conversion in the ROP of *ε*-CL by using **1, 3** and **8**; Right: M_n *vs*. monomer conversion in the ROP of *δ*-VL by using **1, 3** and **8**; Conditions: T=130 °C, $n_{Monomer}$: n_V: BnOH= 500: 1: 1.

2.2.4 Co-polymerization of ε-CL and δ-VL

The complexes exhibited moderate conversions, with the mixed-metal complex **1** performing best (72.6%), with **5** (p-CF_3) and the known complex **I** also producing conversions > 60%. Under the conditions employed, the systems **5**, **6, 7** and **8** showed a preference for CL incorporation (50 – 66%), and in the case of **5** and **6**, this was despite the initial addition of *δ*-VL. Complex **4** exhibited the highest preference

(67%) for VL incorporation. In general, the systems appeared to be relatively well behaved with PDIs in the range 1.17-1.84; NMR spectra were consistent with the presence of BnO and OH end groups (Figure 2-14). The composition of the copolymer was further investigated by ^{13}C NMR spectroscopy. In fact, diagnostic resonances belonging to CL–VL, CL–CL, VL–VL and VL–CL dyads can be observed in the region between δ 63.91 and 64.13 ppm (Figure 8-10, Chapter 8). Based on the current results, the number-average sequence length was found to be 7.16 and 5.30 for CL and VL, respectively, consistent with a randomness degree R of 0.33, which suggests the copolymers possess a "blocking" tendency (Figure 8-10, Equations 8-1 to 8-3, Chapter 8).[20]

Table 2-4. ROP of co-polymer (ε-CL +δ-VL) using **1 – 8** and **I – IV** in the presence of BnOH**.**

Run	Cat	CL:VL:V:BnOH	T/^{o}C	CL:VL[a]	Conv[b] (%)	$M_{n,GPC}\times10^{-3}$[c]	$M_{w}\times10^{-3}$[c]	PDI[d]
1	**1**[e]	250:250:1:1	130	45:55	72.6	12.16	22.37	1.84
3	**2**[e]	250:250:1:1	130	45:55	25.3	1.32	2.31	1.75
4	**3**[e]	250:250:1:1	130	40:60	45.2	4.68	6.23	1.33
5	**4**[e]	250:250:1:1	130	33:67	47.5	5.29	6.88	1.30
6	**5**[e]	250:250:1:1	130	40:60	59.5	7.21	8.45	1.17
7	**5**[f]	250:250:1:1	130	66:34	63.7	7.44	8.95	1.20
8	**5**[g]	250:250:1:1	130	58:42	35.8	4.22	7.12	1.69
9	**6**[e]	250:250:1:1	130	40:60	57.9	6.01	7.52	1.25
10	**6**[f]	250:250:1:1	130	62:38	55.4	6.21	7.69	1.24
11	**6**[g]	250:250:1:1	130	50:50	38.5	5.98	8.15	1.36
12	**7**[e]	250:250:1:1	130	50:50	58.4	6.12	7.14	1.17
13	**8**[e]	250:250:1:1	130	51:49	60.8	6.85	8.69	1.27
15	**I**[e]	250:250:1:1	130	46:54	61.1	6.95	8.69	1.25
16	**II**[e]	250:250:1:1	130	45:55	58.1	3.67	4.98	1.36
17	**III**[e]	250:250:1:1	130	40:60	49.5	4.53	7.21	1.59
18	**IV**[e]	250:250:1:1	130	35:65	38.4	4.21	6.49	1.54

[a] Ratio of ε-CL to δ-VL observed in the co-polymer by ^{1}H NMR spectroscopy. [b] Determined

by ^{1}H NMR spectroscopy. [c] $M_{n/w}$, GPC values corrected considering Mark–Houwink method from polystyrene standards in THF, $M_{n/w}$ GPC = [0.56 × $M_{n/w}$ measured × (1-%CL) + 0.57 × $M_{n/w}$ measured ×(1-%VL)] × 10^3. [d] From GPC. [e] ε-Caprolactone was firstly added for 24 h, then δ-valerolactone was added and heating for 24 h. [f] δ-valerolactone was firstly added for 24 h, then ε-caprolactone was added and heating for 24 h. [g] ε-caprolactone and δ-valerolactone were added at the same time and heating for 24 h. Solvent used in the ROP: toluene.

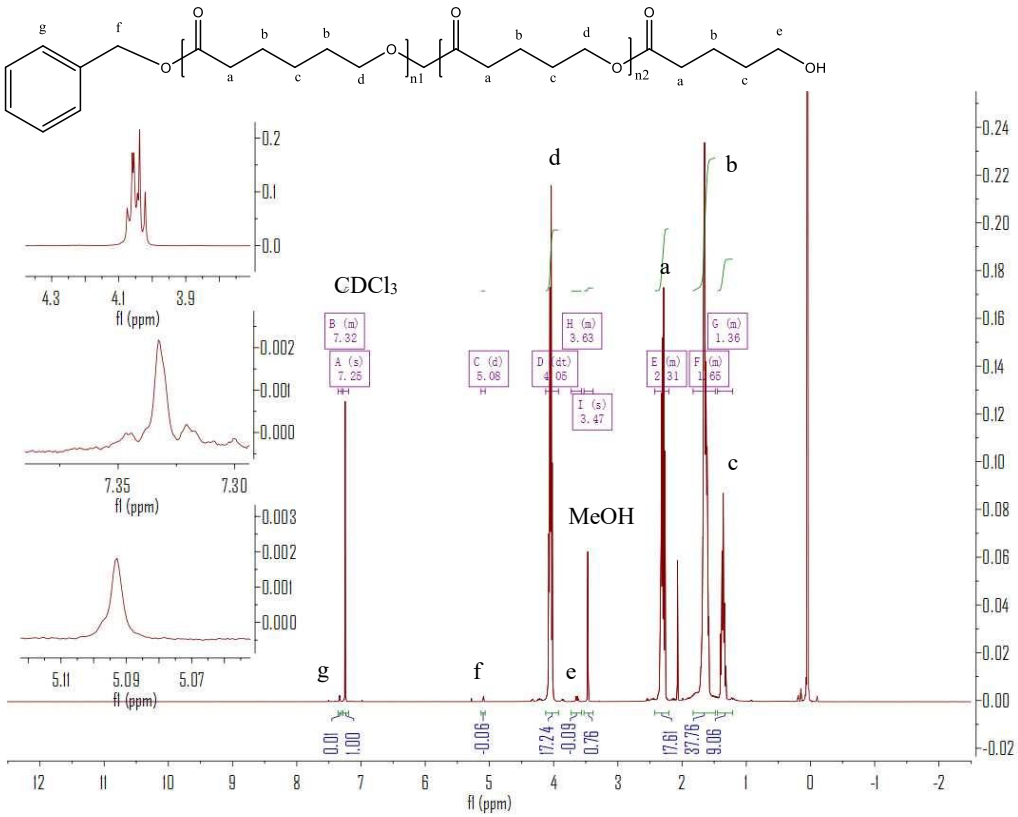

Figure 2-14. ^{1}H NMR spectrum ($CDCl_3$, 400 MHz, 298 K) of the CL-VL copolymer (1:1 ratio CL/VL) synthesized with **1**/BnOH. (run 1, Table 2-4).

2.2.5 ROP of *r*-lactide

To enhance the thermal properties of the polymers obtained herein, we also investigated the ROP of the *r*-lactide. Unfortunately, none of the systems herein proved to be effective as catalysts for the ROP of *r*-lactide either in solution at high temperatures (130 °C) or as melts.

2.2.6 Ethylene polymerization

In collaboration with the Russian Academy of Sciences in Novosibirsk, the imido complexes **3**–**7** were screened for their ability to polymerize ethylene in the presence of the co-catalysts R_2AlCl (R = Me, Et) and the re-activator ethyltrichloroacetate (ETA), see Table 2-5. High polymerization activities were observed if Me_2AlCl was used as activator (*cf*. entries **1** and **2** of Table 2-5). In the presence of Me_2AlCl+ETA, the catalytic activities followed the trend **3** (*p*-Me) ≈ **5** (*p*-CF_3) > **7** (*p*-F) > **6** (*p*-Cl) > **4** (*p*-OMe). Complexes **3**-**7** exhibited high ethylene consumption rates during 10-20 min of polymerization and virtually lost the activity after 30 min (Figure 2-14(a)). Complex **4** showed the lowest reactivity toward ethylene in the series, which may be explained by the presence of strong electron-donating OMe substituents, reducing its electrophilicity. All systems except **4** were relatively well-controlled with PDIs < 2.5 (Figure 2-14(b)) and afforded highly linear (according to ^{13}C NMR spectroscopy, there were no detectable branches, Figure 8-12, Chapter 8) high molecular weight polyethylene. The ethylene polymerization activities found here for complexes **3**-**7**, are very high, several times higher than those reported for vanadium polyphenolate and phenoxyimine catalysts under comparable conditions.[21]

Table 2-5. Ethylene polymerization data for homogeneous catalysts **3**-**7**.

Entry	Cat	V loading/μmol	Co-catalyst	PE yield/g	Activity[a]	$M_n \times 10^{-3}$	$M_w \times 10^{-3}$	M_z/M_w	PDI[b]
1	**3**	**1.0**	Et_2AlCl	0.7	1.4	-	-	-	-
2	**3**	**0.5**	Me_2AlCl	7.4	14.8	110	245	1.8	2.2
3	**4**	**0.5**	Me_2AlCl	1.2	2.4	72	520	5.0	7.2
4	**5**	**0.5**	Me_2AlCl	7.2	14.2	74	180	2.1	2.4
5	**6**	**0.5**	Me_2AlCl	4.5	9.0	120	290	1.9	2.4
6	**7**	**0.5**	Me_2AlCl	6.7	13.4	74	185	2.0	2.5

[a] In 10^6 g PE/(mol V bar h). [b] PDI= M_w/M_n. For entry 1 of Table 2-5: V loading 1.0 μmol (dissolved in CH_2Cl_2), co-catalyst Et_2AlCl + ETA (molar ratio V: Et_2AlCl: ETA = 1: 1000: 500) in 50 mL of toluene + 100 mL of heptane, T = 70 °C, P(C_2H_4) = 2 bar, for 30 min. For entries 2–6 of Table 2-5: V complex was dissolved in toluene, Co-catalyst Me_2AlCl + ETA (molar ratio V :Me_2AlCl : ETA = 1 : 1000 : 1000) in 100 mL of toluene + 100 mL of heptane; T = 70 °C, P(C_2H_4) = 2 bar, for 30 min.

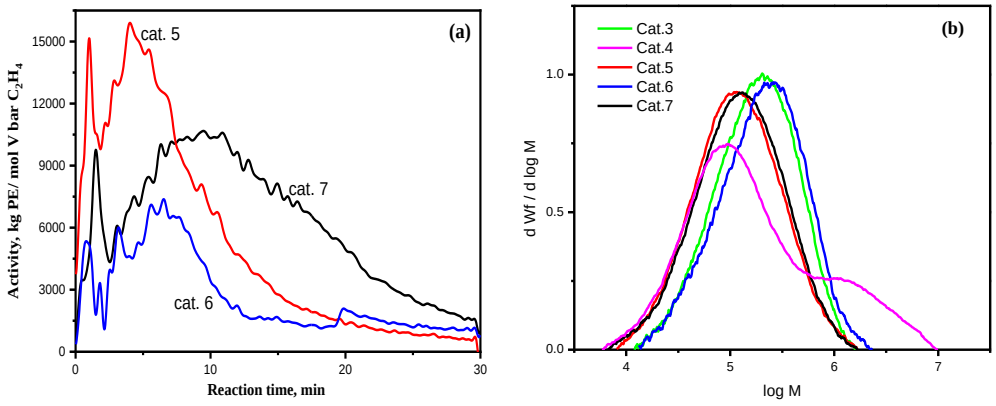

Figure 2-14. (a) Activity *vs*. time plot for entries 4-6 of Table 5. (b) GPC traces of polyethylenes in entries 2-6 of Table 5.

3. Conclusions

In conclusion, the use of p-*tert*-butyltetrahomodioxacalix[6]areneH_6, $L^{6O}H_6$, with [$NaVO(OtBu)_4$] or [$VO(OnPr)_3$] affords the mixed-metal complex [$(VO)_2(\mu\text{-}O)Na_2(L^{6O})(MeCN)_4$] or the tetranuclear complex {$[VO]_4L^{6O}$}, respectively. Use of

imido-alkoxide precursors [V(N*p*-RC_6H_4)(OR')$_3$] leads to the formation of {[V(N*p*-RC_6H_4)]$_2$$L^{6O}$} type complexes. Under the conditions employed, the calixarene ring system can break *in situ*, and result in two 2-(*p*-$CH_3C_6H_4NCH$)-4-*t*Bu-C_6H_2O-6-CH_2)-4-*t*BuC_6H_2OH ($L^{6O'}$), which can bind to the vanadium to form a metallocyclic complex of the form [VO($L^{6O'}$)]$_2$. All complexes were active for the ROP of the cyclic esters ε-CL and δ–VL, with and without benzyl alcohol (BnOH) present, but not for *r*-LA. The co-polymerization of ε-CL with δ-VL was also possible. Low molecular weight products were obtained but with good control. For the imido complexes in the presence of BnOH, kinetic studies indicated the rate order **5** (CF_3) >**6** (Cl)>**7** (F)>**4** (OMe)>**3** (Me) for ε-CL which suggested that the presence of electron withdrawing *para* substituents favour higher activity, and a similar order for δ–VL; in the absence of BnOH, structure/activity trends were less evident. Observed conversion rates were superior to related oxacalix[3]arene species (**I** and **II**) as well as methylene (-CH_2-) bridged calix[6 and 8]arene complexes **III** and **IV** under similar conditions. This suggests the presence and large flexibility of the dioxacalix[6]arene scaffold is beneficial in ROP. For ethylene polymerization (with DMAC/ETA), the imido complexes **3** and **5-7** showed very high catalytic activities of the order 0.9-1.5·10^7 g PE (mol V)$^{-1}$ bar^{-1} h^{-1}, which followed the trend **3** (*p*-Me) ≈ **5** (*p*-CF_3) > **7** (*p*-F) > **6** (*p*-Cl), whilst the activity associated **4** (*p*-OMe) was much lower and was thought to be due to its reduced electrophilicity. The product in each case was highly linear polyethylene. The ethylene polymerization runs were

conducted at the Russian Academy of Sciences in Novosibirsk by the group of Professor Konstantin Bryliakov.

4. References

[1] T. Czigány and F. Ronkay, *eXPRESS Polym. Lett*., 2020, 14, 510-511.

[2] For reviews, see (a) O. Dechy-Cabaret, B. Martin-Vaca and D. Bourissou, *Chem. Rev*., 2004, 104, 6147–6176; (b) M. Labet and W. Thielemans, *Chem. Soc. Rev*., 2009, 38, 3484–3504; (c) C. M. Thomas, *Chem. Soc. Rev*., 2010, 39, 165–173; (d) A. Arbaoui and C. Redshaw, *Polym. Chem*., 2010, 1, 801– 826; (e) Y. Sarazin and J.-F. Carpentier, *Chem. Rev*., 2015, 115, 3564−3614 and references therein.

[3] (a) M. Cozzolino, V. Leo, C. Tedesco, M. Mazzeo and M. Lamberti, *Dalton Trans*., 2018, 47, 13229-13238; (b) C. Redshaw, *Catalyst*, 2017, 7, 165 –176; (c) B. Antelmann, M. H. Chisholm, S.S. Iyer, J.C. Huffman, D. Navarro-Llobet, M. Pagel, W. J. Simonsick and W. Zhong, *Macromolecules*, 2001, 34, 3159–3175; (d). W. Braune and J. Okuda, *Angew. Chem. Int. Ed*., 2003, 42, 64–68.

[4] (a) F. Ge, Y. Dan, Y. Al-Khafaji, T. J. Prior, L. Jiang, M. R. J. Elsegood and C. Redshaw, *RSC Adv*., 2016, 6, 4792-4802; (b) C. Redshaw, *Dalton Trans*., 2016, 45, 9018 – 9030; (c) H. Ishikura, R. Neven, T. Lange, A. Galetová, B. Blom and D. Romano, *Inorg. Chimica Acta*, 2021, 515, 120047-120054.

[5] (a) Y. Onishi, S. Katao, M. Fujiki, and K. Nomura, *Organometallics*, 2008, 27, 2590-2596; (b) A. Arbaoui, D. Homden, C. Redshaw, J. A. Wright, S. H. Dale and M. R. J. Elsegood, *Dalton Trans*., 2009, 8911-8922; (c) S. Zhang and K. Nomura, *J. Am. Chem.*

Soc., 2010, 132, 4960-4965; (d) K. Nomura, A. Igarashi, S. Katao, W. Zhang and W.-H. Sun, *Inorg. Chem*., 2013, 52, 2607-2614; (e) X.-Y. Tang, A. Igarashi, W.-H. Sun, A. Inagaki, J. Liu, W. Zhang, Y.-S. Li and K. Nomura, *Organometallics*, 2014, 33, 1053-1060; (f) N. Diteepeng, X. Tang, X. Hou, Y.-S. Li, K. Phomphrai and K. Nomura, *Dalton Trans*., 2015, 44, 12273-12281; (g) K. Nomura, M. Oshima, T. Mitsudome, H. Harakawa, P. Hao, K. Tsutsumi, G. Nagai, T. Ina, H. Takaya, W.-H. Sun and S. Yamazoe, *ACS Omega,* 2017, 2, 8660-8673; (h) G. Zanchin, L. Vendier, I. Pierro, F. Bertini, G. Ricci, C. Lorber and G. Leone, *Organometallics*, 2018, 37, 3181-3195; (i) G. Zanchin, F. Bertini, L. Vendier, G. Ricci, C. Lorber and G. Leone, *Polym. Chem*., 2019, 10, 6200-6216.

[6] D. M. Homden and C. Redshaw, *Chem. Rev*., 2008, 108, 5086-5130.

[7] C. Redshaw, M. Walton, K. Michiue, Y. Chao, A. Walton, P. Elo, V. Sumerin, C. Jiang and M. R. J. Elsegood, *Dalton Trans*., 2015, 44, 12292-12303.

[8] C. Redshaw, M. Rowan, L. Warford, D. M. Homden, A. Arbaoui, M. R. J. Elsegood, S. H. Dale, T. Yamato, C. P. Casas, S. Matsui and S. Matsuura. *Chem. Eur. J*., 2007, 13, 1090-1107.

[9] B. Masci, Chapter 12 in *Calixarenes 2001*, Eds. M. -Z. Asfari, V. Böhmer, J. Harrowfield, J. Vicens and M. Saadioui, Springer, Netherlands, 2001.

[10] C. Redshaw, M. Walton, D. S. Lee, C. Jiang, M. R. J. Elsegood and K. Michiue, *Chem. Eur. J*., 2015, 21, 5199-5210.

[11] See for example, (a) M. A. Woodruff and D. W. Hutmacher, *Prog. Polym. Sci*., 2010, 35, 1217-1256; (b) Y. F. Al-Khafaji, F. H. Hussein in Green and Sustainable

Advanced Materials: Processing and Characterization, Eds. S. Ahmed and C. M. Hussain, Wiley, 2018, Chapter 6.

[12] M. Bochmann, G. Wilkinson, G. B. Young, M. B. Hursthouse and K. M. A. Malik, *J. Chem. Soc., Dalton Trans*., 1980, 1863-1871.

[13] (a) D. M. Miller-Shakesby, S. Nigam, D. L. Hughes, E. Lopez-Estelles, M. R. J. Elsegood, C. J. Cawthorne, S. J. Archibald and C. Redshaw. *Dalton Trans*., 2018, 47, 8992 – 8999. (b) W. Clegg, M. R. J. Elsegood, V. C. Gibson and C. Redshaw, *Dalton Trans*. 1998, 3037-3039; (c) N. Li, J.-J. Liu, J.-W. Sun, B.-X. Dong, L.-Z. Dong, S.-J. Yao, Z. Xin, S.-L. Li and Y.-Q. Lan, *Green Chem*. 2020, 22, 5325-5332; (d) X.-X. Yang, W.-D. Yu, X.-Y. Yi and C. Liu, *Inorg. Chem*. 2020, 59, 7512-7519.

[14] A. W. Addison, T. N. Rao, J. Reedijk, J. van Rijn, and G. C. Verschoor, *J. Chem. Soc. Dalton Trans*., 1984, 7, 1349-1356.

[15] T. Moriuchi and T. Hirao, *Coord. Chem. Rev*., 2011, 255, 2371– 2377.

[16] (a) D. D. Devore, J. D. Lichtenhan, F. Takusagawa and E. A. Maatta, *J. Am. Chem. Soc*., 1987, 109, 7408-7416. (b) E. A. Maatta, *Inorg. Chem.*, 1984, 23, 2560-2561.

[17] M. Lutz, H. Hagen, A. M. M. Schreurs and G. Van Koten, *Acta Crystallogr. Sect*. C, 1999, 55, 1636-1639.

[18] (a) P. Slavík and P. Lhoták, *Tet. Lett*. 2018, 59, 1757-1759; (b) P. Slavík, H. Dvořáková, M. Krupička and P. Lhoták, *Org. Biomed. Chem*., 2018, 16, 838-843.

[19] See for example, (a) K. Ding, M. O. Miranda, B. Moscato-Goodpaster, N. Ajellal, L. E. Breyfogle, E. D. Hermes, C. P. Schaller, S. E. Roe, C. J. Cramer, M. A. Hillmyer and W. B. Tolman, *Macromolecules*, 2012, 45, 5387-5396; (b) M. Normand, V. Dorcet, E.

Kirillov and J.-F. Carpentier, *Organometallics*, 2013, 32, 1694-1709; (c) Y. Huang, W. Wang, C.-C. Lin, M. P. Blake, L. Clark, A. D. Schwarz and P. Mountford, *Dalton Trans*., 2013, 42, 9313-9324; (d) A. Thevenon, C. Romain, M. S. Bennington, A. J. P. White, H. J. Davidson, S. Brooker and C. K. Williams, *Angew. Chem. Int. Ed*., 2016, 55, 8680-8685.

[20] (a) Q. Hu, S. -Y. Jie, P. Braunstein and B.-G. Lia Chinese *J. Polym. Sci*., 2020, 38, 240–247; (b) M. A. Woodruff and D. W. Hutmacher, *Prog. Polym. Sci.,* 2010, 35, 1217−1256; (c) T. Wu, Z. Wei, Y. Ren, Y. Yu, X. Leng and Y. Li, *Polym. Degrad. Stab.,* 2018, 155, 173−182; (d) M. T. Hunley, N. Sari, and K. L. Beers, *ACS Macro Lett*., 2013, 2, 375−379. (e) Z. Sun, Y. Zhao, O. Santoro, M. R. J. Elsegood, E. V. Bedwell, K. Zahra, A. Walton, and C. Redshaw, *Catal. Sci. Technol.*, 2020, 10, 1619−1639.

[21] (a) I. E. Soshnikov, N. V. Semikolenova, A. A. Shubin, K. P. Bryliakov, V. A. Zakharov, C. Redshaw and E. P. Talsi, *Organometallics*, 2009, 28, 6714–6720. (b) I. E. Soshnikov, N. V. Semikolenova, K. P. Bryliakov, A. A. Shubin, V. A. Zakharov, C. Redshaw and E. P. Talsi, *Macromol. Chem. Phys.*, 2009, 210, 542-548. (c) I. E. Soshnikov, N. V. Semikolenova, K. P. Bryliakov, V. A. Zakharov, C. Redshaw and E. P. Talsi, *J. Mol. Catal. A Chem.*, 2009, 303, 23–29.

Chapter 3

Co-polymerization of propylene oxide and CO_2 using early transition metal (groups IV and V) metallocalix[*n*]arenes (n = 4, 6, 8)

1. Introduction

Given the current issues associated with CO_2 pollution and the environment, there is now a pressing need to develop processes which can utilize and transform CO_2 into other useful materials such as urea, formic acid, dimethyl ether, urethane, isocyanate, and polyurethane, etc.[1] One such process of interest converts CO_2 into polycarbonates via coupling with an epoxide.[2] To-date, this has met with some success,[3] although the resulting polycarbonates have found limited application.[4] For example, salen complexes of the metals chromium and cobalt have been reported, and it was found that they can function as catalysts for the co-polymerization of CO_2 with propylene oxide under mild conditions (Chart 3-1).[5] The product selectivity was good with > 99% head-to-tail linkages observed, and very little cyclic carbonate was present (see B, Chart 3-1). The exploration of new catalysts for this process continues to attract much attention, and a range of metals have been employed from chromium through to zinc.[6] However, reports concerning the use of early transition metals, specifically of groups IV and V are scant.[7] In this chapter, the use of metallocalix[*n*]arenes as catalysts is investigated for this co-polymerization process, given that calixarenes have been described as pseudo oxide surfaces,[8] and that they have exhibited promising catalytic potential in a number of other processes.[9] Calix[*n*]arenes are phenolic macrocycles in which the *n* phenols can be linked via a variety of bridges.[10] In this chapter, the calixarenes shown in Chart 3-2 have been utilized, which differ in both size and the bridging group present. Only the use of the earth abundant metals titanium and vanadium has been investigated, given that the derived calix[*n*]arene species of both are relatively non-toxic[11] and readily accessible.[12] The complexes screened in this chapter are shown in Chart 3-3.

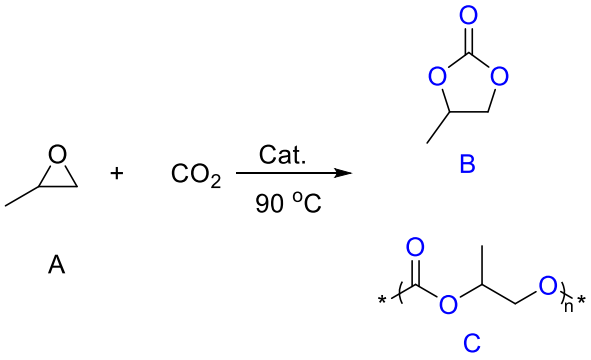

Chart 3-1. Co-polymerization of propylene oxide and CO_2.

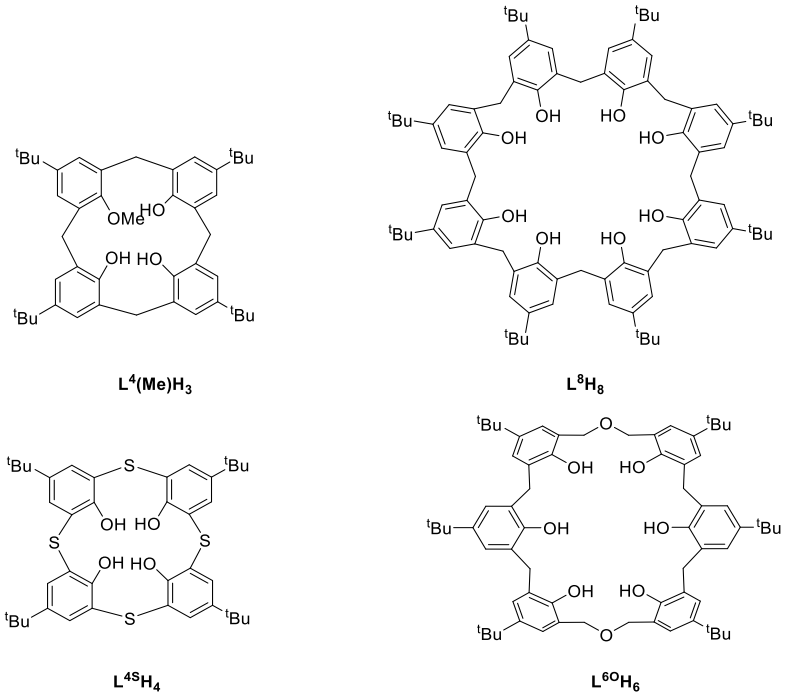

Chart 3-2. Calixarenes employed in the current chapter.

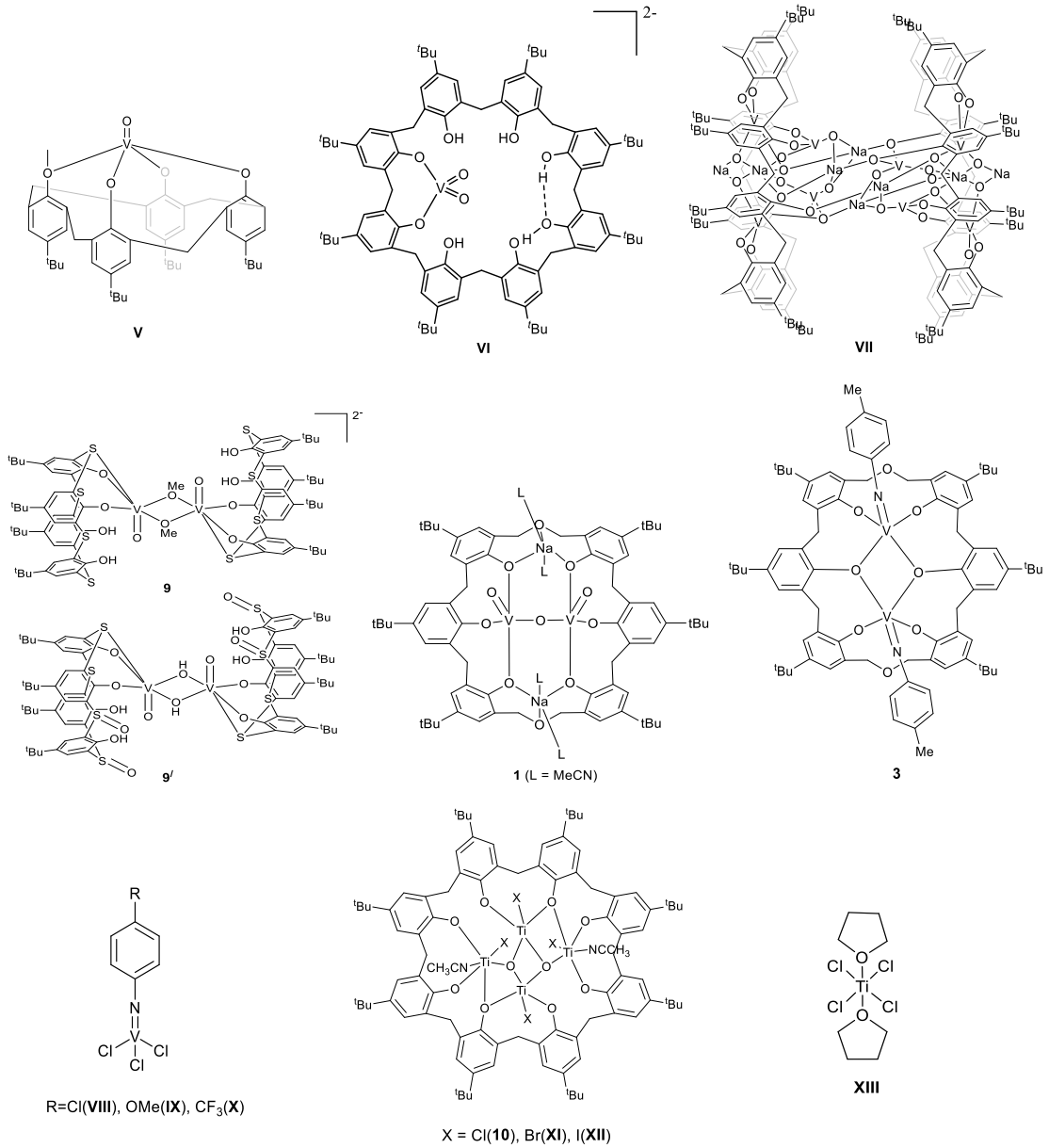

Chart 3-3. The metallocalix[4, 6, and 8]arenes screened herein and the non-calixarene precursors used as benchmarks.

2. Results and discussion

2.1 Vanadium complexes

Given the high activity exhibited for the coupling of epoxides and CO_2 by using vanadyl-containing chelating phenolate species catalyst, the current study investigated a number of vanadyl or vanadium imido containing calixarene systems.[7(j)] The known vanadyl p-*tert*-

butylcalix[4]arene [VO(L^4Me)] (**V**) was initially screened [13] however the results for the co-polymerization of propylene oxide with CO_2 using **V** were disappointing (Run 1, Table 3-1). Similar results were obtained using a VO_2 motif bound to the lower rim of a p-*tert*-butylcalix[8]areneH_8 ligand (derived from L^8H_8), *i.e*. complex **VI** (Run 2, Table 3-1). Then a complex containing multiple vanadyl centres was examined to ascertain if potential cooperativity between the metal centres would enhance the observed catalytic activity. In particular, complex **VII** bearing eight vanadium centres sandwiched between two L^{6O}-derived ligands was screened under the same conditions as for **V** and **VI**, but again only small amounts of polycarbonate (Run 3, Table 3-1) were isolated. Then a thia [-S-] bridged calixarene species was targeted, since changing to this type of bridge has proved beneficial in other catalytic processes,[14] and the bridging sulfur can help to stabilize novel motifs.[15] A new vanadyl complex **9** was isolated by reacting p-*tert*-butylthiacalix[4]areneH_4 ($L^{4S}H_4$) with [$VOSO_4$] in the presence of triethylamine in dry methanol under nitrogen. Following removal of the solvent, the residue was washed with acetonitrile to remove the known (blue) complex $[HNEt_3]_5[(VO)_5(\mu_3\text{-}O)_4(SO_4)_4]$.[16] Subsequent extraction of the remaining residue into dichloromethane afforded the methoxide-bridged salt $[HNEt_3]_2[VO(\mu\text{-}OMe)L^3H_2]_2\cdot 3CH_2Cl_2$ (**9**$\cdot 3CH_2Cl_2$) (*ca.* 15 %) as small, solvent dependent, yellow prisms. The crystals were subjected to a single crystal X-ray diffraction study using synchrotron radiation, and the molecular structure is shown in Figure 3-1, with selected bond lengths and angles given in the caption; crystallographic data are given in Table 8-5, Chapter 8. The molecule lies on a centre of symmetry, with three molecules of CH_2Cl_2 present; two in thiacalixarene cavities, making C–H···π interactions of 2.57 Å and 2.65 Å with rings C(1) >

C(6) and C(21) > C(26) respectively, and two half-occupied molecules *exo*. On each of the thiacalixarenes, two phenolic groups are not involved in bonding to the metal, but are involved in H-bonding to the two coordinated phenolate groups. The $[HNEt_3]^+$ cations are involved in H-bonding to the vanadyl oxygen atoms. Each thiacalix[4]arene cavity possesses a distorted elliptical conformation, with opposite centroid···centroid separations of 6.514 Å and 7.498 Å. This complex has geometrical parameters similar to the bridged hydroxide salt $[VO(\mu\text{-}OH)L^{TC}]_2[PPh_4]_2$, where L^{TC} = 2,2′-thiobis(2,4-di-*tert*-butylphenol), reported by Limberg *et al*.[17] The same group has also reported the structure of the oxo-bridged salt $[VO(\mu\text{-}O)L^{4S}H_2]_2[PPh_4]_2$.[18] The V···V distance [3.060(2) Å] in **9** is non-bonding, (*cf* 3.1705(4) Å in the Limberg hydroxo-bridged complex),[17] with the d^1 centres exhibiting weak antiferromagnetic coupling at ambient temperature (μ_{eff} = 2.06).

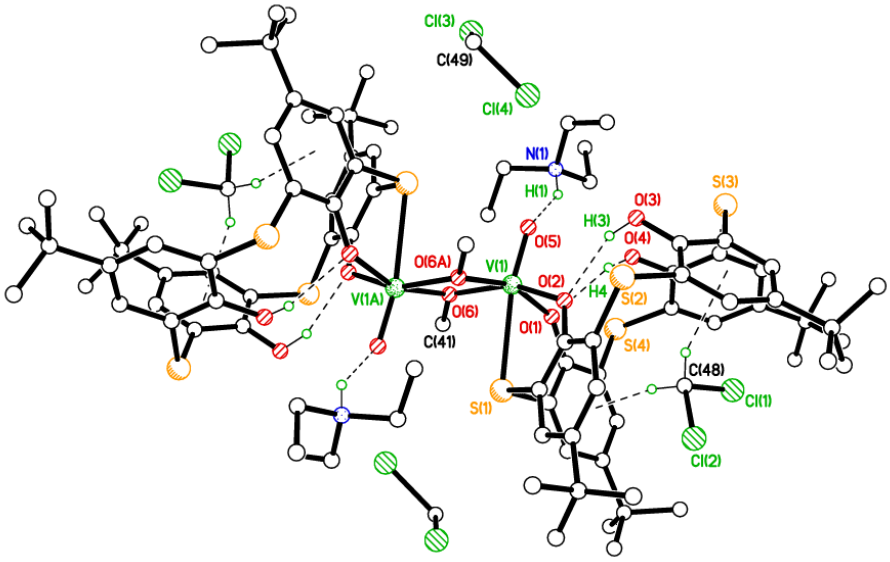

Figure 3-1. Molecular structure for the anion of **9**·$3CH_2Cl_2$. Non H-bonding H atoms removed for clarity. Selected bond lengths (Å) and angles (°): V(1)–O(1) 1.983(4), V(1)–O(2) 1.966(4), V(1)–O(5) 1.610(4), V(1)–O(6) 1.952(4), V(1)–O(6′) 1.970(4), V(1)–S(1) 2.801(2); O(1)–V(1)–O(2) 93.12(18), O(5)–V(1)–S(1) 169.41(16), V(1)–O(6)–V(1′) 102.55(18). Symmetry operator ′ = –x+1, –y+2, –z+1.

Interestingly, on one occasion, following work-up as described above, red/brown needles

were isolated which were found, by X-ray crystallography, to be the hydroxide-bridged dimeric structure $[VO(\mu\text{-}OH)L^{4S/}H_2]_2{\cdot}6CH_2Cl_2$ (**9′**$\cdot 6CH_2Cl_2$), where $L^{4S/}H_2$ is a partially oxidized form of the parent thiacalixarene L^3H_4. This partially oxidized ligand bears bridges of the form $S_2SO_{0.163}SO_{0.382}$, and presumably arises via the presence of adventitious oxygen present during the preparation (the parent $L^{4S}H_4$ appeared to contain no oxidized species). The molecular structure is shown in Figure 3-2, with selected bond lengths and angles given in the caption; crystallographic data are given in Table Table 8-5, Chapter 8.

In **9′**, each vanadium(V) is distorted octahedral and is bounded by two calix phenoxide oxygens, one of the thia calix sulfur bridges, the two hydroxide bridges, and a vanadyl group. The molecule lies on a centre of symmetry. Two calixarene phenol groups remain protonated and form intramolecular H-bonds with metal-coordinated phenolate neighbours, as seen in **9**. The bridging hydroxide forms a H-bond with one of the CH_2Cl_2 molecules. The CH_2Cl_2 molecule in the calixarene cavity forms C–H···π interactions with two C atoms, C(13) and C(16), in one calixarene phenolate ring with distances of 2.94 Å and 2.86 Å respectively. The V···V distance [2.7809(11) Å] in **9′** is non-bonding (*cf* 2.7453(6) Å in the Limberg oxo-bridged complex).[18]

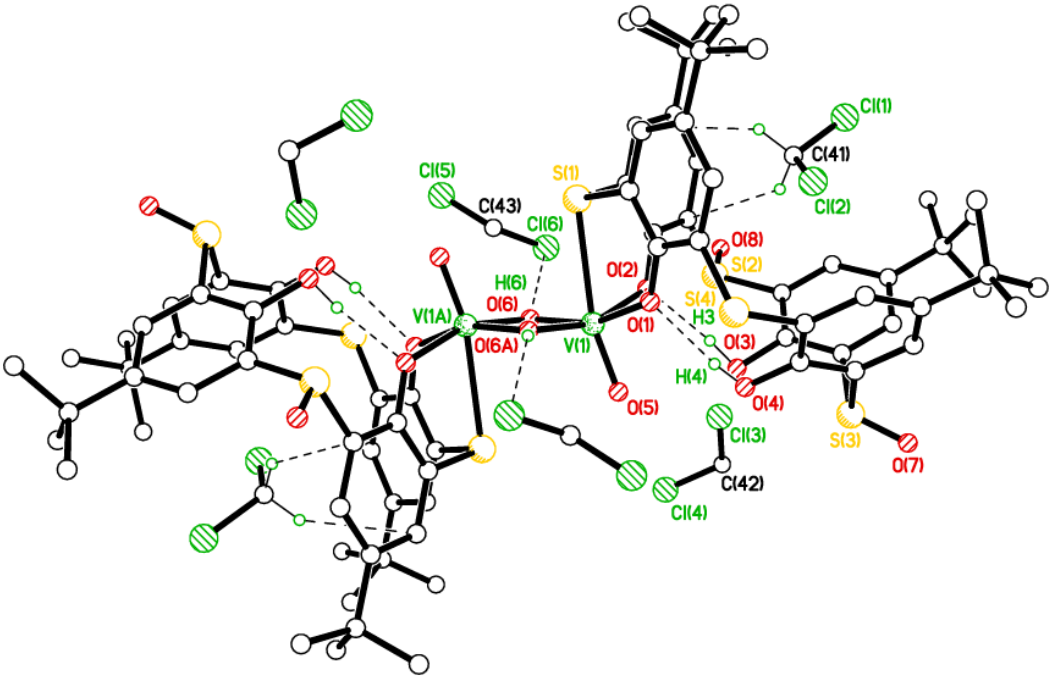

Figure 3-2. Molecular structure of **9**$^{/}$·6CH_2Cl_2. H atoms not involved in H-bonding omitted for clarity. Selected bond lengths (Å) and angles (^{o}): V(1)–O(1) 1.967(3), V(1)–O(2) 1.975(3), V(1)–O(5) 1.606(3), V(1)–O(6) 1.828(3), V(1)–O(6$^{/}$) 1.849(4), V(1)–S(1) 2.7604(10); O(1)–V(1)–O(2) 91.91(10), O(5)–V(1)–S(1) 166.54(9), V(1)–O(6)–V(1$^{/}$) 98.30(11). Symmetry operator $^{/}$ = –x, –y+1, –z.

Disappointingly, results from the screening utilizing this new thia-bridged species also proved to be poor (Run 4, Table 3-1) affording only 0.6 g of polycarbonate per g of catalyst. Furthermore, catalysts based on dimethyloxa (-CH_2OCH_2-) bridged calix[*n*]arenes have shown enhanced performance in other catalytic applications,[13] and so the known complexes **1** and **3** were prepared. Whilst the imido complex **3** was virtually inactive, slightly higher activity was observed for mixed-metal complex **1**, with a TON of 1.523 g/g_{Cat}.

To investigate whether the presence of the calixarene was detrimental to the process, a series of vanadium imido trichlorides was targeted, namely [V(*p*-RC_6H_4N)Cl_3] (R = Cl (**VII**), OMe (**IX**), CF_3 (**X**)).[19] All three of these imido trichlorides were either inactive or

extremely poor catalysts.

2.2 Titanium complexes

For titanium, work focused on titanocalix[8]arenes, namely {$(TiX)_2[TiX(NCMe)]_2(\mu_3\text{-}O)_2(L^2)$} (X = Cl (**10**), Br (**XI**), I (**XII**)) which were prepared, as reported elsewhere, by the interaction of $[TiX_4]$ with the parent p-*tert*-butylcalix[8]areneH_8 (L^8H_8) in toluene and subsequent crystallization from acetonitrile.[20] In the case of X = Cl, the reaction afforded orange/red crystals suitable for a single crystal X-ray diffraction study. The molecular structure was found to be {$(TiCl)_2[TiCl(NCMe)]_2(\mu_3\text{-}O)_2(L^2)$}·6.5(MeCN) **10**·6.5(MeCN), and is shown in Figure 3-3, with selected bond lengths and angles given in the caption; crystallographic data are given in Table 8-5, Chapter 8. For **10**·6.5(MeCN), two Ti_4 complexes and 13 MeCNs of crystallization are found in the asymmetric unit. Each molecule comprises a Ti_4O_4 ladder, with end chlorides 'up', and middle two chlorides 'down'. It is noteworthy that calix[8]arene titanium ladder complexes have recently been isolated and utilized for CO_2 photoreduction and photocatalytic H_2 production.[21] In **10**·6.5(MeCN), there are two triply-bridging oxo bridges, and terminal coordinated MeCNs on the two end Ti ions. Both independent molecules have the same basic arrangement of chlorides, oxos, and coordinated MeCNs. The diffraction data are twinned via twin law: [–1 0 0, 0 –1 0, 0.777 0 1] with a twin ratio 89.08:10.92(11)%. In the packing, the MeCNs of crystallization lie in the clefts of the calixarene ligand and between molecules. Molecules form slightly off-set stacks parallel to *b*. The coordinated MeCN H atoms make weak contacts with the chloride ligands on the next molecule in the stack with H···Cl distances of approx. 3.0 Å – see Figure 3-4.

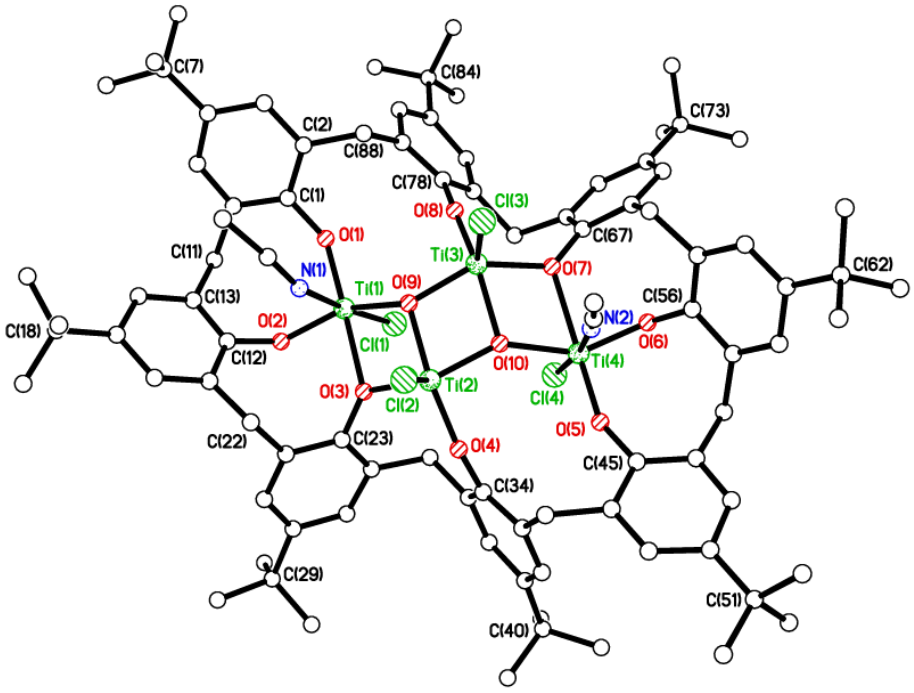

Figure 3-3. Molecular structure of $\{(TiCl)_2[TiCl(NCMe)]_2(\mu_3\text{-}O)_2(L^2)\}\cdot 6.5MeCN$ **10**·6.5MeCN. This is half of the asymmetric unit. There are two similar Ti_4 complexes and 13 MeCNs of crystallization in the asymmetric unit. H atoms and MeCNs of crystallization omitted for clarity. Selected bond lengths (Å) and angles (°): Ti(1)–O(1) 1.822(9), Ti(1)–O(2) 1.798(7), Ti(1)–O(3) 2.173(8), Ti(1)–O(9) 1.986(8), Ti(1)–Cl(1) 2.297(4), Ti(1)–N(1) 2.213(10), Ti(2)–O(3) 1.957(7), Ti(2)–O(4) 1.788(8), Ti(2)–O(9) 1.974(8), Ti(2)–O(10) 1.871(7), Ti(2)–Cl(2) 2.232(4); Ti(1)–O(1)–C(1) 146.6(7), Ti(1)–O(2)–C(12) 136.3(7), Ti(1)–O(3)–C(23) 124.7(6), Ti(2)–O(4)–C(34) 159.2(7), Ti(1)–O(3)–Ti(2) 103.0(3), Ti(1)–O(9)– Ti(3) 139.3(4), O(3)–Ti(2)–O(10) 137.4(3).

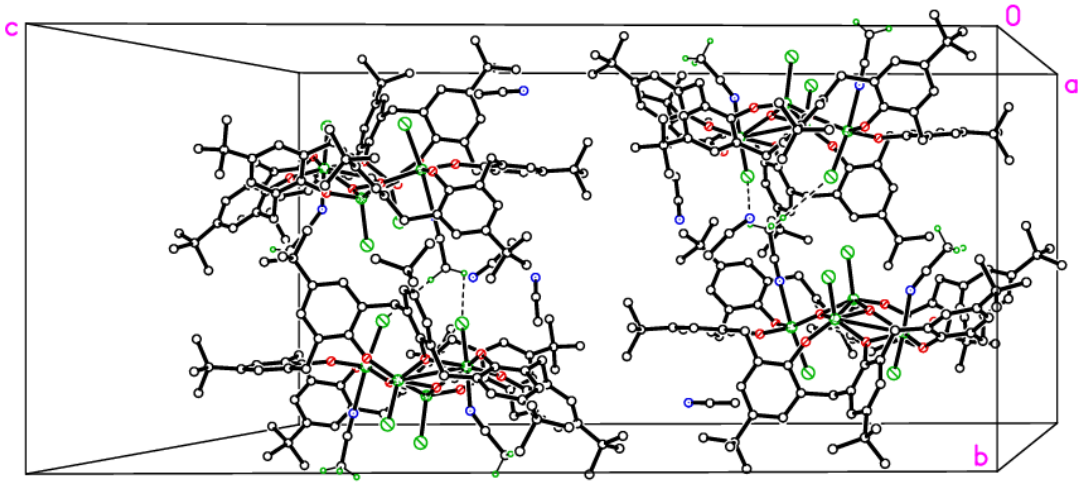

Figure 3-4. Stacking observed in **10**·6.5MeCN showing weak C–H···Cl interaction between a coordinated MeCN on one molecule and the two outer chlorides on the molecule above/below in the *b* direction.

2.3 Co-polymerization of propylene oxide with CO_2

The effect of the catalysts on the co-polymerization of propylene oxide with CO_2 were investigated, and the results are summarized in Table 3-1. All polymers obtained were of low polydispersity (PDI < 1.4), which suggested that these polymerizations occurred without significant side reactions. However, only low molecular weight oligomeric products ($M_n \leq 1665$ g·mol^{-1}) were obtained using the current systems. The absence of a co-catalyst herein such as PPNCl (bis(triphenylphosphine)iminium chloride) or *n*-Bu_4NCl may account for these low molecular weights and conversion. The screening of complexes **V**-**XIII**, **1**, **3**, **9** and **10** revealed that the complexes namely **1**, **10**, **XI** and **XII** herein, exhibited comparatively higher activities (TON > 1 g/g_{Cat}) under the conditions employed. For the vanadium catalysts, it was observed that the poly(propylene carbonate) oligomerization rate followed the order: **1** > **9**> **V**> **3**≈ **VI**> **VIII**> **X**> **VII**> **IX** and for titanium complex, the rate followed the order: **10**> **XI**> **XII**> **XIII**. The ^{1}H NMR spectra of the poly(propylene carbonate) indicated that the selectivity is relatively higher when using catalyst **XI (**Figure 3-5**)**. The generally accepted mechanism for the copolymerization of CO_2 and epoxides involves the alternate enchainment of CO_2 and the epoxide via insertion into either a metal alkoxide or carbonate bond (Chart 3-4). A growing polymer dissociates from an electron-rich metal center leading to the formation of cyclic carbonate.[22]

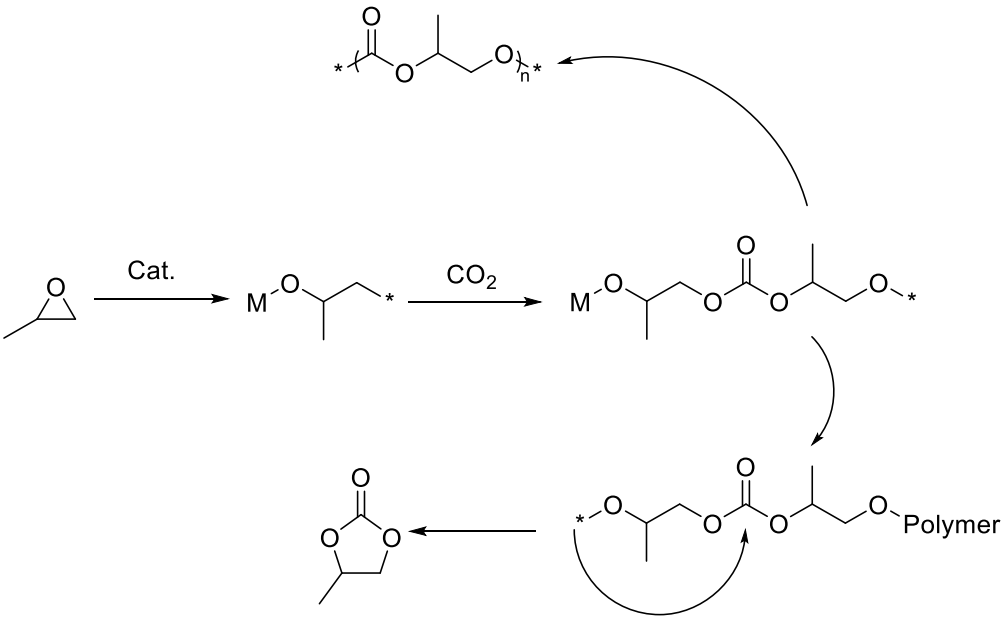

Chart 3-4. Mechanism for the copolymerization of propylene oxide and CO_2.

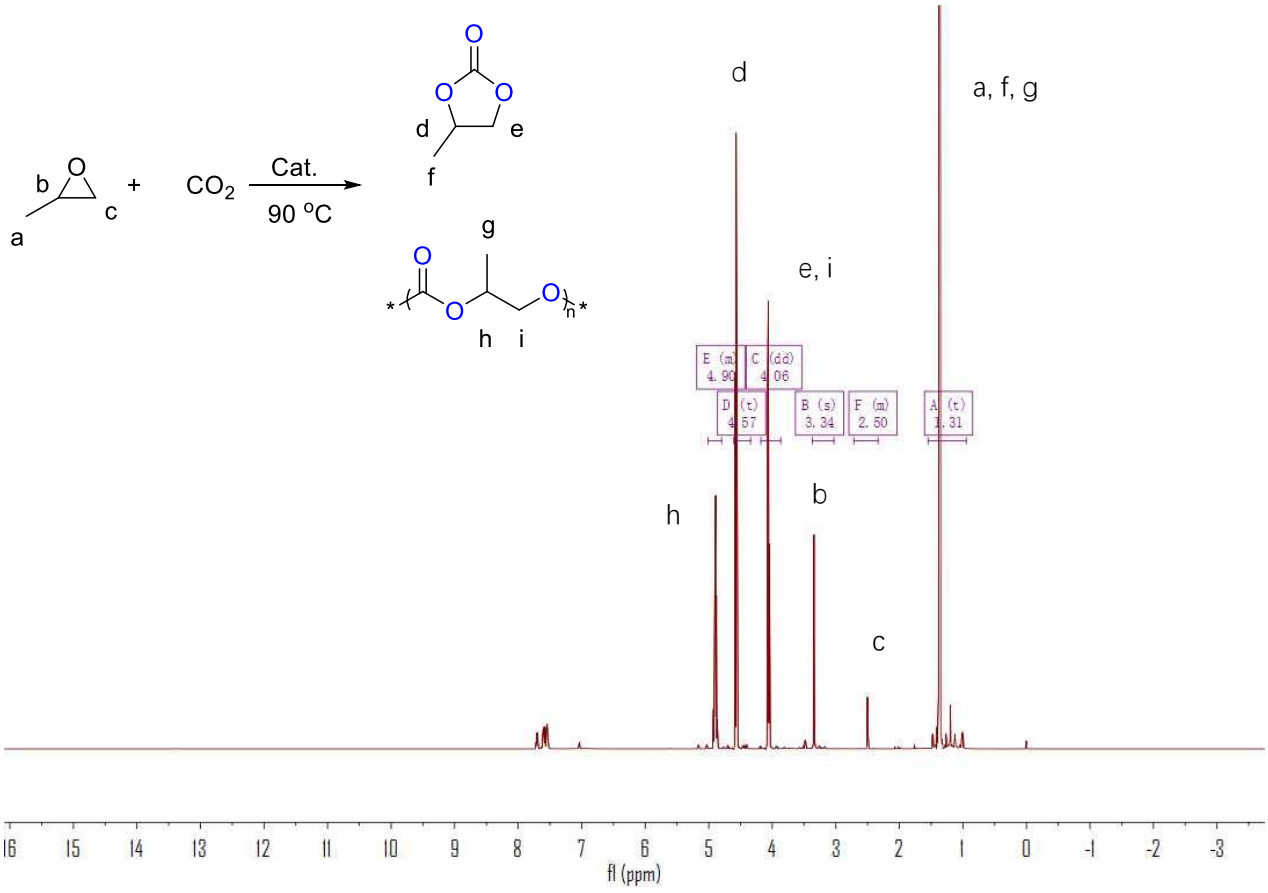

Figure 3-5. ^1H NMR spectrum ($CDCl_3$, 400 MHz, 298 K) of the cyclic/poly(propylene carbonate) synthesized with **XI** (run 12, Table 3-1).

Table 3-1. Results from the catalytic screen of complexes **V-XIII**, **1**, **3**, **9** and **10**.[a]

Run	Cat.[b]	S_B (10^5)[c]	m_B (mg) [d]	TON ($g/g_{Cat.}$)[d]	Selectivity (polymer, %)[e]	Yield (polymer, mg)[f]	M_n ($g \cdot mol^{-1}$)[g]	PDI[g]
1	**V**	7.13	12.24	0.122	62.5	7.62	420	1.05
2	**VI**	3.12	5.36	0.054	30.6	1.65	460	1.08
3	**VII**	0.18	0.31	0.003	55.7	0.17	415	1.34
4	**9**	13.55	23.29	0.233	44.6	10.39	1005	1.06
5	**1**	88.65	152.33	1.523	57.6	87.72	1250	1.03
6	**3**	3.22	5.53	0.055	32.8	1.80	700	1.20
7	**VIII**	1.05	1.80	0.018	20.5	0.37	710	1.11
8	**IX**	0	0	0	-	-	-	-
9	**X**	0.29	0.50	0.005	34.2	0.17	560	1.03
10	**10**	332.37	571.07	5.711	39.2	223.85	1655	1.19
11	**10**[h]	1120.00	1961.5	19.613	48.5	932.93	3515	1.12
12	**XI**	271.56	373.57	3.736	33.7	125.89	1025	1.22
13	**XII**	117.49	201.75	2.017	24.5	49.41	1020	1.25
14	**XIII**	0.69	1.18	0.012	32.8	0.39	835	1.09

Reaction conditions: [a] Propylene oxide: 5 mL, Temperature: 90 °C, Pressure of CO_2: 5 MPa, Reaction time: 6 h; [b] *Cat*.: 100 mg. [c] Measured by GC, S_B = integral area measured by GC; [d] m_B = the mass of afforded product, which derived from S_B; [e] Based on ^{1}H NMR spectroscopy; [f] Yield (polymer) = m_B ×Selectivity (polymer); [g] Determined by gel permeation chromatography in THF, PDI = (M_w/M_n); [h] Reaction performed with PPNCl present as co-catalyst.

Duan *et al* have explored the influence of the co-catalyst bis(triphenylphosphine)iminium chloride (PPNCl) on the copolymerization of propyleneoxide with CO_2 when using a cobalt catalyst bearing a salen-like ligand.[23] In their studies, it was observed that the use of increasing amounts of PPNCl led to enhanced catalytic performance, including an increase in the polymer molecular weight. With this in mind, PPNCl was employed herein with the best of the catalysts in this work, and it was also found that significant increases in polymer yield and molecular weight occur (see run 11, Table 3-1). Co-polymerization of propylene oxide and CO_2 catalyzed by metallocalix[n]arenes in the presence of PPNCl is speculated

as shown in Chart 3-5. The metallocalix[n]arenes serves as a Lewis acid and activates propylene oxide for ring-opening. The $[PPN]^+$ acts as a noncoordinating countercation for the Cl^- group, both of which can nucleophilically attack the metalcoordinated propylene oxide. Assisted by the Cl^- group, CO_2 was then inserted to form a carbonated ester cell, and the growing copolymer chain could migrate to another metal center and attack the activated propylene oxide. When propylene oxide and CO_2 were inserted into the carbonate chains alternately, the target copolymer was obtained.

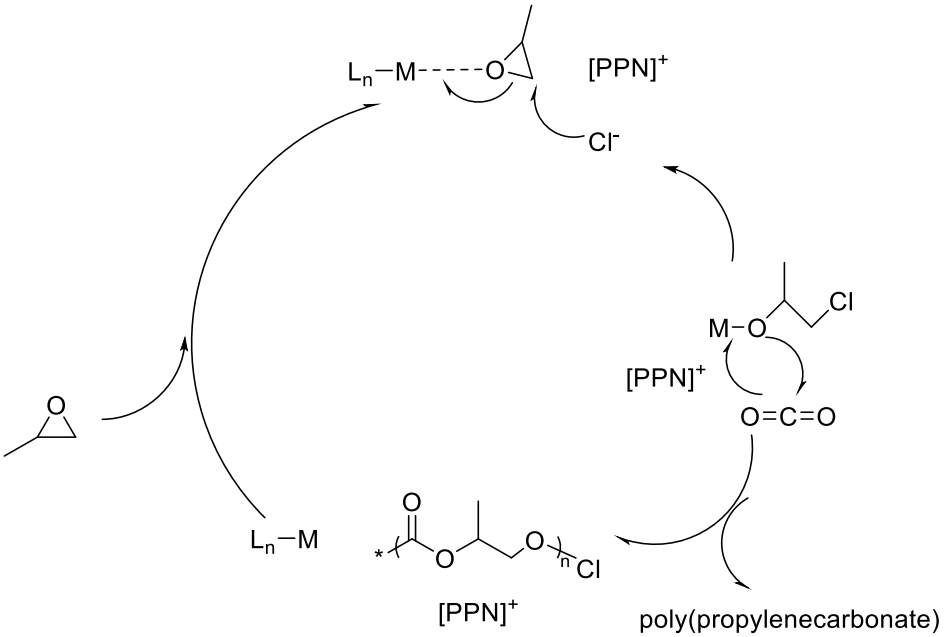

Chart 3-5. Mechanism for the copolymerization of propylene oxide and CO_2 with PPNCl co-catalyst.

3. Conclusions

In summary, a number of metallocalix[*n*]arenes, where n = 4, 6, or 8, of titanium and vanadium which act as catalysts for the co-polymerization of propylene oxide and CO_2 to cyclic polycarbonates have been synthesized. The vanadium-containing catalysts performed poorly affording, in the majority of cases, TONs less than 1 at 90 ℃ within 5 h.

In the case of the titanocalix[8]arenes, which all adopt a similar ladder-type structure, the activity under the same conditions is somewhat higher (TONs > 6) and follows the trend Cl > Br > I. The use of PPNCl significantly improved both the polymer yield and molecular weight.

4. References

[1] (a) T. Sakakura, J.–C. Choi and H. Yasuda, *Chem. Rev*., 2007, 107, 2365-2387. (b) M. T. Ravanchi and S. Sahebdelfar, *Appl. Petrochem. Res.*, 2014, 4, 63-77. (c) S. Liu and X. Wang, *Curr. Opin. Green Sustain. Chem.*, 2017, 3, 61-66.

[2] D. J. Darensbourg, *J. Chem. Educ*., 2017, 94, 1691-1695.

[3] (a) Z. Qin, C. M. Thomas, S. Lee and G. W. Coates, *Angew. Chemie Int. Ed.*, 2003, 42, 5484-5645. (b) C. T. Cohen, T. Chu and G. W. Coates, *J. Am. Chem. Soc.*, 2005, 127, 10869-10878. (c) K. Nakano, S. Hashimoto, M. Nakamura, T. Kamada and K. Nozaki, *Angew. Chemie Int. Ed.*, 2011, 50, 4868-4871. (d) M. R. Kember, A. Buchard and C. K. Williams, *Chem. Commun*., 2011, 47, 141-163. (e) P. P. Pescarmona and M. Taherimehr, *Catal. Sci Technol*., 2012, 2, 2169-2187. (f) Y. Liu, W.-M. Ren, W.-P. Zhang, R.-R. Zhao and X.-B. Lu, *Nat. Commun.*, 2015, 6, 8594-8602.

[4] See for example, (a) M. O. Sonnati, S. Amigoni, E. P. Taffin de Givenchy, T. Darmanin, O. Choulet and F. Guittard, *Green Chem*., 2013, 15, 283-306. (b) V. Besse, F. Camara, C. Voirin, R. Auvergne, S. Caillol and B. Boutevin, *Polym. Chem*., 2013, 4, 4545-4561.

[5] K. Xu, J.-G. Chen, W. Kuan, Z.-W. Liu, J.-Q. Jiang and Z.-T. Liu, *J. Macromol. Sci., A: Pure Appl. Chem.*, 2014, 51, 589-597.

[6] (a) N. Takeda and S. Inoue, *Makromol. Chem.* 1978, 179, 1377-1381. (b) X. Chen, Z. Shen and Y. Zhang, *Macromolecules*, 1991, 19, 5305-5308. (c) D. J. Darensbourg and M. W. Holtcamp, *Macromolecules*, 1995, *28*, 7577-7579. (d) M. Cheng, E. B. Lobkovsky and G. W. Coates, *J. Am. Chem. Soc.*, 1998, 120, 11018-11019. (e) M. Ree, J. Y. Bae, J. H. Jung and T. J. Shin, *Polym. Chem.*, 1999, 37, 1863-1876. (f) D. J. Darensbourg, J. R. Wildeson, J. C. Yarbrough and J. H. Reibenspies, *J. Am. Chem. Soc.*, 2000, 122, 12487–12496. (g) M. Cheng, D. R. Moore, J. J. Recaek, B. M. Chamberlain, E. B. Lobkovsky and G. W. Coates, *J. Am. Chem. Soc.*, 2001, 123, 8738–8749. (h) H. Sugimoto, H. Ohshima and S. Inoue, *J. Polym. Sci. A: Polym. Chem.*, 2003, 41, 3549-3555. (i) I. Kim, M. J. Yi, S. H. Byun, D. W. Park, B. U. Kim and C. S. Ha, *Macromol. Symp.*, 2005, 224, 181-192. (j) D. J. Darensbourg and D. R. Billodeaux, *Inorg. Chem.*, 2005, 44, 1433–1442. (k) X.-B. Lu, L. Shi, Y.-M. Wang, R. Zhang, Y.-J. Zhang, X.-J. Peng, Z.-C. Zhang and B. Li, *J. Am. Chem. Soc.*, 2006, 128, 1664–1674. (l) B. Li, R. Zhang and X.-B. Lu, *Macromolecules*, 2007, 40, 2303–2307. (m) B. Li, G.-P. Wu, W.-M. Ren, Y.-M. Wang, D.-Y. Rao and X.-B. Lu, *J. Polym. Sci. A: Polym. Chem.*, 2008, 46, 6102-6113. (n) B. Liu, Y. Gao, X. Zhao, W. Yan and X. Wang, *J. Polym. Sci. A: Polym. Chem.*, 2010, 48, 359-365. (o) G.-P. Wu, S.-H. Wei, W.-M. Ren, X.-B. Lu, T.-Q. Xu and D. J. Darensbourg, *J. Am. Chem. Soc.*, 2011, 133, 15191–15199. (p) P. K. Saini, C. Romain and C. K. Williams, *Chem. Commun*, 2014, 50, 4164-4167. (q) G. Trott, P. K. Saini and C. K. Williams, *Philos Trans A Math Phys Eng Sci*., 2016, 374, 20150085-20150104. (r) Y. Wang and D. J. Darensbourg, *Coord. Chem. Rev*., 2018, 372, 85-100. (s) B. Grignard, S. Gennen, C. Jérôme, A. W. Kleij and C. Detrembleur, *Chem. Soc. Rev*., 2019, 48, 4466-4514.

[7] (a) K. Nakano, K. Kobayashi and K. Nozaki, *J. Am. Chem. Soc*., 2011, 133, 10720–10723. (b) C. Y. Li, C. J. Yu and B. T. Ko, *Organometallics*, 2013, 32, 172–180. (c) C.–K. Su, H.–J. Chuang, C.–Y. Li, C. –Y. Yu, B.–T. Ko, J.–D. Chen and M.–J. Chen, *Organometallics*, 2014, 33, 7091–7100. (d) Y. Wang, Y. Qin, X. Wang and F. Wang, *Catal. Sci. Technol*., 2014, 4, 3964-3972. (e) C. C. Quadri and E. Le Roux, *Dalton Trans*., 2014, 43, 4242-4246. (f) Y. Wang, Y. Qin, X. Wang and F. Wang, *ACS Catal*., 2015, 5, 393–396. (g) M. Mandel and D. Chakraborty, *J. Polym. Sci., Part A: Polym, Chem*., 2015, 54, 809-824. (h) J. Hessevik, R. Lalrempula, H. Nsiri, K. W. Tornroos, V. R. Jensen and E. Le Roux, *Dalton Trans*., 2016, 45, 14734-14744. (i) J. A. Garden, A. J. P. White and C. K. Williams, *Dalton Trans*., 2017, 46, 2532-2541. (j) C. Miceli, J. Rintjema, E. Martin, E. C. Escudero-Adán, C. Zonta, G. Licini and A. W. Kleij, *ACS Catal.*, 2017, 7, 2367–2373.

[8] C. Floriani, D. Jacoby, C.-V. Angiola and C. Guastini, *Angew. Chem. Int. Ed.*, 1989, 28, 1376-1377.

[9] D. M. Homden and C. Redshaw, *Chem. Rev.*, 2008, 108, 5086–5130.

[10] B. KÖnig and M. H. Fonseca, *Eur. J. Inorg. Chem*., 2000, 2000, 2303-2310.

[11] (a) C. Redshaw, M. R. J. Elsegood, J. A. Wright, H. Baillie-Johnson, T. Yamato, S. De Giovanni and A. Mueller, *Chem. Commun.*, 2012, 48, 1129-1131. (b) D. M. Miller-Shakesby, S. Nigam, D. L. Hughes, E. Lopez-Estelles, M. R. J. Elsegood, C. J. Cawthorne, S. J. Archibald and C. Redshaw, *Dalton Trans.*, 2018, 47, 8992-8999.

[12] A. Arduini, A. Casnati in Macrocycle Synthesis, Ed. D. Parker, Oxford University Press, New York, 1996, Chapter 7.

[13] C. Redshaw, M. A. Rowan, L. Warford, D. M. Homden, A. Arbaoui, M. R. J. Elsegood, S. H. Dale, T. Yamato, C. P. Casas, S. Matsui and S. Matsuura, *Chem. Eur. J.*, 2007, 13, 1090–1107.

[14] C. Redshaw, L. Clowes, D. L. Hughes, M. R. J. Elsegood and T. Yamato, *Organometallics*, 2011, 30, 5620–5624.

[15] (a) N. Morohashi, F. Narumi, N. Iki, T. Hattori and S. Miyano, *Chem. Rev*., 2006, 106, 5291–5316. (b) R. Kumar, Y. O. Lee, V. Bhalla, M. Kumar and J. S. Kim, *Chem. Soc. Rev*., 2014, 43, 4824-4870.

[16] A. Ignaszak, M. Radtke, M. R. J. Elsegood, J. W. A. Frese, J. L. Z. F. Lipman, T. Yamato, S. Sanz, E. Brechin, T. J. Prior and C. Redshaw, *Dalton Trans.*, 2018, 47, 15983-15993.

[17] C. G. Werncke, C. Limberg, C. Knispel and S. Mebs, *Chem. Eur. J*., 2011, 17, 12129-12135.

[18] E. Hoppe and C. Limberg, *Chem. Eur. J*. 2007, 13, 7006-7016.

[19] B. Masci, *J. Org. Chem.*, 2001, 66, 4, 1497-1499.

[20] O. Santoro, M. R. J. Elsegood, E. V. Bedwell, J. A. Pryce, and C. Redshaw, *Dalton Trans.*, 2020, 49, 11978-11996.

[21] (a) N. Li, J. –J. Liu, J. –W. Sun, B. –X. Dong, L. –Z. Dong, S. –J. Yao, Z. Xin, S. –L. Li and Y. Q. Lan, *Green Chem*., 2020, 22, 5325-5332. (b) X.-X Yang, W.-D. Yu, X.-Y. Yi and C. Liu, *Inorg. Chem*. 2020, 59, 7512–7519. (c) X.-X Yang, W.-D. Yu, X.-Y. Yi, L. –J. Li and C. Liu, *Chem Commun*. 2020, 56, 14035-14038.

[22] R. L. Paddock and S. T. Nguyen, *Macromolecules*, 2005, 38, 15, 6251–6253.

[23] J. Huang, Y. Xu, M. Wang and Z. Duan, *J. Macromol. Sci. Part A: Pure & Applied Chem.*, 2020, 57, 131-138.

Chapter 4

Titanium complexes bearing oxa- and azacalix[4, 6]arenes: structural studies and use in the ring opening homo-/co-polymerization of cyclic esters

1. Introduction

Calix[*n*]arenes are a family of macrocyclic molecules consisting of phenol units linked most commonly by methylene (-CH_2-) bridges at their *ortho* positions, and have found a range of applications in supramolecular and coordination chemistry.[1] Investigations into their coordination chemistry have shown that their potential in areas such as catalysis can be greatly improved if the methylene bridges are replaced by heteroatom-containing bridges such as thia (-S-), sulfinyl (-SO-), sulfonyl (-SO_2-) or dimethyleneoxa (-CH_2OCH_2-), which can potentially bind to the metal.[2] Interestingly, there is a lack of such studies involving dimethyleneoxa (-CH_2OCH_2-) containing calix[*n*]arenes, where n ≥6.[3] Furthermore, there is even less data on azacalix[*n*]arenes, where the bridge (-NR-) has an addition group (R) bound to the nitrogen which can potentially be varied to control the sterics and/or electronics of the system.[4] Given this, the current chapter discusses work on the coordination chemistry of both dimethyloxa- and azacalix[*n*]arenes with a view to investigating their potential as catalysts for the ring opening polymerization (ROP) of cyclic esters. Given recent successes using titanocalix[*n*]arenes for ROP (see Chart 4-1),[5] the work here focuses on titanium-containing dimethyloxa- and azacalixarenes, and a number of interesting poly-metallic species (see Chart 4-2) have been structurally characterized. The ability of these complexes to act as catalysts for the ROP of *ε*-caprolactone (*ε*-CL), *δ*-valerolactone (*δ*-VL) and *rac*-lactide (*r*-LA) has been investigated; the copolymerization of *ε*-CL and *r*-LA was also investigated.

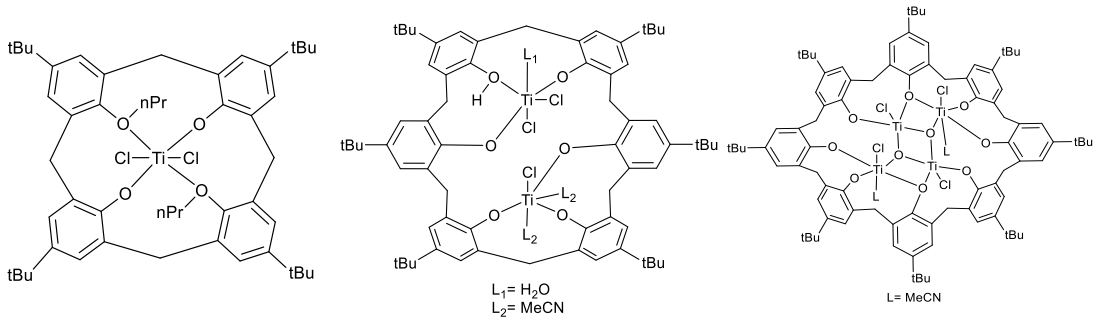

Chart 4-1. Known titanium calixarene pre-catalysts for the ROP of cyclic esters.

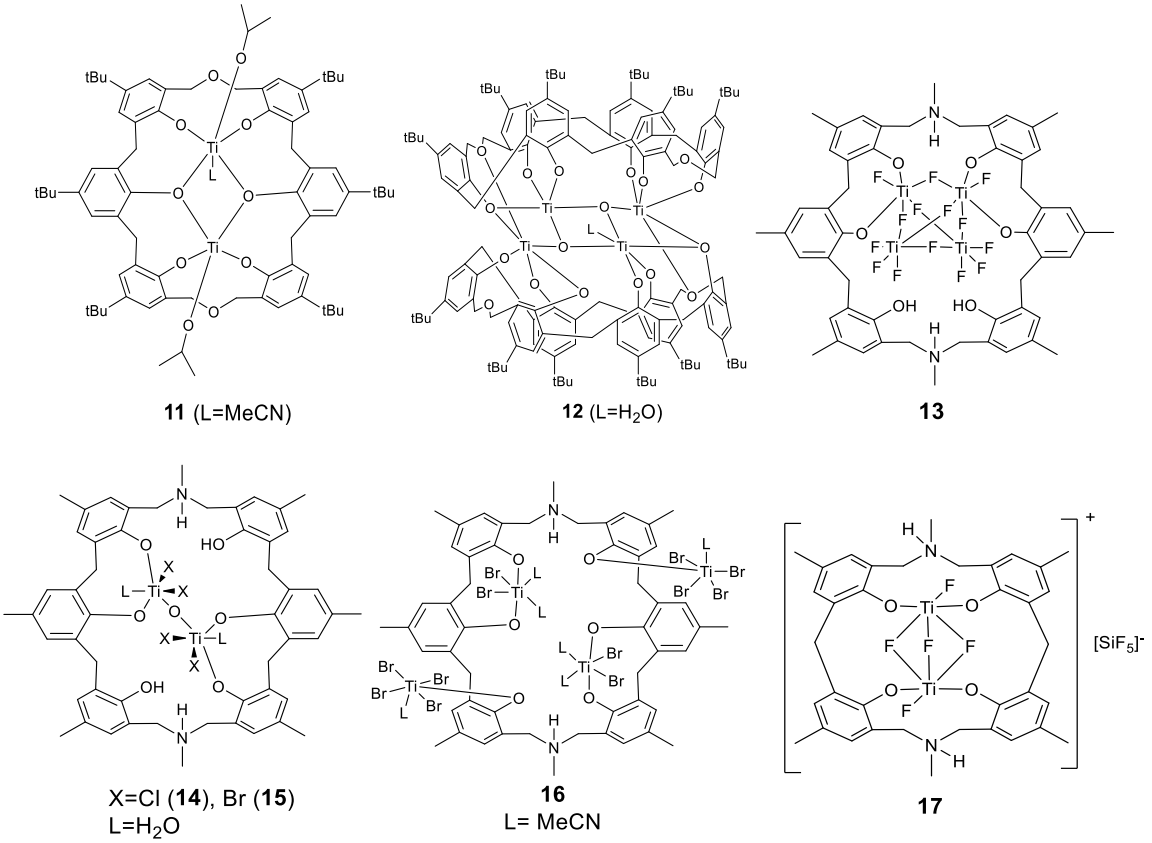

Chart 4-2. Pre-catalysts prepared in Chapter 4.

2. Results and Discussion

2.1 Syntheses and solid-state structures

2.1.1 Dioxacalix[6]arene complexes

Interaction of an excess (3 equiv.) of [Ti(O*i*Pr)$_4$] with p-*tert*-butyltetrahomodioxacalix[6]areneH$_6$ (L^{6O}H$_6$) in refluxing toluene afforded, after work-up

in MeCN, the orange complex $[Ti_2(OiPr)_2(MeCN)L^{6O}]\cdot 3.5MeCN$ (**11**·3.5MeCN) in 52% yield. The molecular structure is shown in Figure 4-1, with selected bond lengths and angles given in the caption; crystallographic data are given in Table 8-6. The complex contains two titanium centres, one of which, Ti(1), is distorted octahedral bound by an isopropoxide ligand, an acetonitrile ligand and four calixarene phenoxide oxygens in a square plane, two of which are shared with Ti(2). Ti(2) is five-coordinate and adopts a slightly distorted rectangular pyramidal ($\tau = 0.015$).[6]

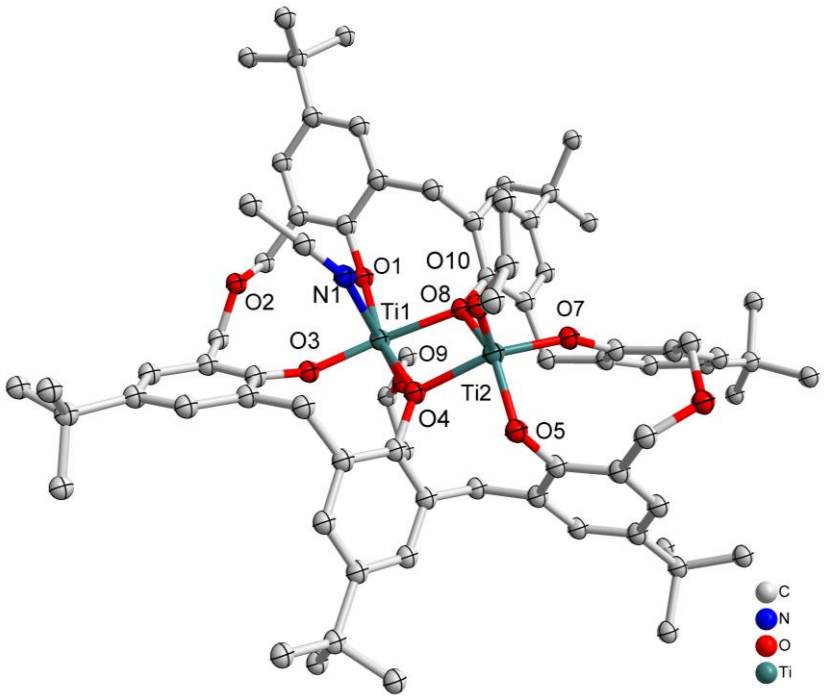

Figure 4-1. Molecular structure of $[Ti_2(OiPr)_2(MeCN)L^{6O}]\cdot 3.5MeCN$ (**11**·3.5MeCN). Solvent molecules and hydrogen atoms omitted for clarity. Selected bond lengths: O(1)-Ti(1) 1.828(3), O(3)-Ti(1) 1.844(3), O(4)-Ti(2) 2.029(3), O(4)-Ti(1) 2.070(3), O(5)-Ti(2) 1.877(3), O(7)-Ti(2) 1.821(3), O(8)-Ti(2) 2.019(3), O(8)-Ti(1) 2.081(3), O(9)-Ti(1) 1.796(3), O(10)-Ti(2) 1.764(3), Ti(2)-O(4)-Ti(1) 106.35(13), Ti(2)-O(8)-Ti(1) 106.31(13), O(9)-Ti(1)-O(1) 99.39(14), O(9)-Ti(1)-O(3) 99.09(13), O(1)-Ti(1)-O(3) 102.70(13), O(9)-Ti(1)-O(4) 94.94(12) O(1)-Ti(1)-O(4) 159.26(12), O(3)-Ti(1)-O(4) 89.65(12).

If the reaction is conducted in the presence of adventitious oxygen/water and using only two equivalents of $[Ti(OiPr)_4]$, then the isopropoxide groups are lost and a structure

involving a titanium-oxygen Ti_4O_4 ladder sandwiched between two oxacalix[6]arenes is formed, namely $[Ti_4O_4(L^{6O})_2]$·MeCN (**12**·MeCN). The molecular structure is shown in Figure 4-2, with selected bond lengths and angles given in the caption. It is noted that calix[8]arene titanium ladder complexes have recently been isolated and utilized for ROP, CO_2 photoreduction and photocatalytic H_2 production.[5b, 7]

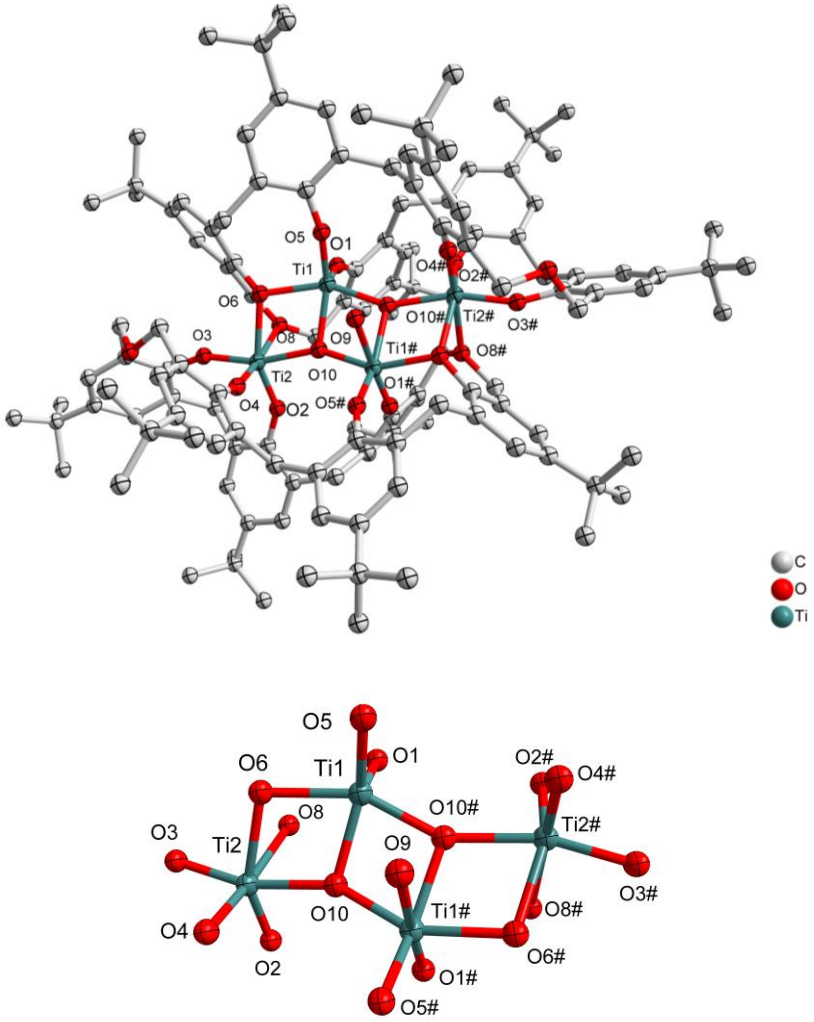

Figure 4-2. Left: molecular structure of $[Ti_4O_4(L^1)_2]$·MeCN (**12**·MeCN); Right: core of the structure. Solvent molecules and hydrogen atoms omitted for clarity; Selected bond lengths: O(9)-Ti(1) 2.313(6), O(1)-Ti (1) 1.785(3), O(2)-Ti (2) 1.814(3), O(3)-Ti (2) 1.818(3), O(4)-Ti(2) 1.803(3), O(5)-Ti(1) 1.788(3), O(10)-Ti(1) 1.890(3), O(6)-Ti(1) 2.032(3), C(1)-O(1)-Ti(1) 152.1(3), C(12)-O(2)-Ti(2) 147.4(3), C(23)-O(3)-Ti(2) 155.7(3), C(35)-O(4)-Ti(2) 163.6(3), C(46)-O(5)-Ti(1) 163.4(3), C(57)-O(6)-Ti(1) 122.3(2), O(1)-Ti(1)-O(5) 103.74(15), O(1)-Ti(1)-O(10) 95.97(14), O(5)-Ti(1)-O(10) 105.68(14), O(1)-Ti(1)-O(6) 95.53(12), O(5)-Ti(1)-O(6) 95.36(13), O(10)-Ti(1)-O(6) 152.80(12).

2.1.2 Azacalixarene complexes

Reaction of *p-methyl*-dimethyldiazacalix[6]areneH$_6$ ($L^{6N}H_6$) with four equivalents of [TiF_4] in refluxing toluene afforded the orange complex [$Ti_4F_{14}L^{6N}H_2(H)_2$]·2.5MeCN (**13**·2.5MeCN). The molecular structure is shown in Figure 4-3, with selected bond lengths and angles given in the caption. The complex contains four distorted octahedral titanium centres each linked via fluoride bridges to give a central Ti_4F_{14} core. The azacalixarene acts as a bidentate *O*,*O*-chelate to Ti(1) and to Ti(2), leaving two uncoordinated phenolic groups on the macrocycle. The ^{1}H NMR spectroscopic data are consistent with the solid-state structure, whilst in the ^{19}F NMR spectrum, only 3 distinct fluorine broad resonances are observed. In the EI mass spectrum, a peak is observed at 1283 Da assigned to the molecular ion –2.5MeCN+Na^+.

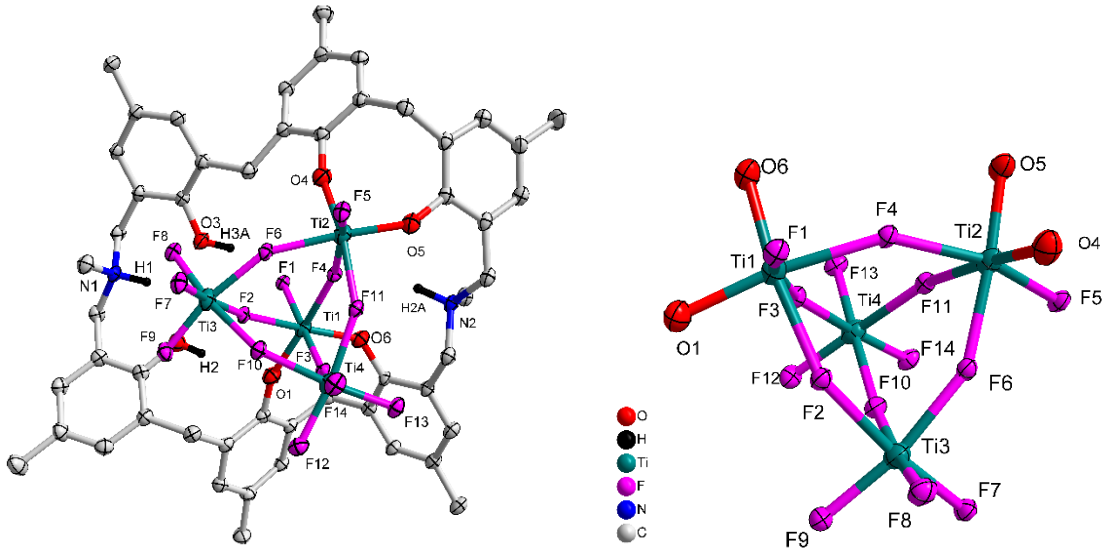

Figure 4-3. Left: molecular structure of [$Ti_4F_{14}L^{6N}H_2(H)_2$]·2.5MeCN (**13**·2.5MeCN); Right: core of the structure. Solvent molecules and hydrogen atoms omitted for clarity; Selected bond lengths: Ti(1)-O(2) 1.762(2), Ti(1)-O(3) 1.822(2), Ti(1)-F(1) 1.8342(19), Ti(1)-F(14) 2.0018(18), Ti(1)-F(3) 2.0315(19), Ti(1)-F(2) 2.0326(19), Ti(2)-F(6) 1.771(2), Ti(2)-F(5) 1.780(2), Ti(2)-F(4) 1.781(2), Ti(2)-F(3) 1.944(2), Ti(2)-F(8) 1.9679(18), Ti(2)-F(12) 1.988(2), O(2)-Ti(1)-O(3) 95.06(11), O(2)-Ti(1)-F(1) 98.77(10), O(3)-Ti(1)-F(1) 97.97(9),

O(2)-Ti(1)-F(14) 94.02(9), O(3)-Ti(1)-F(14) 91.73(9), F(1)-Ti(1)-F(14) 163.16(9), O(2)-Ti(1)-F(3) 87.41(10), O(3)-Ti(1)-F(3) 175.51(9), F(1)-Ti(1)-F(3) 85.33(8), F(6)-Ti(2)-F(5) 97.59(10), F(6)-Ti(2)-F(4) 96.63(10), F(5)-Ti(2)-F(4) 95.67(10), F(6)-Ti(2)-F(3) 167.61(9).

Treatment of $L^{6N}H_6$ with two equivalents of $[TiCl_4(THF)_2]$ in refluxing toluene afforded, after work-up (MeCN), dark red prisms of $[Ti_2Cl_4(H_2O)_2OL^{6N}H_2(H)_2]\cdot 5MeCN$ (**14**·5MeCN) in 41% yield. The molecular structure is shown in Figure 4-4, with selected bond lengths and angles given in the caption. The complex contains two distorted octahedral titanium centres linked via a near linear oxo bridge [Ti(1)-O(7)-Ti(2) 168.84(6)º]. The coordination at each Ti centre is completed by two adjacent phenoxides of the calixarene, a water molecule and two chlorides, one of which is found *trans* to the oxo bridge. The titanium phenoxide bond lengths are typical [1.8324(11) – 1.8975(11) Å], whilst those to the water ligands are, as expected, somewhat longer [2.1445(12) and 2.1570(11) Å].[5b,8] The overall charge is balanced by the protonated aza bridges of the calixarene.

Similar treatment of $L^{6N}H_6$ with two equivalents of $[TiBr_4]$ resulted in the isostructural complex $[Ti_2Br_4(H_2O)_2OL^{6N}H_2(H)_2]\cdot 2MeCN$ (**15**·4.5MeCN) in 32% yield. The molecular structure is shown in Figure 4-5, with selected bond lengths and angles given in the caption. As in **14**, a linear oxo bridge [Ti(2)-O(7)-Ti(1) 172.65(17)º] links the two distorted octahedral centres, and a bromide at each Ti centre can be found *trans* to the μ_2-O. The Ti-O bond length range is similar to that in **14**.

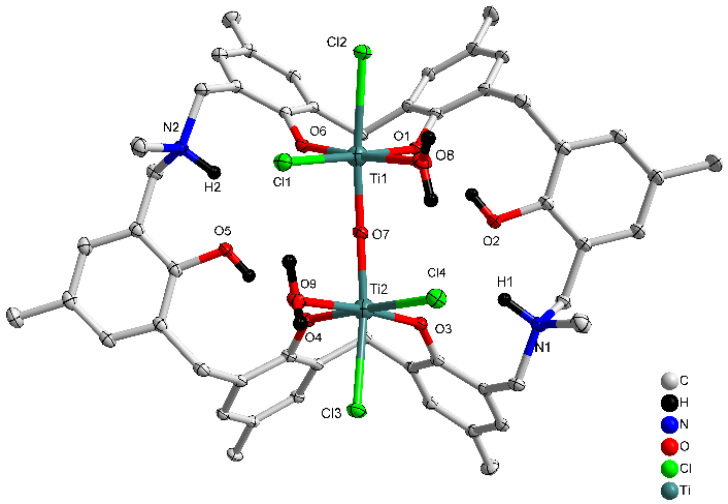

Figure 4-4. Molecular structure of $[Ti_2Cl_4(H_2O)_2OL^{6N}H_2(H)_2]\cdot 5MeCN$ (**14**·5MeCN). Solvent molecules and hydrogen atoms omitted for clarity; Selected bond lengths: O(1)-Ti(1) 1.8975(11), O(3)-Ti(2) 1.8341(11), O(4)-Ti(2) 1.8809(11), O(6)-Ti(1) 1.8324(11), O(7)-Ti(1) 1.8202(10), O(7)-Ti(2) 1.8245(10), Cl(1)-Ti(1) 2.4861(5), Cl(2)-Ti(1) 2.4311(5), Cl(3)-Ti(2) 2.4104(4), Cl(4)-Ti(2) 2.4863(5), Ti(1)-O(8) 2.1445(12), Ti(2)-O(9) 2.1570(11), Ti(1)-O(7)- Ti(2) 168.84(6), O(7)- Ti(1)-O(6) 99.11(5), O(7)-Ti(1)-O(1) 92.62(5), O(6)-Ti(1)-O(1) 98.13(5), O(7)-Ti(1)-O(8) 85.85(5), O(6)-Ti(1)-O(8) 172.84(5), O(1)-Ti(1)-O(8) 86.74(5) O(7)-Ti(1)-Cl(2) 170.03(4), O(6)-Ti(1)-Cl(2) 90.54(4), O(1)-Ti(1)-Cl(2) 88.45(3) O(8)-Ti(1)-Cl(2) 84.32(4).

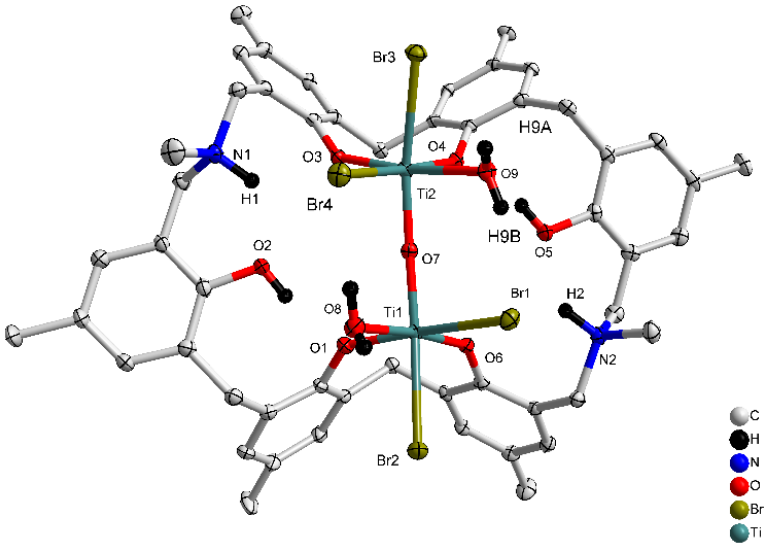

Figure 4-5. Molecular structure of $[Ti_2Br_4(H_2O)_2OL^{6N}H_2(H)_2]\cdot 4.5MeCN$ (**15**·4.5MeCN). Solvent molecules and hydrogen atoms omitted for clarity; Selected bond lengths: O(1)-Ti(1) 1.883(3), O(3)-Ti(2) 1.825(3), O(4)-Ti(2) 1.869(3), O(6)-Ti(1) 1.828(3), O(7)-Ti(2) 1.817(3), O(7)-Ti(1) 1.817(3), Br(1)-Ti(1) 2.6748(8), Br(2)-Ti(1) 2.6040(9), Br(3)-Ti(2) 2.5796(9), Br(4)-Ti(2) 2.6647(9), Ti(1)-O(8) 2.134(3), Ti(2)-O(9) 2.152(3), Ti(2)-O(7)-Ti(1) 172.65(17), O(7)-Ti(1)-O(6) 100.63(13), O(7)-Ti(1)-O(1) 94.90(12), O(6)-Ti(1)-O(1) 99.19(13), O(7)-Ti(1)-O(8) 86.50(13), O(6)-Ti(1)-O(8) 171.03(13), O(1)-Ti(1)-O(8)

85.49(13), O(7)-Ti(1)-Br(2) 168.80(9), O(6)-Ti(1)-Br(2) 89.29(9), O(1)-Ti(1)-Br(2) 88.59(9), O(8)-Ti(1)-Br(2) 83.15(9), O(7)-Ti(1)-Br(1) 88.29(8), O(6)-Ti(1)-Br(1) 91.97(8), O(1)-Ti(1)-Br(1)167.59(10), O(8)-Ti(1)-Br(1) 82.74(9).

Reaction of $L^{6N}H_6$ with excess [$TiBr_4$] led to the isolation of the orange complex [$Ti_4Br_{12}L^{6N}(H)_2(MeCN)_6$]·7MeCN (**16**·7MeCN) in 26% isolated yield. A view of the molecular structure is shown in Figure 4-6, with selected bond lengths and angles given in the caption. The asymmetric unit of **16**·7MeCN contains two independent half molecules each comprising one half a p-methyldimethyldiazacalix[6]arene and two Ti ions (Ti1 and Ti2 in first half molecule; Ti3 and Ti4 in second half molecule). The complete molecule in each case is generated by the inversion centre. The two half molecules are similar but are not related by symmetry. In each, the two octahedral Ti ions have different environments. One (Ti1 or Ti3) is coordinated by four bromide ions in a square plane, with O from the calix and $NCCH_3$ in a *trans* arrangement. The calixarene is twisted so that the phenoxide points away from the centre of the molecule and places Ti1 and Ti1_i on opposite sides of the plane of the calixarene (symmetry operation i = 1–x, –y, –z). A very similar arrangement is observed for Ti3 and Ti3_ii (symmetry operation ii = 2–x, 1–y, 1–z). The second Ti ion (Ti2 & Ti4) is coordinated in an 8-membered chelate ring, by two geminal phenoxides from the calixarene, two *cis* $NCCH_3$ in approximately the same plane, and two *trans* bromide ions. The twisted orientation of the calixarene allows for the formation of an N–H···Br hydrogen bond from the protonated aza linkage.

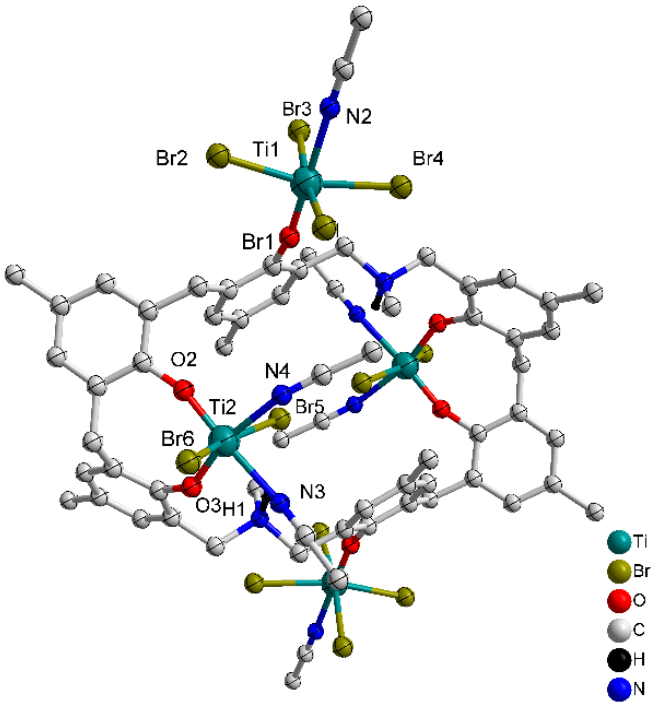

Figure 4-6. Molecular structure of $[Ti_4Br_{12}L^{6N}(H)_2(MeCN)_6]\cdot 7MeCN$ (**16**·7MeCN). Solvent molecules and hydrogen atoms omitted for clarity; Selected bond lengths: Ti(1)-O(1) 1.779(4), Ti(1)-N(2) 2.236(6), Ti(1)-Br(2) 2.4939(13), Ti(1)-Br(1) 2.5058(15), Ti(1)-Br(3) 2.5064(15), Ti(1)-Br(4) 2.5423(13), Ti(2)-O(2) 1.755(4), Ti(2)-O(3) 1.820(4), Ti(2)-N(4) 2.194(5), Ti(2)-N(3) 2.245(5), Ti(2)-Br(6) 2.4998(11), Ti(2)-Br(5) 2.5280(11), O(1)-Ti(1)-N(2) 176.3(2), O(1)-Ti(1)-Br(2) 98.72(14), N(2)-Ti(1)-Br(2) 82.18(15), O(1)-Ti(1)-Br(1) 97.79(15), N(2)-Ti(1)-Br(1) 85.75(17), Br(2)-Ti(1)-Br(1) 90.42(5), O(1)-Ti(1)-Br(3) 91.34(15), O(2)-Ti(2)-O(3) 98.68(18), O(2)-Ti(2)-N(4) 94.27(19), O(3)-Ti(2)-N(4) 165.59(19), O(2)-Ti(2)-N(3) 175.84(18), O(3)-Ti(2)-N(3) 85.48(17), N(4)-Ti(2)-N(3) 81.58(19), O(2)-Ti(2)-Br(6) 95.06(14).

When $L^{4N}H_4$ was treated with four equivalents of $[TiF_4]$, orange prisms were isolated on work-up, albeit in poor yield (< 20%). A crystal structure determination revealed the complex to be $[Ti_2F_2(\mu\text{-}F)_3L^{4N}(H)_2(SiF_5)]\cdot 2MeCN$ (**17**·2MeCN), see Figure 4-7. In **17**·2MeCN, triply bridging fluorides link two distorted octahedral Ti centers, with a terminal fluoride and two adjacent phenoxides of the macrocycle completing the coordination sphere at each metal centre. The SiF_5^- ion is thought to result from the scavenging of HF formed during the reaction. This reaction is performed in a glass vessel without added base, the scavenging of HF can occur via the following reaction: $5HF + SiO_2$

$\rightarrow 2H_2O + H^+ + SiF_5^-$.[9]

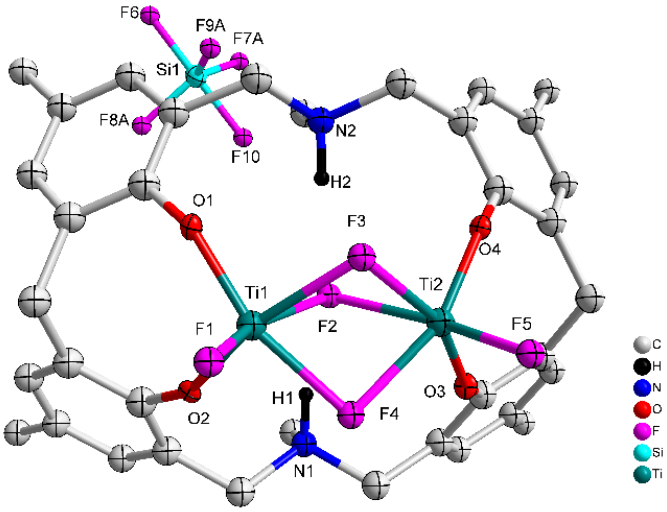

Figure 4-7. Molecular structure of $[Ti_2F_2(\mu\text{-}F)_3L^{4N}(H)_2(SiF_5)]\cdot 2MeCN$ (**17**·2MeCN). Solvent molecules and hydrogen atoms omitted for clarity; Selected bond lengths: O(1)-Ti(1) 1.792(5), O(2)-Ti(1) 1.801(4), O(3)-Ti(2) 1.789(4), O(4)-Ti(2) 1.791(5), F(1)-Ti(1) 1.802(3), F(2)-Ti(1) 2.035(3), F(2)-Ti(2) 2.064(3), F(3)-Ti(2) 2.023(4), F(3)-Ti(1) 2.049(4), F(4)-Ti(1) 2.012(4), F(4)-Ti(2) 2.055(4), F(5)-Ti(2) 1.799(3), O(1)-Ti(1)-O(2) 97.67(19), O(1)-Ti(1)-F(1) 100.70(19), O(2)-Ti(1)-F(1) 101.88(19), O(1)-Ti(1)-F(4) 162.69(19), F(1)-Ti(1)-F(4) 90.92(16), O(1)-Ti(1)-F(2) 91.46(18), F(1)-Ti(1)-F(2) 159.36(16), O(2)-Ti(1)-F(4) 92.36(18), (4)-Ti(1)-F(2) 73.92(15), O(2)-Ti(1)-F(2) 92.85(17).

2.2 Ring opening polymerization studies

General: The performance of these complexes to act as catalysts for the ring opening polymerization (ROP) of *ε*-caprolactone (*ε*-CL), *δ*-valerolactone (*δ*-VL) and *rac*-lactide (*r*-LA), with one equivalent of benzyl alcohol (BnOH) per titanium present, has been investigated. The co-polymerization of *ε*-caprolactone and *rac*-lactide has also been investigated.

2.2.1 ROP of *ε*-caprolactone (*ε*-CL)

Complexes **11**-**17** were screened for their ability to polymerise ε-caprolactone and the results are collated in Table 4-1. The polymerization screening indicated that the best

conditions were 250 equivalents of ε-caprolactone to titanium at 130 °C. The activity of complex **11** increased with temperature and peaked at 250 equivalents of monomer. Complex **11** was also active at low catalyst loading leading to 80.4% conversion after 8 h for 1000 equivalents of monomer. All polymers obtained were of relatively low polydispersity (PDI < 1.75), which suggested that these polymerizations occurred without significant side reactions. The M_n were found to be much lower than the calculated values, which may be rationalized in terms of intramolecular transesterification during the propagation process. The initiation may occur through insertion of monomer into each Ti–O bond, these steps triggering independent polymerization processes (proceeding each via a coordination-insertion mechanism) as well as intramolecular transesterification processes involving the two polymer chains growing at the same Ti centre.[10] Interestingly, complex **11** proved to be active also under aerobic conditions achieving 84% conversion during 8 h (Table 4-1, run 7), which may suggest that the dioxacalix[6]arene based complexes **11** and **12** can tolerate air/water during the ROP catalysis.

After 8 h, the screening of complexes **11**-**17** (Table 4-1, run 1-13) revealed that the titanium-based L^{6O} complexes namely **11** and **12** herein, exhibited higher activities than other complexes under the conditions employed. After 24 h (Table 4-1), complexes **13**, **14** and **17** afforded relatively lower conversions (<90%), whereas higher conversions (>90%) were reached using complexes **11**, **12**, **15** and **16**, under similar conditions. From a kinetic study (Figure 4-8), it was observed that the PCL polymerization rate followed the order: **12**> **11**> 1**5**≈ 1**6**> **14**> **13**> **17**. Compared with the larger titanocalix[6]arene complexes (complexes **11**-**16**), complex **17** was found to be relatively inactive (Table 4-1, run 13 and 20),

presumably due to the its low solubility in toluene. The observed activity of complex **12** surpassed that of the other complexes screened herein, and this may be attributed to the arrangement of and distance between the Ti centers.[5(b)] The higher activity of the chloro- (**14**) and bromo- (**15**, **16**) azacalixarene titanium complexes compared with that of fluoro- (**13**) compound can be explained considering the lability of the ligands present. This is in line with our recent study on titanocalix[4]arenes, in which the presence of a labile ligand (*i.e*. MeCN and H_2O) proved beneficial for the catalyst activity.[5] MALDI-ToF mass spectra of the PCL indicated the presence of an BnO end group (e.g. Figure 4-9), which agrees with the ^{1}H NMR spectra (e.g. Figure 4-9) and indicates that the polymerization proceeded via a coordination insertion mechanism. Indeed, the MALDI-ToF spectrum of the sample displayed a major series of peaks separated by 114 m/z units accountable to two OH terminated PCL *n*-mers (M = 17 (OH)+ 1(H) + n × 114.14 (CL) + 22.99 (Na^+)) and there is a part of peaks consistent with the polymer terminated by OH and BnO end groups (M = n × 114.12 (CL) + 108.05 (BnOH) + 22.99 (Na^+)).

Table 4-1. ROP of ε-CL using **11** – **17**.

Run	Cat.	CL: Ti: BnOH	T/°C	t/h	Conv[a] (%)	$M_{n,GPC}\times10^{-3}$[b]	$M_w\times10^{-3}$[b]	$M_{n,Cal}\times10^{-3}$[c]	PDI[d]
1	**11**	1000: 1: 1	130	8	80.4	7.10	9.71	91.98	1.37
2	**11**	500: 1: 1	130	8	84.9	8.44	13.41	48.66	1.59
3	**11**	250: 1: 1	130	8	92.3	10.58	18.43	26.55	1.74
4	**11**	100: 1: 1	130	8	93.4	5.04	6.54	10.87	1.30
5	**11**	250: 1: 1	100	8	74.2	4.87	5.49	21.38	1.13
6	**11**	250: 1: 1	80	8	28.3	2.95	3.43	8.28	1.16
7	**11**[e]	250: 1: 1	130	8	85.4	9.43	12.03	24.58	1.27
8	**12**	250: 1: 1	130	8	93.5	12.54	15.20	26.89	1.21
9	**13**	250: 1: 1	130	8	62.3	4.37	6.43	17.99	1.47
10	**14**	250: 1: 1	130	8	67.5	6.19	9.97	19.47	1.50
11	**15**	250: 1: 1	130	8	77.1	8.21	12.32	22.21	1.61
12	**16**	250: 1: 1	130	8	84.2	8.84	13.09	24.10	1.48
13	**17**	250: 1: 1	130	8	25.3	-	-	-	-

14	**11**	250: 1: 1	130	24	>99	11.43	16.32	28.46	1.42
15	**12**	250: 1: 1	130	24	>99	13.34	23.14	28.46	1.73
16	**13**	250: 1: 1	130	24	76.4	6.78	7.93	22.01	1.17
17	**14**	250: 1: 1	130	24	82.5	8.40	11.11	23.75	1.32
18	**15**	250: 1: 1	130	24	96.4	8.28	11.64	27.72	1.41
19	**16**	250: 1: 1	130	24	>99	10.04	15.82	28.46	1.58
20	**17**	250: 1: 1	130	24	34.6	2.28	2.63	9.98	1.15
21	**11**	250: 1: 0	130	24	71.6	4.30	5.20	20.49	1.20
22	**12**	250: 1: 0	130	24	74.7	6.13	7.01	21.37	1.14
23	**13**	250: 1: 0	130	24	59.1	2.38	3.62	16.92	1.52
24	**14**	250: 1: 0	130	24	63.8	3.42	5.51	18.26	1.61
25	**15**	250: 1: 0	130	24	69.2	4.18	5.79	19.80	1.39
26	**16**	250: 1: 0	130	24	62.8	4.85	5.78	17.97	1.19
27	**17**	250: 1: 0	130	24	-	-	-	-	-

[a] Determined by ^{1}H NMR spectroscopy. [b] $M_{n/w}$, GPC values corrected considering Mark–Houwink factor (0.56) from polystyrene standards in THF. [c] Calculated from ([monomer]$_0$/Ti) × conv (%) × monomer molecular weight (M_{CL}=114.14) + Molecular weight of BnOH. [d] From GPC. [e] Reaction performed in air. Solvent used in the ROP: toluene.

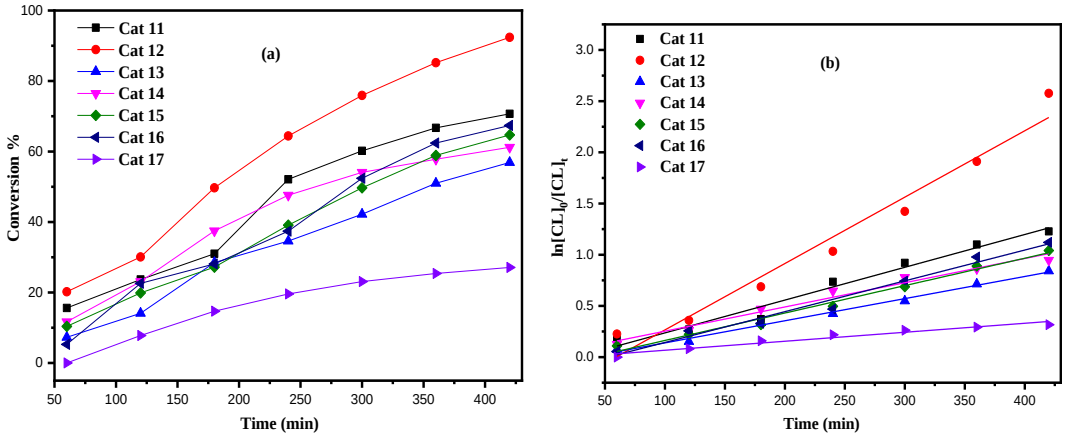

Figure 4-8. (a) Relationship between conversion and time for the polymerization of ε-CL by using complex **11-17**; (b) Plot of ln[CL]$_0$/[CL]$_t$ vs. time for the polymerization of ε-CL by using complexes **11-17**; Conditions: T=130 ºC, $n_{Monomer}$: n_{Ti}: BnOH=250 : 1: 1.

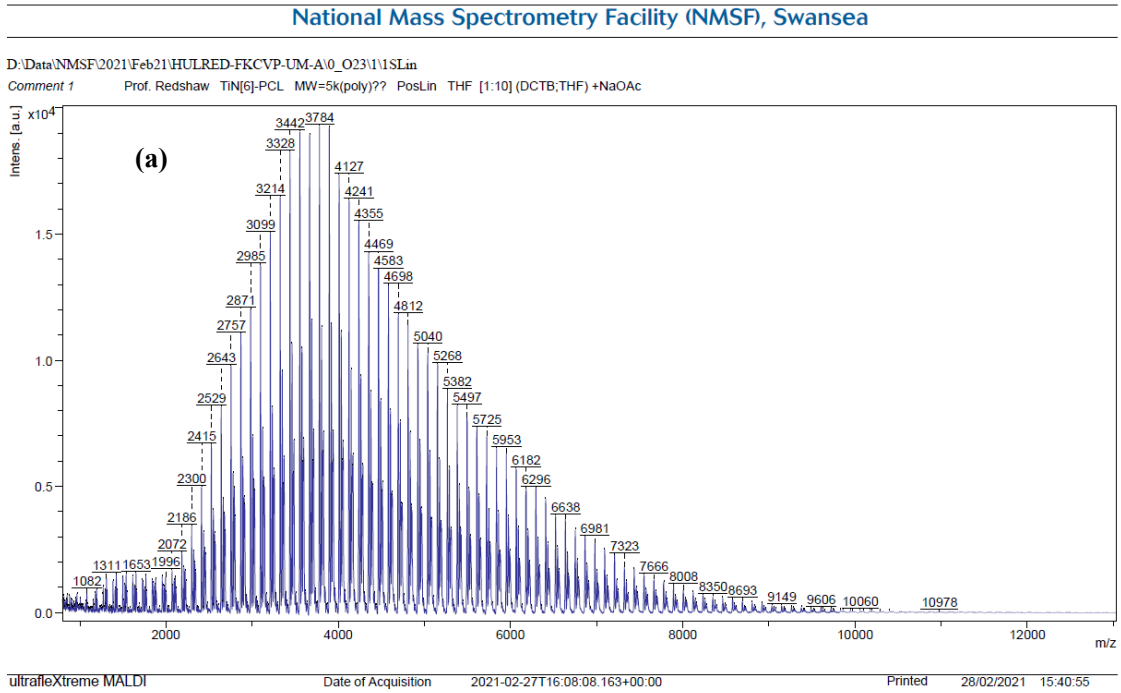

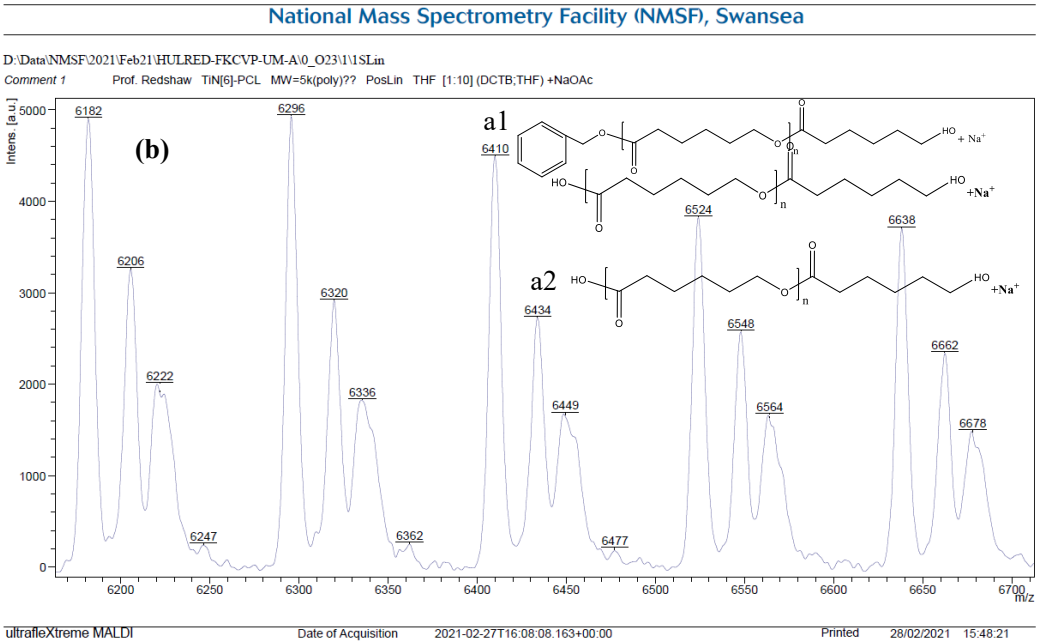

Figure 4-9. (a) Mass spectrum of PCL synthesized with **14**/BnOH (run 10, Table 1) (0-12000 m/z); (b) Mass spectrum of PCL synthesized with **14**/BnOH (run 10, Table 1) (6200-6700 m/z).

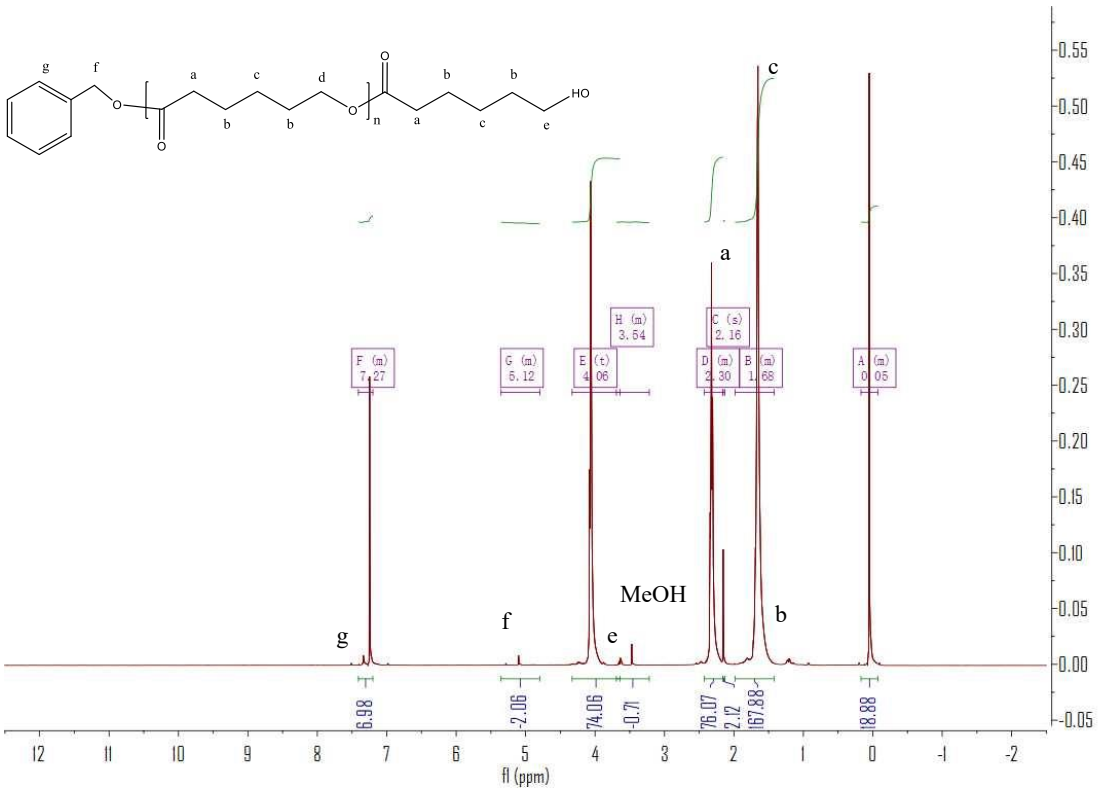

Figure 4-10. ^{1}H NMR spectrum ($CDCl_3$, 400 MHz, 298 K) of the PCL synthesized with **11**/BnOH (run 17, Table 4-1).

2.2.2 ROP of δ-valerolactone (δ-VL)

Furthermore, complexes **11**-**17** were also evaluated as catalysts, in the presence of one equivalent of BnOH, for the ROP of δ-VL (Table 4-2). Using compound **11**, the conditions of temperature and [Ti]: [δ-VL] were varied. On increasing the temperature to 130 °C and lowering the monomer to catalyst ratio, best results were achieved at 130 °C using [Ti]:[δ-VL] at 1:250 over 8 h. As in the case of the ROP of ε-CL, kinetic studies (Figure 4-11) revealed that the catalytic activities followed the order: **12**> **11**> **15**≈ **16**> **14**> **13**> **17**. As for the ROP of ε-Cl, there was evidence of significant transesterification and nearly all observed M_n values were significantly lower than the calculated values. The MALDI-ToF mass spectra (Figure 4-12) exhibited a major family of peaks consistent with BnO end groups [M = 108.05 (BnOH) + n × 100.12 (VL) + 22.99 (Na^+)], and a minor family assigned

to cyclic PVL. The ^{1}H NMR spectra of the PVL also indicated the presence of a BnO end group (e.g. Figure 4-13).

Table 4-2. ROP of δ-VL using **11** – **17**.

Run	Cat.	VL: Ti: BnOH	T/°C	t/h	Conv[a]	$M_{n,GPC}\times10^{-3}$[b]	$M_w\times10^{-3}$[b]	$M_{n,Cal}\times10^{-3}$[c]	PDI[d]
1	**11**	1000: 1: 1	130	8	81.2	11.56	18.23	81.30	1.58
2	**11**	500: 1: 1	130	8	80.1	12.27	17.54	40.10	1.43
3	**11**	250: 1: 1	130	8	89.4	13.49	27.46	22.38	2.03
4	**11**	100: 1: 1	130	8	86.7	5.84	8.12	8.68	1.38
5	**11**	250: 1: 1	100	8	68.1	4.06	4.67	17.05	1.15
6	**11**	250: 1: 1	80	8	-	-	-	-	-
7	**11**[e]	250: 1: 1	130	8	74.6	10.23	14.56	18.67	1.42
8	**12**	250: 1: 1	130	8	90.8	16.44	32.07	22.73	1.95
9	**13**	250: 1: 1	130	8	64.6	6.36	8.02	16.17	1.26
10	**14**	250: 1: 1	130	8	70.3	7.10	9.71	17.60	1.36
11	**15**	250: 1: 1	130	8	83.3	9.58	14.59	20.85	1.52
12	**16**	250: 1: 1	130	8	80.6	10.76	15.96	20.28	1.48
13	**17**	250: 1: 1	130	8	38.1	2.64	3.24	9.54	1.22

[a] Determined by ^{1}H NMR spectroscopy. [b] $M_{n/w}$, GPC values corrected considering Mark–Houwink factor (0.57) from polystyrene standards in THF. [c] Calculated from ([monomer]$_0$/Ti) × conv (%) × monomer molecular weight (M_{VL}=100.16) + Molecular weight of BnOH. [d] From GPC. [e] Reaction performed in air.

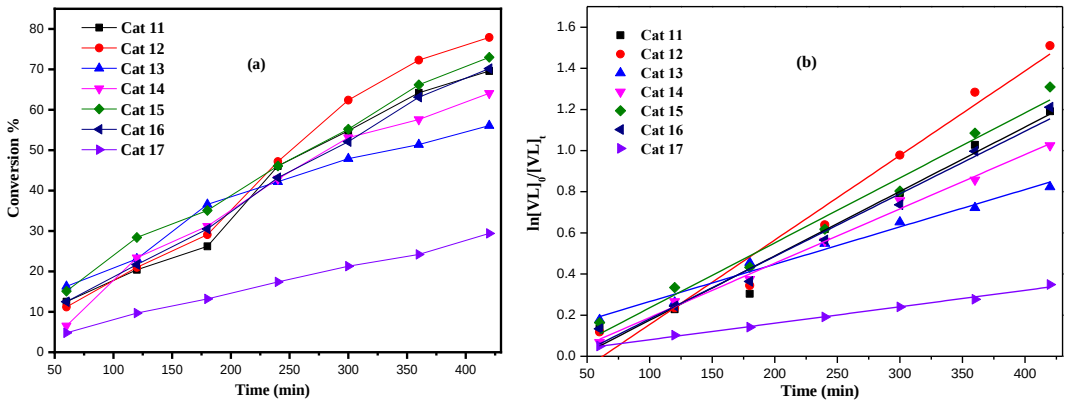

Figure 4-11. (a) Relationship between conversion and time for the polymerization of δ-VL by using complex **11-17**; (b) Plot of ln[VL]$_0$/[VL]$_t$ *vs*. time for the polymerization of δ-VL by using complexes **11-17** ; Conditions: T=130 °C, $n_{Monomer}$: n_{Ti}: BnOH=250 : 1: 1.

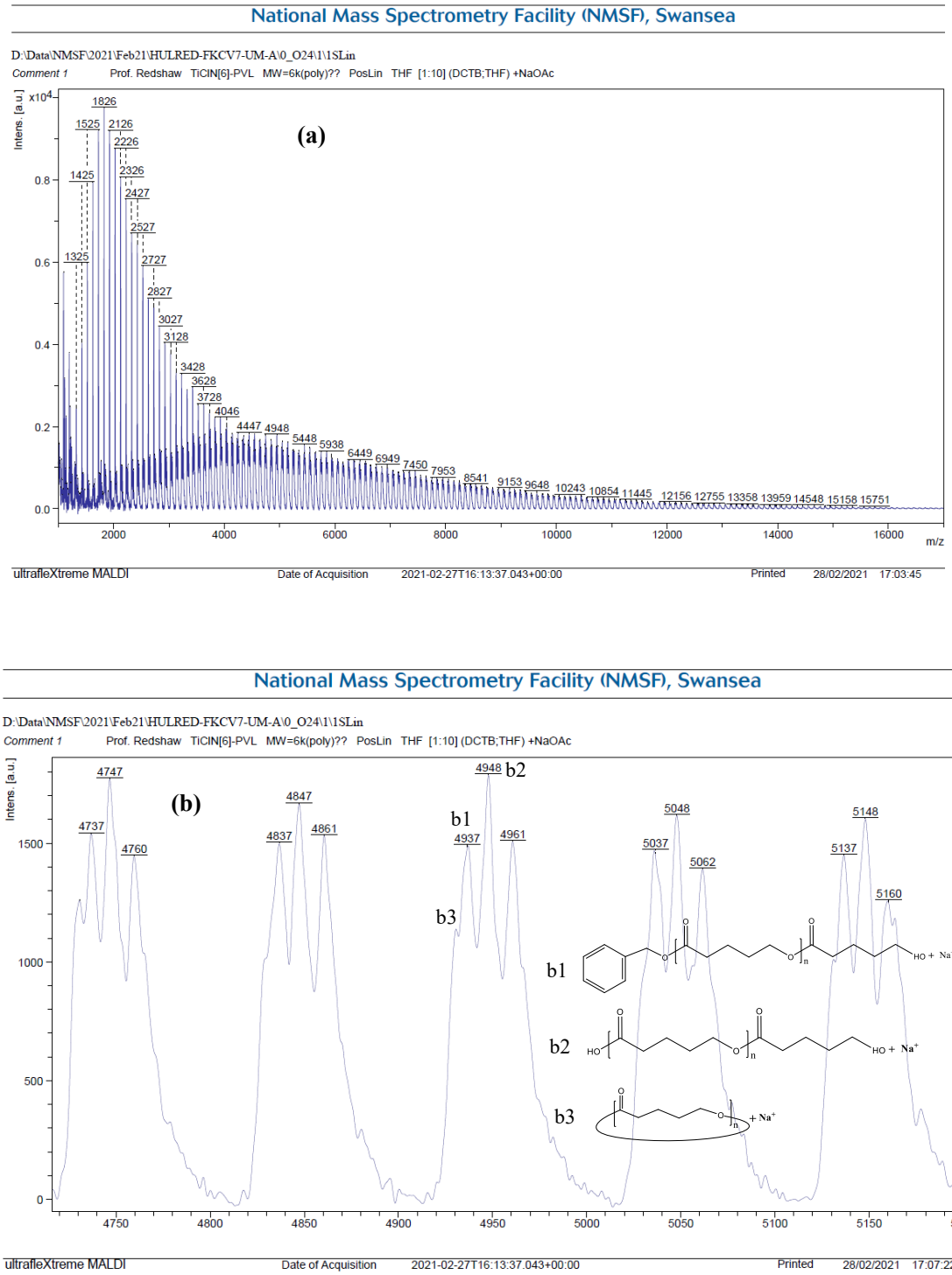

Figure 4-12. (a) Mass spectrum of PVL synthesized with **7**/BnOH (run 13, Table 4-2) (0-16000 m/z); (b) Mass spectrum of PVL synthesized with **7**/BnOH (run 13, Table 4-2) (4750-5200 m/z).

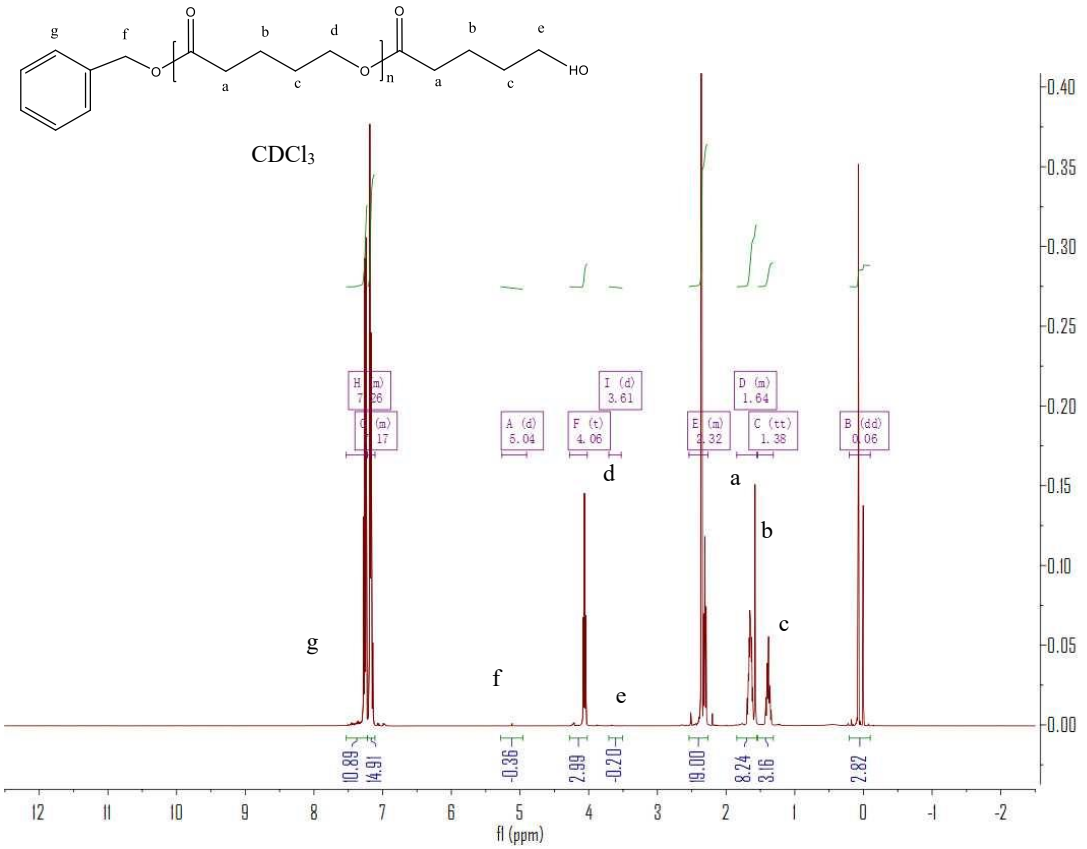

Figure 4-13. ^{1}H NMR spectrum ($CDCl_3$, 400 MHz, 298 K) of the PVL synthesized with **15**/BnOH (run 11, Table 4-2).

2.2.3 ROP of *rac*-lactide

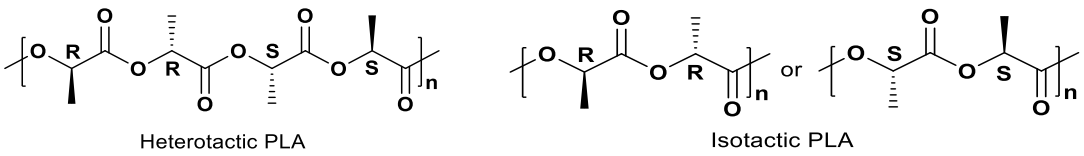

Chart 4-3. Microstructure of heterotactic and isotactic poly-(*rac*-lactide).[12]

Selected complexes were also employed as catalysts in the ROP of *r*-LA (Table 4-3). Best conversion was achieved in the presence of **12** (78.1%, run 2). The M_n of the polymer was lower than the calculated value albeit with narrow molecular weight distribution (7320 and 1.12, respectively). In the case of systems **11**-**17**, all polymers obtained were of low polydispersity (PDI < 1.75), which suggested that there was reasonable control for polymerization. However, **17** only allowed for 25.6% monomer conversion affording low molecular weight species. MALDI-ToF mass spectra of the PLA indicated the presence of

an BnO end group (e.g. Figure 4-14), which agrees with the ^{1}H NMR spectra (e.g. Figure 4-15). The sample was analysed by MALDI-ToF mass spectra in positive-linear mode, the expected series corresponding to repeating unit mass of 72/144 for half/full LA was observed and the polymer chain was terminated by OH and BnO end group [M = 108.05 (BnOH) + n × 72.06 ($C_3H_4O_2$) + 22.99 (Na^+)]. The syndiotactic bias was determined by 2D *J*-resolved ^{1}H NMR spectroscopy, investigating the methine area (5.13-5.20 ppm) of the spectra (e.g. Figure. 8-13, Chapter 8).[11] The peaks were assigned to the corresponding tetrads according to the literature.[11] For *rac*-lactide, when P_r=0.5, the afforded PLA is an atactic polymer, and when P_r=0, an isotactic polymer. The observed values herein (P_r=0.39-0.58) suggested the catalyst **12**, **14**, **15**, **16** and **17** afforded almost isotactic polymers and heterotactic materials were isolated in the case of systems **11** and **13**. (Chart 4-3).

Table 4-3. ROP of *rac*-lactide using complexes **11**- **17**.

Run	Cat.	LA: Ti: BnOH	T/°C	t/h	Conv[a]	$M_{n,GPC}\times10^{-3}$[b]	$M_w\times10^{-3}$[b]	*Pr*[c]	$M_{n,Cal}\times10^{-3}$[d]	PDI[e]
1	**11**	250: 1: 1	130	24	75.4	5.98	10.27	0.52	27.16	1.72
2	**12**	250: 1: 1	130	24	78.1	7.32	8.23	0.40	28.14	1.12
3	**13**	250: 1: 1	130	24	36.9	5.86	8.75	0.58	13.29	1.49
4	**14**	250: 1: 1	130	24	54.3	5.10	7.57	0.39	19.56	1.43
5	**15**	250: 1: 1	130	24	59.1	4.98	7.02	0.46	21.29	1.41
6	**16**	250: 1: 1	130	24	62.6	4.38	5.39	0.41	22.66	1.05
7	**17**	250: 1: 1	130	24	25.6	3.46	4.86	0.42	9.33	1.18

[a] Determined by ^{1}H NMR spectroscopy on crude reaction mixture. [b] $M_{n/w}$, GPC values corrected considering Mark–Houwink factor (0.58) from polystyrene standards in THF. [c] From 2D *J*-resolved ^{1}H NMR spectroscopy. [d] Calculated from ([Monomer]$_0$/Ti) × conv. (%) × Monomer molecular weight (M_{LA}=144.13) + Molecular weight of BnOH. [e] From GPC.

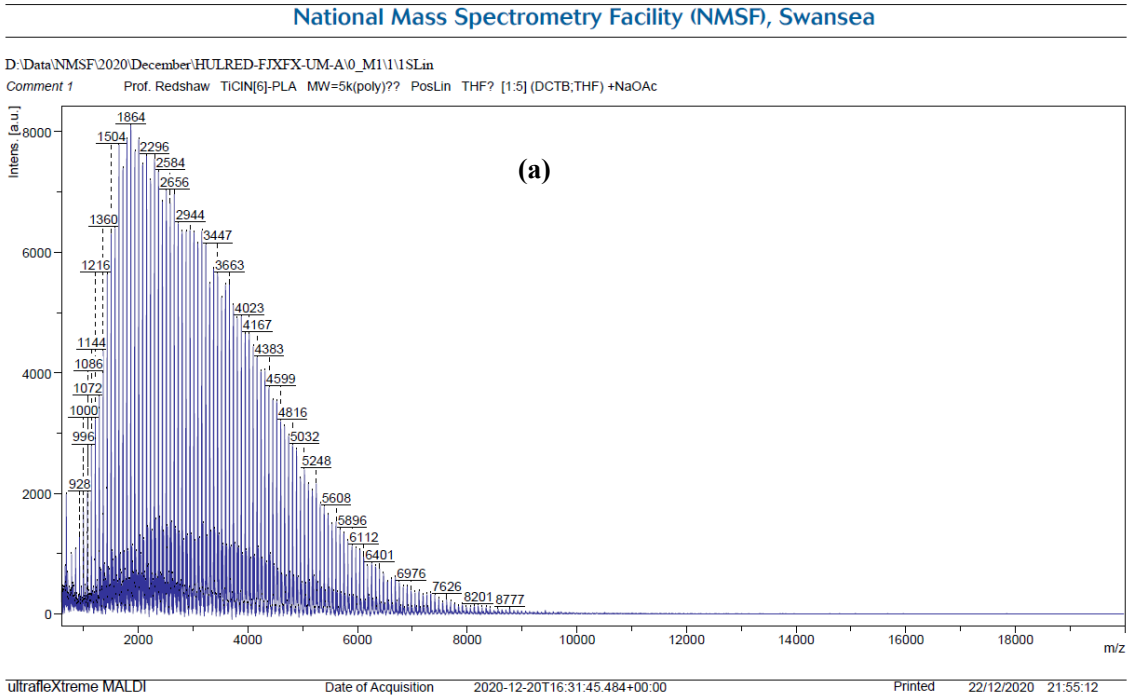

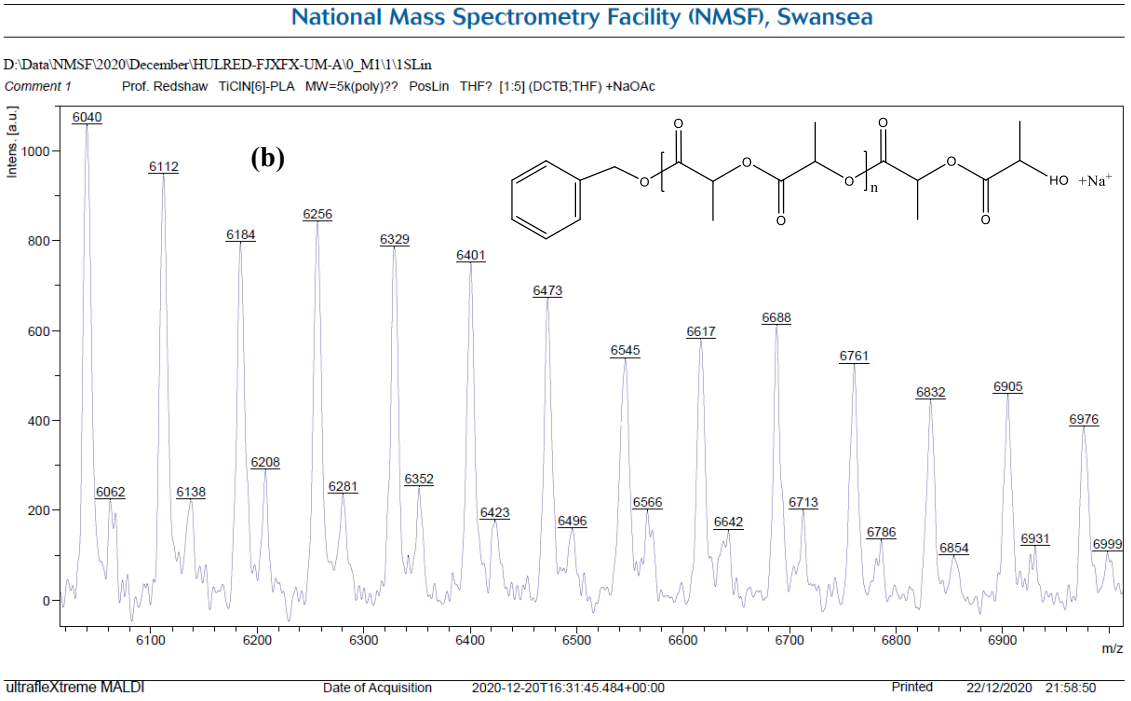

Figure 4-14. (a) Mass spectrum of PLA synthesized with **13**/BnOH (run 3, Table 4-3) (0-15000 m/z); (b) Mass spectrum of PLA synthesized with **13**/BnOH (run 3, Table 4-3) (6100-6900 m/z).

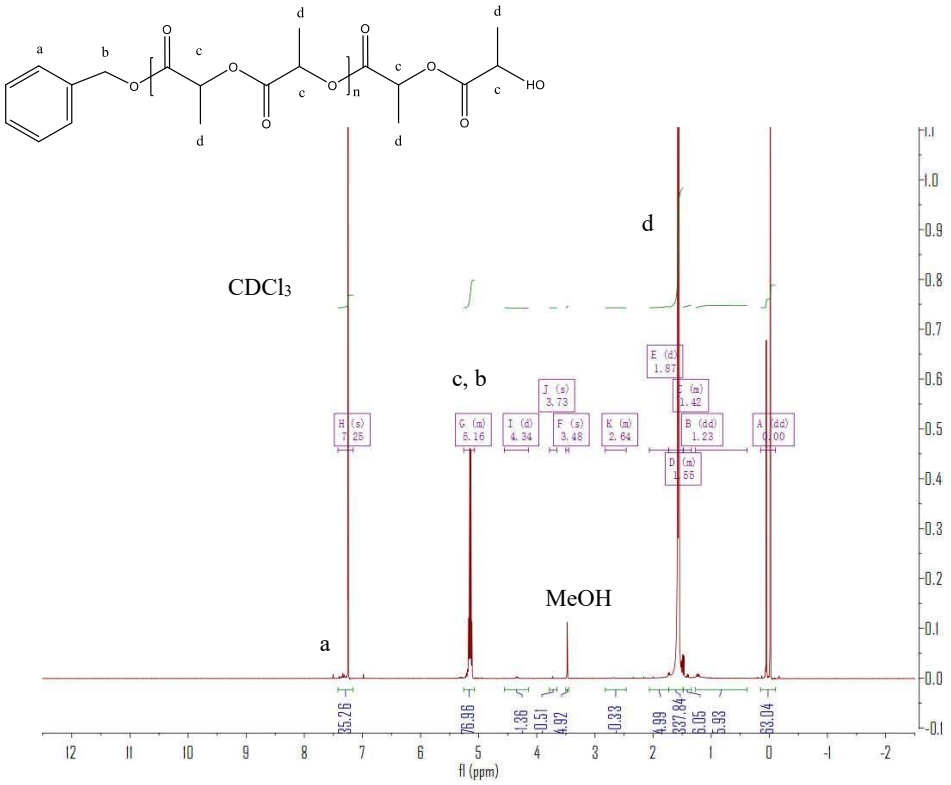

Figure 4-15. ^{1}H NMR spectrum ($CDCl_3$, 400 MHz, 298 K) of the PLA synthesized with **12**/BnOH (run 2, Table 4-3).

2.2.4 Co-polymerization of *r*-LA and *ε*-CL

The co-polymerization of *r*-LA and *ε*-CL was next investigated (Table 4-4). The complexes exhibited moderate conversions, with complex **12** performing best (85.1%), and with **11** and **13**-**16** also producing conversions > 70%. In general, the systems appeared to be relatively well behaved with PDIs in the range 1.16-1.95; ^{1}H NMR spectra were consistent with the presence of BnO and OH end groups (Figure 4-16). The composition of the copolymer was further investigated by ^{13}C NMR spectroscopy. In fact, diagnostic resonances belonging to CL–CL–CL, LA-CL-CL, CL-CL-LA, LA-CL-LA, LA-LA-CL, CL-LA-LA and LA-LA-LA dyads can be observed in the region between *δ* 173.6 and 169.6 ppm (Figure 8-13, Chapter 8). Based on the current results, the number-average sequence length was found to be 1.18 and 5.10 for CL and LA, respectively (Figure 8-13, Equations 8-4 and 8-5). Furthermore, no peaks corresponding to the CL-LA-CL triad at 171.1 ppm

was observed. Such signals arise from the transesterification of the cleavage of the lactyl-lactyl bond in the lactidyl unit.[13]

Table 4-4. Ring opening copolymerization of *r*-LA and *ε*-CL using **11**-**17**.

Run[a]	Cat.	LA: CL: Ti: BnOH	t/h	T/°C	Conv[b] (%)	$M_{n,GPC}\times10^{-3c,d}$	$M_w\times10^{-3c,d}$	PDI[c]
1	**11**	250: 250: 1: 1	130	24	80.2	14.16	26.71	1.88
2	**12**	250: 250: 1: 1	130	24	85.1	16.44	32.07	1.95
3	**13**	250: 250: 1: 1	130	24	72.4	9.48	14.23	1.50
4	**14**	250: 250: 1: 1	130	24	75.9	10.63	17.37	1.63
5	**15**	250: 250: 1: 1	130	24	82.7	14.42	21.98	1.52
6	**16**	250: 250: 1: 1	130	24	80.1	15.01	22.88	1.52
7	**17**	250: 250: 1: 1	130	24	33.8	2.35	2.75	1.16

[a] Testing method: *rac*-lactide was firstly added and heating for 24 h, then *ε*-caprolactone was added and heating for 24 h. [b] Determined by ^{1}H NMR spectroscopy on crude reaction mixture based on *ε*-CL. [c] From GPC. [d] M_n values were determined by GPC in THF vs. PS standards and were corrected with a Mark–Houwink factor $M_{n/w}$ GPC = [($M_{n/w}$ measured × 0.56 × (1-%CL) + $M_{n/w}$ measured × 0.58 × (1-%LA)]. Solvent used in the ROP: toluene.

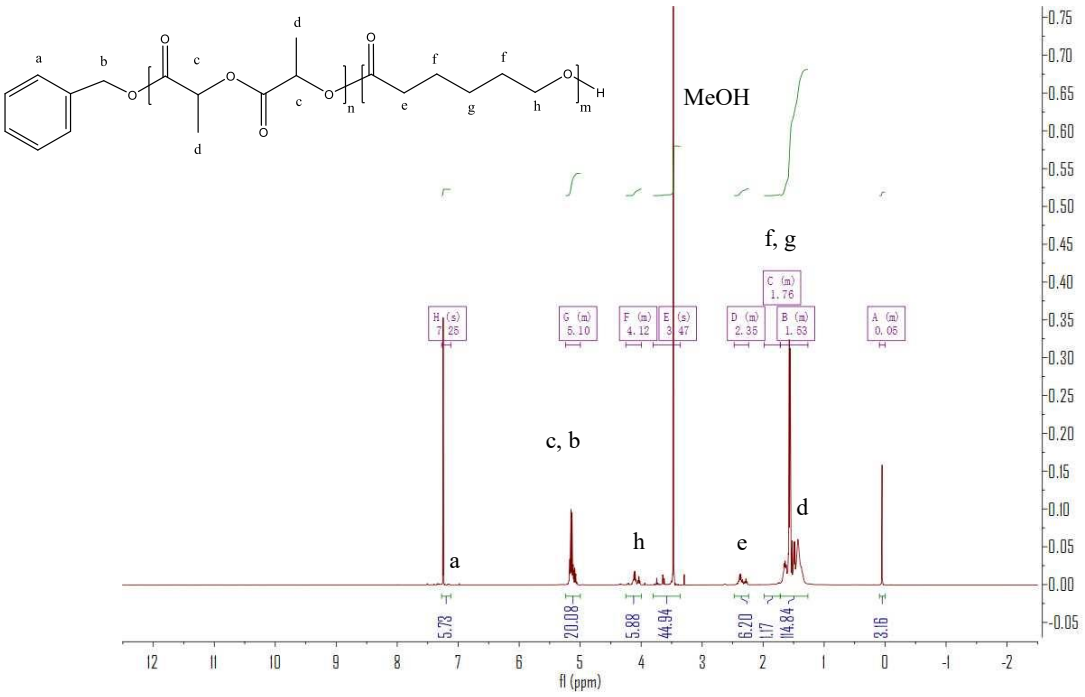

Figure 4-16. ^{1}H NMR spectrum ($CDCl_3$, 400 MHz, 298 K) of the PLA-PCL copolymer synthesized with **16**/BnOH (run 6, Table 4-4).

2.2.5 Kinetics study for *ε*-CL and *δ*-VL

From a kinetic study of the ROP of *ε*-CL using **11**-**17**, it was observed that the polymerization rate exhibited first-order dependence on the *ε*-CL concentration (Figure 4-8(a)), and the conversion of monomer achieved over 420 min was >25%. The activity trend in this case revealed that **12** was the most active and then **11**> **15**≈ **16**> **14**> **13**> **17**. An induction period of **12** hours observed for complexes **11**-**16** could be ascribed to the longer time required for the formation of the catalytically active species. A similar result was also observed in the polymerization of *δ*-VL (Figure 4-9(b)).

The dependence of the M_n and molecular weight distribution on the monomer conversion in the reactions catalyzed by **11**, **13**, **15** with BnOH was also investigated (Figure 4-17). For the ROP of *ε*-CL, the polymer M_n was shown to increase linearly with the conversion, which suggested that the polymerization was well controlled (Figure 4-17, left). A similar outcome was also observed in the reaction involving *δ*-VL (Figure 4-17, right).

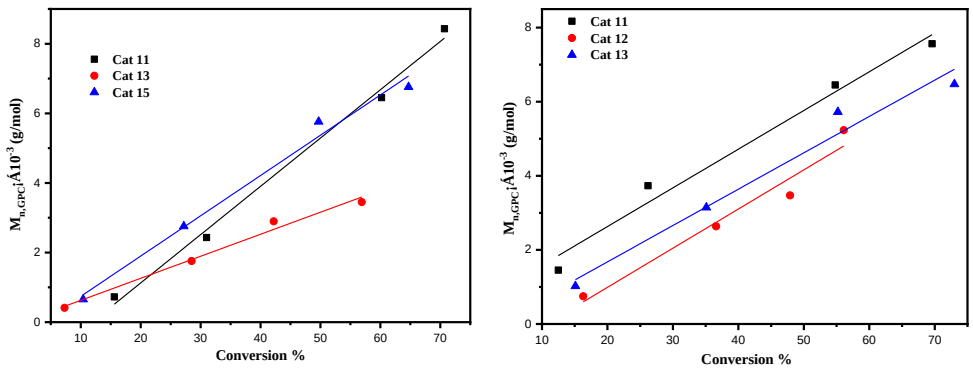

Figure 4-17. Left: M_n *vs*. monomer conversion in the ROP of *ε*-CL by using **11**, **13** and **15**; Right: M_n *vs*. monomer conversion in the ROP of *δ*-VL by using **11**, **13** and **15**; Conditions: T=130 ºC, $n_{Monomer}$: n_{Ti}: BnOH= 250:1:1.

2.2.6 ROP of *ω*-pentadecalactone

To enhance the thermal properties of the polymers obtained herein, the ROP of the *ω*-

pentadecalactone was investigated. Unfortunately, none of the systems herein proved to be effective as catalysts for the ROP of *ω*-pentadecalactone either in solution at high temperatures (130 °C) or as melts.

3. Conclusions

The current chapter reports rare examples of metal (here titanium) complexes of larger dioxacalix[6]arenes and has extended the work to include even rarer examples of titanium complexes bearing azacalixarenes. The molecular structures reveal how these macrocycles can support multiple metal centres which adopt some interesting structural motifs. The complexes are active for the ring opening polymerization of *ε*-caprolactone (*ε*-CL), *δ*-valerolactone (*δ*-VL) and *rac*-lactide (*r*-LA) but not *ω*-pentadecalactone. In all cases, the oxo complex $[Ti_4O_4(L^{6O})_2]$·MeCN (**12**·MeCN) proved to be the most active catalyst with first order kinetics.

4. References

[1] (a) D. H. Homden and C. Redshaw, *Chem. Rev.,* 2008, 108, 5086-5130; (b) Coordination Chemistry and Applications of Phenolic Calixarene–metal Complexes. Y. Li, K.-Q. Zhao, C. Redshaw, B. A. Martínez Ortega, A. Y. Nuñez, T. A. Hanna in Patai's Chemistry of Functional Groups, Wiley 2014.

[2] (a) B. König and M.H. Fonseca, *Eur. J. Inorg. Chem.*, 2000, 2303–2310; (b) P. Lhoták, *Eur. J. Org. Chem.,* 2004, 1675−1692; (c) N. Morohashi, F. Narumi, N. Iki, T. Hattori and S. Miyano, *Chem. Rev.*, 2006, 106, 5291-5316; (d) H. Tsue, K. Ishibashi and R. Tamura,

Top Heterocycl Chem., 2008, 17, 73–96; (e) K. Cottet, P. M. Marcos and P. J. Cragg, *Beilstein J. Org. Chem.,* 2012, 8, 201–226; (f) R. Tamura, M. Miyata (eds.), *Advances in Organic Crystal Chemistry*, Chapter 13, 2015, 241-261; (g) H. Takemura, T. Shinmyozu, H. Miura and I. U. Khan, *J. Incl. Phenom. Macrocycl. Chem.*, 1994, 19, 193-206.

[3] (a) C. Desroches, G. Pilet, S. A. Borshch, S. Parola, and D. Luneau, *Inorg. Chem.,* 2005, 44, 9112−9120; (b) R. Kuriki, T. Kuwabara and Y.i Ishii, *Dalton Trans.,* 2020, 49, 12234−12241; (c) R. Kumar, Y. O. Lee, V. Bhalla, M. Kumar and J. S. Kim, *Chem. Soc. Rev.*, 2014, 43, 4824−4870; (d) P. Thuéry, M. Nierlich, J. Vicens and H. Takemura, *Dalton Trans*., 2000, 279–283; (e) C. Redshaw, M. Rowan, L. Warford, D. M. Homden, A. Arbaoui, M. R. J. Elsegood, S. H. Dale, T. Yamato, C. P. Casas, S. Matsui and S. Matsuura, *Chem. Eur. J.*, 2007, 13, 1090-1107; (f) T. Xing, T. J. Prior, M. R. J. Elsegood, N. V. Semikolenova, I. E. Soshnikov, K. Bryliakov, K. Chen and C. Redshaw, *Catal. Sci. Technol*., 2021, 11, 624-636.

[4] M. Frediani, D. Sémeril, A. Marrioti, L. Rosi, P. Frediani, L. Rosi, D. Matt and L. Toupet, *Macromol. Rapid Comm.,* 2008, 29, 1554-1560.

[5] (a) Z. Sun, Y. Zhao, O. Santoro, M. R. J. Elsegood, E. V. Bedwell, K. Zahra, A. Walton, and C. Redshaw, *Catal. Sci. Technol.*, 2020, 10, 1619-1639; (b) O. Santoro, M. R. J. Elsegood, E. V. Bedwell, J. A. Pryce and C. Redshaw, *Dalton Trans*., 2020, 49, 11978-11996.

[6] A. W. Addison, T. N. Rao, J. Reedijk, J. van Rijn and G. C. Verschoor, *J. Chem. Soc., Dalton Trans*., 1984, 1349–1356.

[7] (a) N. Li, J. –J. Liu, J. –W. Sun, B. –X. Dong, L. –Z. Dong, S. –J. Yao, Z. Xin, S. –L.

Li and Y. Q. Lan, *Green Chem*., 2020, 22, 5325-5332; (b) X. -X Yang, W. -D. Yu, X.-Y. Yi and C. Liu, *Inorg. Chem*., 2020, 59, 7512-7519; (c) X. -X Yang, W. -D. Yu, X. -Y. Yi, L. – J. Li and C. Liu, *Chem Commun*., 2020, 56, 14035-14038.

[8] J. P. Fackler Jr., F. J. Kristine, A. M. Mazany, T. J. Moyer, and R. E. Shepherd *Inorg. Chem.*, 1985, 24, 1857–1860.

[9] A. C. Cooper, J. C. Bollinger, J. C. Huffman and K. G. Caulton, *New J. Chem.*, 1998, 22, 473-480.

[10] M. Frediani, D. Sémeril, A. Marrioti, L. Rosi, P. Frediani, L. Rosi, D. Matt and L. Toupet, *Macromol. Rapid Comm.*, 2008, 29, 1554-1560.

[11] (a) C. Ludwig and M. R. Viant, *Phytochem. Anal*., 2010, 21, 22-32; (b) M. J. Walton, S. J. Lancaster and C. Redshaw, *ChemCatChem*, 2014, 6, 1892-1898.

[12] (a) Z. Zhong, P. J. Dijkstra and J. Feijen, *J. Am. Chem. Soc*., 2003, 125, 11291-11298; (b) P. Hormnirun, E. L. Marshall, V. C. Gibson, A. J. P. White and D. J. Williams, *J. Am. Chem. Soc*., 2004, 126, 2688-2689.

[13] (a) F. Della Monica, E. Luciano, A. Buonerba, A. Grassi, S. Milione and C. Capacchione, *RSC Adv*., 2014, 4, 51262−51267; (b) P. Vanhoorne, P. Dubois, R. Jerome and P. Teyssie, *Macromolecules,* 1992, 25, 37–44; (c) J. Kasperczyk and M. Bero, *Makromol. Chem*., 1991, 192, 1777–1787; (d) J. Kasperczyk and M. Bero, *Makromol. Chem*. 1993, 194, 913–925; (e) N. Nomura, A. Akita, R. Ishii and M. Mizuno, *J. Am. Chem. Soc*., 2010, 132, 1750–1751; (f) G. Li, M. Lamberti, D. Pappalardo and C. Pellecchia, *Macromolecules,* 2012, 45, 8614−8620.

Chapter 5

Lithiated calix[*n*]arenes (n = 6 or 8): Synthetic, structural and use in the ring opening homo-/co-polymerization of cyclic esters

1. Introduction

The versatility of calixarenes is now well documented with applications ranging from their use in nuclear waste to use in hair dyes.[1,2] These uses stem from the facile functionalization of either the lower or upper rims, and the conformational flexibility displayed by such calixarenes which often results in the beneficial presence of π–rich cavities. The interest here stems from their ability to act as useful ancillary ligands in catalysis.[3] Recently, Redshaw *et al.* have reported that a family of lithiated calix[4]arenes can act as efficient catalysts for the ring opening polymerization (ROP) of cyclic esters, albeit with a lack of control.[4] This area is topical given the current issues with petroleum-based plastics, and the need to develop new polymeric materials with more environmentally friendly properties.[5] Studies have shown that larger calix[*n*]arenes have the ability to simultaneously bind multiple metal centers,[6] and, in the area of catalysis, this has the potential to lead to beneficial cooperative effects. Mixed-metal systems can also exhibit interesting catalytic behaviour, and it has been shown that the presence of one metal can impact on the catalytic potential of another.[7] In terms of the larger calix[*n*]arenes, only a limited number of lithiated species have been reported,[8,9] and none have been employed as catalysts for the ROP of cyclic esters. Reports include mixed lithium/strontium complexes available via the use of *n*BuLi with L^8H_8 (or its p-*iso*-propyl analogue) and subsequent treatment with $SrBr_2$.[8] Also, Fromm *et al* have structurally characterized the complex $[Li_2L^8H_6(THF)_7(H_2O)_{12}]_2$, which resulted from the reaction of L^8H_8 with Li_2CO_3 in THF/water.[9] Herein, the reactions between p-*tert*-butylcalix[6 and 8]arene$H_{6,8}$ (L^6H_6 and L^8H_8, Chart 5-1) and the lithium reagents Li*O*t*Bu* or $LiOH·H_2O$ has been investigated,

and a number of intriguing multi-lithiated species have been isolated, see Chart 5-2. The bulk of current synthetic studies have focused on the L^8H_8 system given its cost *versus* L^6H_6 or deBuL^8H_8.[10] The use of lithiated species for the ROP of cyclic esters has been reviewed,[11] whilst a number of lithium-based rings, cages and ladders have been reported as catalytic ROP systems.[12]

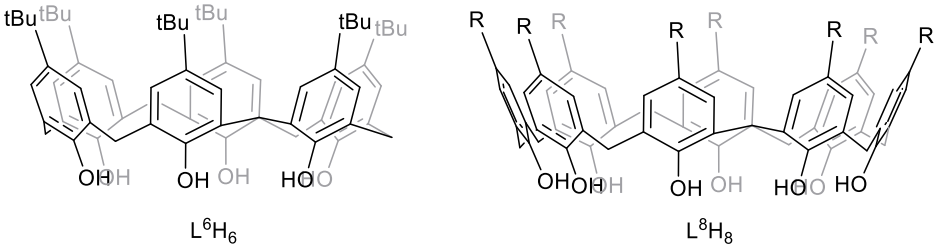

Chart 5-1. Calixarenes used in this chapter (R = H, *t*Bu).

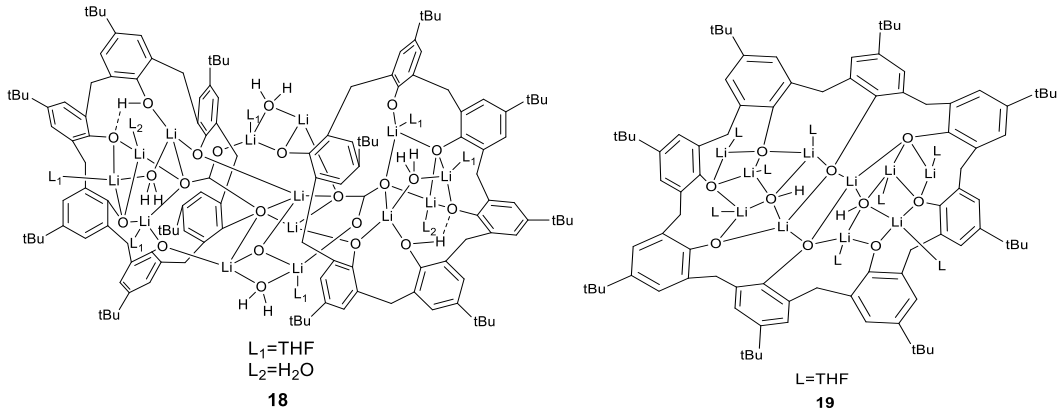

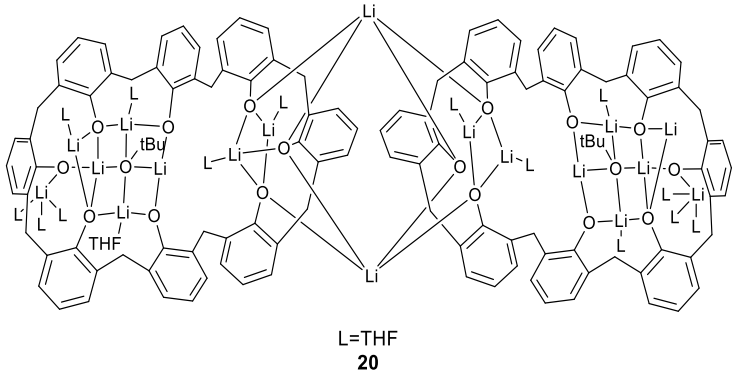

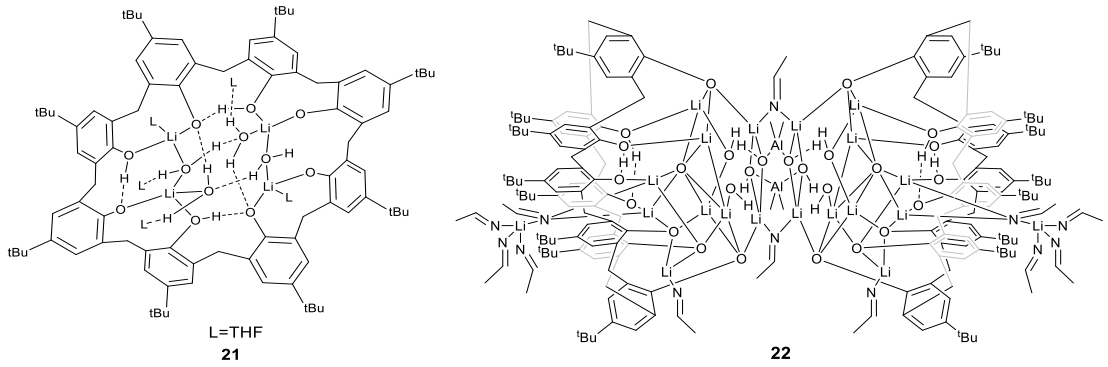

Chart 5-2. Pre-catalysts prepared herein.

2. Results and Discussion

2.1 Syntheses and solid-state structures

Using a modification of the method reported by Fromm *et al*. for the complex [Li_4(p-*tert*-butylcalix[4]arene)$(THF)_4$]·6THF,[13] L^6H_6 was treated with Li*O*tBu in THF at ambient temperature. Following work-up, the complex [$Li_{14}(L^6H)_2(CO_3)_2(THF)_6(OH_2)_6$]·14THF (**18**·14THF) was isolated as the only crystalline product in low yield (*ca.* 15%). The molecular structure is shown in Figure 5-1, with selected bond lengths and angles given in the caption. The molecule lies on a centre of symmetry, and so half of the formula above is the asymmetric unit. ^{1}H NMR spectroscopic data are consistent with the solid-state structure, whilst in the ^{7}Li NMR spectrum, only 5 distinct lithium resonances are observed. In the EI mass spectrum, a peak is observed at 2177 Da assigned to the molecular ion – $6H_2O$–20THF+Na^+.

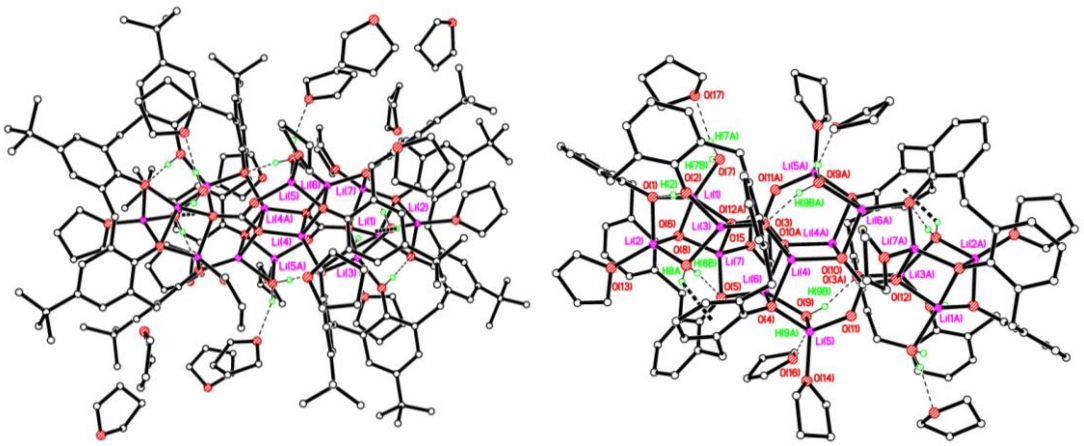

Figure 5-1. Molecular structure of $[Li_{14}(L^6H)_2(CO_3)_2(THF)_6(OH_2)_6]\cdot 14THF$ (**18**·14THF). Selected bond lengths (Å) and angles (°): Li(1)–O(6) 1.933 (12), Li(1)–O(7) 1.954(14), Li(1)–O(1) 1.954 (13), Li(2)–O(1) 1.905(13), Li(2)–O(13) 1.939 (13), Li(3)–O(3) 1.932 (11), Li(3)–O(8) 2.103 (12), Li(4)–O(3) 1.931(12), Li(4)–O(10) 1.959(11), Li(5)–O(4) 1.874(12), Li(5)–O(11) 1.876(11), Li(6)–O(5) 1.924(11), Li(6)–O(4) 1.995(13), Li(7)—O(6) 1.850(11), Li7—O5 1.901 (13), O6—Li1—O1 92.0 (5) O7—Li1—O1 124.1 (7), O1—Li2—O13 114.8 (6) O1—Li2—O6 91.7 (6), O3—Li3—O2 113.2 (6), O3—Li4—O10 124.5 (6), O3—Li4—O4 116.5 (5).

The presence of the carbonate here is not unprecedented in metal phenolate chemistry. For example, McIntosh, Brechin, and Dalgarno *et al*. utilized bis-phenolate 6,6/-methylenebis(4-*tert*-butyl)-2-(hydroxymethyl)phenol to form a cobalt (Co_{15}) cluster, the structure of which was found to incorporate a μ_6-CO_3^{2-} ligand. The carbonate in this Co_{15} cluster was thought to arise via the incorporation of atmospheric CO_2, which, given the limited solubility of the CO_2 under the conditions employed, led to a low product yield.[14] For **18**·14THF, a similarly low yield was observed, and so carbonate incorporation from exposure to atmospheric CO_2 is also proposed here. In **18**·14THF, one calixarene oxygen, O(2), remains protonated and forms an H-bond with a neighbouring phenolate oxygen, O(1). The H atoms of water molecule at O(9) form H-bonds with a calixarene phenolate oxygen O(3A) and a THF oxygen. Water molecules at O(8) & O(9) bridge pairs of Li^+ ions, while that at O(7) is terminal. The H atoms of water molecule at O(8) form an H-bond with

a calixarene phenolate oxygen O(5) and an O–H···π interaction with calixarene aromatic ring C(34) > C(39) with distance 2.37 Å. The water molecule at O(7) forms an H-bond with a THF oxygen for one H atom, but no non-covalent interaction with the other H. There are some clear methylene H atom interactions with Li^+ centres, for example at Li(7) with H(55B) = 2.12 Å, Li(1) with H(66A) = 2.25 Å, and Li(4) with H(33B) = 2.17 Å. The carbonate ions form bonds to a total of 7 Li^+ ions each. Each Li^+ is essentially 4-coordinate, ignoring the interactions with H atoms. Li(2), Li(5), and Li(7) each bind to a terminal THF ligand. The core of the molecule is an elongated array of 14 oxygen-bridged Li^+ ions approx. 12 Å long. The core of the molecule has a chain of 5 Li_2O_2 diamonds (see Figure 8-16, Chapter 8). In terms of charge, the 14+ available from the Li centres is balanced by 10– from the two calix[6]arenes and 4– from the two CO_3^{2-} anions.

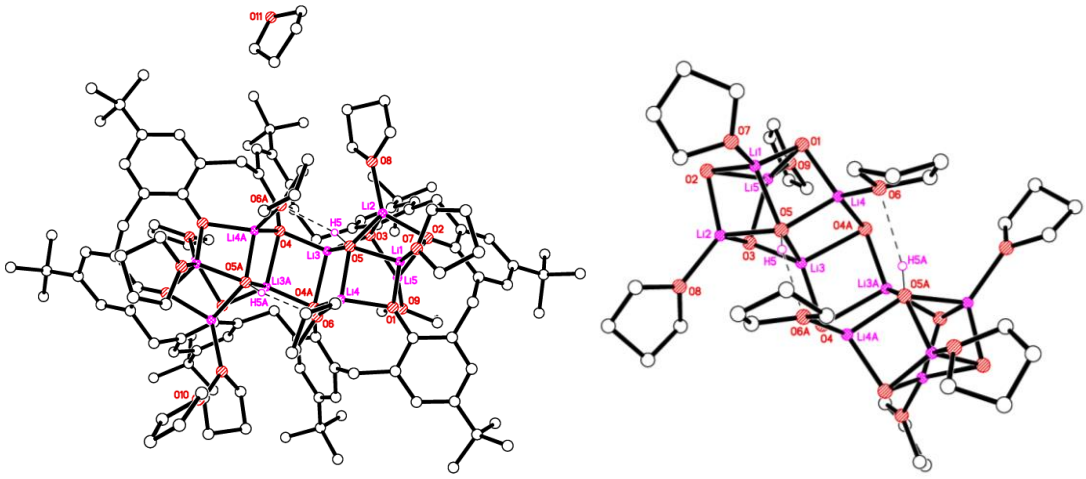

Figure 5-2. Molecular structure and core of $[Li_{10}(L^8)(OH)_2(THF)_8]\cdot 7THF$ (**19**·7THF). Selected bond lengths (Å) and angles (°): Li(1)–O(1) 1.896(2), Li(1)–O(2) 1.896(2), Li(1)–O(3) 1.959(5), Li(2)–O(2) 1.909(5), Li(2)–O(3) 1.876(5), Li(2)–O(8) 1.938(5), Li(3)–O(3) 1.920(5), Li(3)–O(4) 1.940(5), Li(3)–O(5) 1.993(5); O(1)–Li(1)–O(2) 97.9(2), Li(1)–O(5)–Li(3) 130.1(2), Li(3)–O(4)–Li(4A) 110.0(2).

Interaction of L^8H_8 with Li*O*t*Bu* in THF at ambient temperature afforded $[Li_{10}(L^8)(OH)_2(THF)_8]\cdot 7THF$ (**19**·7THF) in moderate isolated yield (*ca*. 50%). The molecular structure is shown in Figure 5-2, with selected bond lengths and angles given in the caption. It is a twinned data set with two twin components related by 177.5° rotation about reciprocal axis [0 1 0]. The molecule lies on a centre of symmetry, and so half is unique. The core of the molecule comprises a six-rung Li – O ladder, and Li(1), Li(2), Li(3), Li(4), and Li(5) all have four bonds which connect with oxygen (for alternative views of the core see Figure 8-27, Chapter 8). There is H-bonding involving two of the Li-bound (at Li(4)/Li(4A)) THFs. Each molecule has two intramolecular H-bonded interactions between oxygen (in THF) to the hydroxyl H. Only 3 distinct lithium resonances were observed in the ^{7}Li NMR spectrum, whilst in the EI mass spectrum, a peak is observed at 1416 Da is assigned to the molecular ion –15THF+Na^+. In terms of charge, the 10+ available from the Li centres is balanced by 8– from the calix[8]arene and 2– from the two OH^- anions.

Similar use of de-butylated calix[8]areneH_8 (deBuL^8H_8) led to an elongated dimer $[Li_{18}(deBuL^8)_2(O$t$Bu)_2(THF)_{14}]\cdot 4THF$ (**20**·4THF). The molecular structure is shown in Figure 5-3, with selected bond lengths and angles given in the caption. The molecule sits on a centre of symmetry. Two calix[8]arene ligands, which possess a wave like conformation, form bridges to link three separate Li_xO_y clusters. Li(1), Li(2), Li(4), Li(6), Li(8), and Li(9) all have four bonds which connect with oxygen, whilst Li(3), Li(5), and Li(7) have three bonds; a view of the core is given in Figure 8-18, Chapter 8. Li(7) makes some weak π interactions with C atoms in the neighbouring calixarene rings attached to O(1) and O(7). In terms of charge, the 18+ available from the Li centres is balanced by 16–

from the two calix[8]arenes and 2– from the two O*t*Bu^{-} anions.

Interaction of L^8H_8 with $LiOH \cdot H_2O$ afforded $[Li_4(L^8H_4)(OH_2)_4(THF)_6] \cdot 5.5THF$ (**21**·5.5THF). Crystals suitable for a diffraction study were obtained from a saturated THF solution on standing at ambient temperature. The molecular structure is shown in Figure 5-4, with selected bond lengths and angles given in the caption. The molecule sits on a centre of symmetry, so half is unique. The calix[8]arene adopts a wave-like conformation. Both Li(1) and Li(2) have four bonds which connect with oxygen. Two views of the core are given in Figure 8-19. Hydrogens on water O(7) H-bond to oxygen on the THF, including O(9) and water molecule O(8A). Hydrogens on water O(8) H-bond to oxygen on calixarene O(2) (phenolate, which has strong electronegativity) and oxygen on the THF, including O(6). The intramolecular H-bond interactions involving Li, O, and H construct a cage in the core of the structure with six and eight-membered rings. In the ^{7}Li NMR spectrum, only one peak was observable, whilst in the EI mass spectrum, a peak observed at 1645 Da is assigned to the molecular ion $–2H_2O–7.5THF$. In terms of charge, the 4+ available from the Li centres is balanced by 4– from calix[8]areneH_4.

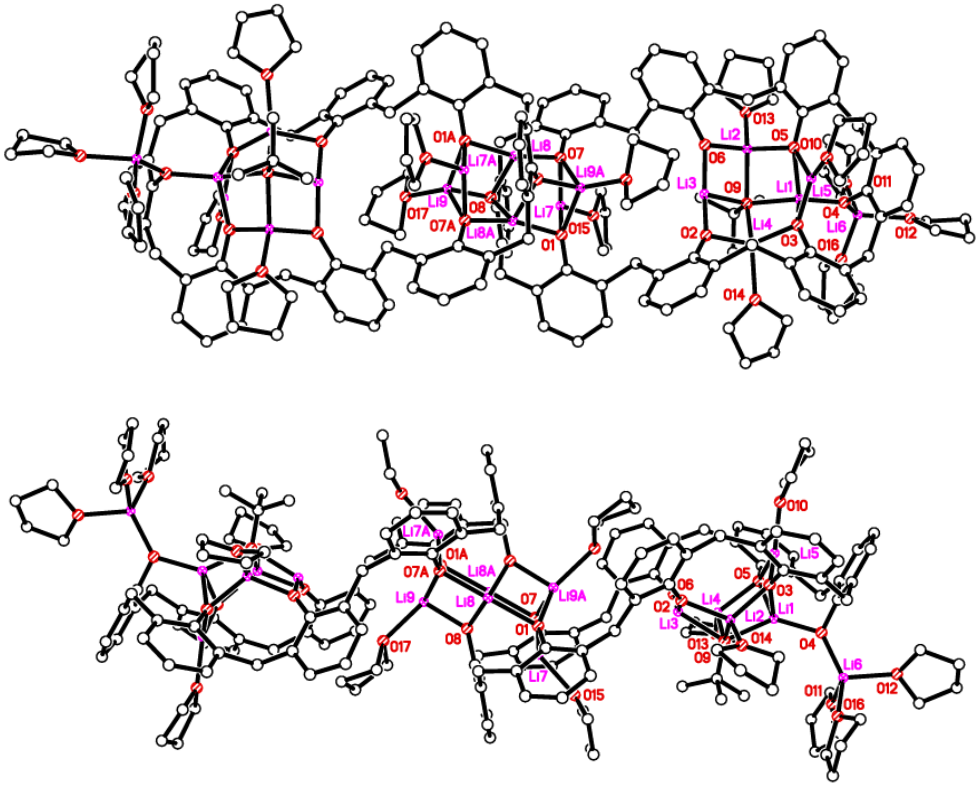

Figure 5-3. Two views of the molecular structure of $[Li_{18}(deBuL^{8})_2(OtBu)_2(THF)_{14}]\cdot 4THF$ (**20**·4THF). Selected bond lengths (Å) and angles (°): Li(1)–O(3) 1.965(14), Li(1)–O(4) 1.855(16), Li(1)–O(5) 2.066(13), Li(1)–O(9) 2.001(17), Li(2)–O(5) 1.967(16), Li(2)–O(6) 1.814(15), Li(2)–O(9) 2.048(13), Li(2)–O(13) 2.044(13), Li(3)–O(2) 1.798(12), Li(3)–O(6) 1.809(12), Li(3)–O(9) 2.036(14), Li(4)–O(2) 1.895(15), Li(4)–O(3) 1.963(16), Li(4)–O(9) 2.045(13), Li(5)–O(3) 1.824(15), Li(5)–O(5) 1.933(13), Li(6)–O(4) 1.882(15), Li(7)–O(1) 1.898(12), Li(7)– O(7) 1.947(12), Li(8)–O(7) 2.034(15), Li(8)–O15) 1.937(15); Li(1)–O(3)–Li(4) 81.2(7), Li(1)–O(3)–Li(5) 79.6(6), Li(1)–O(4)–Li(6) 132.9(8), Li(1)–O(9)–Li(3) 123.7(6).

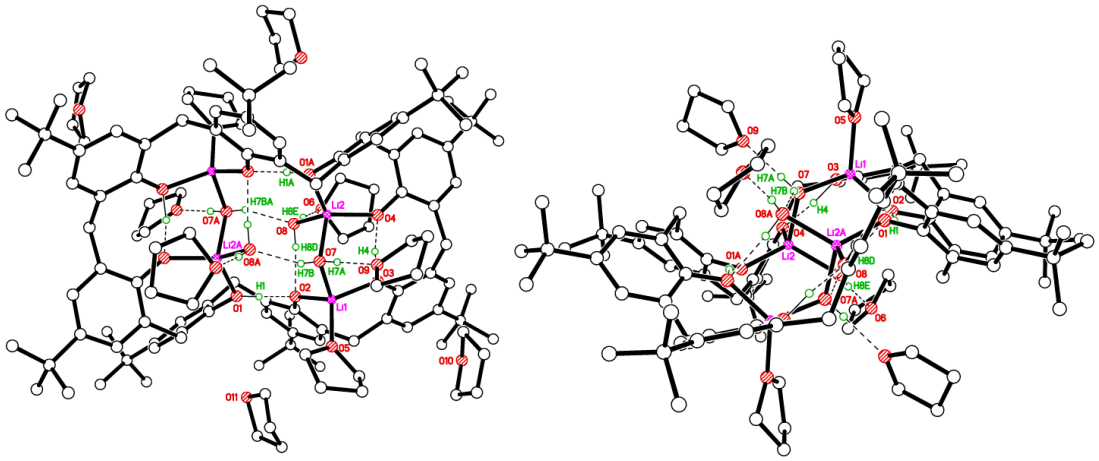

Figure 5-4. Two views of the molecular structure of $[Li_4(L^{8}H_4)(OH_2)_4(THF)_6]\cdot 5.5THF$ (**21**·5.5THF). Selected bond lengths (Å) and angles (°): Li(1)–O(2) 1.903(8), Li(1)–O(3)

1.929(8), Li(1)–O(7) 1.969(9), Li(2)–O(1) 1.919(8), Li(2)–O(4) 1.907(7), Li(2)–O(8) 1.970(8); Li(1)–O(7)–Li(2) 103.7(3), O(1)–Li(2)–O(8) 112.5(3), O(4)–Li(2)–O(8) 114.8(4).

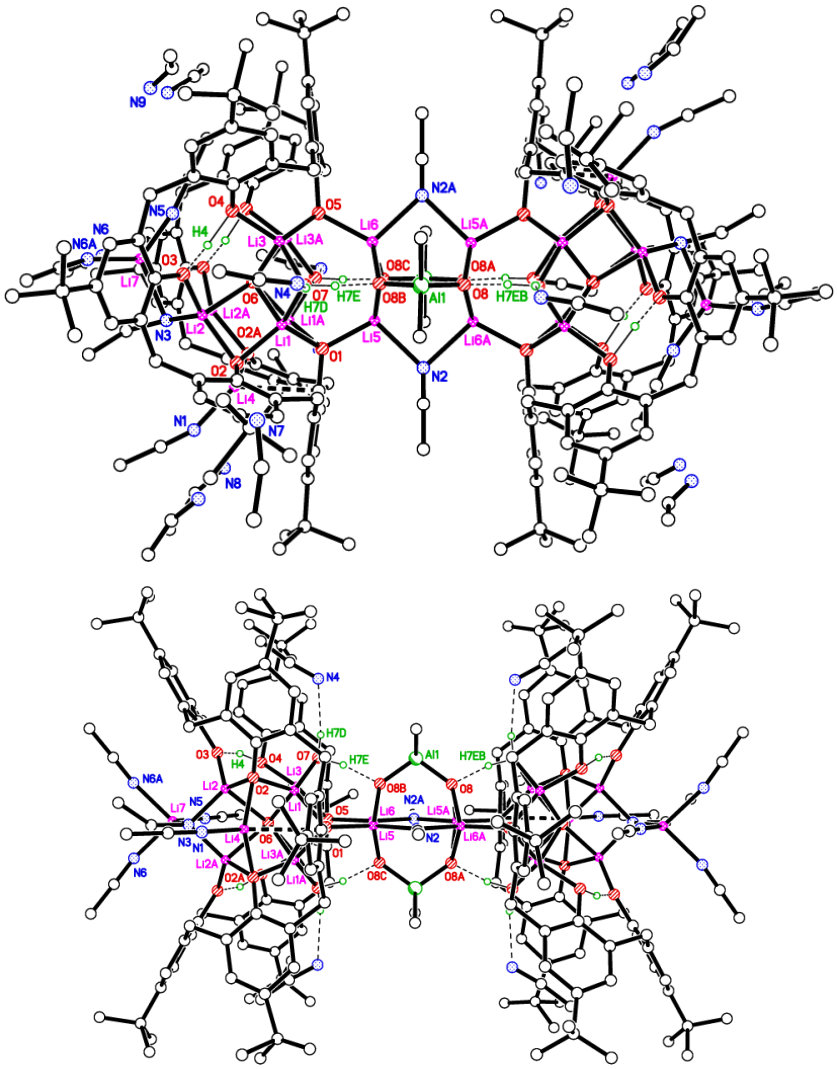

Figure 5-5. Two views of the molecular structure of $[(AlMe_2)_2Li_{20}(L^8H_2)_2(OH_2)_4(O^{2-})_4(OH)_2(NCMe)_{12}]\cdot 10MeCN$ (**22**·10MeCN). Selected bond lengths (Å) and angles (°): Li(1)–O(1) 1.927(7), Li(1)–O(2) 1.879(3), Li(1)–O(6) 2.074(7), Li(1)–O(7) 1.901(7), Li(2)–O(2) 1.908(9), Li(2)–O(3) 1.877(9), Li(2)–O(6) 2.200(9), Li(2)–N(3) 1.858(9), Li(3)–O(4) 1.900(7), Li(3)–O(5) 1.926(7), Li(3)–O(6) 2.200(6), Li(3)–O(7) 2.085(8), Li(4)–O(2) 1.994(9), Li(4)–N(1) 1.92(2), Li(5)–O(1) 1.904(9), Li(5)–N(2) 2.173(10), Li(6)–O(5) 1.942(10), Al(1)–O(8) 1.625(3); O(8)–Al(1)–O(8B) 108.75(19), Li(1)–O(1)–Li(3) 109.0(3), Li(1)–O(1)–Li(1A) 81.4(4), Li(2)–O(2)–Li(4) 93.6(7).

Given that mixed aluminium-lithium complexes have displayed favourable ROP characteristics *versus* their homo-metallic counterparts,[15] the solution generated from L^8H_8 and Li*O*t*Bu* was treated with Me_3Al. This led, following work-up, to the isolation of

the complex $[(AlMe_2)_2Li_{20}(L^8H_2)_2(OH_2)_4(O^{2-})_4(OH)_2(NCMe)_{12}]\cdot 10MeCN$ (**22**·10MeCN). The molecular structure is shown in Figure 5-5, with selected bond lengths and angles given in the caption. One quarter of the above formula comprises the asymmetric unit. The molecule sits on a centre of symmetry and there is a mirror plane running long-ways through the molecule with all atoms having their y-coordinate = 0.0000 lying on the mirror, *i.e*. Li(4) > Li(7), O(1), O(5), & O(6), N(1), N(2), N(3), N(5), & N(7). The calix[8]arene adopts a bowl conformation, and Li, O, Al, and N build a polyhedral center. Li(1), Li(2), Li(3), Li(5), Li(6), Li(7), and Al(1) all make four bonds, however, Li(4) has five bonds (the core is shown in Figure S5, ESI). H(7D) and H(7E) on the water link to N(4) on MeCN and O(8B), respectively via H-bonds. There is an intramolecular H-bond interaction between H(4) and O(3) within the calixarene. Li(4) makes a weak π interaction with the C(1) atom in the neighbouring calixarene ring attached to O(1). The voids are filled with MeCN molecules between molecules of the complex. In the ^{1}H NMR spectrum, the Al*Me*$_2$ appears at δ–0.81, whilst in the ^{7}Li NMR spectrum, only 4 distinct lithium resonances are observed. In terms of charge, the 20+ available from the Li centres and the 2+ from the $(AlMe_2)^+$ is balanced by 12– from the two calix[8]areneH_2s and 8– from the four oxo anions and 2– from the two hydroxide anions.

2.2 Ring opening polymerization studies

General: Given the track record of lithium-based systems for the ring opening polymerization (ROP) of cyclic esters,[4,11] the performance of the complexes herein to act as catalysts for the ROP of ε-caprolactone (ε-CL), δ-valerolactone (δ-VL), and *rac*-lactide

(*r*-LA), in the presence of one equivalent of benzyl alcohol (BnOH) per lithium present, has been investigated. Results are compared against the reported calixarene complexes **XIV** – **XVI** (Chart 5-3).[4,16]

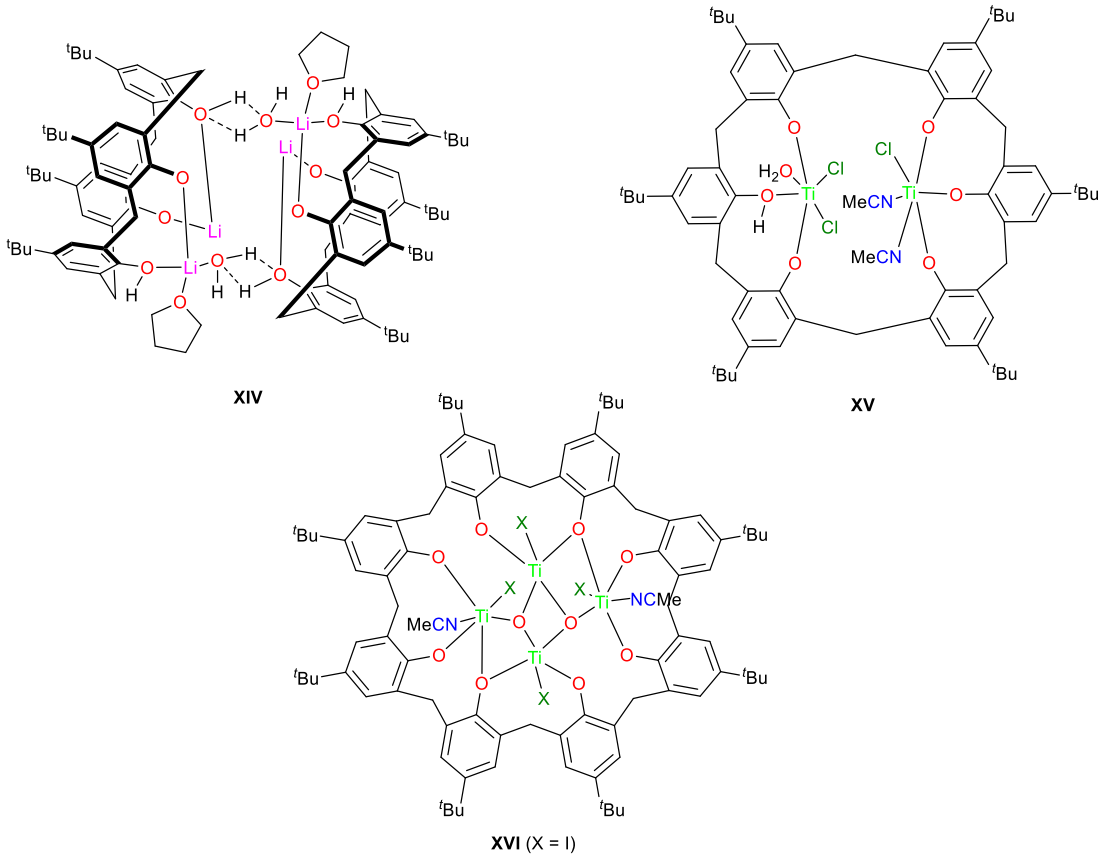

Chart 5-3. Literature complexes **XIV** - **XVI**.[4,16]

2.2.1 ROP of ε-caprolactone (ε-CL)

Complexes **18**-**22** were screened for their ability to polymerise ε-caprolactone and the results are collated in Table 5-1. The polymerization screening indicated that the best conditions were 500 equivalents of ε-caprolactone to lithium at 130 °C. The activity of **18** increased with temperature and peaked at 500 equivalents of monomer. Complex **18** was also active at low catalyst loading leading to 56% conversion after 8 h for 1000 equivalents of monomer. Highest conversion and molecular weight were achieved under no solvent

conditions, with the run showing good control (Polydispersity Index, PDI, 1.18), which is consistent with former reports.[17] The polymers obtained possessed PDI < 1.85, whilst the M_n were found to be much lower than the calculated values, suggesting the occurrence of transesterification processes.[18]

The screening of **18**-**22** (Table 5-1) revealed that the lithium/aluminium-based complex, namely **22**, exhibited higher activities *versus* the other complexes herein, under the conditions employed. After 24 h (Table 5-1), complexes **18**-**21** afforded conversions <90%, whereas higher conversions (>90%) were achieved using **22** under similar conditions. From a kinetic study (Figure 5-6), it was observed that the CL polymerization rate followed the order: **22** >**18** >**19** >**20** >**21**. Compared with the lithiated calix[6]arene complex **18**, complexes **19**-**21**, derived from calix[8]arenes, were found to be relatively inactive (Table 5-1, runs 12-14). The observed activity of **22** surpassed that of the other complexes screened herein, and this may be attributed to the presence of the Al centers.[19] The higher activity of the **18** compared with **19**-**21** can be explained considering the lability of ligands present. This is in line with a recent study on titanocalix[4]arenes, in which the presence of a labile ligand (*i.e.* MeCN or H_2O) proved beneficial for the catalyst activity.[20] ^{1}H NMR spectra of the polycaprolactone (PCL) indicated the presence of an BnO end group (e.g. Figure 5-7). This agrees with the MALDI-ToF mass spectra (e.g. Figure 5-8) and indicates that the polymerization proceeded via a coordination-insertion mechanism. The MALDI-ToF spectrum of the sample displayed a major series of peaks separated by 114 m/z units, accountable by two OH terminated PCL *n*-mers (M = 17 (OH)+ 1(H) + n × 114.14 (CL), whilst there is also a minor family of peaks consistent with the polymer terminated by OH

and BnO end groups (M = n × 114.12 (CL) + 108.05 (BnOH) + 45.98 ($2Na^+$)).

On comparison with the methylene-bridged lithiated calix[4]arene **XIV** (Chart 5-3, left), at 130 °C over 24h in the presence of one equivalent of BnOH, a higher conversion for the systems herein is achieved (e.g. runs 4 and 21 *versus* run 29, Table 5-1). In the absence of solvent, the conversion achieved by the mixed Al/Li system **22** over 1h (run 27) was somewhat less than that of **XIV** (run 30) though with slightly better control. However, over 24h under air, the trend was reversed with **22** outperforming **XIV** (runs 25 v 31). In the case of the titanocalix[6 and 8]arenes **XV** and **XVI**, complex **XV** (run 34) performs less well than those herein in terms of conversion affording in general lower molecular weight products but with slightly better control. The titanocalix[8]arene **XVI** performs slightly better than lithiated calix[8]arenes **20** and **21** (runs 35, 36) under the same conditions.

Table 5-1. ROP of ε-CL using **18** – **22** and **XIV - XVI**.

Run	Cat.	CL: Li: BnOH	T/°C	t (h)	Conv[a]	$M_{n,GPC}\times10^{-3}$[b]	$M_w\times10^{-3}$[b]	$M_{n,cal}\times10^{-3}$[c]	PDI[d]
1	**18**	1000: 1: 1	130	8	56.0	5.20	7.45	63.92	1.42
2	**18**	500: 1: 1	130	8	59.4	5.34	7.87	33.90	1.21
3	**18**	250: 1: 1	130	8	49.9	4.63	5.58	14.24	1.21
4	**18**	100: 1: 1	130	8	52.4	4.49	6.64	5.98	1.33
5	**18**	500: 1: 1	100	8	29.7	1.96	2.37	16.95	1.20
6	**18**	500: 1: 1	80	8	-	-	-	-	-
7	**19**	500: 1: 1	130	8	55.6	5.58	7.84	31.73	1.40
8	**20**	500: 1: 1	130	8	50.7	4.93	6.45	28.93	1.30
9	**21**	500: 1: 1	130	8	28.4	1.54	1.68	16.21	1.09
10	**22**	500: 1: 1	130	8	95.3	12.78	19.20	54.39	1.50
11	**18**	500: 1: 1	130	24	81.2	6.35	7.36	46.34	1.16
12	**19**	500: 1: 1	130	24	75.9	5.85	9.37	43.32	1.60
13	**20**	500: 1: 1	130	24	67.2	5.23	6.94	38.35	1.33
14	**21**	500: 1: 1	130	24	34.9	2.25	4.12	19.92	1.82
15	**22**	500: 1: 1	130	24	98.5	13.54	20.11	56.21	1.48

16	**18**	500: 1: 0	130	24	55.2	4.10	5.78	31.50	1.40
17	**19**	500: 1: 0	130	24	52.4	4.18	4.68	29.90	1.12
18	**20**	500: 1: 0	130	24	-	-	-	-	-
19	**21**	500: 1: 0	130	24	-	-	-	-	-
20	**22**	500: 1: 0	130	24	69.1	6.43	9.28	39.44	1.44
21	**22**	100: 1: 1	130	24	>99	9.85	12.95	11.30	1.31
22	**18**[e]	100: 1: 0	130	24	74.5	7.61	8.41	8.50	1.11
23	**20**[e]	100: 1: 0	130	24	60.7	6.82	7.69	6.93	1.13
24	**22**[e]	100: 1: 0	130	24	>99	9.92	13.56	11.30	1.37
25	**22**[e,f]	100: 1: 0	130	24	27.9	1.43	1.67	3.18	1.17
26	**22**[e]	100: 1: 0	130	6	89.7	7.65	10.85	10.24	1.42
27	**22**[e]	100: 1: 0	130	1	34.5	1.86	2.79	3.94	1.50
28	**22**[e]	100: 1: 0	130	15	15.4	0.72	0.95	1.76	1.32
29	**XIV**	100: 1: 1	130	24	20	-	-	-	-
30	**XIV**[e]	100: 1: 0	130	1	80	16.13	28.71	9.13	1.78
31	**XIV**[e,f]	100: 1: 0	130	24	14	-	-	-	-
32	**20**	500: 1: 3	130	24	75.4	5.24	7.21	43.15	1.37
33	**22**	500: 1: 3	130	24	>99	13.54	22.91	56.62	1.69
34	**XV**	500: 1: 3	130	24	20	2.69	3.22	3.86	1.20
35	**20**	250: 1: 1	130	24	60.1	3.86	5.12	17.27	1.33
36	**21**	250: 1: 1	130	24	39.7	1.64	2.24	11.45	1.37
37	**XVI**	250: 1: 1	130	24	74	6.61	8.13	21.11	1.23

[a] Determined by ^{1}H NMR spectroscopy. [b] Values corrected considering Mark–Houwink factor (0.56) from polystyrene standards in THF. [c] Calculated from ([monomer]$_0$/Li) × conv (%) × monomer molecular weight (M_{CL}=114.14) + Molecular weight of BnOH. [d] From GPC. [e] Reaction performed without solvent.

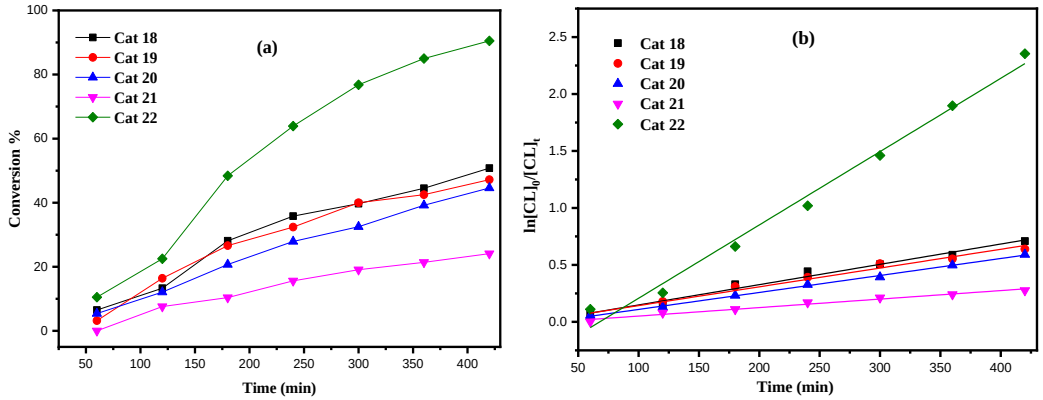

Figure 5-6. (a) Relationship between conversion and time for the polymerization of ε-CL by using complex **18-22**; (b) Plot of ln[CL]$_0$/[CL]$_t$ *vs*. time for the polymerization of ε-CL by using complexes **18-22**; Conditions: T=130 ºC, $n_{Monomer}$: n_{Li}: BnOH=500: 1: 1.

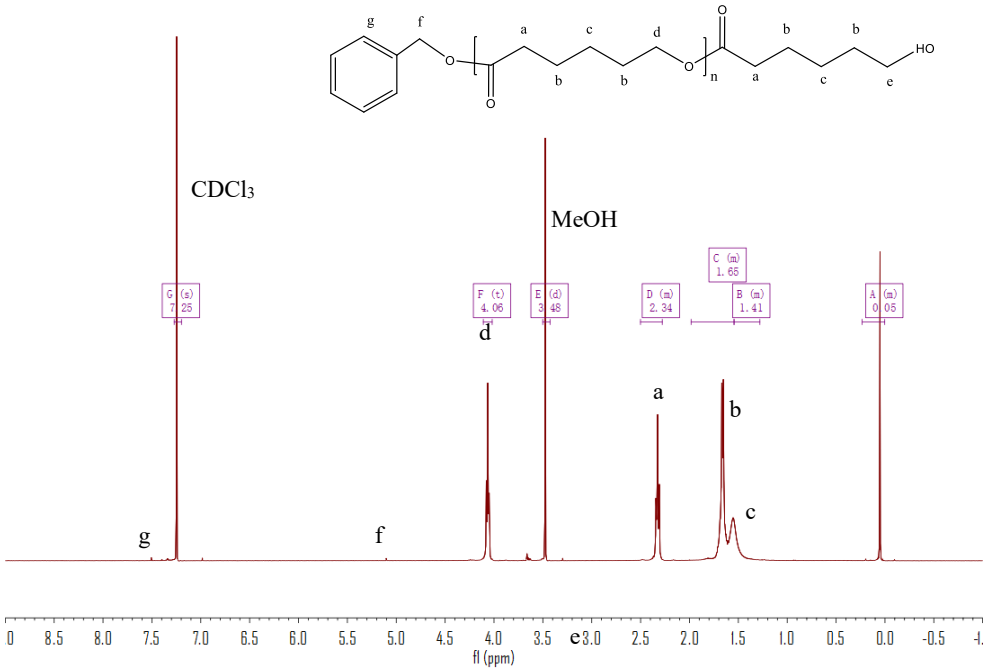

Figure 5-7. ^{1}H NMR spectrum ($CDCl_3$, 400 MHz, 298 K) of the PCL synthesized with **18**/BnOH (run 11, Table 5-1).

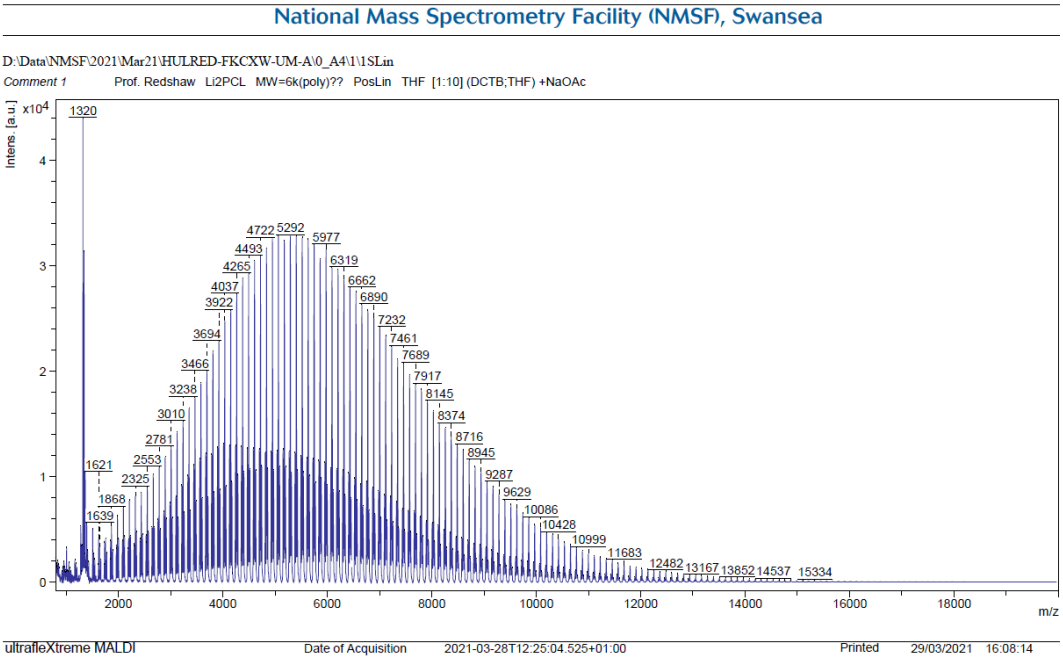

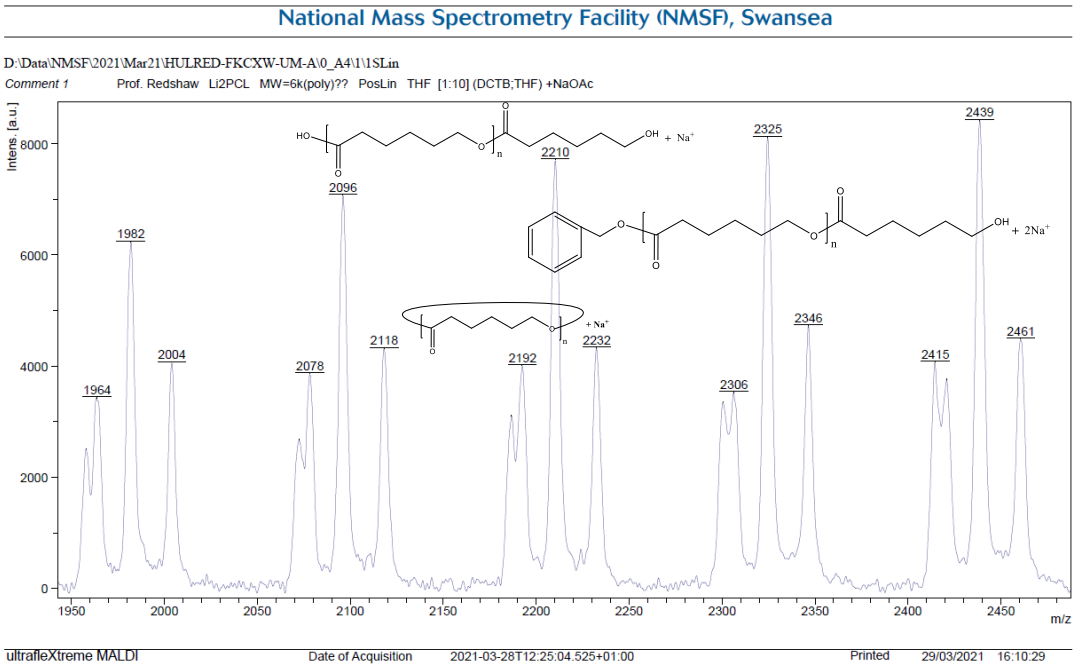

Figure 5-8. Mass spectrum of the PCL synthesized with **22**/BnOH (run 15, Table 5-1).

2.2.2 ROP of *δ*-valerolactone (*δ*-VL)

Complexes **18**-**22** were also evaluated as catalysts, in the presence of one equivalent of BnOH, for the ROP of δ-VL (Table 5-2). Using **18**, the conditions of temperature and [Li]:[δ-VL] were varied. On increasing the temperature to 130 °C and lowering the monomer to catalyst ratio, best observed results were achieved at 130 °C using [Li]:[*δ*-VL] at 1:500 over 8 h. As in the case of the ROP of *ε*-CL, kinetic studies (Figure 5-9) revealed that the catalytic activities followed the order: **22** >**18** >**19** >**20** >**21**. As for the ROP of *ε*-Cl, there was evidence of transesterification and nearly all observed M_n values were significantly lower than the calculated values. The MALDI-ToF mass spectra (e.g. Figure 5-10) exhibited a major family of peaks consistent with BnO end groups [M = 108.05 (BnOH) + n × 100.12 (VL) + 22.99 (Na^+)], and a family assigned to cyclic PVL [n × 100.12

(VL) + 22.99 (Na^+)]. The ^1H NMR spectra of the PVL also indicated the presence of a BnO end group (e.g. Figure 5-11).

Comparison of **22** *versus* lithiated calix[4]arene **XIV** in the absence of solvent over 1 h (runs 13 v 18) indicated a better performance for **XIV**, with a slightly higher conversion, a larger molecular weight product and better control. In the case of the titanocalix[6]arene **XV**, conversion is comparable with the lithiated complex **20** but inferior to the mixed-metal complex **22** (runs 19-21) under related conditions (only the amount of BnOH varied); X**V** exhibited better control. For **XVI**, the trend was similar with better conversion shown by the mixed-metal system **22**, but poorer conversion seen for lithiated **20** under the same conditions.

Table 5-2. ROP of δ-VL using **18** – **22** and **XIV - XVI**.

Run	Cat.	VL: Li: BnOH	T/°C	t (h)	Conv[a] (%)	$M_{n,GPC}\times10^{-3}$[b]	$M_w\times10^{-3}$[b]	$M_{n,cal}\times10^{-3}$[c]	PDI[d]
1	**18**	1000: 1: 1	130	8	52.4	5.23	9.59	59.81	1.83
2	**18**	500: 1: 1	130	8	58.1	5.97	9.42	33.16	1.58
3	**18**	250: 1: 1	130	8	49.5	5.52	6.11	14.12	1.11
4	**18**	100: 1: 1	130	8	44.8	3.64	5.69	5.11	1.56
5	**18**	500: 1: 1	100	8	35.2	2.56	4.26	20.09	1.66
6	**18**	500: 1: 1	80	8	-	-	-	-	-
7	**19**	500: 1: 1	130	8	54.9	5.96	9.45	31.33	1.59
8	**20**	500: 1: 1	130	8	47.9	3.73	4.16	27.34	1.12
9	**21**	500: 1: 1	130	8	33.0	1.68	2.11	18.83	1.26
10	**22**	500: 1: 1	130	8	89.4	11.54	18.65	51.02	1.62
11	**22**[e]	100: 1: 0	130	24	>99	15.69	16.56	9.91	1.06
12	**22**[e]	100: 1: 0	130	12	96.1	12.14	14.33	9.62	1.18
13	**22**[e]	100: 1: 0	130	1	36.5	2.12	4.45	3.66	2.10
14	**20**	500: 1: 3	130	24	62.1	4.85	6.24	31.09	1.28
15	**22**	500: 1: 3	130	24	>99	12.39	15.35	49.57	1.24
16	**20**	100: 1: 0	130	1	8.5	-	-	-	-
17	**22**	100: 1: 0	130	1	20.9	1.76	3.35	2.09	1.90

18	**XIV**	100: 1: 0	130	1	46.0	16.36	22.74	4.61	1.39
19	**XV**	250: 1: 3	130	24	45.8	6.36	7.18	11.47	1.13
20	**20**	250: 1: 2	130	24	41.5	3.48	5.61	10.39	1.61
21	**22**	250: 1: 2	130	24	>99	8.93	15.19	24.78	1.70
22	**XVI**	250: 1: 2	130	24	69.6	13.00	17.81	17.42	1.37

[a] Determined by ^{1}H NMR spectroscopy. [b] Values corrected considering Mark–Houwink factor (0.57) from polystyrene standards in THF. [c] Calculated from ([monomer]$_0$/Li) × conv (%) × monomer molecular weight (M_{CL}=100.12) + Molecular weight of BnOH. [d] From GPC. [e] Reaction performed without solvent. Solvent used in the ROP: toluene.

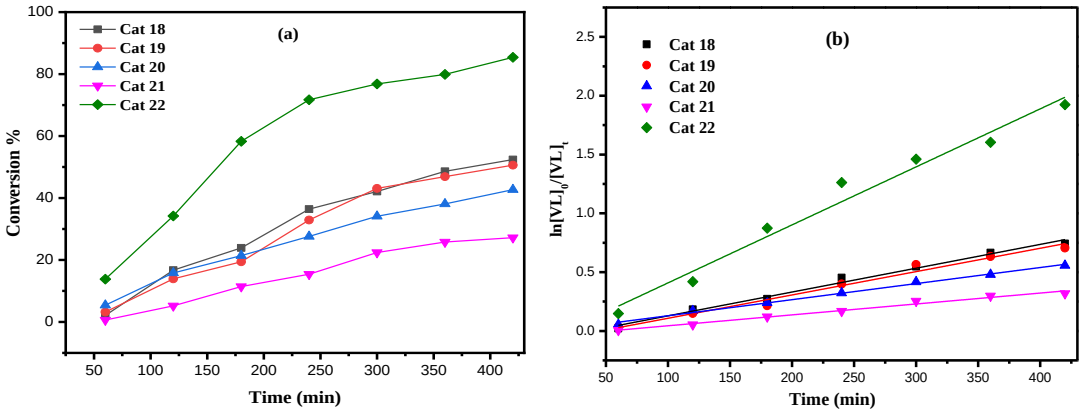

Figure 5-9. (a) Relationship between conversion and time for the polymerization of *δ*-VL by using complex **18** – **22**; (b) Plot of ln[VL]$_0$/[VL]$_t$ *vs*. time for the polymerization of *δ*-VL by using complexes **18** – **22**; Conditions: T=130 ºC, $n_{Monomer}$: n_{Li}: BnOH=500: 1: 1.

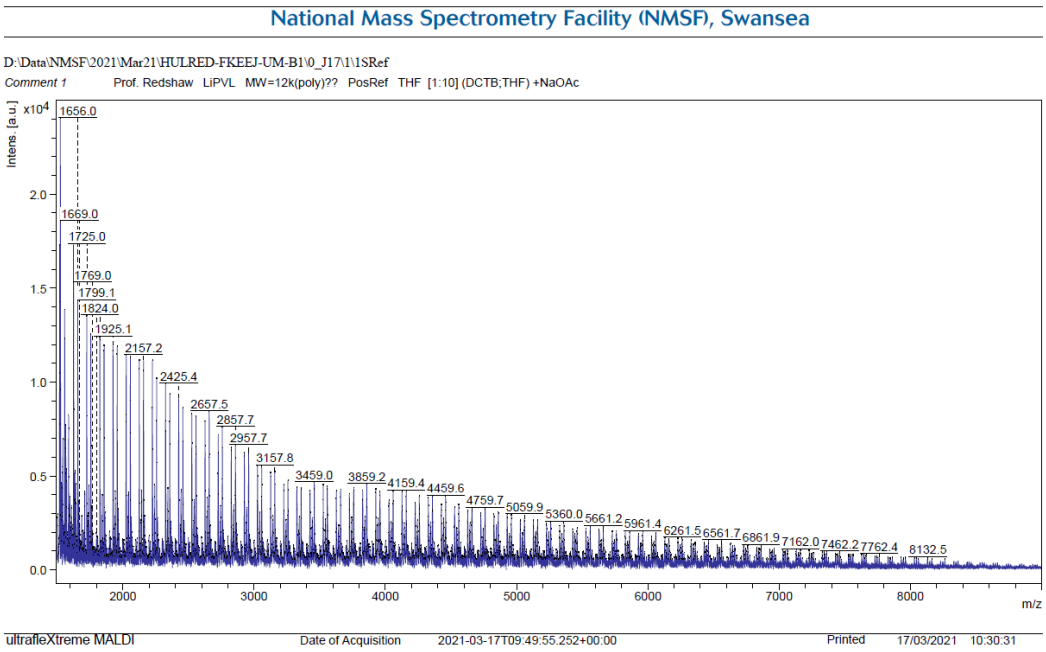

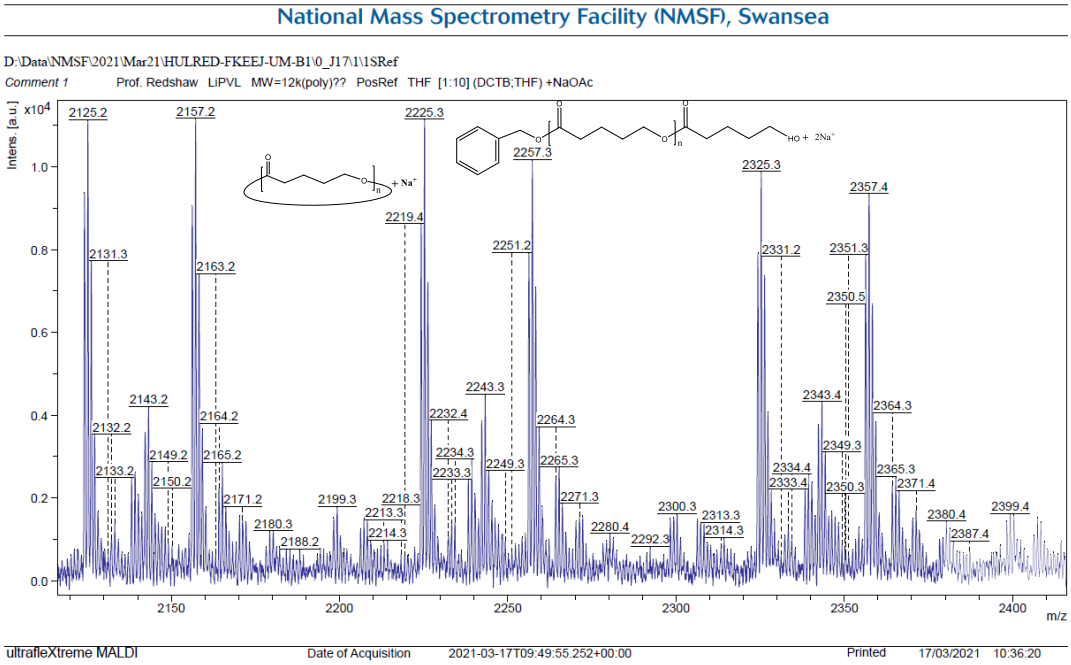

Figure 5-10. Mass spectrum of the PVL synthesized with **22**/BnOH (run 10, Table 5-2).

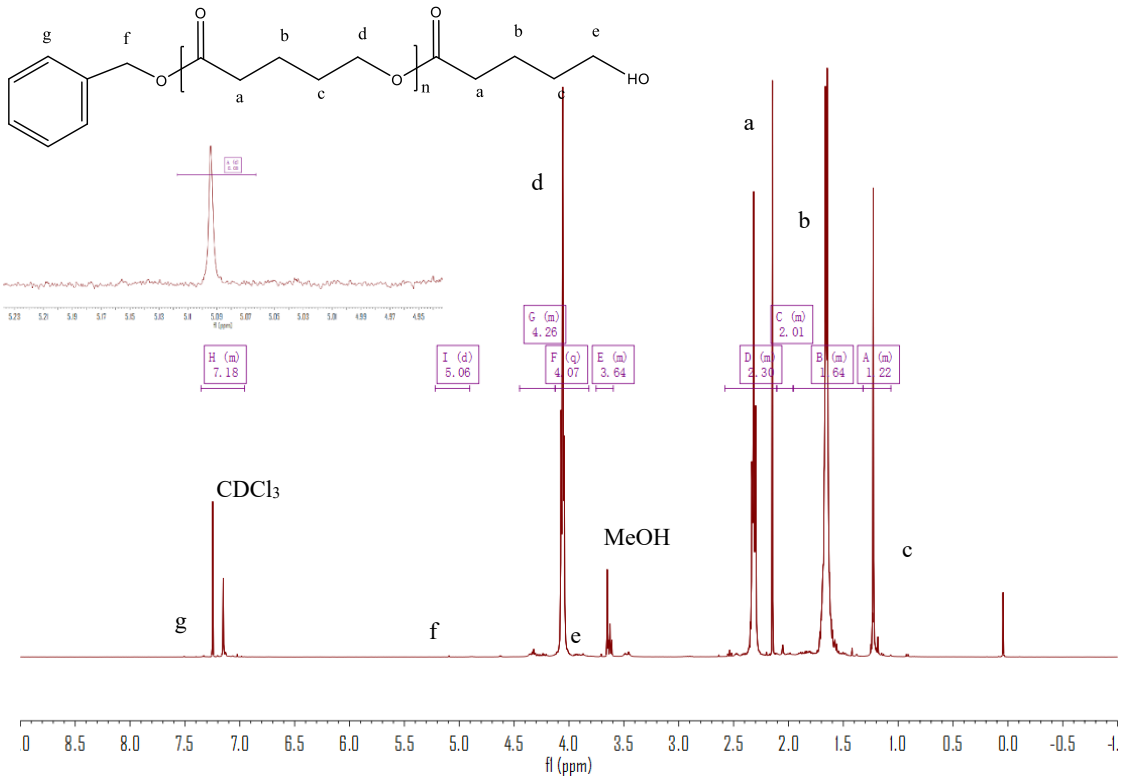

Figure 5-11. ^{1}H NMR spectrum ($CDCl_3$, 400 MHz, 298 K) of the PVL synthesized with **22**/BnOH (run 10, Table 5-2).

2.2.3 ROP of *r*-lactide

The complexes were also employed as catalysts in the ROP of *r*-LA (Table 5-3). Best conversion was achieved in the presence of **22** (56.6%, Table 5-3, run 5). The M_n of the polymer was lower than the calculated value albeit with narrow molecular weight distribution (6580 and 1.16, respectively). In the case of systems **18**-**22**, all polymers obtained were of relatively low polydispersity (PDI < 1.75), which suggested that there was moderate control of the polymerization. However, **21** only afforded 32.5% monomer conversion, affording low molecular weight species. ^{1}H NMR spectra of the PLA indicated the presence of a BnO end group (e.g. Figure 5-12), which agrees with the MALDI-ToF mass spectra (e.g. Figure 5-13). The sample was analysed by MALDI-ToF mass spectra in positive-linear mode with the expected series corresponding to repeating unit mass of 72/144 for half/full LA being observed and the polymer chain was terminated by OH and BnO end groups [M = 108.05 (BnOH) + n × 72.06 ($C_3H_4O_2$) + 22.99 (Na^+)]. The syndiotactic bias was determined by 2D *J*-resolved ^{1}H NMR spectroscopy, investigating the methine area (5.13-5.20 ppm) of the spectra (e.g. Figure 8-21, in Chapter 8).[21] The peaks were assigned to the corresponding tetrads according to the literature reports.[22] The observed value *Pr* (*Pr* = probability of racemic linkages) suggested all the catalysts afforded almost heteroatactic polymers.

Comparison *versus* lithiated **XIV** indicated that under solvent-free conditions (runs 7, 8) complex **22** outperforms **XIV**, whilst in toluene at 150 ^{o}C, **22** exhibits comparable behaviour to titanocalix[6]arene **XV** (runs 9, 10) and outperforms **XVI** (run 12) under the same conditions.

Table 5-3. ROP of *rac*-lactide using **18** – **22** and **XIV - XVI**.

Run	Cat.	LA: Li: BnOH	T/°C	t/h	Conv[a] (%)	$M_{n,GPC}\times10^{-3}$[b]	$M_w\times10^{-3}$[b]	Pr[c]	$M_{n,Cal}\times10^{-3}$[d]	PDI[e]
1	**18**	500: 1: 1	130	24	55.1	4.63	7.56	0.45	39.82	1.63
2	**19**	500: 1: 1	130	24	50.7	4.45	6.78	0.51	36.64	1.52
3	**20**	500: 1: 1	130	24	39.4	2.36	3.20	0.46	28.50	1.35
4	**21**	500: 1: 1	130	24	32.5	1.08	1.24	0.54	23.53	1.16
5	**22**	500: 1: 1	130	24	56.6	6.58	11.18	0.56	40.90	1.70
6	**22**	100: 1: 0	150	24	62.1	6.68	9.42	0.60	8.95	1.61
7	**22**[h]	100: 1: 0	150	24	84.1	12.23	17.39	0.56	12.14	1.42
8	**XIV**[h]	100: 1: 0	150	24	18	-	-	-	-	-
9	**22**	500: 1: 3	150	24	85.6	8.23	12.52	0.45	61.79	1.52
10	**XV**	500: 1: 3	150	24	87	8.19	10.56	0.51	21.00	1.29
11	**22**	250: 1: 1	150	24	91.4	7.55	10.52	0.45	33.04	1.39
12	**XVI**	250: 1: 1	150	24	8.2	-	-	-	-	-

[a] Determined by ^{1}H NMR spectroscopy on crude reaction mixture. [b] Values corrected considering Mark–Houwink factor (0.58) from polystyrene standards in THF. [c] From 2D *J*-resolved ^{1}H NMR spectroscopy. [d] Calculated from ([Monomer]$_0$/Li) × conv. (%) × Monomer molecular weight (M_{LA}=144.13) + Molecular weight of BnOH. [e] From GPC.

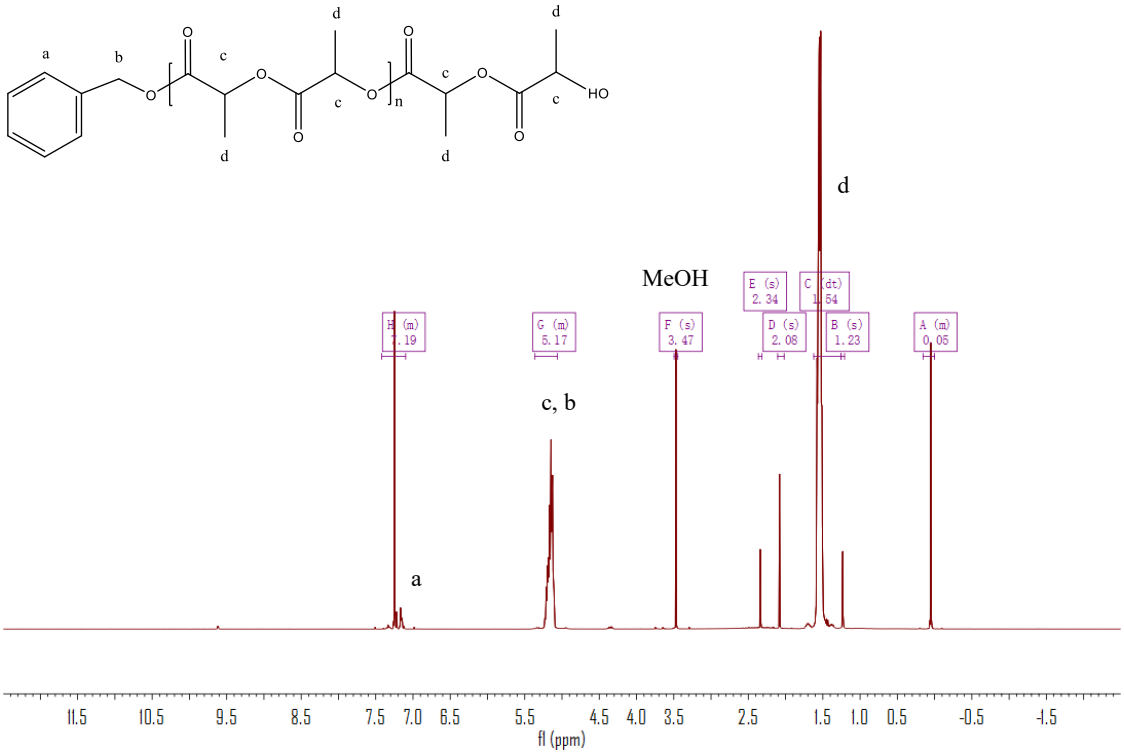

Figure 5-12. ^{1}H NMR spectrum ($CDCl_3$, 400 MHz, 298 K) of the PLA synthesized with **22**/BnOH (run 5, Table 5-3).

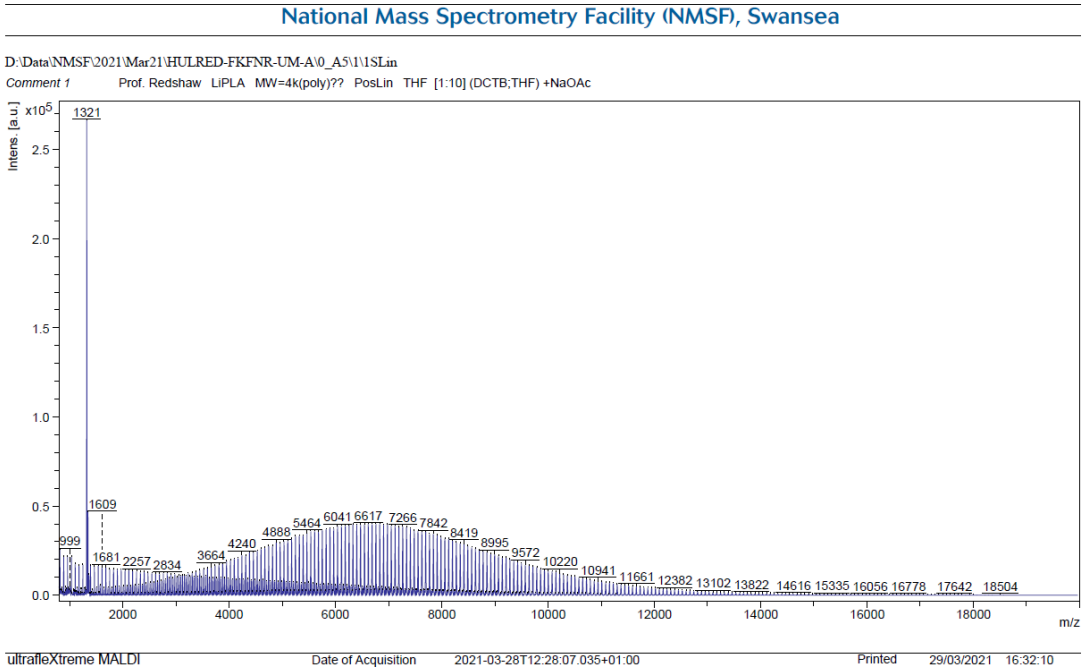

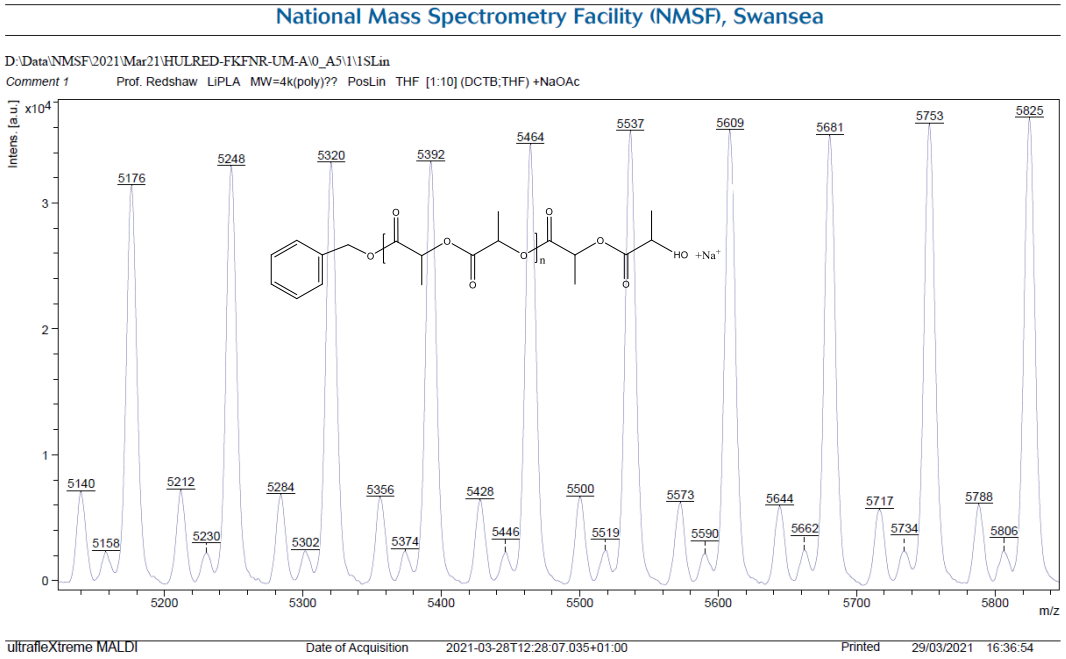

Figure 5-13. Mass spectrum of the PLA synthesized with **22**/BnOH (run 5, Table 5-3).

2.2.4 ROP of ω-pentadecalactone

To enhance the thermal properties of the polymers obtained herein, the current work also investigated the ROP of the ω-pentadecalactone. Unfortunately, none of the systems herein proved to be effective as catalysts for the ROP of ω-pentadecalactone either in solution at high temperatures (130 °C) or as melts.

2.2.5 Kinetics study of ε-CL and δ-VL

From a kinetic study of the ROP of ε-CL using **18**-**22**, it was observed that the polymerization rate exhibited first-order dependence on the ε-CL concentration (Figure 5-6), and the conversion of monomer achieved over 420 min was >20%. The activity trend in this case revealed that **22** was the most active and then **22** >**18** >**19** >**20** >**21**. An induction period of 2 h was observed for complexes **18**-**22** ascribed to the time required for the formation of the catalytically active species; a similar result was observed in the polymerization of δ-VL (Figure 5-9).

The dependence of the M_n and molecular weight distribution on the monomer conversion in the reactions catalyzed by **18**, **20**, **22** with BnOH was also investigated (Figure 5-13). For the ROP of ε-CL, the polymer M_n was shown to increase linearly with conversion, which suggested that the polymerization was well controlled (Figure 5-13, left). A similar outcome was also observed in the reaction involving δ-VL (Figure 5-13, right).

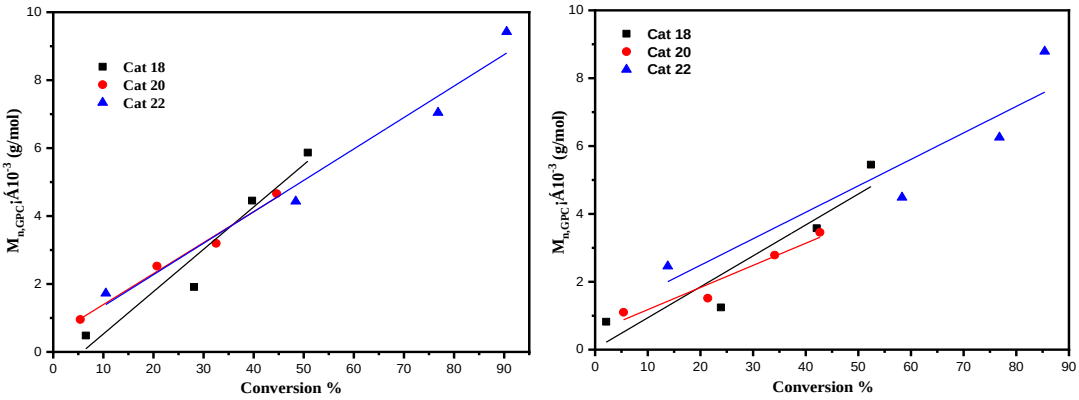

Figure 5-13. Left: M_n *vs*. monomer conversion in the ROP of ε-CL by using **18**, **20** and **22**; Right: M_n *vs*. monomer conversion in the ROP of δ-VL by using **18**, **20** and **22**; Conditions: T=130 ºC, $n_{Monomer}$: n_{Li}: BnOH= 500:1:1.

3. Conclusions

This chapter reports some rare examples of lithium complexes of larger p-*tert*-butylcalix[*n*]arenes (n = 6, 8). The molecular structures reveal how these macrocycles can support multiple metal centres which adopt some interesting structural motifs. The complexes are active for the ring opening polymerization of ε-caprolactone (ε-CL), δ-valerolactone (δ-VL) and *rac*-lactide (*r*-LA), with the mixed lithium-aluminum complex $[(AlMe_2)_2Li_{20}(L^8H_2)_2(OH_2)_4(O^{2-})_4(OH)_2(NCMe)_{12}]\cdot 10MeCN$ (**22**·10MeCN) proving to be the most active with first order kinetics. Low molecular weight products were obtained but with good control.

4. References

[1] (a) P. Jose and S. Menon, *Bioinorg. Chem. Appl*. 2007, 2007, 1-16; (b) S. B. Nimse and T. Kim, *Chem. Soc. Rev*. 2013, 42, 366-386; (c) 'Coordination Chemistry and Applications of Phenolic Calixarene–metal Complexes'. Y. Li, K.-Q. Zhao, C. Redshaw, B. A. Martínez

Ortega, A. Y. Nuñez, T. A. Hanna in Patai's Chemistry of Functional Groups. Wiley 2014; (d) M. Deska, B. Dondela, and W. Silwa, Arkivov 2015, (vi) 393-416; (e) R. Kumar, A. Sharma, H. Singh, P. Suating, H. S. Kim, K. Sunwoo, I. Shim, B. C. Gibb and J. S. Kim, *Chem. Rev*. 2019, 119, 9657-9721; (f) J. Wang and S. Zhuang, *Nucl. Eng. Technol*. 2020, 52, 328-336.

[2] A. Ikeda and S. Shinkai, *Chem. Rev*. 1997, 97, 1713-1734.

[3] D. M. Homden and C. Redshaw, *Chem. Rev*. 2008, 108, 5086-5130.

[4] O. Santoro, M. R. J. Elsegood, S. J. Teat, T. Yamato and C. Redshaw, *RSC Adv*. 2021, 11, 11304-11317.

[5] J. –M. Raquez, R. Mincheva, O. Coulembier, and P. Dubois, Ring-opening Polymerization of Cyclic Esters: Industrial Synthesis, Properties, Applications, and Perspectives. In Polymer Science: A Comprehensive Reference; Elsevier: Amsterdam, The Netherlands, 2012, 761–777.

[6] C. Redshaw, *Coord. Chem. Rev*. 2003, 244, 45-70.

[7] K. Wang, T. J. Prior and C. Redshaw, *Chem. Commun*. 2019, 55, 11279-11282.

[8] N. P. Clague, J. D. Crane, D. J. Moreton, E. Sinn, S. J. Teat and N. A. Young, *J. Chem. Soc.*, *Dalton Trans*., 1999, 3535-3536.

[9] R. D. Bergougnant, A. Y. Robin and K. M. Fromm, *Tetrahedron* 2007, 63, 10751-10757.

[10] For example, as of 17.6.21 on the Sigma-Aldrich website, the cost of L^8H_8 = 5 g for £46.60 (USD 64.94); L^6H_6 = 5 g for £130; deBuL^8H_8 = 1 g for £57.50.

[11] (a) A. K. Sutar, T. Maharana, S. Dutta and C. -T. Chen, *Chem. Soc. Rev*. 2010, 39, 1724-1746; (b) J. Gao, D. Zhu, W. Zhang, G. A. Solan, Y. Ma, and W. -H. Sun, *Inorg. Chem. Front*. 2019, 6, 2619-2652.

[12] (a) B. –T. Ko and C. –C. Lin, *J. Am. Chem. Soc*. 2001, 123, 7973-7977; (b) M. H. Chisholm, C. –C. Lin, J. C. Gallucci and B. –T. Ko, *Dalton Trans*. 2003, 406-412; (c) C. –A. Huang and C. –T. Chen, *Dalton Trans*. 2007, 5561-5566; (d) W. Clegg, M. G. Davidson, D. V. Graham, G. Griffen, M. D. Jones, A. R. Kennedy, C. T. O'Hara, L. Russo and C. M. Thomson, *Dalton Trans*. 2008, 1295-1301; (e) Y. Huang, Y. –H. Tsai, W. –C. Hung, C. –S. Lin, W. Wang, J. –H. Huang, S. Dutta and C. –C. Lin, *Inorg. Chem*. 2010, 49, 9416-9425; (f) W. –Y. Lu, M. –W. Hsiao, S. C. N. Hsu, W. –T. Peng, Y. –J. Chang, Y. –C. Tsou, T. –Y. Wu, Y. –C. Lai, Y. Chen and H. –Y. Chen, *Dalton Trans*. 2012, 41, 3659-3667; (g) N. Ikpo, C. Hoffmann, L. N. Dawe and F. M. Kerton, *Dalton Trans*. 2012, 41, 6651-6660; (h) R. K. Dean, A. M. Reckling, H. Chen, L. N. Dawe, C. M. Schneider and C. M. Kozak, *Dalton Trans*. 2013, 42, 3504-3520; (i) D. Alhashmialameer, N. Ikpo, J. Collins, L. N. Dawe, K. Hattenhauer and F. M. Kerton, *Dalton Trans*. 2015, 44, 20216-20231; (j) K. Devaine-Pressing, F. J. Oldenburg, J. P. Menzel, M. Springer, L. N. Dawe and C. M. Kozak, *Dalton Trans*. 2020, 49, 1531-1544.

[13] E. D. Gueneau, K. M. Fromm and H. Goesmann, *Chem. Eur. J*. 2003, 9, 509-514.

[14] R. McLellan, J. Rezé, S. M. Taylor, R. D. McIntosh, E. K. Brechin and S. J. Dalgarno, *Chem. Commun*. 2014, 50, 2202-2204.

[15] M. T. Muñoz, T. Cuenca and M. E. G. Mosquera, *Dalton Trans*. 2014, 43, 14377-14385.

[16] O. Santoro, M. R. J. Elsegood, E. V. Bedwell, J. A. Pryce and C. Redshaw, *Dalton Trans*., 2020, 49, 11978-11996.

[17] A. J. Chmura, M. G. Davidson, C. J. Frankis, M. D. Jones, and M. D. Lunn, *Chem.*

Commun., 2008, 1293-1295.

[18] M. Frediani, D. Sémeril, A. Marrioti, L. Rosi, P. Frediani, L. Rosi, D. Matt and L. Toupet, *Macromol. Rapid Comm.*, 2008, 29, 1554-1560.

[19] (a) Y. Wei, S. Wang and S. Zhou, *Dalton Trans*. 2016, 45, 4471–4485; (b) T. Fuoco and D. Pappalardo, *Catalysts*, 2017, 7, 64–81; (c) Y. Li, K.-Q. Zhao, M. R. J. Elsegood, T. J. Prior, X. Sun, S. Mo and C. Redshaw, *Catal. Sci. Technol*. 2014, 4, 3025–3031; (d) B. Antelmann, M. H. Chisholm, S.S. Iyer, J. C. Huffman, D. Navarro-Llobet, M. Pagel, W. J. Simonsick and W. Zhong, *Macromolecules*, 2001, 34, 3159–3175; (e) W. Braune and J. Okuda, *Angew. Chem. Int. Ed*. 2003, 42, 64–68; (f) C. Redshaw, *Catalysts* 2017, 7, 165.

[20] Z. Sun, Y. Zhao, O. Santoro, M. R. J. Elsegood, E. V. Bedwell, K. Zahra, A. Walton, and C. Redshaw, *Catal. Sci. Technol*., 2020, 10, 1619-1639.

[21] (a) C. Ludwig and M. R. Viant, *Phytochem. Anal*. 2010, 21, 22-32; (b) M. J. Walton, S. J. Lancaster and C. Redshaw, *ChemCatChem*, 2014, 6, 1892-1898.

[22] (a) Z. Zhong, P. J. Dijkstra and Jan Feijen, *J. Am. Chem. Soc*. 2003, 125, 11291-11298; (b) P. Hormnirun, E. L. Marshall, V. C. Gibson, A. J. P. White and D. J. Williams, *J. Am. Chem. Soc*. 2004, 126, 2688-2689.

Chapter 6

Lead calix[*n*]arenes (n = 4, 6, 8): Structures and ring opening polymerization capability for cyclic esters

1. Introduction

The ring opening polymerization (ROP) of cyclic esters is attracting much attention in light of the current environmental issues with petroleum-derived plastics.[1] As seen in previous chapters, coordination chemistry can play a crucial role in the development of new greener polymers with desirable features, given that control over the ligands at the metal centre of the catalyst employed for ROP can allow for control over the resultant polymer properties.[2] Ideally, the metal centre needs to be highly active, as well as abundant and non-toxic, however sometimes it is necessary for one of these criteria to become secondary if one or more of the others is exemplary. With this in mind, the report by Sarazin *et al* that for main group elements of group IV, systems employing the ligand set 2-CH_2NR_2-4,6-*t*Bu_2-C_6H_2OH (*i* = 1, NR_2 = $N((CH_2)_2OCH_3)_2$; *i* = 2, NR_2 = NEt_2; *i* = 3, NR_2 = aza-15-crown-5) were ROP active is of interest. The ROP activity followed the trend $Ge^{II} \ll Sn^{II} \ll Pb^{II}$,[3] whilst for a subsequent report on $[M(\mu_2\text{-O}i\text{Pr})_2]_n$, the trend was Ge ≪ Sn < Pb.[4] Thus, despite the issue of toxicity associated with lead compounds, and given the interest herein on metallocalix[*n*]arenes as ROP catalysts,[5] combined with the lack of lead calixarenes,[6] this chapter has utilized the calix[*n*]arenes shown in Chart 6-1, which differ in both size (n = 4, 6, 8) and/or bridge (-CH_2- or -CH_2OCH_2-), with focus on lead-containing calixarene complexes. A number of interesting multi-metallic species (see Chart 6-2) have been structurally characterized. The ability of these complexes to act as catalysts for the ROP of ε-caprolactone (ε-CL) and δ-valerolactone (δ-VL) has been investigated; the copolymerization of ε-CL and δ-VL was also investigated.

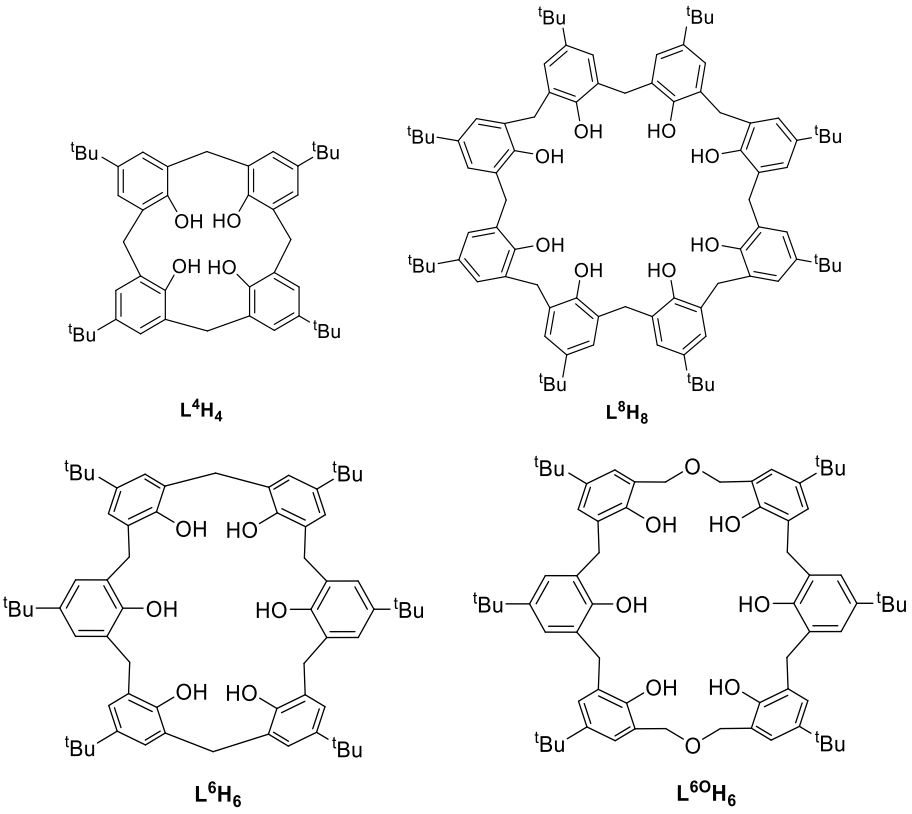

Chart 6-1. Calix[*n*]arenes used in this chapter.

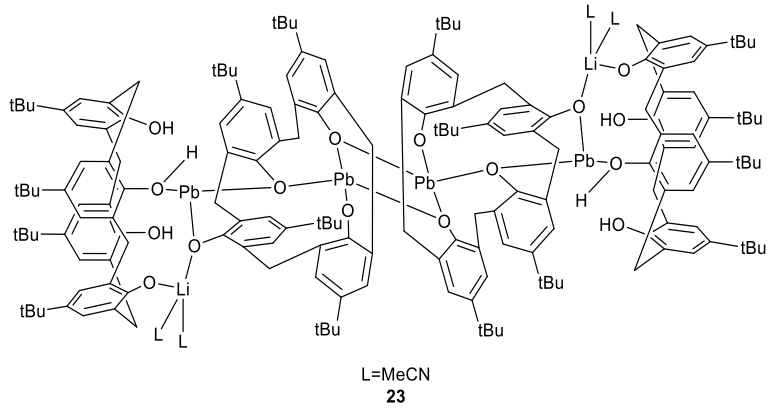

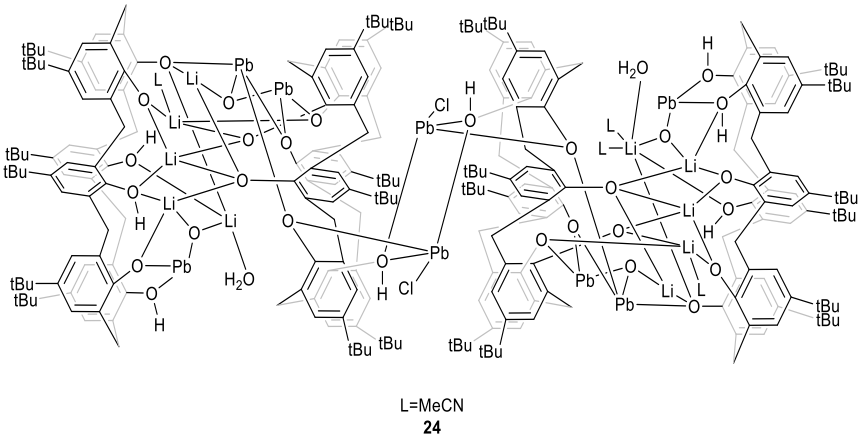

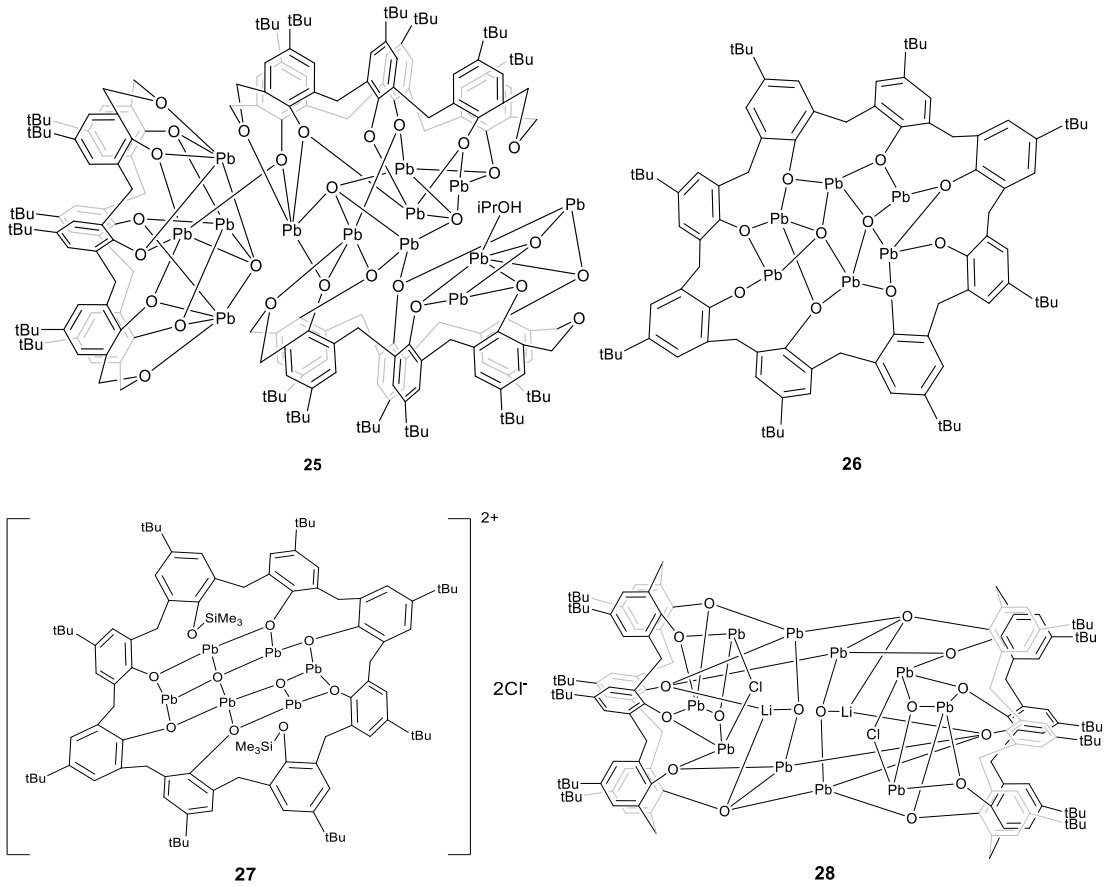

Chart 6-2. Pre-catalysts prepared herein.

2. Results and Discussion

2.1 Syntheses and solid-state structures

Given that previous reports have found the metallocalixarenes generated from heterobimetallic reagents of the form Li[M(OR)$_x$] tend to be highly crystalline,[7] the current work selected as the entry point the reagent [LiPb(O*i*Pr)$_3$]$_2$, which was generated *in-situ* from [Pb(O*i*Pr)$_2$] and LiO*i*Pr using a method similar to that for [LiPb(O*t*Bu)$_3$]$_2$.[4] Subsequent reaction with one equivalent of *p-tert*-butylcalix[4]areneH$_4$ (L^{4}H$_4$) in refluxing toluene led, following work-up (extraction into acetonitrile), to the complex [Pb$_4$Li$_2$(L^4)$_4$H$_6$(MeCN)$_3$]·4.5MeCN (**23**·4.5MeCN) in moderate yield (37%). The

molecular structure of **23**·4.5MeCN is shown in Figure 6-1, with selected bond lengths and angles given in the caption. The cluster is centosymmetric and contains four Pb atoms and two lithium centres. At the centre of the cluster are two Pb atoms (Pb2) and two oxygen atoms (O2) from a calix[4]arene in a diamond formation (Figure 6-1 bottom). On either side of this lie calix[4]arene molecules that are twisted so that one of the aromatic rings points downwards from the bowl of the calix; this enables it bind Pb2 on one side and Pb1 on the other. There is a further calix[4]arene at each end of the cluster (in bowl configuration) and this forms one O-Pb bond to Pb1. The lithium ions are coordinated by one oxygen from each of the two calixarenes; coordination about the Li is completed by MeCN. In essence, the complex can be described as a cluster of four stacked calix[4]arene molecules threaded by an LiOPbOPb(μ_2-O)PbOPbOLi chain.

Using a similar method to **23**, but using the larger calixarene *p-tert*-butylcalix[6]areneH_6 (L^6H_6) led to the isolation of the complex $[Pb_8Li_{10}Cl_2(L^6)_4(H)_8(O)_4(H_2O)_2(MeCN)_4]$·14MeCN (**24**·14MeCN) in moderate yield (47%). The molecular structure of **24**·14MeCN is shown in Figure 6-2, with selected bond lengths and angles given in the caption. The cluster is reasonably close to being centrosymmetric and is composed of four calixarenes that bind 8 lead ions and 10 lithium ions. At the centre of the cluster there is a Pb_2O_2 diamond which is linked to further lead atoms via bridging chloride ions. Two further Pb ions are bound near the plane of the six oxygen atoms by each calixarene adjacent to the centre. One more Pb is bound on each side by the terminal calixarenes, which also binds 5 lithium ions. There are additional oxide and hydroxide anions between the Pb and Li ions and bound acetonitrile.

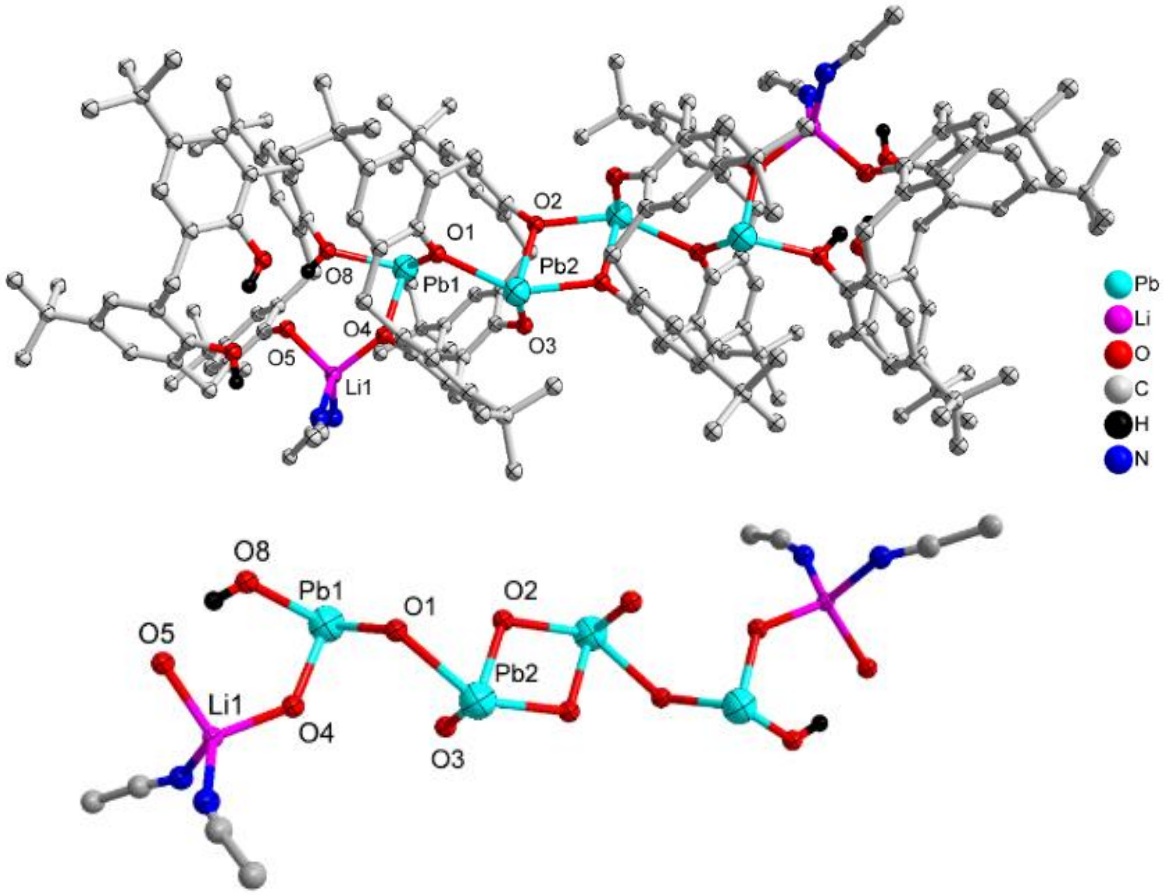

Figure 6-1. Molecular structure and core of $[Pb_4Li_2(L^4)_4H_6(MeCN)_3]\cdot 4.5MeCN$ (**23**·4.5MeCN). Non coordinated solvent molecules have been removed for clarity. Selected bond lengths (Å) and angles (°): Pb(1)-O(1) 2.235(5), Pb(1)-O(4) 2.260(6), Pb(1)-O(8) 2.357(6), Pb(2)-O(1) 2.528(6), Pb(2)-O(2) 2.283(6), O(1)-Pb(1)-O(4) 82.7(2), O(1)-Pb(1)-O8 101.3(2), O(4)-Pb(1)-O(8) 81.5(2), O(2)-Pb(2)-O(1) 77.74(19), O(3)-Pb(2)-O(1) 98.7(2), O(4)-Li(1)-O(5) 102.4(8), O(4)-Li(1)-N(2) 126.5(11), O(4)-Li(1)-N(1) 102.9(10), O(5)-Li(1)-N(1) 121.2(12).

Use of the precursors $[Pb(OR)_2]$ (R = *i*Pr or *t*Bu) or $\{Pb[N(TMS)_2]\}$ also allows access to metallocalix[*n*]arene species. Indeed, interaction of five equivalents of $[Pb(O{i}Pr)_2]$ with *p*-*tert*-butyltetrahomodioxacalix[6]areneH_6 ($L^{6O}H_6$) afforded, following work-up, the complex $[Pb_{13}(L^{6O})_3O_4(i\text{PrOH})]\cdot 11MeCN$ (**25**·11MeCN). The molecular structure of **25**·11MeCN is shown in Figure 6-3, with selected bond lengths and angles given in the caption. The complex is a large cluster of 13 unique Pb atoms composed of two smaller clusters. A pair of calixarenes are arranged roughly on top of each other. Between these lie

nine lead atoms (Pb5 – Pb13), and four oxide anions (O26-O29). Each lead is coordinated by the oxygen atoms of the calixarene and the oxide. Uniquely, the coordination of Pb11 is completed by an isopropoxide. The second part of the cluster is approximately perpendicular to the first and linked to it through the bond Pb2-O9. This contains four lead atoms (Pb1-Pb4) which surround a central oxide (O25). Around the cluster there are 11 unbound molecules of MeCN, some of which are ordered, others located by SQUEEZE.

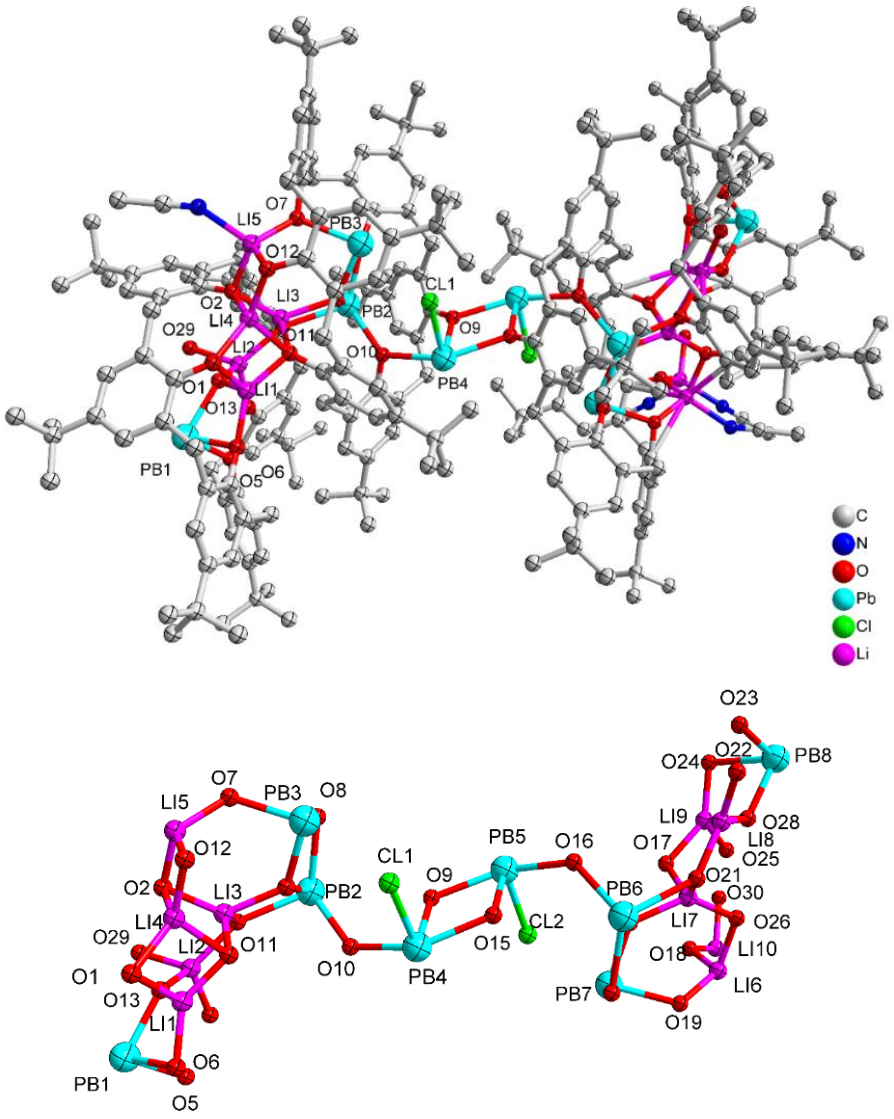

Figure 6-2. Molecular structure and core of $[Pb_8Li_{10}Cl_2(L^6)_4(H)_8(O)_4(H_2O)_2(MeCN)_4]\cdot 14MeCN$ (**24**·14MeCN). Selected bond lengths (Å) and angles (°): O(1)-Li(1) 2.063(16), O(1)-Li(4) 1.964(17), O(2)-Li(3) 1.978(15), O(2)-Li(4) 1.960(17), O(2)-Li(5) 1.943(16), O(3)-Pb(2) 2.496(6), O(3)-Li(2) 2.064(19), O(5)-Pb(1)

2.266(6), O(6)-Pb(1) 2.288(6), O(7)-Pb(3) 2.318(5), O(8)-Pb(3) 2.313(6), O(9)-Pb(4) 2.280(6), O(9)-Pb(5) 2.467(6), O(10)-Pb(2) 2.342(6), O(10)-Pb(4) 2.390(6), Li(4)-O(2)-Li(3) 81.2(6), Li(5)-O(2)-Li(3) 105.2(6), Li(5)-O(2)-Li(4) 83.2(7), Li(2)-O(3)-Pb(2) 157.1(6), Li(3)-O(3)-Pb(2) 93.9(5), Li(3)-O(3)-Li(2) 95.1(7), Pb(3)-O(8)-Pb(2) 104.7(2), Li(5)-O(7)-Pb(3) 122.3(5).

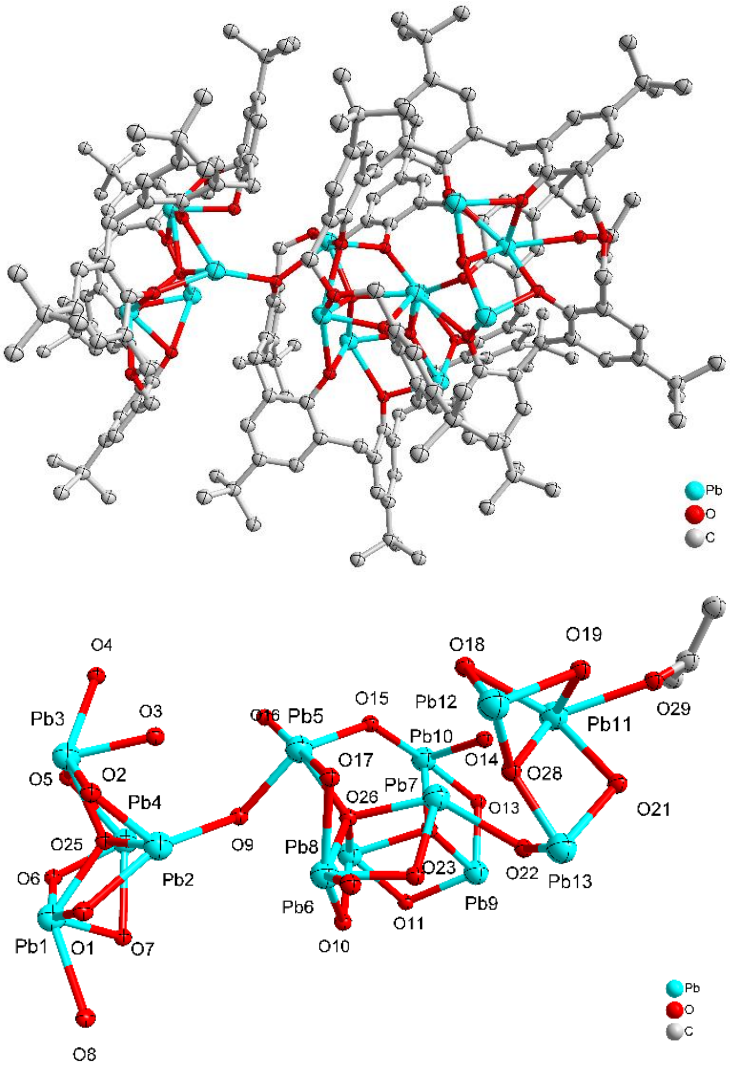

Figure 6-3. Molecular structure and core of $[Pb_{13}(L^{6O})_3O_4(i\text{PrOH})]\cdot 11\text{MeCN}$ (**25**·11MeCN). Selected bond lengths (Å) and angles (°): Pb(1)-Pb(2) 3.6746(6), Pb(1)-O(1) 2.356(8), Pb(1)-O(6) 2.553(8), Pb(1)-O(7) 2.359(8), Pb(2)-Pb(3) 3.5012(7), Pb(2)-O(1) 2.405(8), Pb(2)-O(2) 2.224(9), Pb(2)-O(9) 2.738(8), Pb(3)-O(2) 2.483(8), Pb(3)-O(3) 2.340(9), Pb(3)-O(4) 2.757(9), Pb(3)-O(5) 2.365(9), Pb(4)-O(5) 2.379(10), Pb(4)-O(6) 2.208(8), Pb(4)-O(7) 2.751(8), Pb(5)-O(9) 2.447(7), Pb(5)-O(15) 2.503(8), Pb(5)-O(16) 2.586(7), Pb(6)-O(17) 2.581(7), Pb(6)-O(23) 2.251(7), Pb(7)-Pb(10) 3.5418(6), O(1)-Pb(1)-Pb(2) 39.97(19), O(1)-Pb(1)-Pb(4) 108.51(19), O(1)-Pb(1)-O(6) 145.6(2), O(1)-Pb(1)-O(7) 106.6(3), Pb(5)-O(9)-Pb(2) 118.6(3), O(1)-Pb(2)-Pb(1) 38.99(19), O(1)-Pb(2)-O(9) 149.7(3), O(2)-Pb(2)-O(1) 76.6(3), O(2)-Pb(2)-O(9) 128.1(3), O(3)-Pb(3)-O(2) 68.7(3), O(5)-Pb(3)-O(4) 70.5(3), O(5)-Pb(4)-O(7) 132.0(3), O(9)-Pb(5)-O(15) 127.1(3).

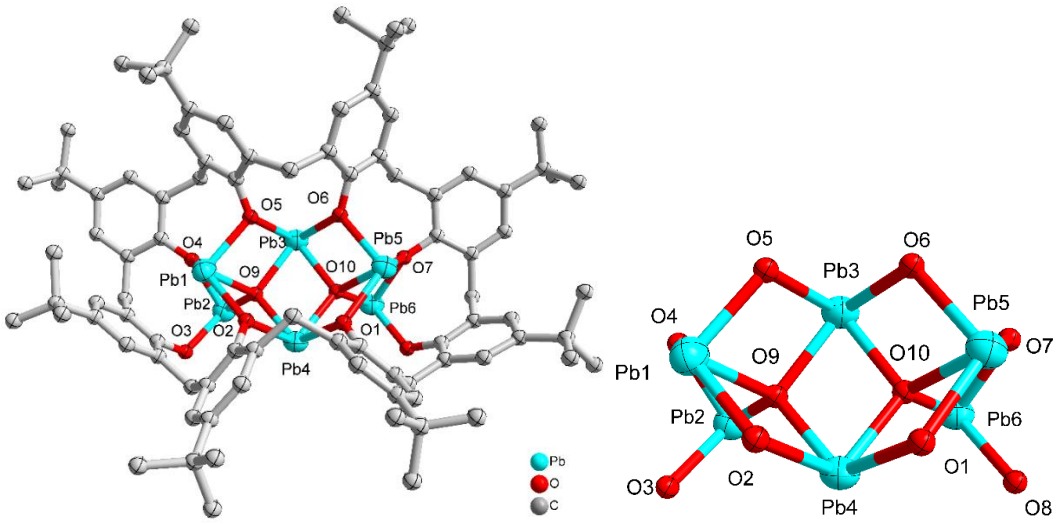

Figure 6-4. Molecular structure and core of $[Pb_{12}(L^8)_2O_4]\cdot 8.7C_7H_8$ (**26**·$8.7C_7H_8$). Selected bond lengths (Å) and angles (°): Pb(1)-O(9) 2.297(4), Pb(1)-O(5) 2.336(5), Pb(1)-O(2) 2.419(5), Pb(1)-O(4) 2.432(5), Pb(2)-O(3) 2.206(4), Pb(2)-O(9) 2.268(5), Pb(2)-O(4) 2.287(4), Pb(3)-O(5) 2.258(4), Pb(3)-O(10) 2.317(4), Pb(3)-O(6) 2.341(4), Pb(3)-O(9) 2.350(4), O(9)-Pb(1)-O(2) 69.91(15), O(5)-Pb(1)-O(2) 101.56(17), O(9)-Pb(1)-O(4) 68.63(16), O(3)-Pb(2)-O(9) 91.99(16), O(3)-Pb(2)-O(4) 90.09(17), O(9)-Pb(2)-O(4) 71.73(16), O(5)-Pb(3)-O(6) 79.54(16), O(10)-Pb(3)-O(6) 71.26(15), O(5)-Pb(3)-O(9) 73.37(16).

Similar use of $[Pb(O\textit{t}Bu)_2]$, but with p-*tert*-butylcalix[8]areneH_8 (L^8H_8) afforded the colourless dimer $[Pb_{12}(L^8)_2O_4]\cdot 8.7C_7H_8$ (**26**·$8.7C_7H_8$). The molecular structure of half of the dimer of **26**·8.7MeCN is shown in Figure 6-4, with selected bond lengths and angles given in the caption. In each half dimer, a hexanuclear lead cluster (Figure 6-4, right) sits on the open face of an L^8 bowl. The μ_4-oxo centres are thought to arise via adventitious oxygen. Two Pb-aryl interactions present result in the formation of the observed dimers (see Figure 8-22, Chapter 8).

The same calix[8]arene, namely L^8H_8, on interaction with {$Pb[N(TMS)_2]$} (TMS = $SiMe_3$) afforded after, work-up (MeCN), the product $[Pb_6(SiMe_3)_2(L^8)O_2Cl_2]$ (**27**). The complex is a centrosymmetric Pb cluster that contains a single calix[8]arene. The asymmetric unit contains one half of the calixarene, three Pb ions and one oxide. The molecular structure of **27** is shown in Figure 6-5, with selected bond lengths and angles given in the caption. Two

of the phenols of the calixarene on opposite sides of the ring carry $SiMe_3$ groups and do not bind to a metal. At the centre of the ring there is a cluster with composition Pb_6O_2 that is formed from two edge-sharing OPb_4 tetrahedra (oxide surrounded by four Pb ions). The coordination about the Pb ions is completed by the oxygen atoms of the calixarene. Pb1 sits at the apex of a square pyramid; the other unique Pb ions are three coordinate. The Cl atoms are thought to result from unreacted $PbCl_2$ during the synthesis of $\{Pb[N(TMS)_2]\}$.

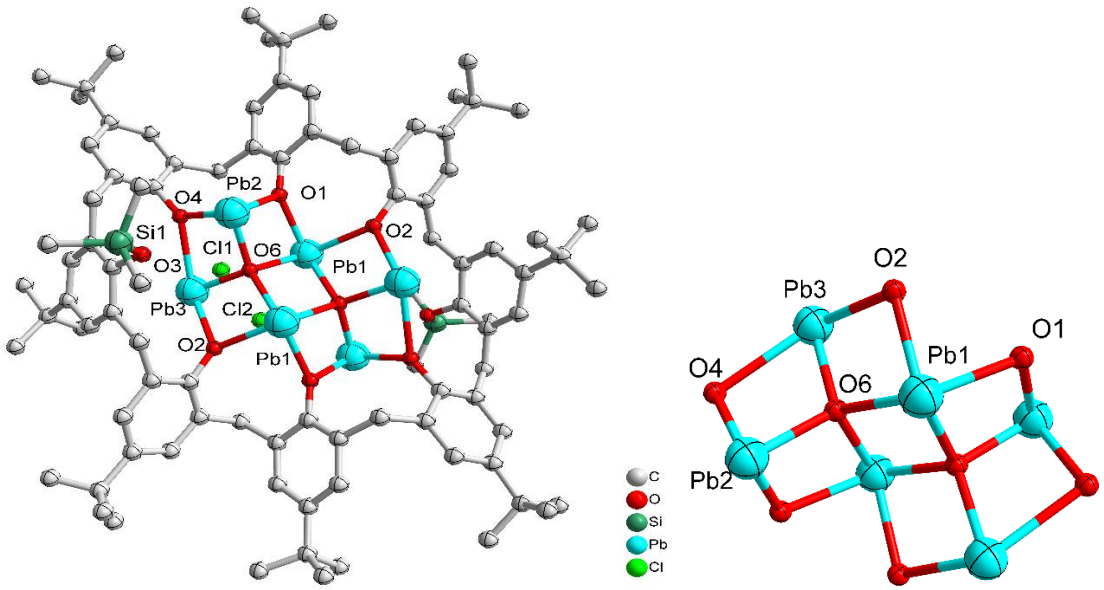

Figure 6-5. Molecular structure and core of $[Pb_6(SiMe_3)_2(L^8)O_2Cl_2]$ (**27**). Selected bond lengths (Å) and angles (°): O(1)-Pb(1) 2.416(12), O(1)-Pb(2) 2.244(13), O(2)-Pb(1) 2.485(13), O(2)-Pb(3) 2.442(12), O(3)-Si(1) 1.729(14), O(4)-Pb(2) 2.249(11), O(4)-Pb(3) 2.678(11), Pb(1)-O(6) 2.369(10), Pb(2)-O(6) 2.236(10), Pb(3)-O(6) 2.227(10), Pb(2)-O(1)-Pb(1) 104.9(4), Pb(3)-O(2)-Pb(1) 100.9(4), Pb(2)-O(4)-Pb(3) 95.8(4), O(1)-Pb(1)-O(2) 76.4(4), O(6)-Pb(1)-O(1) 120.3(4), O(6)-Pb(1)-O(2) 72.2(4), O(2)-Pb(3)-O(4) 131.7(4), O(6)-Pb(3)-O(2) 75.4(4), Pb(2)-O(6)-Pb(1) 114.8(5), Pb(3)-O(6)-Pb(1) 111.5(4), Pb(3)-O(6)-Pb(2) 110.5(4).

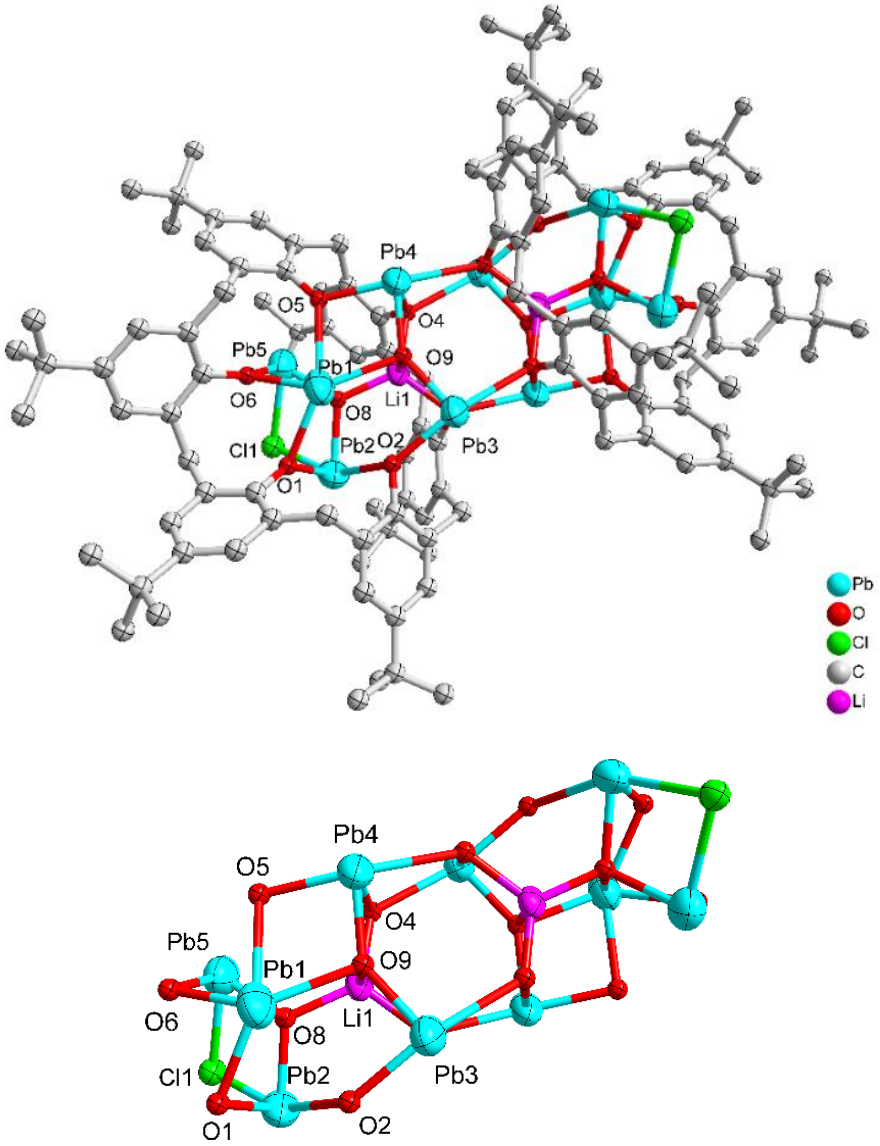

Figure 6-6. Molecular structure and core of $[Pb_5Li(L^6)O_{2.5}Cl_{0.5}]\cdot 4.75MeCN$ (**28**·4.75MeCN). Selected bond lengths (Å) and angles (°): Pb(3)-O(9) 2.158(3), Pb(3)-O(4) 2.728(3), Pb(3)-O(3) 2.392(3), Pb(3)-O(2) 2.306(3), Pb(5)-Cl(1) 2.669(4), Pb(4)-O(9) 2.159(3), Pb(4)-O(4) 2.428(3), Pb(4)-O(3) 2.719(3), Pb(4)-O(5) 2.313(3), O(9)-Pb(4)-O(4) 79.83(11), O(9)-Pb(4)-O(3) 99.61(10), O(9)-Pb(4)-O(5) 84.26(10), O(9)-Pb(4)-Li(1) 40.34(19), O(4)-Pb(4)-O(3) 70.32(9), O(8)-Pb(1)-O(1) 73.17(11), O(8)-Pb(1)-O(6) 74.46(10), O(6)-Pb(1)-O(1) 72.49(10), O(6)-Pb(1)-O(1) 72.49(10), O(8)-Pb(2)-O(1) 77.32(11), O(8)-Pb(2)-Li(1) 29.17(15), O(8)-Pb(2)-O(7) 72.2(3).

Finally, the precursor{$Pb[N(TMS)_2]$}, which was generated *in-situ* from $(Me_3Si)_2NH$, *n*BuLi and $PbCl_2$, was treated with L^6H_6. Following work-up (MeCN), the complex $[Pb_5Li(L^6)O_{2.5}Cl_{0.5}]\cdot 4.75MeCN$ (**28**·4.75MeCN) was isolated. The molecular structure of **28**·4.75MeCN is shown in Figure 6-6, with selected bond lengths and angles given in the

caption. The compound features a centrosymmetric cluster comprised of two symmetry-equivalent parts. Each calixarene binds one lithium ion and five lead ions, but between these ions there are oxide anions surrounded by four metal ions. In addition, there are hydroxide and chloride bridging between two lead ions (each 50% occupied and sharing a site). The two calixarenes do not lie face-on in the solid state but one is translated related to the other so that the bonding holing the $Pb_{10}Li_2$ cluster together is two pairs of Pb-O(calix) bonds; hydroxide and oxide are not involved in bridging.

2.1 Ring opening polymerization studies

General: The performance of these complexes to act as catalysts for the ring opening polymerization (ROP) of *ε*-caprolactone (*ε*-CL) (Table 6-1), *δ*-valerolactone (*δ*-VL) (Table 6-2), the co-polymerization of *ε*-caprolactone and *δ*-valerolactone (Table 6-3) and the ROP of *rac*-lactide (*r*-LA) (Table 6-4) has been investigated.

2.1.1 Polymerization of *ε*-caprolactone (*ε*-CL)

Complexes **23**-**27** were screened for their ability to polymerise *ε*-caprolactone and the results are collated in Table 6-1. The polymerization screening indicated that the best conditions were 500 equivalents of *ε*-caprolactone to metal at a temperature of 130 ^{o}C. Complex **23** was also active at low catalyst loading leading to *ca*. 54% conversion after 8 h for 1000 equivalents of monomer. All polymers obtained were of relatively low polydispersity (PDI < 2), which suggested that these polymerizations occurred without significant side reactions. Interestingly, complex **23** proved to be active also under aerobic conditions achieving *ca*. 49% conversion over 8 h (Table 6-1, run 7).

The screening of complexes **23**-**27** (Table 6-1) showed that the lead/lithium-based complexes **23** and **24** exhibited higher activities than other complexes under the conditions employed. After 24 h (Table 1), complexes **25**-**27** afforded relatively lower conversions (<70%), whereas higher conversions (>70%) were reached using complexes **23** and **24**, under similar conditions. The higher conversions achieved using **23** and **24** may be attributed to the presence of the lithium centres, although it should be noted that the lability of the MeCN ligands present in these species may also prove beneficial. This is in line with a recent study by our group on titanocalix[4]arenes, in which the presence of a labile ligand (*i.e*. MeCN and H_2O) proved beneficial for the catalyst activity.[8] From a kinetic study (Figure 6-7), it was observed that the PCL polymerization rate followed the order: **24** >**23** >**25** >**26** ≈ **27** (with first order dependence, see kinetics section). Compared with the larger lead-calix[8]arene complexes **26** and **27**, complexes **23**-**25** were found to be relatively more active (Table 6-1, run 12-14), which may due to the oxacalix[*n*]arene complexes with dimethyleneoxa bridges (–CH_2OCH_2–) showed more favourable conformational flexibility than calix[*n*]arene ligand with methylene bridges (–CH_2–).[9] Furthermore, compared with **26** and **27**, the higher activity of **25** was thought to be due to the higher flexibility of the –CH_2OCH_2– bridge allowing better access to the active centre(s) and/or to the stabilization of the active species by the oxygen atoms of said bridge.[10] The MALDI-ToF mass spectra (e.g. Figure 6-8) indicated the presence of an BnO end group, which agrees with the ^{1}H NMR spectra of the PCL (e.g. Figure 6-9) and indicates that the polymerization proceeded via a coordination insertion mechanism. Indeed, the MALDI-ToF spectrum of the sample displayed a major series of peaks separated by 114

m/z units accountable to two OH terminated PCL *n*-mers [M = 17 (OH)+ 1(H) + n × 114.14 (CL) + 22.99 (Na^+)]. Additionally, there is a family of peaks consistent with the polymer terminated by OH and BnO end groups [M = n × 114.12 (CL) + 108.05 (BnOH) + 22.99 (Na^+)].

Table 6-1. ROP of ε-CL using **23-27**.

Run	Cat.	CL: Pb: BnOH	T/°C	t (h)	Conv[a] (%)	$M_{n,GPC}\times10^{-3}$[b]	$M_w\times10^{-3}$[b]	$M_{n,cal}\times10^{-3}$[c]	PDI[d]
1	**23**	1000: 1: 1	130	8	54.2	8.05	15.34	61.86	1.91
2	**23**	500: 1: 1	130	8	60.4	8.49	14.55	34.47	1.71
3	**23**	250: 1: 1	130	8	57.3	6.52	9.45	16.35	1.45
4	**23**	100: 1: 1	130	8	52.4	3.56	5.14	5.98	1.44
5	**23**	500: 1: 1	100	8	35.4	4.38	5.79	20.20	1.32
6	**23**	500: 1: 1	80	8	24.8	1.23	1.43	14.15	1.16
7	**23**[e]	500: 1: 1	130	8	49.1	3.22	5.42	28.02	1.69
8	**24**	500: 1: 1	130	8	72.6	8.94	11.57	41.43	1.29
9	**25**	500: 1: 1	130	8	55.2	6.72	8.09	31.50	1.20
10	**26**	500: 1: 1	130	8	40.7	2.95	3.57	23.23	1.21
11	**27**	500: 1: 1	130	8	49.1	3.75	4.50	28.02	1.20
12	**23**	500: 1: 1	130	24	70.5	10.59	14.24	40.24	1.34
13	**24**	500: 1: 1	130	24	92.1	11.25	12.45	52.56	1.11
14	**25**	500: 1: 1	130	24	66.9	6.81	8.06	38.18	1.18
15	**26**	500: 1: 1	130	24	59.4	4.20	4.81	33.90	1.15
16	**27**	500: 1: 1	130	24	62.6	5.11	6.09	35.73	1.19
17	**23**	500: 1: 0	130	24	44.7	8.33	8.73	25.51	1.05
18	**24**	500: 1: 0	130	24	72.4	5.23	6.98	41.32	1.33
19	**25**	500: 1: 0	130	24	58.1	3.21	4.53	33.16	1.41
20	**26**	500: 1: 0	130	24	35.2	2.51	3.70	20.09	1.47
21	**27**	500: 1: 0	130	24	52.8	2.86	4.21	30.13	1.47

[a] Determined by ^{1}H NMR spectroscopy. Values corrected considering Mark–Houwink factor (0.56) from polystyrene standards in THF. [c] Calculated from ($[monomer]_0$/Pb) × conv (%) × monomer molecular weight (*M*CL=114.14) + Molecular weight of BnOH. [d] From GPC. [e] Reaction performed in air. Solvent used in the ROP: toluene.

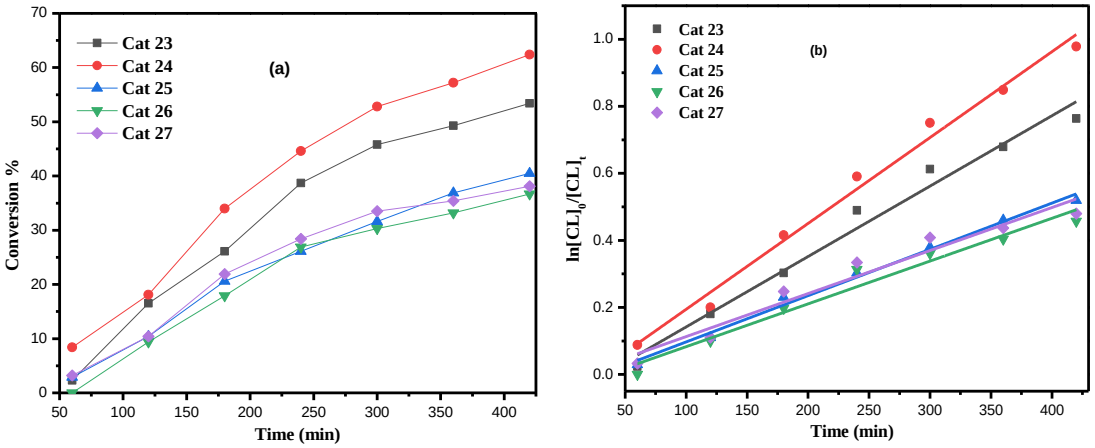

Figure 6-7. (a) Relationship between conversion and time for the polymerization of ε-CL by using complex **23-27**; (b) Plot of $\ln[CL]_0/[CL]_t$ *vs*. time for the polymerization of ε-CL by using complexes **23-27**; Conditions: T=130 °C, $n_{Monomer}$: n_{Pb}: BnOH=500: 1: 1.

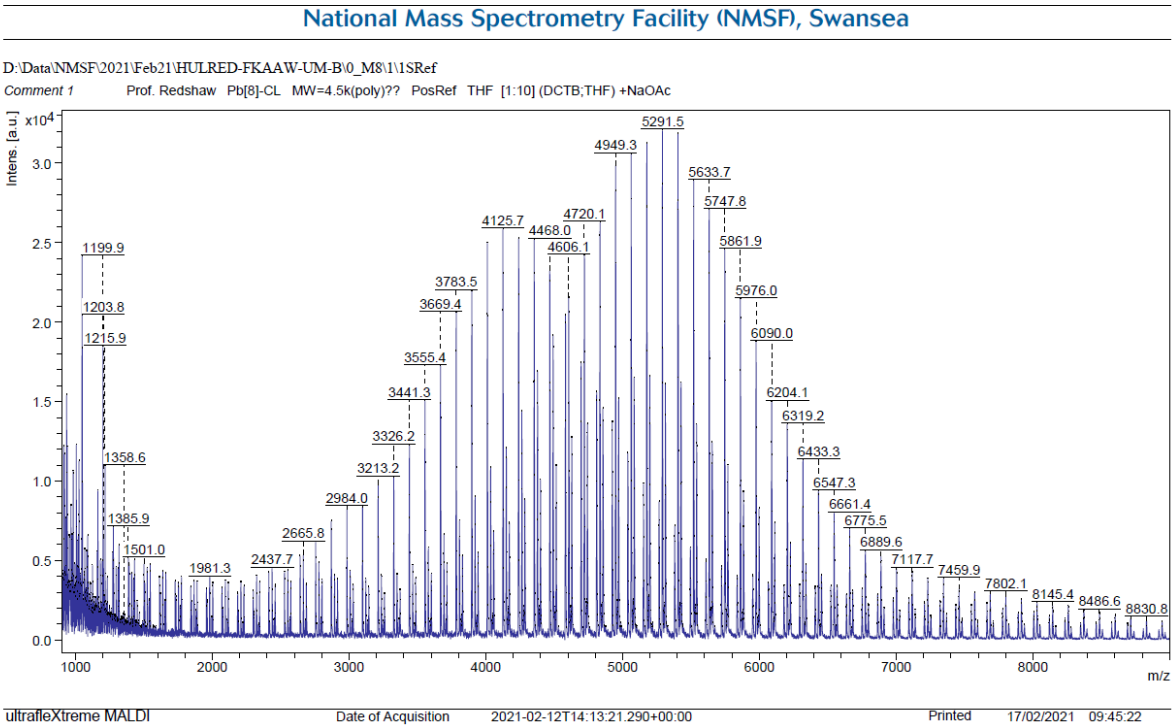

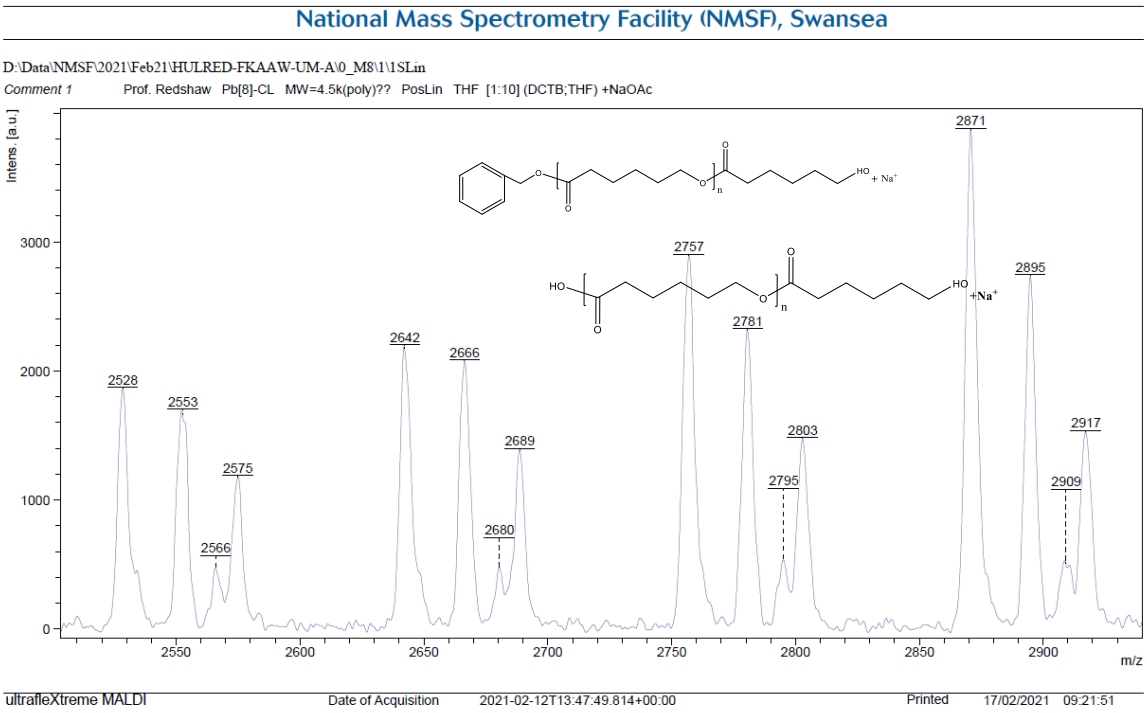

Figure 6-8. Mass spectrum of PCL synthesized with **26**/BnOH (run 15, Table 6-1).

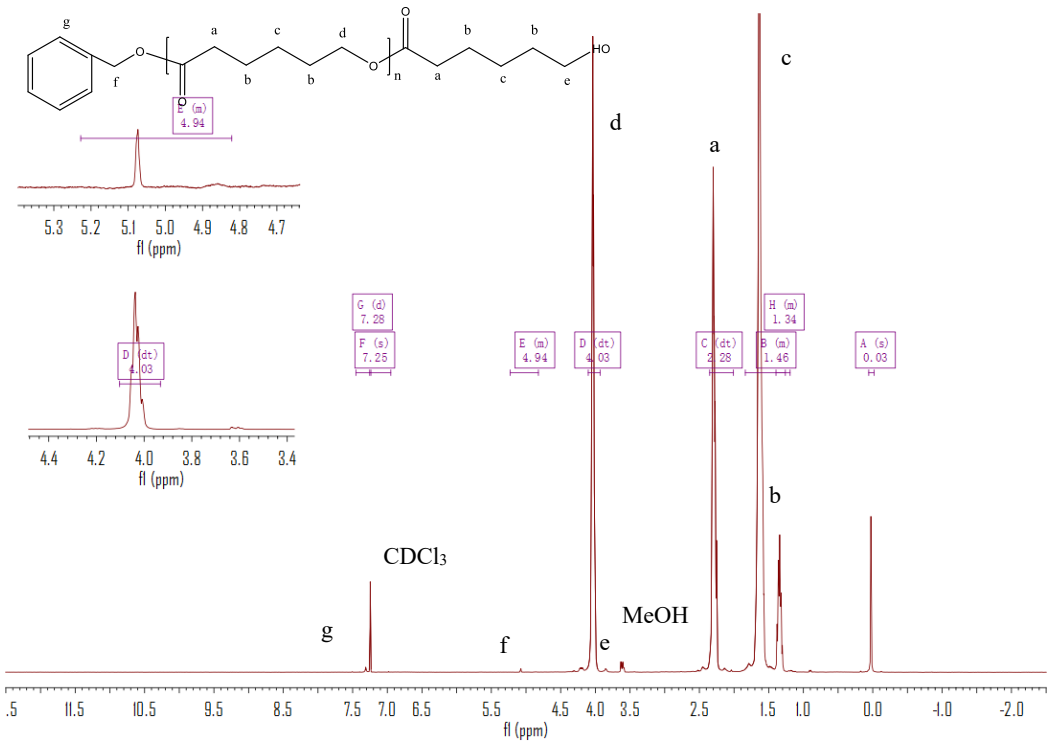

Figure 6-9. ^{1}H NMR spectrum ($CDCl_3$, 400 MHz, 298 K) of the PCL synthesized with **24**/BnOH (run 13, Table 6-1).

2.1.2 Polymerization of *δ*-valerolactone (*δ*-VL)

Complexes **23-27** were also evaluated as catalysts, in the presence of one equivalent of BnOH, for the ROP of δ-VL (Table 6-2). Using **23**, the conditions of temperature and [Pb]: [δ-VL] ratio were varied. On increasing the temperature to 130 °C and lowering the monomer to catalyst ratio, best observed results were achieved at 130 °C using [V]: [*δ*-VL] at 1:500 over 8 h. As in the case of the ROP of *ε*-CL, kinetic studies (Figure 6-10) revealed that the catalytic activities followed the order: **24** >**23** >**25** >**26** ≈ **27**. As for the ROP of *ε*-Cl, there was evidence of significant transesterification and nearly all observed M_n values were significantly lower than the calculated values. The MALDI-ToF mass spectra (Figure 6-11) exhibited a major family of peaks consistent with BnO end groups [M = 108.05 (BnOH) + n × 100.12 (VL) + 22.99 (Na^+)], and a family assigned to the PVL with two OH end groups [M = 17 (OH)+ 1(H) + n × 114.14 (CL) + 22.99 (Na^+)]. The ^{1}H NMR spectra of the PVL also indicated the presence of a BnO end group (e.g. Figure 6-12).

Table 6-2. ROP of *δ*-VL using **23-27**.

Run	Cat.	VL: Pb: BnOH	T/°C	t (h)	Conv[a] (%)	$M_{n,GPC}\times10^{-3}$[b]	$M_w\times10^{-3}$[b]	$M_{n,cal}\times10^{-3}$[c]	PDI[d]
1	**23**	1000: 1: 1	130	8	61.2	7.53	12.57	61.29	1.67
2	**23**	500: 1: 1	130	8	68.9	7.90	12.87	34.50	1.63
3	**23**	250: 1: 1	130	8	61.0	5.12	8.56	15.27	1.67
4	**23**	100: 1: 1	130	8	55.5	2.52	3.96	5.56	1.57
5	**23**	500: 1: 1	100	8	41.2	3.49	7.12	20.63	2.04
6	**23**	500: 1: 1	80	8	31.5	-	-	-	-
7	**23**[e]	500: 1: 1	130	8	43.1	4.01	6.54	21.58	1.63
8	**24**	500: 1: 1	130	8	75.9	10.98	13.83	38.00	1.26
9	**25**	500: 1: 1	130	8	52.4	5.32	6.00	26.24	1.13
10	**26**	500: 1: 1	130	8	36.2	2.15	2.65	18.13	1.23
11	**27**	500: 1: 1	130	8	34.3	1.97	2.38	17.18	1.20

[a] Determined by ^{1}H NMR spectroscopy. [b] Values corrected considering Mark–Houwink factor (0.57) from polystyrene standards in THF. [c] Calculated from ([monomer]$_0$/Pb) × conv

(%) × monomer molecular weight (M_{VL}=100.16) + Molecular weight of BnOH. [d] From GPC. [e] Reaction performed in air. Solvent used in the ROP: toluene.

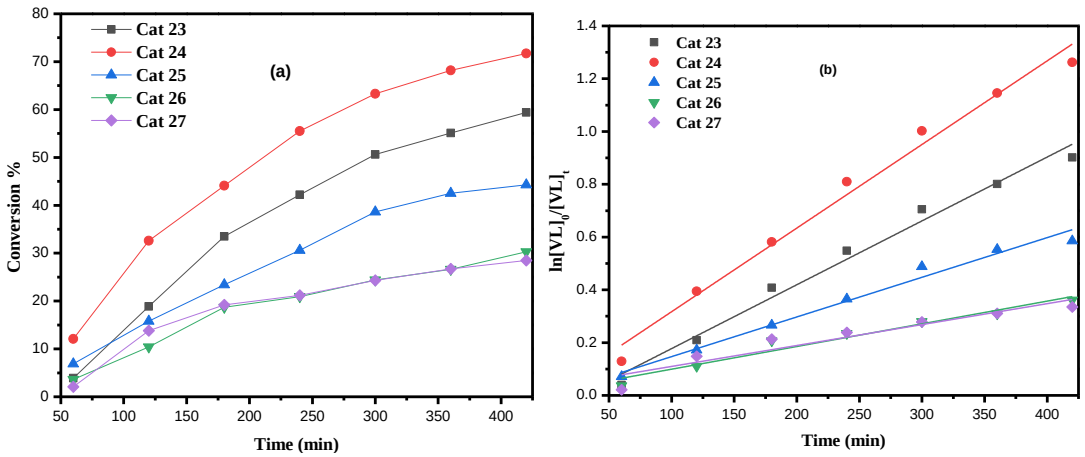

Figure 6-10. (a) Relationship between conversion and time for the polymerization of *δ*-VL by using complex **23-27**; (b) Plot of $\ln[VL]_0/[VL]_t$ *vs*. time for the polymerization of *δ*-VL by using complexes **23-27**; Conditions: T=130 ºC, $n_{Monomer}$: n_{Pb}: BnOH=500: 1: 1.

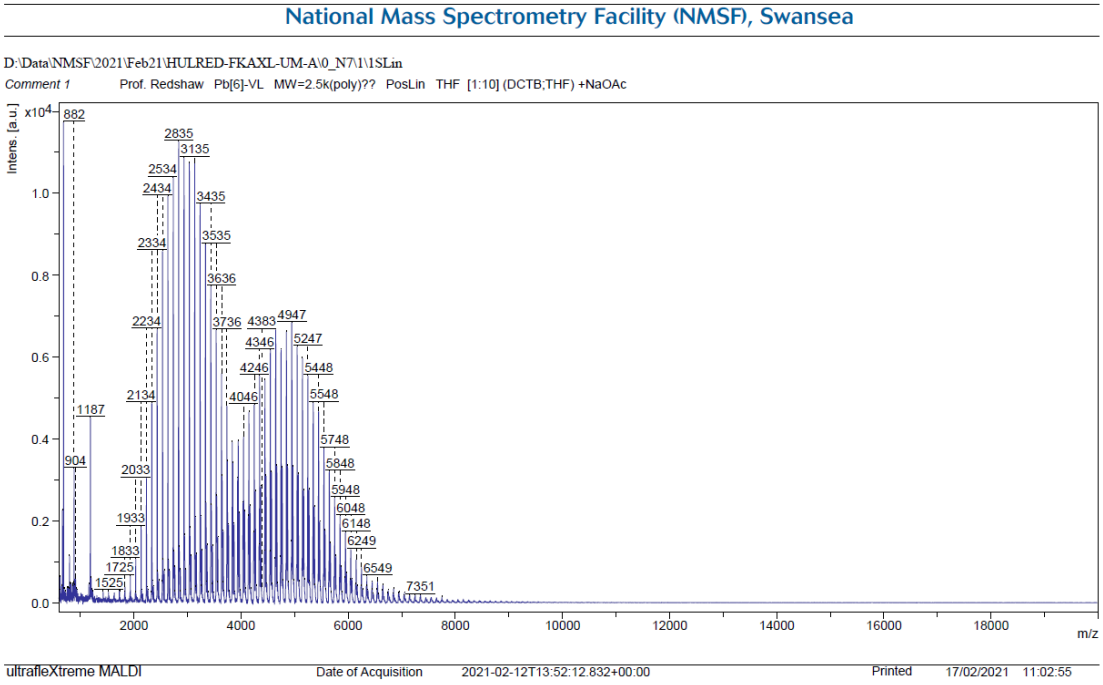

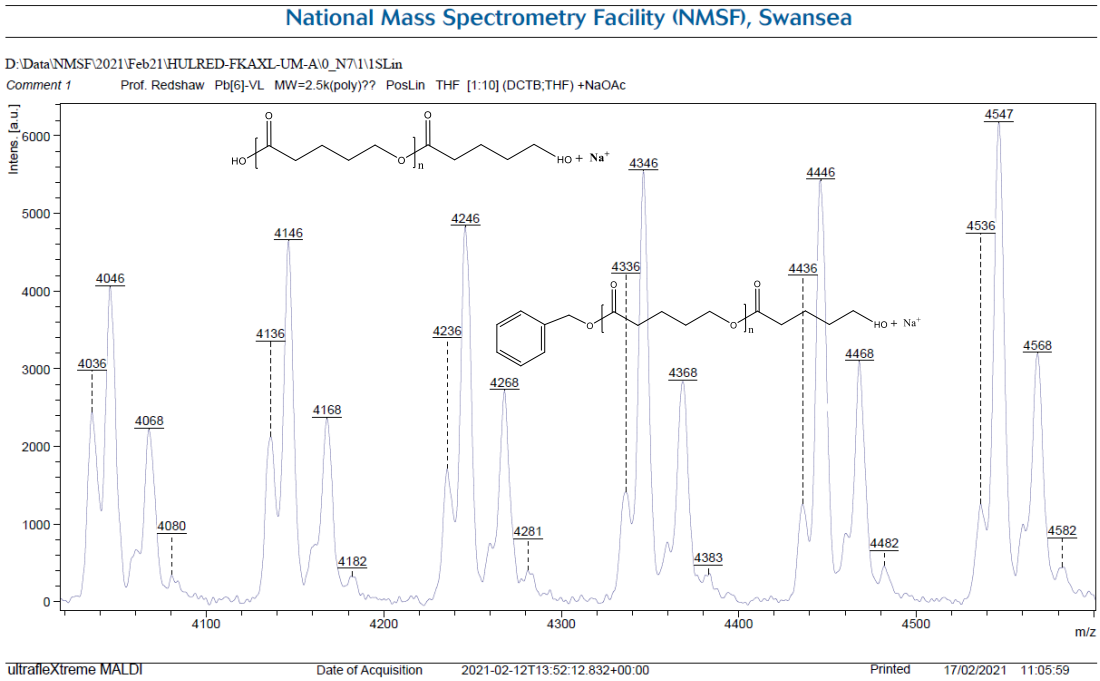

Figure 6-11. Mass spectrum of PVL synthesized with **24**/BnOH (run 8, Table 6-2).

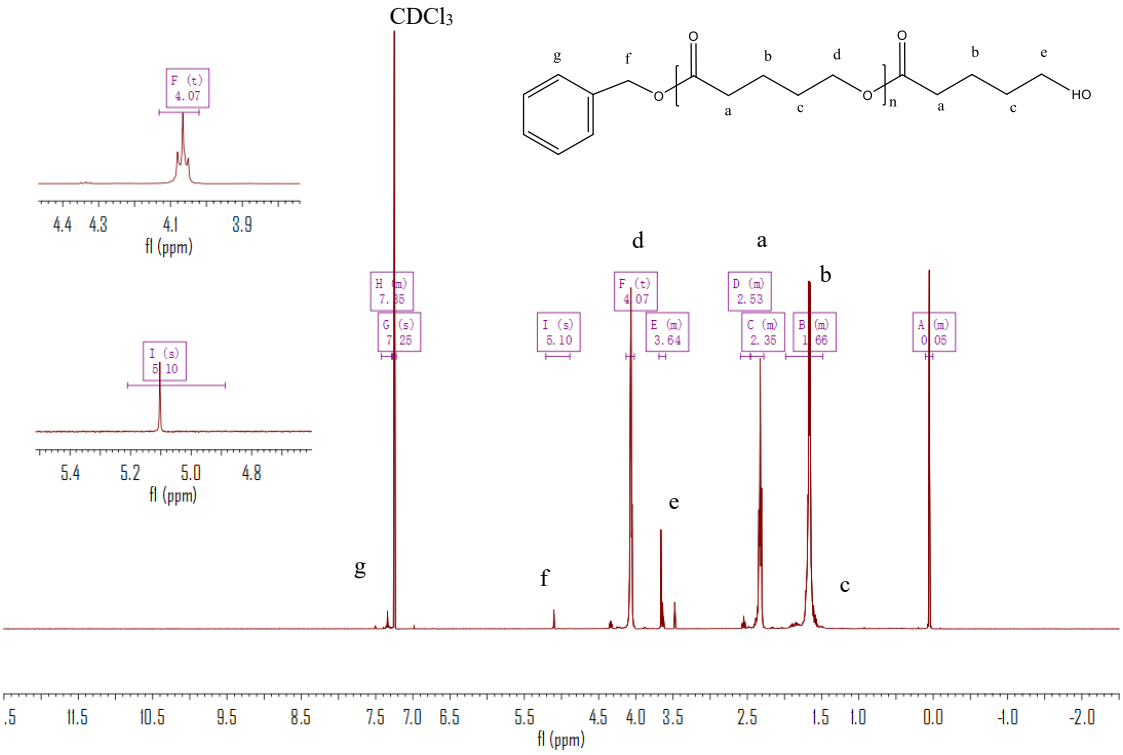

Figure 6-12. ^{1}H NMR spectrum ($CDCl_3$, 400 MHz, 298 K) of the PVL synthesized with **25**/BnOH (run 9, Table 6-2).

2.1.3 Co-polymerization of *ε*-CL and *δ*-VL

The complexes exhibited moderate conversions, with the mixed-metal complex **24** performing best (68.4%). Under the conditions employed, the systems **24**, **25** and **27** showed a preference for CL incorporation (50–64%), and in the case of **27**, this was despite the initial addition of *δ*-VL. Complex **23** exhibited the highest preference (58%) for VL incorporation. In general, the systems appeared to be relatively well behaved with PDIs in the range 1.23-1.51; ^{1}H NMR spectra were consistent with the presence of BnO and OH end groups (Figure 6-13). The composition of the copolymer was further investigated by ^{13}C NMR spectroscopy. In fact, diagnostic resonances belonging to CL–VL, CL–CL, VL–VL and VL–CL dyads can be observed in the region between δ 63.73 and 64.35 ppm (Figure 8-23, Chapter 8). Based on the current results, the number-average sequence length was found to be 1.35 and 3.09 for CL and VL, respectively, consistent with a randomness degree R of 0.98, which suggests the copolymers possess a "blocking" tendency (Figure 8-23, Equations 8-6 to 8-8, Chapter 8).[11]

Table 6-3. ROP of co-polymer (*ε*-CL + *δ*-VL) using **23**-**27**.

Run	Cat	CL: VL: Pb: BnOH	T/°C	CL:VL[a]	Conv[b] (%)	$M_{n,GPC}\times10^{-3}$[c]	$M_w\times10^{-3}$[c]	PDI[d]
1	**23**[e]	250:250:1:1	130	42: 58	61.0	10.98	13.83	1.26
3	**24**[e]	250:250:1:1	130	50: 50	68.4	11.10	15.97	1.44
4	**25**[e]	250:250:1:1	130	52: 48	52.6	6.97	8.69	1.25
5	**26**[e]	250:250:1:1	130	45: 55	53.1	5.60	8.37	1.50
6	**27**[e]	250:250:1:1	130	43: 57	47.2	4.56	6.89	1.51
7	**27**[f]	250:250:1:1	130	64: 36	53.9	6.16	7.56	1.23
8	**27**[g]	250:250:1:1	130	49:51	46.2	3.96	5.89	1.49

[a] Ratio of *ε*-CL to *δ*-VL observed in the co-polymer by ^{1}H NMR spectroscopy. [b] Determined by ^{1}H NMR spectroscopy. [c] $M_{n/w}$, GPC values corrected considering Mark–Houwink method from polystyrene standards in THF, $M_{n/w}$ GPC = [0.56 × $M_{n/w\ measured}$ × (1-%CL) + 0.57 × $M_{n/w}$ measured ×(1-%VL)] × 10^3. [d] From GPC. [e] *ε*-Caprolactone was firstly added for 24 h, then *δ*-

valerolactone was added and heating for 24 h. [f] δ-valerolactone was firstly added for 24 h, then ε-caprolactone was added and heating for 24 h. [g] ε-caprolactone and δ-valerolactone were added at the same time and heating for 24 h. Solvent used in the ROP: toluene.

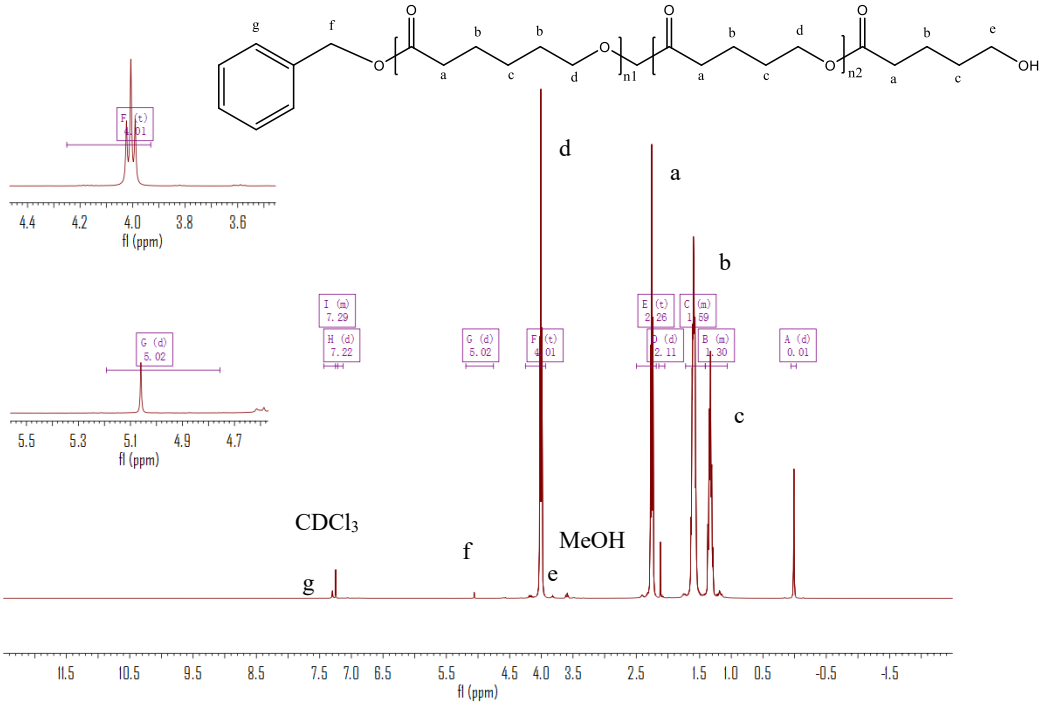

Figure 6-13. ^{1}H NMR spectrum ($CDCl_3$, 400 MHz, 298 K) of the PCL-PVL co-polymer synthesized with **3**/BnOH (run 4, Table 3).

2.1.4 ROP of *r*-lactide

Selected complexes were also employed as catalysts in the ROP of *r*-LA (Table 6-4). Best conversion was achieved in the presence of **23** (64.3%, run 1). The M_n of the polymer was lower than the calculated value albeit with narrow molecular weight distribution (5330 and 1.69, respectively). In the case of systems **23**-**27**, all polymers obtained were of low polydispersity (PDI < 2.2), which suggested that there was reasonable control for polymerization. However, **25** only allowed for 24.9% monomer conversion affording low molecular weight species. ^{1}H NMR spectra of the PLA indicated the presence of a BnO end group (e.g. Figure 6-14), which agrees with the MALDI-ToF mass spectra (e.g. Figure 6-15). The sample was analysed by MALDI-ToF mass spectra in positive-linear mode, the

expected series corresponding to repeating unit mass of 72/144 for half/full LA was observed and the polymer chain was terminated by OH and BnO end group [M = 108.05 (BnOH) + n × 72.06 ($C_3H_4O_2$) + 22.99 (Na^+)]. The syndiotactic bias was determined by 2D *J*-resolved ^{1}H NMR spectroscopy, investigating the methine area (5.13-5.20 ppm) of the spectra (e.g. Figure. 8-24).[12] The peaks were assigned to the corresponding tetrads according to the literature.[12] For *rac*-lactide, when P_r=0.5, the afforded PLA is an atactic polymer, and when P_r=0, an isotactic polymer. The observed values herein (P_r=0.39-0.61) suggested the catalysts **24**, **25** and **27** afforded almost heterotactic polymers and catalysts **23** and **26** afforded almost isotactic polymer.

Table 6-4. ROP of *rac*-lactide using complexes using **23**-**27**.

Run	Cat.	LA: Pb: BnOH	T/°C	t (h)	Conv[a] (%)	$M_{n,GPC}\times10^{-3}$[b]	$M_w\times10^{-3}$[b]	Pr[c]	$M_{n,cal}\times10^{-}$	PDI[e]
1	**23**	500: 1: 1	130	24	64.3	5.33	9.01	0.45	46.40	1.69
2	**24**	500: 1: 1	130	24	56.2	6.82	14.51	0.61	40.57	2.13
3	**25**	500: 1: 1	130	24	24.9	1.45	2.46	0.52	18.04	1.70
4	**26**	500: 1: 1	130	24	34.9	1.64	3.05	0.39	25.24	1.86
5	**27**	500: 1: 1	130	24	30.5	1.63	2.76	0.55	22.07	1.69

[a] Determined by ^{1}H NMR spectroscopy on crude reaction mixture. [b] Values corrected considering Mark–Houwink factor (0.58) from polystyrene standards in THF. [c] From 2D J-resolved ^{1}H NMR spectroscopy. [d] Calculated from ([Monomer]$_0$/Li) × conv. (%) × Monomer molecular weight (M_{LA}=144.13) + Molecular weight of BnOH. [e] From GPC. Solvent used in the ROP: toluene.

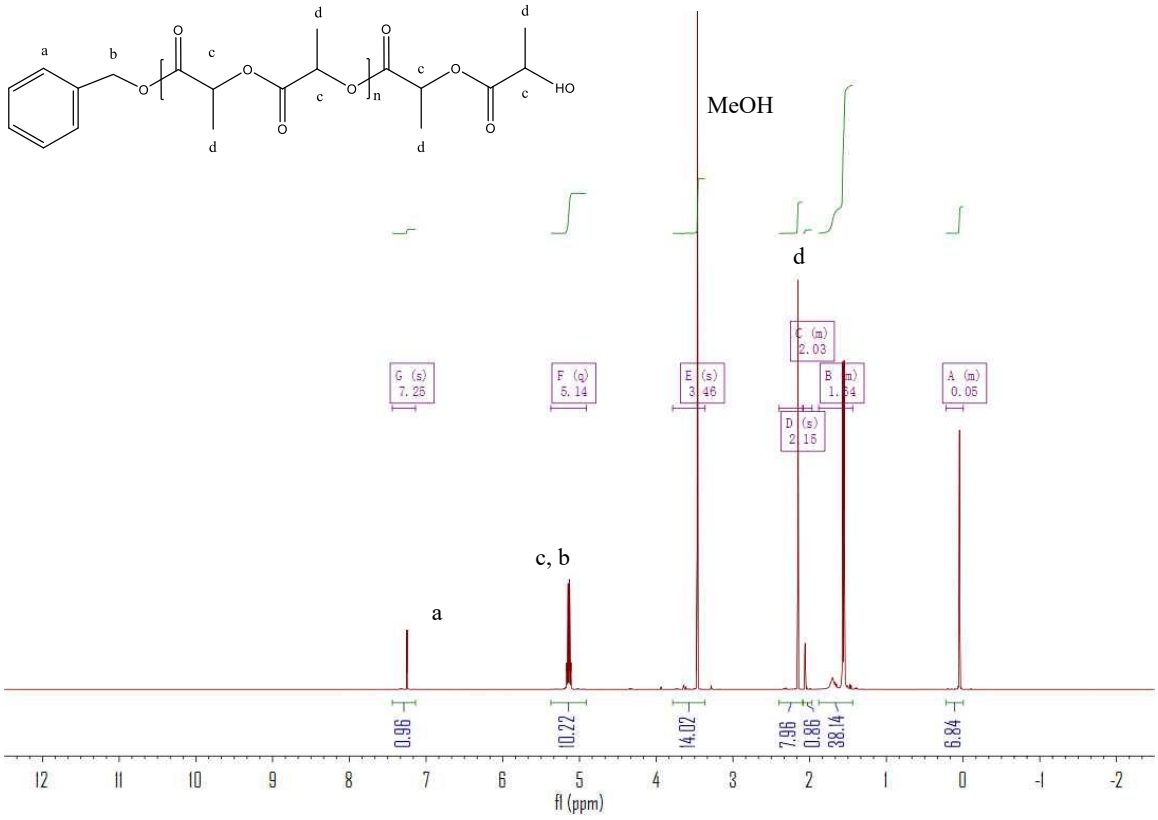

Figure 6-14. ^{1}H NMR spectrum ($CDCl_3$, 400 MHz, 298 K) of the PLA synthesized with **1**/BnOH (run 1, Table 3).

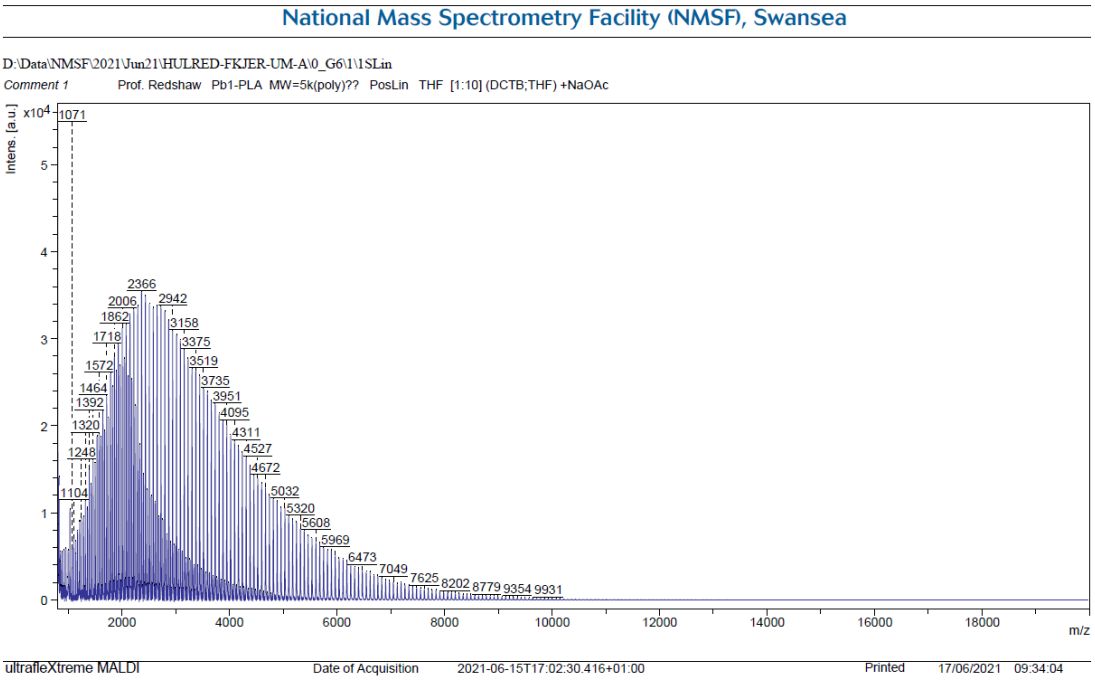

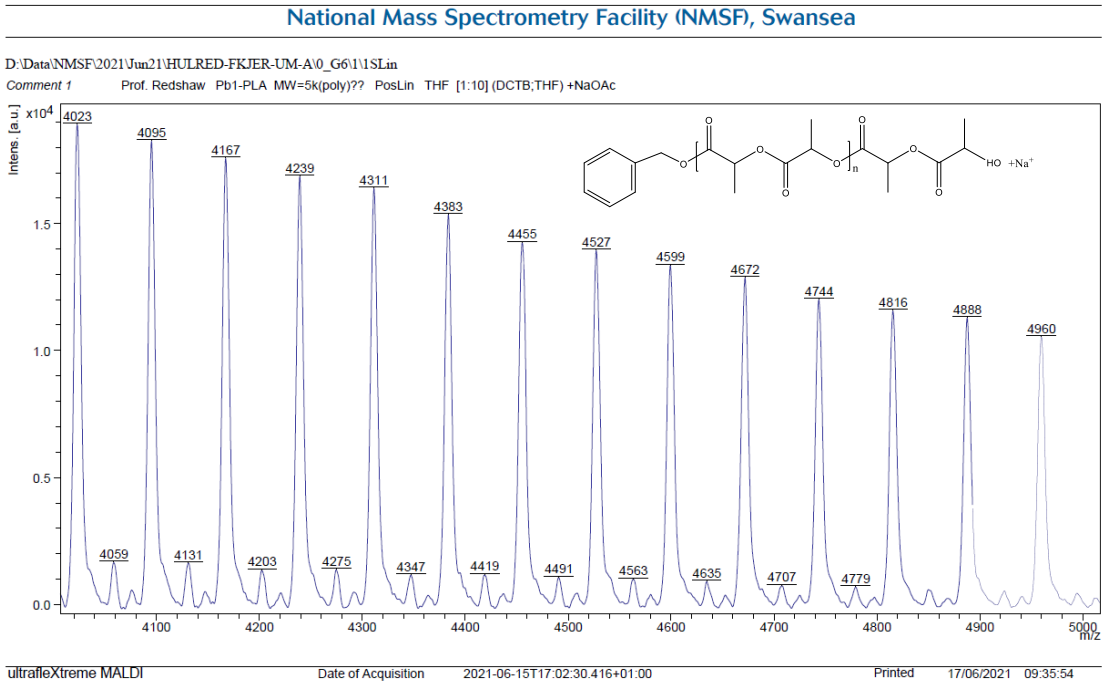

Figure 6-15. Mass spectrum of PLA synthesized with **24**/BnOH (run 2, Table 6-4).

2.1.5 Kinetics study

From a kinetic study of the ROP of ε-CL using **23**-**27**, it was observed that the polymerization rate exhibited first-order dependence on the ε-CL concentration (Figure 6-7), and the conversion of monomer achieved over 420 min was >20%. The activity trend in this case revealed that **24** was the most active followed by **23** >**25** >**26** ≈ **27**. An induction period of 2 h was observed for complexes **23**-**27** which could be ascribed to the longer time required for the formation of the catalytically active species. A similar result was also observed in the polymerization of δ-VL (Figure 6-10).

The dependence of the M_n and molecular weight distribution on the monomer conversion in the reactions catalyzed by **23**, **25**, **27** with BnOH was also investigated (Figure 6-16). For the ROP of ε-CL, the polymer M_n was shown to increase linearly with the conversion,

which suggested that the polymerization was well controlled (Figure 6-16, left). A similar outcome was also observed in the reaction involving δ-VL (Figure 6-16, right).

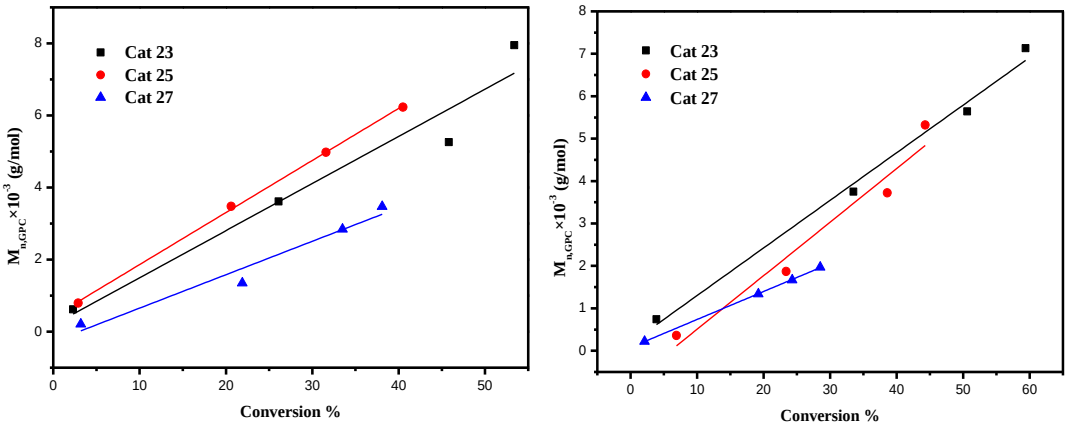

Figure 6-16. Left: M_n *vs*. monomer conversion in the ROP of ε-CL by using **23**, **25** and **27**; Right: M_n *vs*. monomer conversion in the ROP of δ-VL by using **23**, **25** and **27**; Conditions: T=130 °C, $n_{Monomer}$: n_{Pb}: BnOH= 500:1:1.

3. Conclusions

In conclusion, the use of the precursors [LiPb(O*i*Pr)$_3$], Pb(O*i*Pr)$_2$, Pb(O*t*Bu)$_2$ or Pb(N(TMS)$_2$)$_2$, on interaction with a series of calix[*n*]arenes (n = 4, 6, 8) allowed access to a number of rather complicated lead compounds (see Chart 6-2). The molecular structures reveal how these macrocycles can support multiple metal centres which adopt some interesting structural motifs. Complex **23**-**26** proved active in the ring opening homo-/co-polymerization of ε-caprolactone (ε-CL) and δ-valerolactone (δ-VL) under the conditions employed, and the activity trend was found to be **24** >**23** >**25** >**26** ≈ **27**; first order kinetics were observed for the ROP of ε-CL. The NMR spectroscopy and mass spectrometry (MALDI-ToF) characterization of selected polymer samples suggested the formation of linear PCLs and PVLs ended by -BnO and -OH groups. The catalysts **23**-**27** also be proved

to be active in the ROP of the *rac*-lactide (*r*-LA), the activity trend was found to be **24** >**23** >**25** >**26** ≈ **27**, affording near heterotactic polymers.

4. References

[1] (a) A. Chamas, H. Moon, J. Zheng, Y. Qiu, T. Tabassum, J. H. Jang, M. Abu-Omar, S. L. Scott, and S. Suh, *ACS Sustainable Chem. Eng.* 2020, 8, 3494–3511; (b) M. Labet and W. Thielemans, *Chem. Soc. Rev.* 2009, 38, 3484–3504. (c) O. Dechy-Cabaret, B. Martin-Vaca and D. Bourissou, *Chem. Rev.* 2004, 104, 6147–6176. (d) K.S. Anderson, K.M. Schreck and M.A. Hillmyer, *Polym. Rev.* 2008, 48, 85–108. (d) K. Madhavan Nampoothiri, N.R. Nair and R.P. John, *Bioresour. Technol.* 2010, 101, 8493–8501.

[2] (a) D. M. Homden and C. Redshaw, *Chem. Rev.*, 2008, 108, 5086–5130. (b) C. Redshaw, *Dalton Trans.*, 2016, 45, 9018–9030. (c) J. M. Kaiser and B. K. Long, *Coord. Chem. Rev*., 2018, 372, 141-152.

[3] L. Wang, S.-C. Roşca, V. Poirier, S. Sinbandhit, V. Dorcet, T. Roisnel, J.-F. Carpentier and Y. Sarazin, *Dalton Trans*., 2014, 43, 4268-4286.

[4] L. Wang, S. Fadlallah, C. Bellini, C. Orione, V. Dorcet, J.-. Carpentier, and Y. Sarazin, *Organometallics*, 2015, 34, 1321−1327.

[5] (a) T. Xing, T. J. Prior, K. Chen and C. Redshaw, *Dalton Trans.*, 2021, 50, 4396-4407. (b) T. Xing, T. J. Prior, M. R. J. Elsegood, N. V. Semikolenova, I. E. Soshnikov, K. Bryliakov, K. Chen and C. Redshaw, *Catal. Sci. Technol*. 2021, 11, 624-636. (c) M. J. Walton, S. J. Lancaster, J. A. Wright, M. R. J. Elsegood and C. Redshaw, *Dalton Trans*. 2014, 43, 18001-18009. (d) M. Frediani, D. Se´meril, A. Mariotti, L. Rosi, P. Frediani, L.

Rosi and D. Matt, L. Toupet, *Macromol. Rapid Commun*. 2008, 29, 1554–1560.

[6] R. Kuriki, T. Kuwabara and Y. Ishii, *Dalton Trans*., 2020, 49, 12234-12241.

[7] C. Redshaw, M. Walton, K. Michiue, Y. Chao, A. Walton, P. Elo, V. Sumerin, C. Jiang and M. R. J. Elsegood, *Dalton Trans.*, 2015, 44, 12292-12303.

[8] (a) Z. Sun, Y. Zhao, O. Santoro, M. R. J. Elsegood, E. V. Bedwell, K. Zahra, A. Walton, and C. Redshaw, *Catal. Sci. Technol*., 2020, 10, 1619-1639; (b) O. Santoro, M. R. J. Elsegood, E. V. Bedwell, J. A. Pryce and C. Redshaw, *Dalton Trans*., 2020, 49, 11978-11996.

[9] Y. Li, K. Zhao, C. Feng, M. R. J. Elsegood, T. J. Prior, X. Sun and C. Redshaw, *Dalton Trans.*, 2014, 43, 13612-13619

[10] O. Santoro, M. R. J. Elsegood, S. J. Teat, T. Yamato and C. Redshaw, *RSC Adv*. 2021, 11, 11304-11317.

[11] (a) Q. Hu, S.-Y. Jie, P. Braunstein and B.-G. Lia, *Chinese J. Polym. Sci*. 2020, 38, 240–247; (b) M. A. Woodruff and D. W. Hutmacher, *Prog. Polym. Sci.,* 2010, 35, 1217−1256; (c) T. Wu, Z. Wei, Y. Ren, Y. Yu, X. Leng and Y. Li, *Polym. Degrad. Stab.,* 2018, 155, 173−182; (d) M. T. Hunley, N. Sari, and K. L. Beers, *ACS Macro Lett*., 2013, 2, 375−379. (e) Z. Sun, Y. Zhao, O. Santoro, M. R. J. Elsegood, E. V. Bedwell, K. Zahra, A. Walton, and C. Redshaw, *Catal. Sci. Technol.*, 2020, 10, 1619−1639.

[12] (a) C. Ludwig and M. R. Viant, *Phytochem. Anal*. 2010, 21, 22-32; (b) M. J. Walton, S. J. Lancaster and C. Redshaw, *ChemCatChem*, 2014, 6, 1892-1898.

Chapter 7

Experimental section

1. Experimental section for Chapter 2

General

The known compounds $L^{6O}H_6$, L^3H_3, [V(N*p*-RC_6H_4)(O*i*Pr)$_3$] (R= OMe, CF_3, Cl), [V(Np-$CH_3C_6H_4$)(O*t*Bu)$_3$] and [V(N*p*-$CH_3C_6H_4$)(OEt)$_3$], [VOL^3] (L^3H_3 = oxacalix[3]arene) (**I**), [V(N*p*-$CH_3C_6H_4$)L^3]$_2$ (**II**), [Li(MeCN)$_4$][$V_2(O)_2$Li(MeCN)(L^6H_2)$_2$] (L^6H_6 = p-*tert*-butylcalix[6]areneH_6) (**III**) and [$(VO)_2L^8H$] (L^8H_8 = p-*tert*-butylcalix[8]areneH_8) (**IV**) were prepared by the literature methods.[1] All reactions were conducted under an inert atmosphere using standard Schlenk techniques. Toluene was dried from sodium, acetonitrile was distilled from calcium hydride, diethylether was distilled from sodium benzophenone, and all solvents were degassed prior to use. IR spectra (nujol mulls, KBr or NaCl windows) were recorded on a Nicolet Avatar 360 FT IR spectrometer.

^{1}H NMR spectra were recorded at room temperature on a Varian VXR 400 S spectrometer at 400 MHz or a Gemini 300 NMR spectrometer or a Bruker Avance DPX-300 spectrometer at 300 MHz. ^{1}H and ^{13}C NMR spectra of polyethylene samples (1,2-dichlorobenzene-d_4, 100 °C) were recorded on a Bruker Avance 400 MHz NMR spectrometer at 400.130 and 100.613 MHz, respectively. ^{1}H NMR spectra were calibrated against the residual protio impurity of the deuterated solvent. All other chemicals were purchased from Sigma Aldrich and Tokyo Chemical Industry UK Ltd.

Crystal structure data were collected at the UK National Crystallography Service (**1**-**6**) and the SRS at Daresbury (**8**). Full details are given in Table 8-4, Chapter 8. Elemental analyses were performed by the elemental analysis service at the University of Hull. Matrix Assisted Laser Desorption/Ionization Time of Flight (MALDI-TOF) mass spectrometry was

performed in a Bruker autoflex III smart beam in linear mode, and the spectra were acquired by averaging at least 100 laser shots. 2,5-Dihydroxybenzoic acid was used as the matrix and THF as solvent. Sodium chloride was dissolved in methanol and used as the ionizing agent. Samples were prepared by mixing 20 μL of matrix solution in THF (2 $mg \cdot mL^{-1}$) with 20 μL of matrix solution (10 $mg \cdot mL^{-1}$) and 1 μL of a solution of ionizing agent (1 $mg \cdot mL^{-1}$). Then 1 mL of these mixtures was deposited on a target plate and allowed to dry in air at ambient temperature.

Weight-average (M_w) and number-average (M_n) molecular weights, molecular weight distributions (MWD), and polydispersities (M_w/M_n) were measured on a Waters-150 chromatograph at 150 °C, with trichlorobenzene as solvent.

Procedure for ROP of ε-caprolactone/δ-valerolactone

A toluene solution of pre-catalyst (0.010 mmol, 1.0 mL toluene) was added into a Schlenk tube in the glove-box at room temperature. The solution was stirred for 2 min, and then the appropriate equivalent of BnOH (from a pre-prepared stock solution of 1 mmol BnOH in 100 mL toluene) and the appropriate amount of *ε*-CL or *δ*-VL along with 1.5 mL toluene was added to the solution. For example, for Table 2-2, run 1, a toluene solution of pre-catalyst **1** (0.010 mmol, 1.0 mL toluene) was added into a Schlenk tube, then 2 mL BnOH solution (1 mmol BnOH/100 mL toluene) and 20 mmol *ε*-CL along with 1.5 mL toluene was added to the solution. The reaction mixture was then placed into an oil/sand bath pre-heated at 130 °C, and the solution was stirred for the prescribed time (8 or 24 h). The polymerization mixture was quenched on addition of an excess of glacial acetic acid (0.2 mL) into the solution, and the resultant solution was then poured into methanol (200 mL).

The resultant polymer was then collected on filter paper and was dried *in vacuo*.

Kinetic studies

The polymerizations were carried out at 130 °C in toluene (2 mL) using 0.010 mmol of complex. The molar ratio of monomer to initiator was fixed at 500:1, and at appropriate time intervals, 0.5 μL aliquots were removed (under N_2) and were quenched with wet $CDCl_3$. The percent conversion of monomer to polymer was determined using ^{1}H NMR spectroscopy.

Procedure for ethylene polymerization

The catalytic activates of complexes **1**-**8** for ethylene polymerization were collected by the Boreskov Institute of Catalysis, Russian Academy of Sciences. Ethylene polymerization experiments were performed in a steel 500 mL autoclave. The reactor was evacuated at 80 °C, cooled down to 20 °C and then charged with the freshly prepared solution of the co-catalyst in heptane/toluene. Pre-catalysts were introduced into the reactor in sealed glass ampoules, containing 0.5 or 1.0 μmol of appropriate V-complex in 0.5 mL of solvent. After setting up the desired temperature and ethylene pressure, the reaction was started by breaking the ampoule with the pre-catalyst. During the polymerization, ethylene pressure (2 bar), temperature (70 °C) and stirring speed (2000 rpm) were maintained constant. After 30 min (during which time the ethylene consumption rate declined to nearly zero level), the reactor was opened to the atmosphere and the polymeric product was dried in a fume-hood to a constant weight.

Polymerization conditions. For run 1 of Table 2-5: V loading 1.0 μmol (dissolved in CH_2Cl_2), co-catalyst Et_2AlCl + ETA (molar ratio V: Et_2AlCl: ETA= 1: 1000: 500) in 50 mL

of toluene + 100 mL of heptane, T pol 70 °C, P C_2H_4 = 2 bar, for 30 min. For runs 2-6 of Table 2-5: V complex was dissolved in toluene, Co-catalyst Me_2AlCl + ETA (molar ratio V:Me_2AlCl:ETA= 1:1000:1000) in 100 mL of toluene + 100 mL of heptane; T pol 70 °C, P C_2H_4 = 2 bar, for 30 min.

Preparation of **[(VO)$_2$(μ-O)Na$_2$(L^{6O})(MeCN)$_4$]·5MeCN (1·5MeCN)**

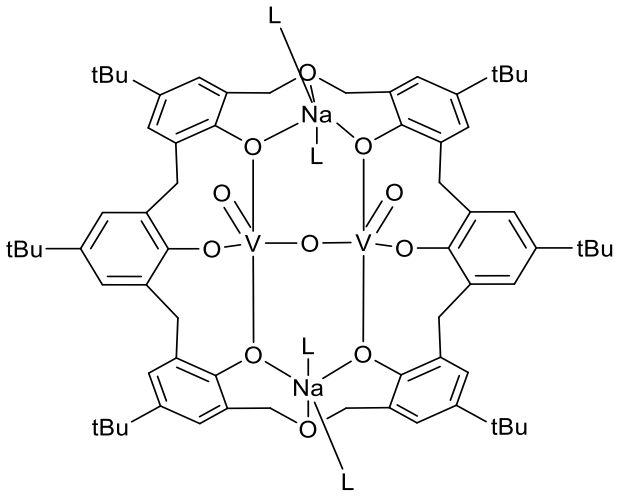

1 (L = MeCN)

To *in-situ* Na[VO(O*t*Bu)$_4$] (generated from 0.98 mmol from $VOCl_3$ and 4*t*BuONa) in Et_2O (30 mL) was added $L^{6O}H_6$ (0.50 g, 0.49 mmol) and at -78 ºC. The mixture was allowed to warm to ambient temperature and then the volatiles were removed *in-vacuo*. Toluene (30 mL) was then added and the system was refluxed for 12 h. On cooling, volatiles were removed *in-vacuo*, and the residue was extracted into warm MeCN (30 mL). On prolonged standing at 0 ºC, green prisms of **1** formed. Yield 0.46 g, 58%. Anal. Cald for $C_{86}H_{109}N_9Na_2O_{11}V_2$: C, 64.85; H, 6.90; N 7.92%; found C, 65.22; H, 7.5%; 7.23%. IR (nujol mull, KBr): 3901w, 3422w, 1747w, 1260s, 1227w, 1199m, 1059s, 1021s, 965m, 903w, 868m, 831w, 796s, 708w, 658m, 641m, 623m, 602w, 553w, 453w. ^{1}H NMR ($CDCl_3$)

δ: 8.00-7.5 (m, 12H, aryl*H*), 5.71 (d, *J*=8.1, 4H, -OCH_2), 4.90 (d, *J*=8.1, 4H, OCH_2), 4.05 (d, *J*=8.0, 4H, -CH_2-), 3.53 (d, *J*=8.0, 4H, -CH_2), 2.05 (s, CH_3CN), 1.35-1.24 (m, 54H, C(CH_3)$_3$). ^{51}V NMR ($CDCl_3$): δ: -675.3 ppm ($\omega_{1/2}$ 272 Hz). Mass Spec (ESI): 1592 $[M]^+$.

Preparation of **$[(VO)_4L^{6O}]$·6MeCN (2·6MeCN)**

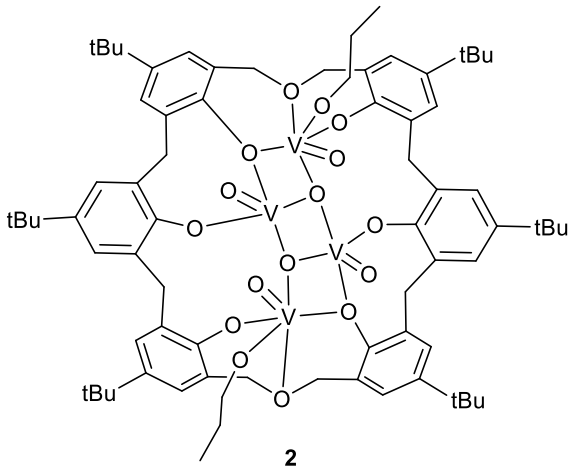

2

$[VO(OnPr)_3]$ (0.49 g, 2.0 mmol) and $L^{6O}H_6$ (0.50 g, 0.49 mmol) were combined in toluene (20 mL). After refluxing for 12h, volatiles were removed *in-vacuo*, and the residue was extracted into MeCN (20 mL). Prolonged standing at 0 ºC afforded **2**·6MeCN as dark blue prisms. Yield 0.32 g, 45%. Anal. Cald for $C_{74}H_{96}O_{16}V_4$ (sample dried *in-vacuo* for 12h): C, 61.49; H, 6.70%. Found C, 61.49; H, 6.53%. IR (nujol mull, KBr): 1651w, 1599m, 1461s, 1377s, 1363m, 1304w, 1260s, 1206m, 1092s, 1052s, 1016s, 986m, 922w, 873m, 851m, 799s. ^{1}H NMR ($CDCl_3$) δ: 6.88-7.35 (m, 12H, aryl*H*), 6.07 (d, *J*=4.8 Hz, 2H, -OCH_2-), 5.77 (m, 2H, -OCH_2-), 5.51 (d, *J*=4.8 Hz, 2H, -OCH_2-) 5.15 (m, 4H, -OCH_2CH$_2$CH$_3$), 4.86 (d, *J*=4.8 Hz, 2H, -OCH_2-), 4.20 (m, 4H, -CH_2-), 3.40 (d, *J*=12.4 Hz, 4H, -CH_2-), 2.32 (m, 4H, -OCH$_2$CH_2CH$_3$), 1.13-1.49 (m, 54H, C(CH_3)$_3$), 1.02 (m, 6H, -OCH$_2$CH$_2$CH_3). ^{51}V NMR ($CDCl_3$) δ: -411.7 ($\omega_{1/2}$ 524 Hz), -461.5 ppm ($\omega_{1/2}$ 735 Hz). Mass Spec (ESI): 1351 [M+Na-

2O*n*Pr]$^{+}$.

Preparation of **{[V(Np-CH$_3$C$_6$H$_4$)]$_2$L^{6O}}·7MeCN·0.5CH$_2$Cl$_2$ (3·7MeCN·0.5CH$_2$Cl$_2$)**

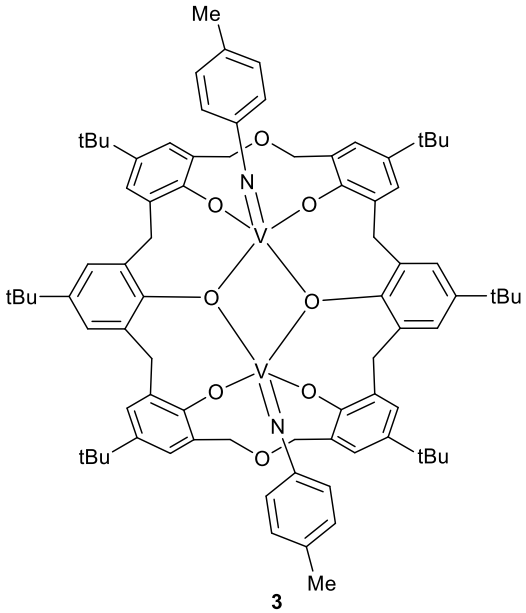

3

To [V(Np-CH$_3$C$_6$H$_4$)(O*t*Bu)$_3$] (0.37 g, 0.99 mmol) and L^{6O}H$_6$ (0.50 g, 0.49 mmol) was added toluene (30 mL) and then the system was refluxed for 12 h. On cooling, the volatiles were removed *in vacuo*, and the residue was extracted into warm MeCN (30 mL). On prolonged standing at 0 ^{o}C, an orange crystalline material formed. Single orange prisms of **3**·7MeCN·0.5CH$_2$Cl$_2$ were grown from a saturated MeCN solution containing CH$_2$Cl$_2$ (2 mL) at 0 ^{o}C (yield 0.61 g, 93%). Anal. Cald for C$_{82}$H$_{96}$N$_2$O$_8$V$_2$: C, 73.41; H, 7.21; N, 2.12%; Found C, 73.32%; H, 7.41 %, N, 2.24%. IR (nujol mull, KBr): 3236w, 2727w, 2349w, 2288w, 2248w, 1614m, 1592m, 1556w, 1300m, 1261s, 1073s, 1020s, 990m, 937m, 878m, 840s, 819s, 763s, 754w, 722w, 696w, 639w, 584w. ^{1}H NMR (CDCl$_3$) δ: 7.78–6.85 (m, 12H, aryl-*H*), 6.46 (d, *J*=8.4 Hz, 4H, -N-C$_6$*H*$_4$-), 6.16 (d, *J*=8.4 Hz, 4H, -N-C$_6$*H*$_4$-), 4.86-5.10 (d, *J*=7.6 Hz, 4H, OC*H*$_2$-), 4.53-4.66 (m, 4H, -OC*H*$_2$-), 4.34-4.25 (m, 4H, -C*H*$_2$) 3.66-4.00 (d, *J*=12.4 Hz, 4H, -C*H*$_2$), 2.35 (m, 6H, *p*-tolyl-C*H*$_3$), 2.05 (s, 3H, MeCN) 1.49 (m, 54H,

C(CH_3)$_3$) ^{51}V NMR ($CDCl_3$) δ: -312.2 ($\omega_{1/2}$ 650 Hz)ppm. Mass Spec (ESI): 1362 $[M+Na]^+$, 1379 $[M+K]^+$.

Preparation of **{[V(Np-(OMe)C$_6$H$_4$)]$_2$L^{6O}}·4MeCN (4·4MeCN)**

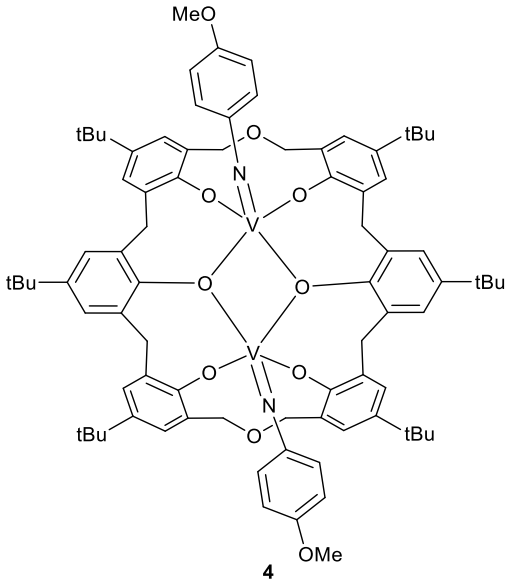

4

As for **2**, but using [V(Np-(OMe)C$_6$H$_4$)(O*i*Pr)$_3$] (0.35 g, 1.0 mmol) and L^{6O}H$_6$ (0.50 g, 0.49 mmol) affording **4**·4MeCN as orange/red prisms. Single orange prisms were grown from a saturated MeCN (30 mL) solution at 0 ºC (yield 0.43 g, 61%). Anal. Cald for $C_{82}H_{96}N_2O_{10}V_2$ (sample dried *in-vacuo* for 12h): C, 71.80; H, 7.06; N, 2.04%. Found C, 71.78; H, 7.14; N, 2.38%. IR (nujol mull, KBr): 3237w, 1613w, 1585m, 1554w, 1540w, 1486m, 1459s, 1383m, 1362w, 1297w, 1260s, 1206m, 1159m, 1075s, 1023s, 910w, 872m, 800s, 754w, 688m. ^{1}H NMR ($CDCl_3$) δ: 6.87-7.54 (m, 12H, aryl*H*), 6.49 (d, *J*=8.0 Hz, 4H, -NC$_6$*H*$_4$-OMe), 5.88 (d, *J*=8.0 Hz, 4H, -NC$_6$*H*$_4$-OMe), 5.11 (d, *J*=6.8 Hz, 4H, -OC*H*$_2$-), 4.95 (d, *J*=6.8 Hz, 4H, -OC*H*$_2$-), 4.47-4.67 (m, 4H, -C*H*$_2$-), 3.64 (d, *J*=5.2 Hz, 4H, -C*H*$_2$-), 3.51 (s, 6H, *p*-C$_6$H$_4$-OC*H*$_3$), 2.01 (s, 3H, *Me*CN), 1.35-1.15 (m, 54H, C(C*H*$_3$)$_3$). ^{51}V NMR ($CDCl_3$) δ: -178.1 ($\omega_{1/2}$ 470 Hz) ppm. Mass Spec (ESI): 1470 $[M+Na]^+$.

Preparation of **{[V(Np-(CF$_3$)-C$_6$H$_4$)]$_2$L^{6O}} (5)**

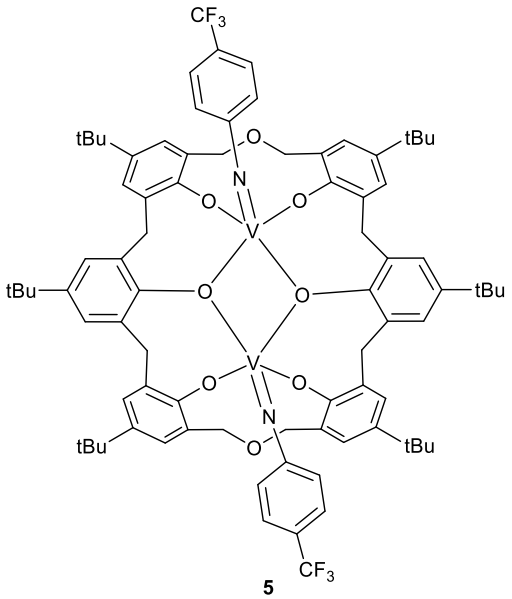

5

As for **2**, but using [V(Np-(CF$_3$)C$_6$H$_4$)(O*i*Pr)$_3$] (0.38 g, 1.0 mmol) and L^{6O}H$_6$ (0.50 g, 0.49 mmol) affording **5** as orange/brown prisms. Single orange prisms were grown from a saturated MeCN (30 mL) solution at 0 ^{o}C (yield 0.26 g, 36%). Anal. Cald for $C_{82}H_{90}F_6N_2O_8V_2$: C, 68.04; H, 6.27; N, 1.94%. Found: C, 67.36; H, 6.45; N, 2.32 %. IR (nujol mull, KBr): 1730w, 1598m, 1557m, 1509m, 1456s, 1383s, 1363w, 1324s, 1260s, 1201w, 1163m, 1059s, 1067s, 1071s, 956w, 877m, 849m, 799s, 723m. ^{1}H NMR ($CDCl_3$) δ: 6.84-7.82 (m, 12H, aryl*H*), 6.51 (d, *J*=8.8 Hz, 4H, -C$_6$*H*$_4$-CF$_3$), 6.19 (m, 4H, -C$_6$*H*$_4$-CF$_3$), 5.02-4.91 (m, 4H, -OC*H*$_2$-), 4.52 (d, *J*=5.2 Hz, 4H, -OC*H*$_2$-), 4.27-4.16 (m, 4H, -C*H*$_2$-) ,3.72 (m , 4H, -C*H*$_2$-), 1.95 (s, 3H, *Me*CN), 1.35-1.06 (m, 54H, C(C*H*$_3$)$_3$). ^{51}V NMR ($CDCl_3$) δ: -408.1 ppm ($\omega_{1/2}$ 474 Hz). ^{19}F NMR ($CDCl_3$): δ = -62.69 ppm. Mass Spec (ESI): 1441 [M].

Preparation of **{[V(Np-Cl-C_6H_4)]$_2$$L^{6O}$} (6)**

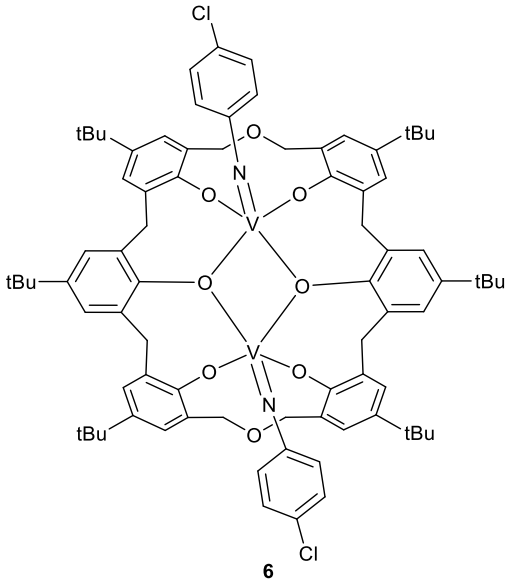

6

As for **2**, but using [V(Np-Cl-C_6H_4)(O*i*Pr)$_3$] (0.35 g, 1.0 mmol) and $L^{6O}H_6$ (0.50 g, 0.49 mmol) affording **6** as dark brown prisms from a saturated MeCN (30 mL) solution at 0 ºC (yield 0.35 g, 51%). Anal. Cald for $C_{80}H_{90}Cl_2N_2O_8V_2$·MeCN C, 69.29; H, 6.89; N, 2.96%. Found C, 67.72; H, 7.43; N 2.25 %.[23] IR (nujol mull, KBr): 2359m, 1737w, 1593m, 1554m, 1513m, 1461s, 1377m, 1294m, 1260m, 1200m, 1117s, 1088w, 822w, 795w, 726w. ^{1}H NMR ($CDCl_3$) δ: 6.88-7.69 (m, 12H, aryl*H*), 6.50 (d, *J*=10.0 Hz, 4H, -C_6H_4-Cl), 6.35 (d, *J*=10.0 Hz, 4H, -C_6H_4-Cl), 4.86-5.09 (m, *J*=10.0 Hz, 4H, -OCH_2-), 4.68 (d, *J*=10.0 Hz, 4H, -OCH_2-), 4.31-4.53 (m, 4H, -CH_2-) ,3.67 (d, *J*=12.8 Hz, 4H, -CH_2-), 1.13-1.35 (m, 54H, C(CH_3)$_3$). ^{51}V NMR ($CDCl_3$) δ: -335.3 ppm ($\omega_{1/2}$ 120 Hz). Mass Spec (ESI): 1386 $[M]^+$.

Preparation of **{[V(Np-F-C_6H_4)]$_2$$L^{6O}$}·MeCN (7·MeCN)**

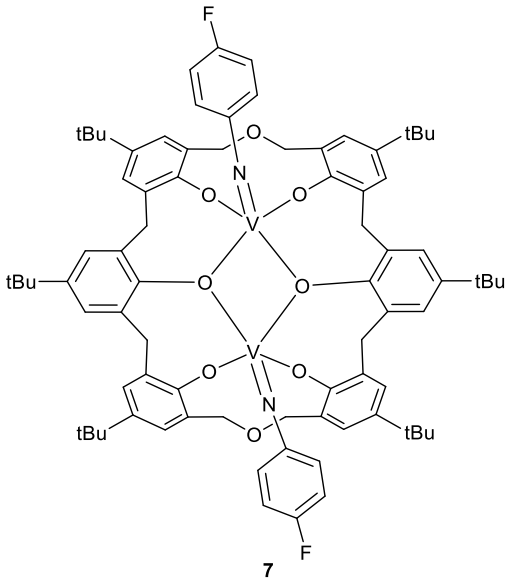

7

As for **2**, but using [V(Np-F-C_6H_4)(O*n*Pr)$_3$] (0.34 g, 0.99 mmol) and $L^{6O}H_6$ (0.50 g, 0.49 mmol) affording **7**·MeCN as red/brown crystals from a saturated MeCN (30 mL) solution at 0 ^{o}C. Yield: 0.57 g, 86%. Anal. Cald for $C_{80}H_{90}F_2N_2O_8V_2$·MeCN C, 70.92; H, 6.75; N, 3.03%. Found C, 70.72; H, 6.89; N 3.38 %. IR (nujol mull, KBr): 2360w, 2341w, 1682w, 1510m, 1411w, 1299w, 1260s, 1228m, 1202s, 1155w, 1144w, 1096s, 1064s, 1017s, 988m, 912w, 872w, 832s, 821s, 806s, 722m, 668w, 581w, 460w. ^{1}H NMR ($CDCl_3$) δ: 6.84-7.81 (m, 12H, aryl*H*), 6.49 (d, *J*=6.8 Hz, 4H, -NC$_6$*H*$_4$-Cl), 5.91 (d, *J*=6.8 Hz, 4H, -NC$_6$*H*$_4$-Cl), 4.91-4.98 (d, *J*=8.8 Hz, 4H, -OC*H*$_2$-), 4.49 (d, *J*=8.8 Hz, 4H, -OC*H*$_2$-), 4.13-4.26 (m, 4H, -C*H*$_2$-), 3.69 (d, *J*=5.2 Hz, 4H, -C*H*$_2$-), 1.36-1.09 (m, 54H, C(C*H*$_3$)$_3$). ^{19}F NMR ($CDCl_3$) δ: -108.30 ppm. ^{51}V NMR ($CDCl_3$): δ: -173.4 ppm ($\omega_{1/2}$ 265 Hz).

Preparation of **[VO(L$^{6O'}$)]$_2$·4MeCN (L$^{6O'}$ = 2-(p-tolylNCH)-4-*t*Bu-C$_6$H$_2$O-6-CH$_2$)-4-*t*BuC$_6$H$_2$OH) (8·4MeCN).**

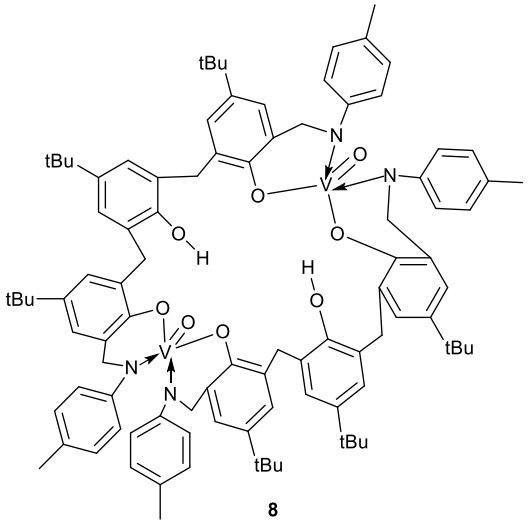

8

[V(Np-tolyl)(OEt)$_3$] (0.29 g, 0.99 mmol) and L^{6O}H$_6$ (0.50 g, 0.49 mmol) were refluxed in toluene (30 mL) for 12 h. Following removal of volatiles *in-vacuo*, the residue was dissolved in hot MeCN (30 mL), filtered and left to stand (1–2 days) at 0 ºC to afford **8** as orange-brown prisms (0.43 g, 57% yield). Anal. Cald for $C_{96}H_{108}N_4O_8V_2$ (sample dried *in-vacuo* for 12 h, -4MeCN): C, 74.49; H, 7.03; N 3.62%; found C, 73.60; H, 7.12; N, 2.88 %. IR (nujol mull, KBr): 3231w, 1613m, 1593m, 1555w, 1505w, 1459s, 1377s, 1363m, 1299w, 1261s, 1209s, 1073s, 1019s, 991, 965m, 878s, 871s, 839m, 818m, 802s, 765w, 764m, 753m, 737m. ^{1}H NMR ($CDCl_3$) δ: 9.01 (s, 2H, -O*H*), 6.84-7.68 (m, 12H, aryl*H*), 6.45 (d, *J*=8.4 Hz, 4H, -NC$_6$*H*$_4$-Me), 6.16 (d, *J*=8.4 Hz, 4H, -NC$_6$*H*$_4$-Me), 4.85-5.10 (d, *J*=9.6 Hz, 4H, -N-CH$_2$-), 4.53-4.65 (d, *J*=9.6 Hz, 4H, -N-C*H*$_2$-), 4.25-4.34 (m, 4H, -C*H*$_2$-), 3.65 (d, *J*=12.8 Hz, 4H, -C*H*$_2$-), 2.33 (m, 12H, -C*H*$_3$), 2.01 (s, 3H, *Me*CN), 1.11-1.36 (m, 54H, C(C*H*$_3$)$_3$) Mass Spec (ESI): 1556 [M+Na$^+$-3MeCN].

2. Experimental section for Chapter 3

General

All complexes were prepared under nitrogen using standard Schlenk techniques using dried and degassed solvents. The precursors [$TiCl_4$] (99%), [$TiBr_4$] (99%), and [TiI_4] (99%) were purchased from Sigma Aldrich. The compounds p-*tert*-butylcalix[8]areneH_8 (98%) and p-*tert*-butylthiacalix[4]areneH_4 were obtained from Tokyo Chemical Industry UK Ltd. Tetrahydrofuran (99%), toluene (99%) and acetonitrile were purchased from Adamas-Beta. N_2 (99.99%) and CO_2 (99.995%) were purchased from Xi'an Teda Cryogenic Equipment Co., Ltd. Methylether-*p*-*tert*-butylcalix[4]areneH_3 and p-*tert*-butyltetrahomodioxacalix[6]areneH_6 were prepared according the methods reported in literature.[1(h),2] The complexes [V(*p*-RC_6H_4N)Cl_3] were prepared according the method reported by Maatta *et al*.[3] [$TiCl_4(THF)_2$] was prepared by the method of Schrock *et al*.[4] All other chemicals were purchased from commercial companies and used without further purification. The complexes **V**,[5] **VI**,[6] **VII**,[7] **1**, **3**,[8] and **10**, **XI** and **XII**,[9] were prepared by the literature methods. Crystal structure data were collected at the UK National Crystallography Service (**9, 9′** and **10**).

Catalytic reaction

The co-polymerization reaction of propylene oxide and CO_2 to cyclic polycarbonates was carried out in a 16 mL stainless steel autoclave with a Teflon inner container in a batch mode of operation. In a typical reaction, propylene oxide (5 mL) and catalyst (100 mg) were added into the inner container, which was transferred into the autoclave. The reactor was sealed and charged with 1 MPa of N_2 to remove the air three times. After that, it was

charged with 5 MPa of CO_2 and heated to 90 °C and stirred for 5 h. Upon reaction, the solid catalyst was separated using an extra magnet, and the liquid was analyzed on a gas chromatograph (GC9720, Zhejiang Fuli Analytical Instruments Co., Ltd., China) equipped with a flame ionization and GC-MS (Agilent 6890N-5975) with an HP-5 capillary column (30 m × 0.32 mm × 0.25 μm). The afforded products (cyclic/polycarbonates) were analyzed on a Gel Permeation Chromatography (Waters 1525 & Agilent PL-GPC220) at room temperature.

Crystallography experimental

Diffraction data for **9**·3CH_2Cl_2 was collected using silicon 111 mono-chromated synchrotron radiation at the ALS station 11.3.1.[10] That for **9**$^{/}$·6CH_2Cl_2 was collected using a conventional fine-focus sealed beam source on a CCD diffractometer with graphite mono-chromation,[11] while data for **10**·6.5MeCN were collected using a rotating anode X-ray tube and a hybrid pixel array detector. All data sets were corrected for absorption and Lp effects.[12] Structures were solved by direct methods or a dual space charge-flipping algorithm.[13] Refinement was on F^2[14] and proceeded routinely except as described as follows: for **9**·3CH_2Cl_2 the crystals degraded rapidly when exposed to the air, most likely due to desolvation. Me groups on *t*Bu groups at C(7) and C(17) were refined as two-fold disordered with major occupancy 72.6(12) and 71.2(17)% respectively. The CH_2Cl_2 containing C(49) was refined at half weight. For **9**$^{/}$·6CH_2Cl_2 the data were non-merohedrally twinned with both twin components used in refinement with a twin ratio of 0.6053:0.3947(18). The twin law is a 180° rotation about reciprocal axis [1 0 0]. Three

unique CH_2Cl_2 molecules per asymmetric unit. Those at C(41) and C(43) were refined as disordered over two sets of positions with major occupancies of 0.622(19) and 0.512(5)%, respectively, while that at C(42) was refined at exactly half weight due to it being very diffuse or low occupancy. In addition, another CH_2Cl_2 per unit cell or per dimer was modelled as an area of diffuse electron density by the Platon Squeeze method which recovered 48 electrons in one void on a centre of symmetry.[15,16] CH_2Cl_2 has 42 electrons, and this tallied with the point atom observations. The disordered CH_2Cl_2 at C(41) resides in the calixarene cavity. For **10**·6.5MeCN the data were also merohedrally twinned with twin law [–1 0 0, 0 –1 0, 0.777 0 1] with a twin ratio 0.8908:0.1092(11). Two-fold disorder was modelled for the entire *t*Bu group at C(51) with major component occupancy 70(2)%. Also, two-fold disorder of the Me groups in the *t*Bu groups at C(17A) and C(84A) was modelled with major occupancy 73(3) and 58(3)% respectively. MeCN of crystallisation at N(12) was modelled as disordered over two sets of positions with major component 71.3(18)%.

Preparation of **$[HNEt_3]_2[VO(\mu\text{-}O)L^{4S}H_2]_2{\cdot}3CH_2Cl_2$ ($9{\cdot}3CH_2Cl_2$)**

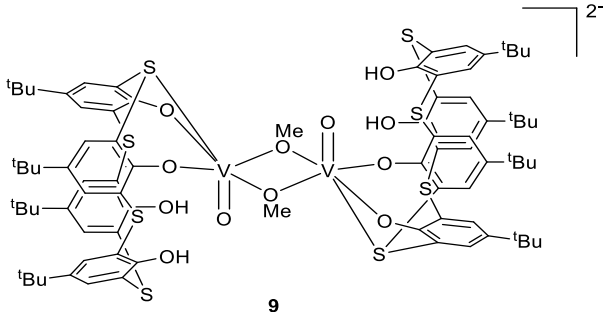

9

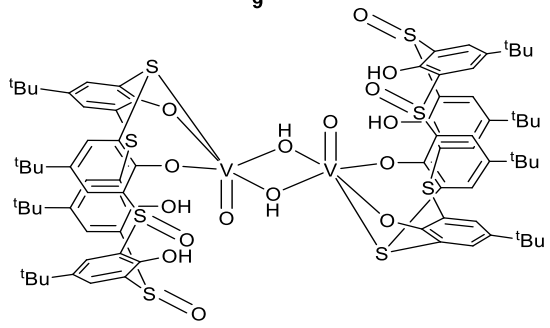

9/

p-tert-Butylthiacalix[4]areneH_4 (0.108 g, 0.15 mmol), [$VOSO_4$] (0.147 g, 0.90 mmol), and Et_3N (1.51 mL, 10.8 mmol) were refluxed for 12 h in methanol (10 mL) under a nitrogen atmosphere. On cooling, volatiles were removed *in-vacuo* and the residue was washed with acetonitrile (30 mL), and then extracted in CH_2Cl_2 (10 mL). A layer of hexane (10 mL) was carefully added and the solvent system left to diffuse for 7 days to afford yellow prisms of **9** (*ca*. 15% yield). Anal. $C_{97}H_{136}Cl_6N_2O_{12}S_8V_2$ requires C, 55.66; H, 6.55; N, 1.34 %. Found: C, 55.83; H, 6.59; N, 1.38 %. IR: 3545w, 3406bw, 1403m, 1260s, 1178m, 1096bs, 1018bs, 938m, 869m, 800s, 722m, 638m. As for **9**, but using undried methanol affording **9/** as yellow prisms (yield, 21%). ^{1}H NMR ($CDCl_3$, 400 MHz, 298K) δ: 10.72 (s, 4H, O*H*), 7.63 – 7.21 (m, 16H, aryl*H*), 5.23 (s, 12H, CH_2Cl_2), 1.08, 1.06 (2 x s, 72H, C(CH_3)$_3$); (μ-OH not observed). ^{51}V NMR ($CDCl_3$) δ: –475.1.

3. Experimental section for Chapter 4

All reactions were conducted under an inert atmosphere using standard Schlenk techniques. Toluene was dried from sodium, acetonitrile was distilled from calcium hydride, diethylether was distilled from sodium benzophenone, and all solvents were degassed prior to use. The dioxacalix[6]arene and azacalixarenes were prepared according to the literature methods.[1(i),17] All other chemicals were purchased from commercial sources. IR spectra (nujol mulls, KBr windows) were recorded on a Nicolet Avatar 360 FT IR spectrometer; ^{1}H NMR spectra were recorded at room temperature on a Varian VXR 400 S spectrometer at 400 MHz or a Gemini 300 NMR spectrometer or a Bruker Advance DPX-300 spectrometer at 300 MHz. The ^{1}H NMR spectra were calibrated against the residual protio impurity of the deuterated solvent. Elemental analyses were performed by the elemental analysis service at the University of Hull. Matrix Assisted Laser Desorption/Ionization Time of Flight (MALDI-TOF) mass spectrometry was performed in a Bruker autoflex III smart beam in linear mode, and the spectra were acquired by averaging at least 100 laser shots. 2,5-Dihydroxybenzoic acid was used as the matrix and THF as solvent. Sodium chloride was dissolved in methanol and used as the ionizing agent. Samples were prepared by mixing 20 μl of matrix solution in THF (2 mg·mL^{-1}) with 20 μL of matrix solution (10 mg·mL^{-1}) and 1 μL of a solution of ionizing agent (1 mg·mL^{-1}). Then 1 mL of these mixtures was deposited on a target plate and allowed to dry under air at ambient temperature.

Procedure for ROP of ε-caprolactone, δ-valerolactone and rac-lactide

A toluene solution of pre-catalyst (0.010 mmol, 1.0 mL toluene) was added into a Schlenk tube in the glove-box at room temperature. The solution was stirred for 2 min, and then the appropriate equivalent of BnOH (from a pre-prepared stock solution of 1 mmol BnOH in 100 mL toluene) and the appropriate amount of *ε*-CL, *δ*-VL or *r*-LA along with 1.5 mL toluene was added to the solution. The reaction mixture was then placed into an oil/sand bath pre-heated at 130 °C, and the solution was stirred for the prescribed time (8 or 24 h). The polymerization mixture was quenched on addition of an excess of glacial acetic acid (0.2 mL) into the solution, and the resultant solution was then poured into methanol (200 mL). The resultant polymer was then collected on filter paper and was dried *in-vacuo*.

Kinetic studies

The polymerizations were carried out at 130 °C in toluene (2 mL) using 0.010 mmol of complex. The molar ratio of monomer to initiator to co-catalyst was fixed at 250:1:1, and at appropriate time intervals, 0.5 μL aliquots were removed (under N_2) and were quenched with wet $CDCl_3$. The percent conversion of monomer to polymer was determined using ^1H NMR spectroscopy.

X-ray Crystallography

In all cases, crystals suitable for an X-ray diffraction study were grown from a saturated MeCN solution at either ambient temperature or 0 ºC. Single crystal X-ray diffraction data (except **15**) were collected at the UK National Crystallography service using Rigaku Oxford Diffraction ultra-high intensity instruments employing modern areas detectors. X-ray diffraction data for **15**·4.5MeCN were collected using a stoe ipds2 image plate

diffractometer operating with molybdenum radiation.In all cases standard procedures were employed for integration and processing of data.

Crystal structures were solved using dual space methods implemented within SHELXT.[13] Completion of structures was achieved by performing least squares refinement against all unique F^2 values using SHELXL-2018.[14] All non-H atoms were refined with anisotropic displacement parameters. Hydrogen atoms were placed using a riding model. Where the location of hydrogen atoms was obvious from difference Fourier maps, C-H and O-H bond lengths were refined subject to chemically sensible restraints. Minor disorder was treated using standard methods.

SQUEEZE[15] was used to model the disordered solvent in structures **11**, **13**, **14**, **15** and **16**.

Synthesis of **[Ti_2(O*i*Pr)$_2$(MeCN)L^{6O}]·3.5MeCN (11·3.5MeCN).**

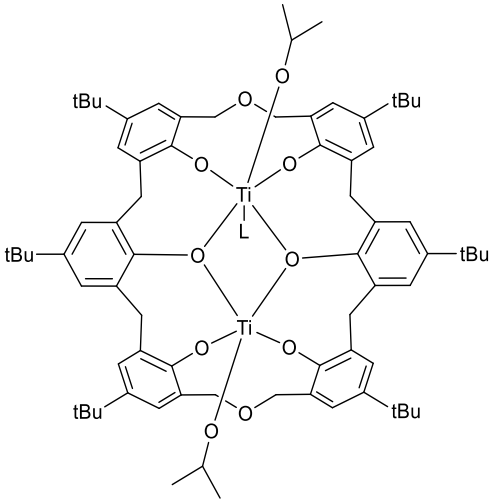

11 (L=MeCN)

To [Ti(O*i*Pr)$_4$] (0.43 g, 1.50 mmol) and $L^{6O}H_6$ (0.50 g, 0.49 mmol) was added toluene (30 mL) and then the system was refluxed for 12 h. On cooling, the volatiles were removed in *vacuo*, and the residue was extracted into warm MeCN (30 mL). On prolonged standing at

0 °C, an orange crystalline material formed, yield 0.32 g, 52%. Anal. Cald for $C_{82}H_{108}N_4O_{10}Ti_2$ (sample dried *in-vacuo* for 12 h, -3.5MeCN): C, 71.60; H, 7.06; found C, 71.92; H, 7.28%. IR (nujol mull, KBr): 3231w, 2923s, 2853s, 2349w, 1641.9w, 1461m, 1413w, 1377m, 1303w, 1260s, 1212w, 1092s, 1019s, 863w, 799s. ^{1}H NMR ($CDCl_3$) δ: 6.86-7.32 (m, 12H, aryl*H*), 5.44 (m, 2H, -OC*H*(CH_3)$_2$), 5.04-5.21 (m, 4H, -OCH_2-), 4.87 (d, J=4.8 Hz, 4H, -OCH_2-), 4.48 (m, 4H, -CH_2-), 3.40 (d, J=12.4 Hz, 4H, -CH_2-), 2.03 (s, 3H, *Me*CN), 1.56 (m, 12H, -OCH(CH_3)$_2$), 2.03 (s, 3H, MeCN) 1.21-1.34 (m, 54H, -C(CH_3)$_3$). Mass Spec (EI): 1267.6 [M+Na^+-3.5MeCN].

Synthesis of **[$Ti_4O_4(L^{6O})_2$]·MeCN (12·MeCN).**

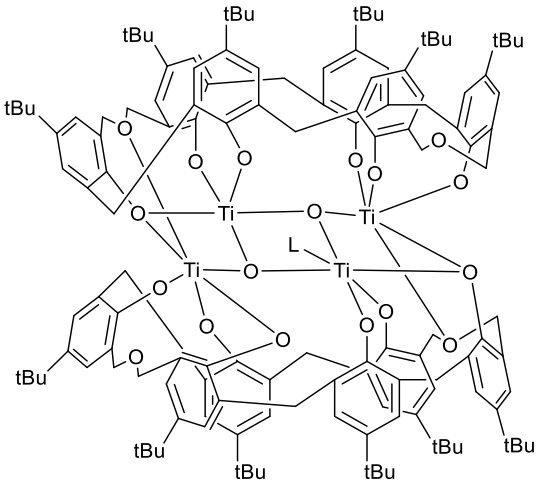

12 (L=H_2O)

As for **11**, but using [Ti(O*i*Pr)$_4$] (0.29 g, 1.00 mmol) and $L^{6O}H_6$ (0.50 g, 0.49 mmol) affording **12** as orange prisms. Single orange prisms were grown from a saturated MeCN (30 mL) solution at 0 °C (yield 0.25 g, 44%). Anal. Cald for $C_{136}H_{164}O_{18}Ti_4$ (sample dried *in-vacuo* for 12 h): C, 71.50; H, 7.26; found C, 71.91; H, 7.38 %; IR (nujol mull, KBr): 2726w, 2359w, 2340w, 1651w, 1463s, 1377s, 1301m, 1260m, 1209m, 1080m, 1020m,

941w, 926w, 899w, 899m, 798s. ^{1}H NMR ($CDCl_3$) δ: 6.89-7.32 (m, 12H, aryl*H*), 5.36 (d, J=6.8 Hz, 4H, -OC*H*$_2$-), 5.02-5.17 (m, 4H, -OC*H*$_2$-), 4.88 (d, d, J=6.8 Hz, 4H, -OC*H*$_2$-), 4.64 (d, J=6.8 Hz, 4H, -OC*H*$_2$-), 4.34 (m, 4H, -C*H*$_2$-), 3.49-3.87 (m, 8H, -C*H*$_2$-), 2.01 (s, 3H, *Me*CN), 1.13-1.36 (m, 108H, -C(C*H*$_3$)$_3$). Mass Spec (EI): 2292 [M].

Synthesis of **[$Ti_4F_{14}L^{6N}H_2(H)_2$]·2.5MeCN (13·2.5MeCN).**

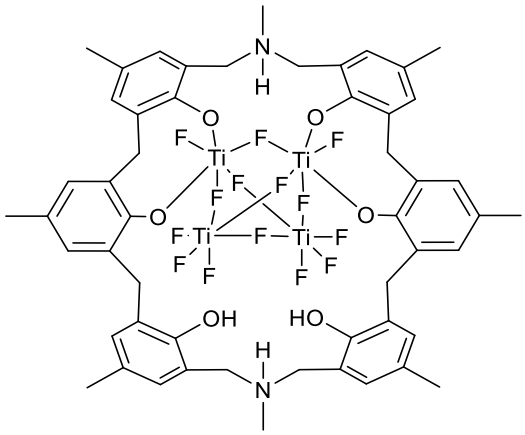

13

As for **11**, but using [TiF_4] (0.31 g, 2.48 mmol) and $L^{6N}H_6$ (0.50 g, 0.62 mmol) affording **13** as red prisms. Single orange prisms were grown from a saturated MeCN (30 mL) solution at room temperature (yield 0.44 g, 56%). Anal. Cald for $C_{52}H_{56}F_{14}N_2O_6Ti_4$ (sample dried *in-vacuo* for 12 h, -2.5MeCN): C, 49.47; H, 4.47; N, 2.22%. Found C, 50.03; H, 4.85; N, 2.06%. IR (nujol mull, KBr): 3849w, 3435s, 1737w, 1692w, 1552w, 1536s, 1461m, 1383m, 1260s, 1220w, 1093s, 1020s, 928w, 866m, 800m, 688m. ^{1}H NMR ($CDCl_3$) δ: 6.98-7.50 (m, 12H, aryl*H*), 3.48-3.73 (m, 8H, -C*H*$_2$-), 3.22-3.42 (m, 8H, -NC*H*$_2$-), 2.34 (s, 6H, -NC*H*$_3$), 2.05-2.18 (m, 18H, -C*H*$_3$). ^{19}F NMR ($CDCl_3$) δ: -110.18 (bs, 6F), -98.32 (bs, 6F), -69.12 (bs, 2F). Mass Spec (EI): 1283 [M+Na^+-2.5MeCN].

Synthesis of **[$Ti_2Cl_4(H_2O)_2OL^{6N}H_2(H)_2$]·5MeCN (14·5MeCN).**

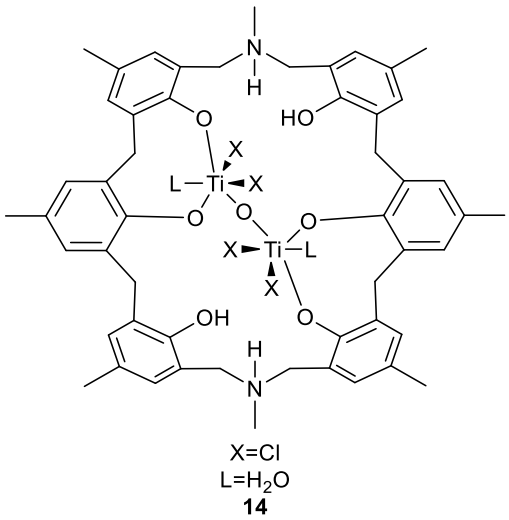

14

As for **11**, but using [$TiCl_4(THF)_2$] (0.41 g, 1.24 mmol) and $L^{6N}H_6$ (0.50 g, 0.62 mmol) affording **14** as dark red prisms. Single orange prisms were grown from a saturated MeCN (30 mL) solution at room temperature (yield 0.28 g, 41%). Anal. Cald for $C_{52}H_{60}Cl_4N_2O_9Ti_2$ (sample dried *in-vacuo* for 12 h, -5MeCN): C, 57.06; H, 5.53; N, 2.56%. Found C, 56.39; H, 5.25; N, 2.26%., IR (nujol mull, KBr): 3428m, 2745w, 2365w, 2278m, 1705m, 1628w, 1425s, 1357s, 1325m. 1232m, 1029s, 1015w, 799m, 754s. ^{1}H NMR ($CDCl_3$) δ: 6.88-7.49 (m, 12H, aryl*H*), 3.71 (d, *J*=4.8 Hz, 8H, -CH_2-), 3.56 (d, *J*=4.8 Hz, 8H, -NCH_2-), 2.34 (s, 6H, -NCH_3), 2.00-2.26 (m, 18H, -CH_3), 1.53 (s, 2H, H_2O). Mass Spec (EI): 1053 [M-2H_2O-5MeCN].

Synthesis of **[$Ti_2Br_4(H_2O)_2OL^{6N}H_2(H)_2$]·4.5MeCN (15·4.5MeCN).**

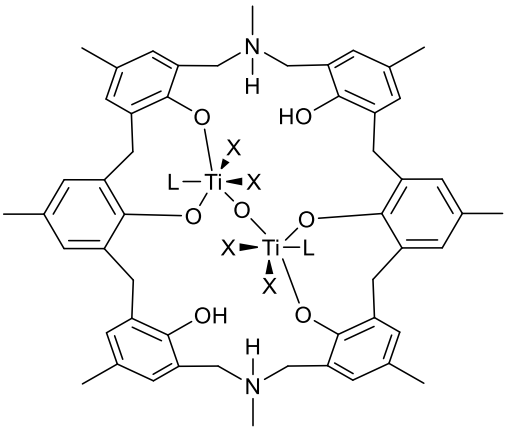

15

As for **11**, but using [$TiBr_4$] (0.46 g, 1.24 mmol) and $L^{6N}H_6$ (0.50 g, 0.62 mmol) affording 1**5** as dark orange prisms. Single orange prisms were grown from a saturated MeCN (30 mL) solution at room temperature (yield 0.25 g, 32%). Anal. Cald for $C_{54}H_{63}Br_4N_3O_9Ti_2$ (sample dried in-vacuo for 12 h, -3.5MeCN): C, 49.38; H, 4.83; N, 3.20%. Found C, 49.62; H, 5.03; N, 2.86%. IR (nujol mull, KBr): 3427m, 2729w, 2348w, 2285m, 2248w, 1605m, 1461s, 1377s, 1302w. 1260s, 1156w, 1039m, 1021m, 863m, 800s. ^{1}H NMR ($CDCl_3$) δ: ^{1}H NMR ($CDCl_3$) δ: 6.80-7.38 (m, 12H, aryl*H*), 3.79 (m, 8H, -CH_2-), 3.52 (m, 8H, -NCH_2-), 2.30 (s, 6H, -NCH_3), 2.05-2.23 (m, 18H, -CH_3), 1.51 (s, 2H, H_2O). Mass Spec (EI): 1274 [M-4.5MeCN].

Synthesis of [**$Ti_4Br_{12}L^{6N}(H)_2(MeCN)_6$**]**·7MeCN (16·7MeCN).**

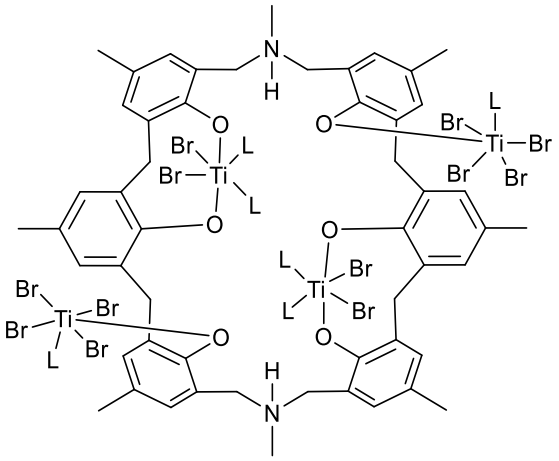

16
L=MeCN

As for **11**, but using [$TiBr_4$] (1.00 g, 2.69 mmol) and $L^{6N}H_6$ (0.50 g, 0.62 mmol) affording **16** as orange/red prisms. Single orange prisms were grown from a saturated MeCN (30 mL) solution at 0 ºC (yield 0.34 g, 26.0%). Anal. Cald for $C_{60}H_{66}Br_{12}N_6O_6Ti_4$ (sample dried *in-vacuo* for 24h, -3MeCN): Anal. Cald for C, 34.03 H, 3.14; N, 3.97%. Found: C, 33.59 H, 3.10; N, 4.42%. IR (nujol mull, KBr): 2957s, 2852s, 2727w, 2350w, 2283w, 1693w, 1645m, 1567w, 1456s, 1377s, 1308w, 1259m, 1094m, 1019m, 927w, 856m, 800s. ^{1}H NMR (CD_2Cl_2) δ: 7.24-6.81 (m, 12H, aryl*H*), 3.91 (m, 8H, -CH_2-), 3.41 (m, 8H, -NCH_2-), 2.88 (s, 6H, -NCH_3), 2.24 (m, 18H, -CH_3), 1.95 (s, 12H, *Me*CN).

Synthesis of **[$Ti_2F_2(\mu\text{-}F)_3L^{4N}(H)_2(SiF_5)$]·2MeCN (17·2MeCN).**

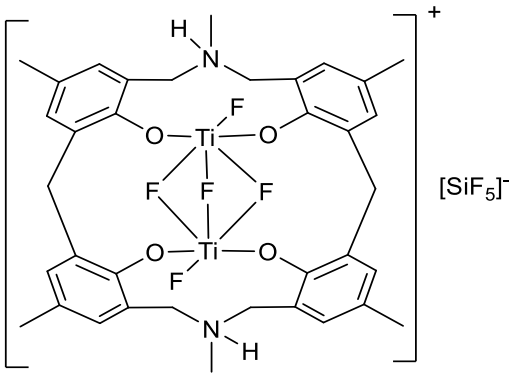

17

As for **11**, but using [TiF_4] (0.44 g, 3.53 mmol) and $L^{4N}H_4$ (0.50 g, 0.88 mmol) affording **17** as orange/red prisms. Single orange prisms were grown from a saturated MeCN (30 mL) solution at 0 ºC (yield 0.15 g, 17%). Anal. Cald for $C_{36}H_{40}F_{10}N_2SiO_4Ti_2$ (sample dried *in-vacuo* for 12h, -2MeCN): Anal. Cald for C, 49.22 H, 4.59; N, 3.19%. Found C, 49.82; H, 5.03; N, 3.59%. IR (nujol mull, KBr): 3353w, 2729w, 2360m, 2340w, 2251w, 1606w, 1463s, 1377s, 1304w, 1260m, 1231m, 1162w, 1093m, 1019m, 945w, 927w, 870m, 801m. ^{1}H NMR ($CDCl_3$) δ: 6.98-7.50 (m, 8H, aryl*H*), 3.72 (m, 4H -CH_2-), 3.46 (m, 8H,-NCH_2-), 2.34(s, 6H, -CH_3) 1.99 (s, 12H, -NCH_3), ^{19}F NMR ($CDCl_3$) δ: -107.27 (bs, 5F), -82.16 (bs, 3F), -72.06 (bs, 2F). Mass Spec (EI): 879 [M-2MeCN].

4. Experimental section for Chapter 5

General

All manipulations were carried out under an atmosphere of nitrogen using Schlenk and cannula techniques or in a conventional nitrogen-filled glove-box. Solvents were refluxed over an appropriate drying agent, and distilled and degassed prior to use. Elemental analyses were performed by the microanalytical services at the London Metropolitan University or the Chemistry Department at the University of Hull. NMR spectra were recorded on a Varian VXR 400 S spectrometer at 400 MHz or a Gemini at 300 MHz (^{1}H) at 298 K; chemical shifts are referenced to the residual protio impurity of the deuterated solvent. IR spectra (nujol mulls, KBr windows) were recorded on Perkin-Elmer 577 and 457 grating spectrophotometers. All other chemicals were purchased from Sigma Aldrich and Tokyo Chemical Industry UK Ltd. Crystal structure data were collected at the UK National Crystallography Service (**18**-**22**).

Procedure for ROP of ε-caprolactone, δ-valerolactone and rac-lactide

A toluene solution of pre-catalyst (0.010 mmol, 1.0 mL toluene) was added into a Schlenk tube in the glove-box at room temperature. The solution was stirred for 2 min, and then the appropriate equivalent of BnOH (from a pre-prepared stock solution of 1 mmol BnOH in 100 mL toluene) and the appropriate amount of *ε*-CL, *δ*-VL, or *r*-LA along with 1.5 mL toluene was added to the solution. The reaction mixture was then placed into an oil/sand bath pre-heated at 130 °C, and the solution was stirred for the prescribed time (8 or 24 h). The polymerization mixture was quenched on addition of an excess of glacial acetic acid

(0.2 mL) into the solution, and the resultant solution was then poured into cold methanol (200 mL, 0 °C). The resultant polymer was then collected on filter paper and was dried *in-vacuo*.

Solvent-free conditions: Under an inert atmosphere, a THF solution of the complex (1 mM) was added into a Schlenk tube and the solvent was removed under reduced pressure at room temperature. The monomer (9.0 mmol) was then added, and the reaction was stirred at 130 °C for 12-24 h, or until a mass of polymer blocking the stirring formed. The mixture was then taken up in CH_2Cl_2 and quenched with acidified methanol (200 mL). The resultant polymer was then collected on filter paper and dried under air at room temperature.

Kinetic studies

The polymerizations were carried out at 130 °C in toluene (2 mL) using 0.010 mmol of complex. The molar ratio of monomer to initiator to co-catalyst was fixed at 500:1:1, and at appropriate time intervals, 0.5 μL aliquots were removed (under N_2) and were quenched with wet $CDCl_3$. The percent conversion of monomer to polymer was determined using ^1H NMR spectroscopy.

Crystal Structure Determinations

Diffraction data were measured on sealed tube sources for **18**·14THF & **19**·7THF, rotating anode sources for **20**·4THF & **22**·10MeCN, and using synchrotron radiation for **21**·5.5THF. Data were corrected for absorption and structures solved by a charge-flipping algorithm. All non-H atoms were refined anisotropically and a riding model was used for all H atoms

except those on hetero- atoms when the quality of the data permitted.[13] In general, these lithium calixarenes crystals are very weakly diffracting due to the lack of any heavy elements and their inherently large unit cells. They are also subject the usual difficulties encountered with calixarene crystallography, namely *t*Bu group and solvent of crystallisation disorder, as well as a significant solvent of crystallisation loading. The number of solvent molecules of crystallisation should therefore be regarded as approximate in each case. Where disorder was modelled restraints were applied to anisotropic displacement parameters and geometry. In pathological cases, Platon Squeeze was used to model badly disordered solvent molecules as diffuse regions of electron density and this solvent was accounted for in the formula.[14,16]

For **18**·14THF, *t*Bu groups at C(18), C(29), C(51), and C(62), were modelled with the methyl groups split over two sets of positions with major occupancies of 84.8(16), 52(3), 73.9(14), and 74(3)%, respectively. In the THF containing O(22), atoms C(105) & C(106) were modelled as split over two sets of positions with major occupancy 59(2)%. Geometric and vibration parameter restraints were applied to some badly behaved THF molecules. Distance restraints were applied to assist geometry in two of the water molecules. There remains some unresolved disorder, and hence some less than ideal geometry, in some of the non-coordinated THF molecules.

For **19**·7THF, in each calix[8]arene complex molecule there are eight bonded molecules of THF and seven THF solvent of crystallisation of which four are well defined (two of these unique). Twelve molecules of THF modelled per unit cell as a diffuse area of electron density by the Platon Squeeze procedure, *i.e*. three extra per calixarene complex.[14,16] Four

THFs lie above the calixarene plane, two are in calixarene cavities and two lie in clefts within the calixarene's undulating ruffles. Three unique *t*Bu groups modelled as disordered over two sets of positions: including that at C(7), with major component = 78.7(6)%; that including C(18) with major component = 66.6(7)%; that including C(40) with major component = 80(4)%. Five THFs were disordered: that including O(6): C(46) split with major component = 50.9(17)%; that including O(8): C(54) split with major component = 51.3(19)%; that including O(9): all C atoms split with major component = 58.4(9)%; that including O(10): all C & O atoms split except C(62) with major component = 71.0(7)%; that including O(11): O(11) & C(68) split with major component = 50.7(14)%.

For **20**·4THF, in each calix[8]arene complex molecule there are 16 Li-coordinated THF molecules and 2 O*t*Bu groups. 8 molecules of THF were modelled per unit cell as a diffuse area of electron density by the Platon Squeeze procedure.

For **21**·5.5THF, in each *t*Bucalix[8]arene complex molecule there are two Li-bonded molecules of THF. 8 THF solvent molecules of crystallisation were modelled as point atoms per complex molecule, of which 4 are H-bonded to the calixarene complex molecule. One and a half molecules of THF were modelled as diffuse areas of electron density by the Platon Squeeze procedure. Two THFs including O(10) {C(58) & C(59) split} and O(11) {C(62) – C(64) split) modelled as disordered over two sets of positions with major components = 81.6(13)% and 60.3(17)% respectively.

For **22**·10MeCN, the *t*Bu group including C(15) > C(18) was modelled as disordered over two sets of positions: with major component = 67.3(12)%; part of a calixarene ring and *t*Bu group including C(33) > C(35) & C(37) > C(40) was also modelled as 2-fold disordered

with major component = 73.5(11)%, *t*Bu group C(47) > C(49) was disordered across a symmetry element, so was modelled at 50% occupancy; the MeCN including N(1) was also modelled as disordered with major component = 56.7(10)% while that including N(8) was similarly disordered in the vicinity of MeCN including N(1), so their occupation factors were linked.

Synthesis of **$[Li_{14}(L^6H)_2(CO_3)_2(THF)_6(OH_2)_6]\cdot 14THF$ (18·14THF)**

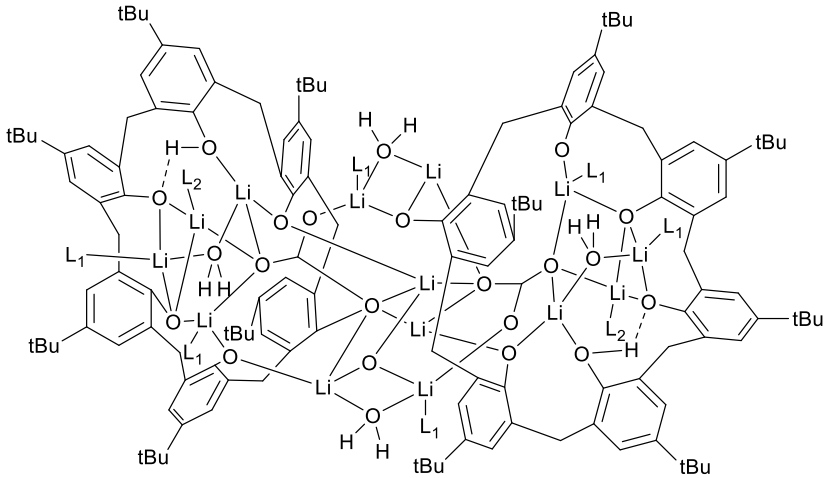

18

A solution of lithium *tert*-butoxide (8.22 mL, 1.0 M in THF, 8.22 mmol) was added to L^6H_6 (1.00 g, 1.03 mmol) in THF (30 mL) at ambient temperature. After stirring for 4 h, the orange solution was concentrated to about 20 mL and was left to stand for 48 h to afford small colorless crystals of the **18**·14THF in *ca* 15 % yield. Calcd for $C_{158}H_{218}Li_{14}O_{30}$ (**18**·14THF–14THF requires C, 70.43; H, 8.15%); found C, 70.56; H, 7.89%. IR: 1616w, 1411w, 1365m, 1290w, 1261s, 1198w, 1095bs, 1020bs, 871w, 800bs, 736w, 721w, 704w, 661w. ^{1}H NMR (THF-d_8, 400 MHz) δ: 7.24−6.79 (m, 24H, arylH), 4.35 (m, 8H, $-CH_2-$), 3.72 (m, 8H, $-CH_2-$), 3.36 (d, 4H, $-CH_2-$), 3.24 (d, 4H, $-CH_2-$), 2.66 (s, 12H, H_2O), 1.69

(THF), 1.24−1.28 (m, 108H, C(CH_3)$_3$), calixO*H* not observed. ^{7}Li NMR (THF-d_8, 194.3 MHz, 298 K) δ: 3.20 (bs), 2.72 (bs), 1.93 (s), 1.86 (s), 1.33 (s). Mass Spec (EI): 2177 [M–$6H_2O$–20THF+Na^+]

Synthesis of **[$Li_{10}(L^8)(OH)_2(THF)_8$]·7THF (19·7THF)**

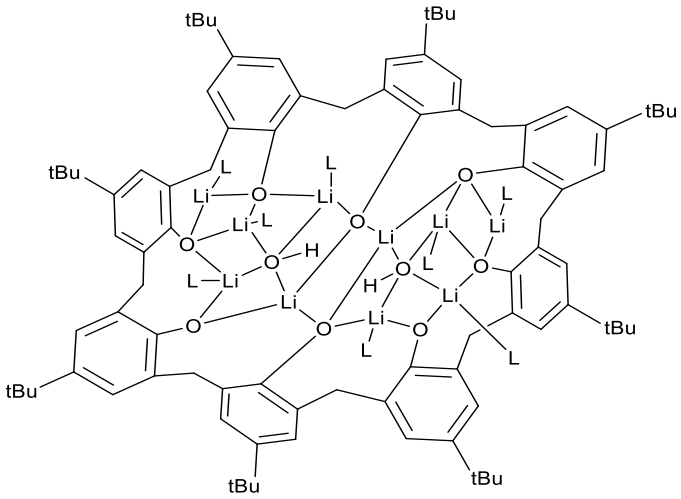

19

A solution of lithium *tert*-butoxide (8.01 mL, 1.0 M in THF, 8.01 mmol) was added to L^8H_8 (1.00 g, 0.77 mmol) in THF (30 mL) at ambient temperature. Following stirring for 12h, the system was filtered and stored at 0 °C for 24h to afford **19**·7THF in *ca*. 50% yield. Calcd for $C_{120}H_{170}Li_{10}O_{18}$ (**19**·7THF–7THF requires C, 73.16; H, 8.70%) found C, 72.69; H, 8.71%. IR: 3339bw, 3171bw, 2360w, 1738w, 1657m, 1614m, 1557m, 1297s, 1260s, 1202s, 1094bs, 1020bs, 872s, 804bs, 734s, 723s, 663m. ^{1}H NMR (THF_d8, 400MHz) δ: 7.32-6.75 (m, 16H, aryl*H*), 4.64 (overlapping d, 4H, -CH_2-), 4.37 (d, *J*=8.0 Hz, 4H, -CH_2-), 3.59 (THF), 3.20 (m, 4H, -CH_2-), 3.04 (d, *J*=8.0 Hz, 4H, -CH_2-), 1.74 (THF), 1.23 (s, 72H, C(CH_3)$_3$), calixO*H* not observed. ^{7}Li NMR (THF-d_8, 194.3 MHz, 298 K) δ: 3.11 (s), 3.49 (bs), 3.61 (bs). Mass Spec (EI): 1416 [M–15THF+Na^+].

Synthesis of **[Li$_{18}$(deBuL^{8})$_2$(O*t*Bu)$_2$(THF)$_{14}$]·4THF (20·4THF)**

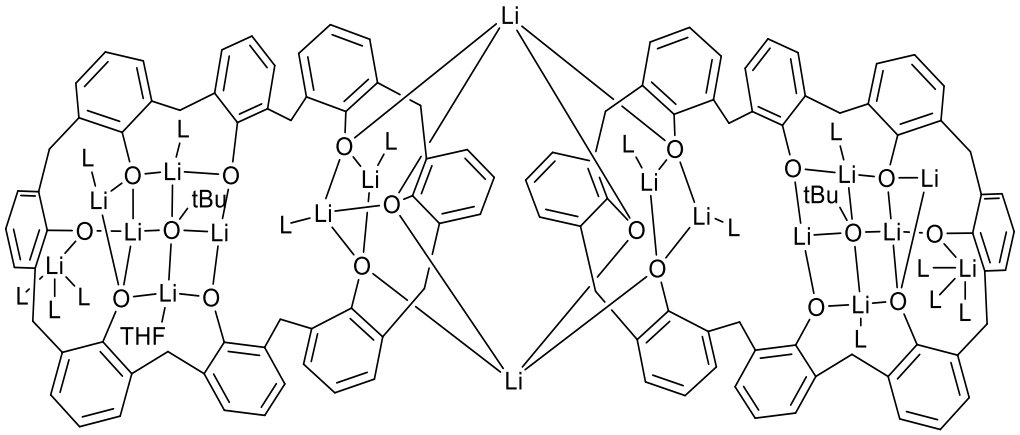

20

A solution of lithium *tert*-butoxide (12.25 mL, 1.0 M in THF, 12.2 mmol) was added to deBuL^{8}H$_8$ (1.00 g, 1.18 mmol) in THF (30 mL) at ambient temperature. After stirring for 4 h, the system was filtered and on prolonged standing (1 week) at ambient temperature, colorless prisms of **20**·4THF were formed (in *ca*. 35% yield). Anal. Calcd for $C_{184}H_{226}Li_{18}O_{34}$ (sample dried *in-vacuo* for 12 h, –4THF) requires C, 71.14; H, 7.33%. Found C 70.96, H 7.22%. IR: 2727w, 1589m, 1460s, 1436s, 1377s, 1261s, 1091s, 1041s, 1019s, 907w, 840m, 799s, 752m, 722w, 695w. ^{1}H NMR (THF-d_8, 400MHz) δ: 7.14−6.89 (m, 48H, arylH), 4.54 (d, 8H, −CH_2−), 4.44 (d, 8H, −CH_2−), 4.29 (d, 4H, −CH_2−), 4.14 (d, 4H, −CH_2−) 3.56 (THF), 3.22−3.32 (m, 8H, −CH_2−),1.74 (THF), 1.12 (s, 18H, −OC(CH_3)$_3$). ^{7}Li NMR (THF-d_8, 194.3 MHz, 298 K) δ: 4.87 (s), 4.10 (s), 1.27 (bs). Mass spec (EI): 1066 [(M-18THF)/2 -Li^++Na^+]

Synthesis of **[Li$_4$(L^{8}H$_4$)(OH$_2$)$_4$(THF)$_6$]·5.5THF (21·5.5THF)**

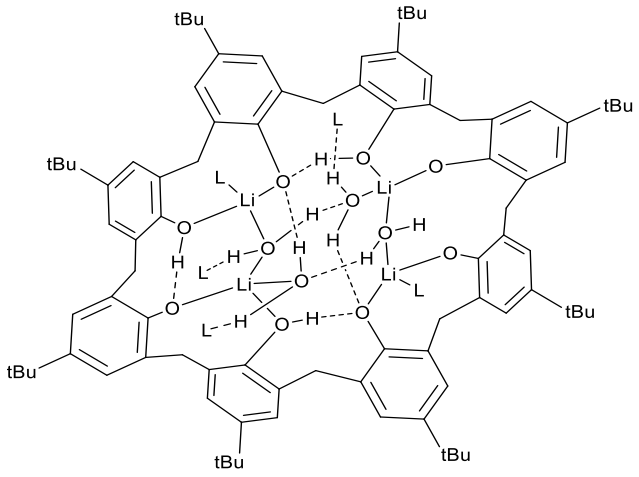

21

To L^{8}H$_8$ (1.00 g, 0.77 mmol) and LiOH·H$_2$O (0.07 g, 1.67 mmol) was added THF (30 mL) and the system was refluxed for 12h. On cooling, filtration followed by prolonged standing at 0 °C afforded **21**·5.5THF in *ca*. 28% yield. Cald for C$_{112}$H$_{156}$Li$_4$O$_{14}$ (**21**·5.5THF–5.5THF–4H$_2$O, requires C, 76.69; H, 8.96%), found C, 76.89; H, 9.05%. IR: 2727w, 2359m, 1620w, 1614w, 1539w, 1462s, 1414w, 1377s, 1260s, 1093s, 1019s, 872w, 799s, 739w, 722w. ^{1}H NMR (THF$_d$8, 400 MHz) δ: 7.11-6.92 (m, 16H, aryl*H*), 4.72 (d, *J*=4.8 Hz, 4H, -C*H*$_2$-), 4.40 (d, *J*=4.8 Hz, 8H, -C*H*$_2$-), 3.57 (THF), 3.35 (s, 4H, O*H*), 3.20 (d, *J*=4.8 Hz, 4H, -C*H*$_2$-), 2.60 (s, 8H, *H*$_2$O), 1.73 (THF), 1.22-1.28 (overlapping s, 72H, C(C*H*$_3$)$_3$). ^{7}Li NMR (THF-d$_8$, 194.3 MHz, 298 K) δ: 3.55 (s). Mass Spec (EI): 1645 [M–2H$_2$O–7.5THF].

Synthesis of **[(AlMe$_2$)$_2$Li$_{20}$(L^{8}H$_2$)$_2$(OH$_2$)$_4$(O^{2-})$_4$(OH)$_2$(NCMe)$_{12}$]·10MeCN (22·10MeCN)**

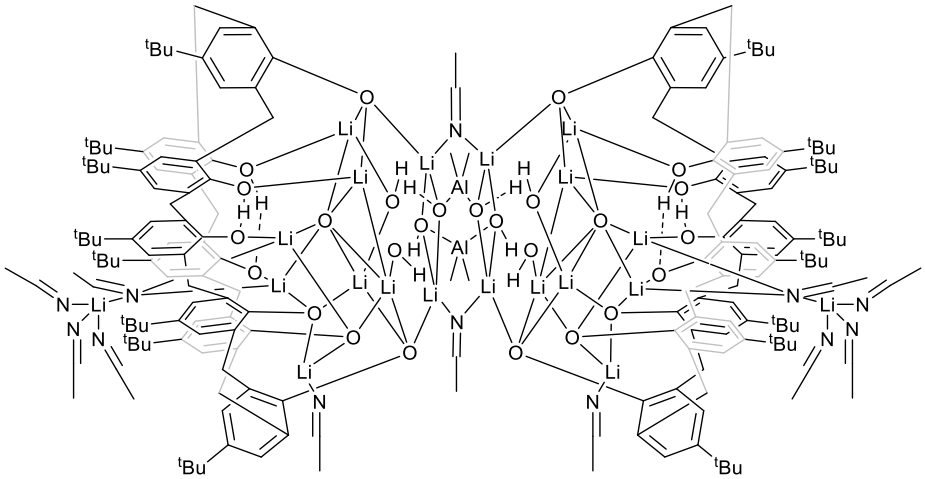

22

A solution of lithium *tert*-butoxide (8.01 mL, 1.0M in THF, 8.01 mmol) was added to L^{8}H$_8$ (1.00 g, 0.77 mmol) in THF (30 mL) at ambient temperature. After stirring for 1 h, Me_3Al (1.0 M, 1.50 mmol) was added to the orange solution. After refluxing for 12 h, the volatiles were removed *in-vacuo*, and the residue was extracted into MeCN (30 mL), and the solution was left to stand for 48 h to afford colorless crystals of **22**·10MeCN in *ca* 20 % yield. Calcd for $C_{196}H_{258}Al_2Li_{20}O_{26}N_8$ (**22**·10MeCN–14MeCN requires C, 70.59; H, 7.80; N, 3.35%), found C, 70.74; H, 7.45; N 3.03%. IR (MeCN product): 2727w, 2261w, 1700w, 1657w, 1604w, 1462s, 1377m, 1362m, 1296m, 1260s, 1296m, 1260s, 1207m, 1093s, 1019s, 909w, 872w, 800s. ^{1}H NMR (THF-d$_8$, 400MHz) δ: 7.19-6.93 (m, 32H, aryl*H*), 4.54 (d, *J*=12 Hz, 8H, -C*H*$_2$-), 4.38 (d, *J*=12 Hz, 8H, -C*H*$_2$-), 4.27 (d, *J*=12 Hz, 8H, -C*H*$_2$-), 4.14 (d, *J*=6.8 Hz, 4H, -C*H*$_2$-), 3.25 (s, 2H, O*H*), 3.20 (m, 4H, -C*H*$_2$-), 2.47 (s, 8H, *H*$_2$O), 1.91 (s, 12H, *Me*CN), 1.28-1.13 (overlapping s, 144H, C(C*H*$_3$)$_3$), -0.81 (s, 12H, Al*Me*$_2$); calixO*H* not observed. ^{7}Li NMR (THF-d$_8$, 194.3 MHz, 298 K) δ: 5.18 (bs), 4.75 (bs), 4.43 (s), 3.88(s). Mass spec (EI): 1527 [(M-22MeCN)/2+Na$^+$]

5. Experimental section for Chapter 6

General

All reactions were conducted under an inert atmosphere using standard Schlenk techniques. Toluene was dried from sodium, acetonitrile was distilled from calcium hydride, diethylether was distilled from sodium benzophenone, and all solvents were degassed prior to use. The dioxacalix[6]arene,[1(i)] [LiPb(O*i*Pr)$_3$],[18] [Pb(N(TMS)$_2$)$_2$],[19] Pb(O*i*Pr)$_2$ and Pb(O*t*Bu)$_2$[20] were prepared according to the literature methods. All other chemicals were purchased from commercial sources. IR spectra (nujol mulls, KBr windows) were recorded on a Nicolet Avatar 360 FT IR spectrometer; ^{1}H NMR spectra were recorded at room temperature on a Varian VXR 400 S spectrometer at 400 MHz or a Gemini 300 NMR spectrometer or a Bruker Advance DPX-300 spectrometer at 300 MHz. The ^{1}H NMR spectra were calibrated against the residual protio impurity of the deuterated solvent. Elemental analyses were performed by the elemental analysis service at the University of Hull. Matrix Assisted Laser Desorption/Ionization Time of Flight (MALDI-TOF) mass spectrometry was performed in a Bruker autoflex III smart beam in linear mode, and the spectra were acquired by averaging at least 100 laser shots. 2,5-Dihydroxybenzoic acid was used as the matrix and THF as solvent. Sodium chloride was dissolved in methanol and used as the ionizing agent. Samples were prepared by mixing 20 μl of matrix solution in THF (2 mg·mL^{-1}) with 20 μL of matrix solution (10 mg·mL^{-1}) and 1 μL of a solution of ionizing agent (1 mg·mL^{-1}). Then 1 mL of these mixtures was deposited on a target plate and allowed to dry in air at ambient temperature. Crystal structure data were collected at the UK National Crystallography Service (**23**-**28**).

Procedure for ROP of ε-caprolactone, δ-valerolactone and rac-lactide

A toluene solution of pre-catalyst (0.010 mmol, 1.0 mL toluene) was added into a Schlenk tube in the glove-box at room temperature. The solution was stirred for 2 min, and then the appropriate equivalents of BnOH (from a pre-prepared stock solution of 1 mmol BnOH in 100 mL toluene) and the appropriate amount of *ε*-CL, *δ*-VL or *r*-LA along with 1.5 mL toluene was added to the solution. The reaction mixture was then placed into an oil/sand bath pre-heated at 130 °C, and the solution was stirred for the prescribed time (8 or 24 h). The polymerization mixture was quenched on addition of an excess of glacial acetic acid (0.2 mL) into the solution, and the resultant solution was then poured into methanol (200 mL). The resultant polymer was then collected on filter paper and was dried *in-vacuo*.

Kinetic studies

The polymerizations were carried out at 130 °C in toluene (2 mL) using 0.010 mmol of complex. The molar ratio of monomer to initiator to co-catalyst was fixed at 250:1:1, and at appropriate time intervals, 0.5 μL aliquots were removed (under N_2) and were quenched with wet $CDCl_3$. The percent conversion of monomer to polymer was determined using ^1H NMR spectroscopy.

Preparation of **[$Pb_4Li_2(L^4)_4H_6(MeCN)_3$]·4.5MeCN (23·4.5MeCN)**

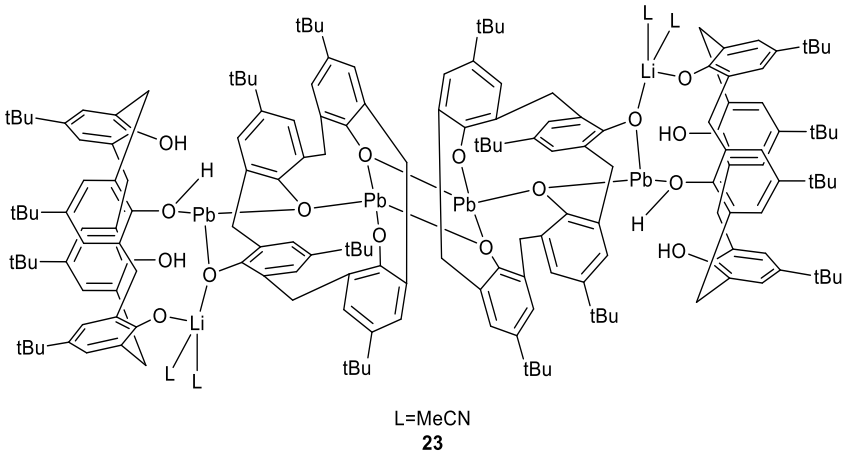

L^4H_4 (1.00 g, 1.54 mmol) and [LiPb(O*i*Pr)$_3$] (0.63 g, 1.57 mmol) were combined in toluene (20 mL) and the system was refluxed for 12 h. On cooling, the volatiles were removed *in-vacuo*, and the residue was extracted into MeCN (20 mL). On standing at 0 ºC for 2 days, colourless prisms formed. Yield, 0.53 g, 37 %. Anal. calcd for $C_{191}H_{236.5}Li_2N_{7.5}O_{17}Pb_4$ (sample dried *in-vacuo* for 12 h, –4.5MeCN): C, 61.55; H, 6.33; N, 1.18%; found C, 61.40; H, 6.25%; N, 1.51%; IR (nujol mull, KBr): 2726w, 2263w, 1607w, 1460s, 1377s, 1304m, 1280m, 1260s, 1204m, 1125m, 1093m, 1018m, 914w, 872m, 818s, 795s. ^{1}H NMR ($CDCl_3$) δ: 10.33 (s, 6H, -O*H*), 6.98-7.48 (m, 32H, aryl*H*), 4.42-4.38 (m, 4H, -CH_2), 4.24 (d, *J*=14 Hz, 12H, -CH_2-), 3.83-3.89 (m, 4H, -CH_2-), 3.48 (d, *J*=14 Hz, 12H, -CH_2-), 1.96 (s, 12H, *Me*CN), 1.13-1.36 (m, 144H, -C(CH_3)$_3$), ^{7}Li ($CDCl_3$): δ: 3.61(bs). Mass Spec (EI): 1761 ([M-7.5MeCN]/2+2Na^+].

Preparation of **[Pb$_8$Li$_{10}$Cl$_2$(L^6)$_4$(H)$_8$(O)$_4$(H$_2$O)$_2$(MeCN)$_4$]·14MeCN (24·14MeCN)**

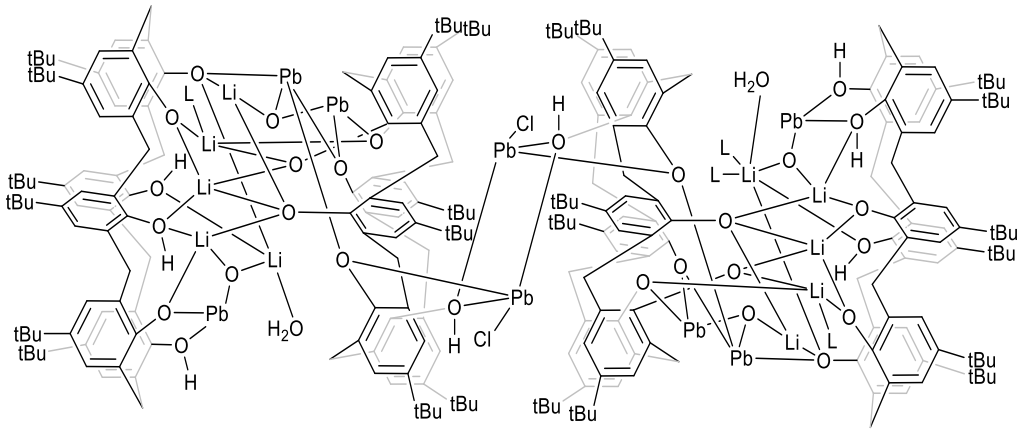

24

L^{6}H$_6$ (1.00 g, 1.03 mmol) and [LiPb(O*i*Pr)$_3$] (0.82 g, 2.04 mmol) were combined in toluene (20 mL) and the system was refluxed for 12 h. On cooling, the volatiles were removed *in-vacuo*, and the residue was extracted into MeCN (20 mL). On standing at 0 ºC for 2 days, colourless prisms formed. Yield, 0.79 g, 47 %. Anal. calcd for $C_{268}H_{323}Cl_2Li_{10}N_2O_{30}Pb_8$ (sample dried *in-vacuo* for 12 h, –16MeCN): C, 55.02; H, 5.57; N, 0.48%; found C, 54.75; H, 5.24; N, 0.79%; IR: 2726w, 2359w, 1645w, 1462s, 1377m, 1364m, 1297w, 1260m, 1203m, 1093m, 1021m, 909w, 872w, 801m, 735m, 527w. ^{1}H NMR ($CDCl_3$): δ: 6.95-7.29 (m, 48H, aryl*H*), 4.56 (d, *J*=12 Hz, 12H, -C*H*$_2$-), 3.98 (d, *J*=12 Hz, 12H, -C*H*$_2$-), 3.46 (d, *J*=4.8 Hz, 6H, -C*H*$_2$-), 3.08-3.18 (m, 18H, -C*H*$_2$-), 1.97 (s, 18H, *Me*CN), 1.13-1.30 (m, 216H, -C(C*H*$_3$)$_3$). ^{7}Li ($CDCl_3$) δ: 3.82 (bs), 3.04 (s), 2.83 (bs), 2.61 (bs), 2.41 (bs).

Preparation of **[Pb$_{13}$(L^{6O})$_3$O$_4$(iPrOH)]·11MeCN (25·11MeCN)**

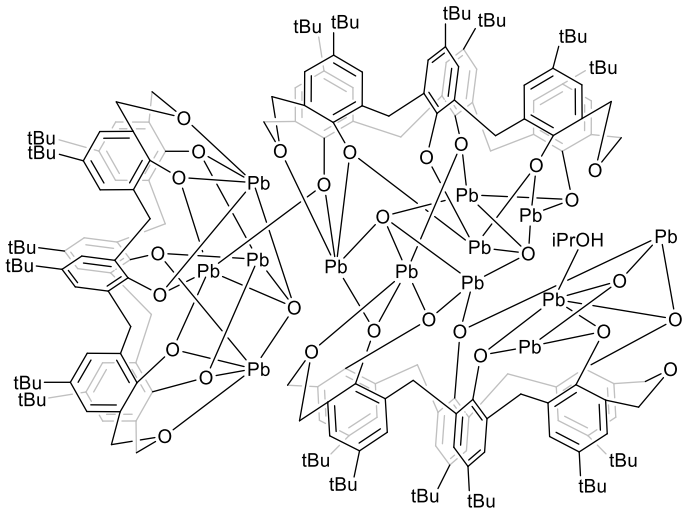

25

To Pb(O*i*Pr)$_2$ (0.96 g, 2.94 mmol) and L^{6O}H$_6$ (0.5 g, 0.49 mmol) was added toluene (30 mL) and the system was refluxed for 12 h. On cooling, the volatiles were removed *in-vacuo*, and the residue was extracted into MeCN (30 mL). On standing at room temperature for 3 days, colourless prisms formed. Yield, 0.35 g, 35 %. Anal. calcd for $C_{207}H_{253}O_{29}Pb_{13}$ (sample dried *in-vacuo* for 12 h, –11MeCN): C, 42.15; H, 4.32%; found C, 42.62; H, 4.58%; IR (nujol mull, KBr): 2726w, 2359w, 1651w, 1539w, 1462s, 1377m, 1260s, 1092s, 1018s, 871s, 799s, 722w. ^{1}H NMR ($CDCl_3$) δ: 6.91-7.62 (m, 36H, aryl*H*), 5.48 (d, *J*=12.4 Hz, 1H, –OC*H*(CH$_3$)$_2$), 4.85-5.20 (m, 12H, -OC*H*$_2$-), 4.45-4.60 (m, 12H, -OC*H*$_2$-), 4.02-4.22 (m, 12H, -C*H*$_2$-), 3.39-3.47 (m, 6H, -C*H*$_2$-), 3.22-3.30 (m, 6H, -C*H*$_2$), 1.70-1.72 (m, 6H, –OCH(C*H*$_3$)$_2$), 1.10-1.32 (m, 162H, -C(C*H*$_3$)$_3$).

Preparation of **[$Pb_{12}(L^8)_2O_4$]·8.7C_7H_8 (26·8.7C_7H_8)**

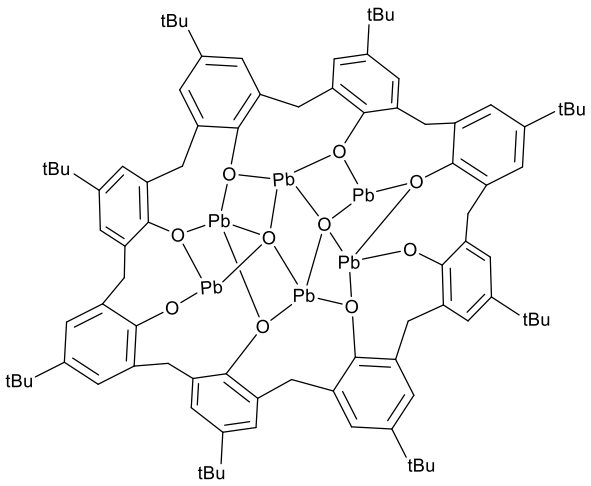

26

To $Pb(OtBu)_2$ (1.63 g, 4.62 mmol) and L^8H_8 (1.00 g, 0.77 mmol) was added toluene (30 mL) and the system was refluxed for 3 h. On cooling, the volatiles were removed in *vacuo*, and the residue was extracted into MeCN (30 mL). On standing at 0 ºC for 2 days, colourless prisms formed. Yield, 0.68 g, 35 %. Anal. calcd for $C_{176}H_{208}O_{20}Pb_{12}$ (sample dried in vacuo for 12 h, –8.7C_7H_8): C, 41.21; H, 4.09%; found C, 41.25; H, 4.50%; IR (nujol mull, KBr): 1685w, 1601w, 1493m, 1362s, 1296s, 1280s, 1260s, 1197s, 1163m, 1117s, 1094bs, 1020bs, 946w, 912w, 899w, 878m, 870m, 817s, 800s, 728s, 702w, 693m, 664w, 634w, 611w, 552w, 528m, 539m, 488m, 475m, 463s. ^{1}H NMR ($CDCl_3$) δ: 6.98-7.34 (m, 16H, aryl*H*), 4.94-5.12 (m, 2H, -CH_2-), 4.30-4.40 (m, 4H, -CH_2-) 4.13-4.15 (m, 4H, -CH_2-), 3.34-3.45 (m, 6H, -CH_2-), 1.19-1.27 (m, 72H, -C(CH_3)$_3$). Mass Spec (EI): 2614.7 [M+2Na^+].

Preparation of **[Pb$_6$(SiMe$_3$)$_2$(L^8)O$_2$Cl$_2$] (27)**

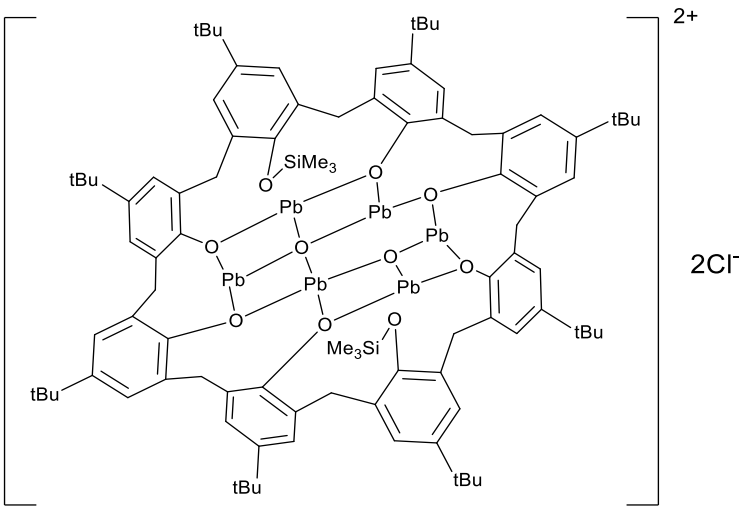

27

To Pb(N(TMS)$_2$)$_2$ (2.44 g, 4.62 mmol) and L^{8}H$_8$ (1.0 g, 0.77 mmol) was added toluene (30 mL) and the system was refluxed for 12 h. On cooling, the volatiles were removed *in-vacuo*, and the residue was extracted into MeCN (30 mL). On standing at 0 ºC for 3 days, colourless prisms formed. Yield, 0.71 g, 33 %. $C_{94}H_{122}Cl_2O_{10}Pb_6Si_2$ (sample dried *in-vacuo* for 12 h) requires C, 40.58; H, 4.42%; found C, 40.23; H, 4.85%. IR (nujol mull, KBr): 2727w, 2359m, 2341s, 1657w, 1461m, 1414s, 1377m, 1260s, 1200w, 1091s, 1019s, 908w, 867w, 799s, 722w, 703w, 667w. ^{1}H NMR ($CDCl_3$) δ: 6.98-7.24 (m, 16H, aryl*H*), 5.11 (d, *J*=12 Hz, 2H, -C*H*$_2$), 4.87 (m, 4H, -C*H*$_2$), 4.47 (m, 4H, -C*H*$_2$), 3.97 (d, *J*=12 Hz, 2H, -C*H*$_2$), 3.33 (m, 6H, -C*H*$_2$), 1.13-1.34 (m, 72H, -C(C*H*$_3$)$_3$), 0.07-0.12 (m, 27H, -Si*Me*$_3$). Mass Spec (EI): 2568.1 [M-2SiMe$_3$-2Cl$^-$].

Preparation of **[$Pb_5Li(L^6)O_{2.5}Cl_{0.5}$]·4.75MeCN (28·4.75MeCN)**

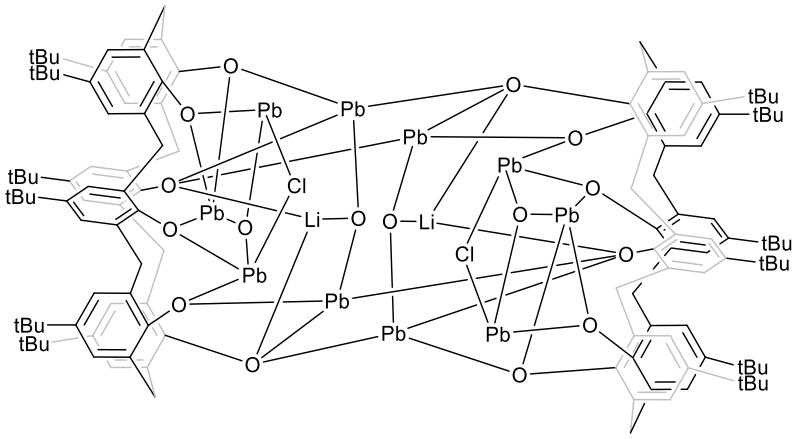

28

To [$Pb(N(TMS)_2)_2$] (1.46 mL, 3.06 mmol), generated *in-situ* from hexamethyldisilazane (19.78 g, 73.58 mmol), *n*BuLi (1.6 M in heptane, 45.99 mL, 73.58 mmol) and $PbCl_2$ (10.23 g, 36.79 mmol) in THF (10 mL), was added L^6H_6 (0.5 g, 0.51 mmol) in toluene (30 mL) and the system was refluxed for 3 h. On cooling, the volatiles were removed *in-vacuo*, and the residue was extracted into MeCN (30 mL). On standing at room temperature for 3 days, colourless prisms formed. Yield, 0.49 g, 46%. $C_{66}H_{78}Cl_{0.5}LiO_{8.5}Pb_5$ (sample dried *in-vacuo* for 12 h, –3.75MeCN) requires C, 38.73; H, 3.87; N, 0.66%; found C, 39.11; H, 3.69; N, 0.74%, IR (nujol mull, KBr): 2727w, 2359w, 2340w, 1716w, 1652w, 1505w, 1457s, 1377m, 1260s, 1199w, 1092s, 1018s, 872w, 799s, 722m. ^{1}H NMR ($CDCl_3$) δ: 6.98-7.24 (m, 16H, aryl*H*), 5.23-5.29 (m, 4H, -CH_2-), 4.65 (d, *J*=4.8 Hz, 8H, -CH_2-) 3.91-4.00 (m, 4H, -CH_2-), 3.47 (d, *J*=4.8 Hz, 8H, -CH_2-), 1.99 (s, 6H, *Me*CN), 1.20-1.35 (m, 72H, -C(CH_3)$_3$). ^{7}Li ($CDCl_3$) δ: 4.38(s). Mass Spec (EI): 2056.9 [M+Na^+-4.75MeCN-Cl].

6. References

[1] (a) C. Redshaw, M. Walton, K. Michiue, Y. Chao, A. Walton, P. Elo, V. Sumerin, C. Jiang, M. R. J. Elsegood, *Dalton Trans*., 2015, 44, 12292-12303. (b) C. Redshaw, M. Rowan, L. Warford, D. M. Homden, A. Arbaoui, M. R. J. Elsegood, S. H. Dale, T. Yamato, C. P. Casas, S. Matsui, S. Matsuura. *Chem. Eur. J*., 2007, 13, 1090-1107. (c) C. Redshaw, M. Walton, D. S. Lee, C. Jiang, M. R. J. Elsegood and K. Michiue, *Chem. Eur. J*., 2015, 21, 5199-5210. (d) T. Moriuchi, T. Hirao, *Coord. Chem. Rev*., 2011, 255, 2371– 2377. (e) D. D. Devore, J. D. Lichtenhan, F. Takusagawa, E. A. Maatta, *J. Am. Chem. Soc*., 1987, 109, 7408-7416. (f) E. A. Maatta, *Inorg. Chem.,* 1984, 23, 2560-2561. (g) M. Lutz, H. Hagen, A. M. M. Schreurs, G. Van Koten, *Acta Crystallogr. Sect*. C, 1999, 55, 1636-1639. (h) B. Masci, *J. Org. Chem*., 2001, 66, 1497-1499. (i) B. Dhawan, C. D. Gutsche, *J. Org. Chem*., 1983, 48, 1536-1539.

[2] A. Zanotti-Gerosa, E. Solari, L. Giannini, C. Floriani, N. Re, A. Chiesi-Villa, C. Rizzoli, *Inorg. Chim. Acta*, 1998, 270, 298-311.

[3] D. D. Devore, J. D. Lichtenhan, F. Takusagawa, E. A. Maatta, *J. Am. Chem. Soc*., 1987, 109, 7408–7416.

[4] L. E. Manxzer, J. Deaton, P. Sharp, R. R. Schrock, in *Inorg. Synth*., John Wiley & Sons, Inc., 2007, 135-140.

[5] C. Redshaw, M. A. Rowan, L. Warford, D. M. Homden, A. Arbaoui, M. R. J. Elsegood, S. H. Dale, T. Yamato, C. P. Casas, S. Matsui, S. Matsuura, *Chem. Eur. J*., 2007, 13, 1090-1107.

[6] A. Ignaszak, M. Radtke, M. R. J. Elsegood, J. W. A. Frese, J. L. Z. F. Lipman, T. Yamato, S. Sanz, E. Brechin, T. J. Prior, C. Redshaw, *Dalton Trans.*, 2018, 47, 15983-15993.

[7] C. Redshaw, M. J. Walton, D. S. Lee, C. Jiang, M. R. J. Elsegood, K. Michiue, *Chem. Eur. J.*, 2015, 21, 5199-5210.

[8] T. Xing, T. J. Prior, M. R. J. Elsegood, N. V. Semikolenova, I. E. Soshnikov, K. Bryliakov, K. Chen, C. Redshaw, *Cat. Sci & Tech*., 2021, 11, 624-636.

[9] O. Santoro, M. R. J. Elsegood, E. V. Bedwell, J. A. Pryce, C. Redshaw, *Dalton Trans*. 2020, 49, 11978-11996.

[10] SAINT and APEX 2 (2009) software for CCD diffractometers. Bruker AXS Inc., Madison, USA.

[11] CrysAlis PRO, Rigaku Oxford Diffraction, 2018.

[12] *CrysAlis PRO*, Rigaku Oxford Diffraction, 2017-2018.

[13] G. M. Sheldrick, *Acta Crystallogr., Sect. A: Found.* Adv., 2015, 71, 3–8.

[14] G. M. Sheldrick, *Acta Crystallogr., Sect. C: Struct. Chem*., 2015, 71, 3–8.

[15] A. L. Spek, *Acta Crystallogr. Sect. C-Struct. Chem*., 2015, 71, 9-18.

[16] P. V. D. Sluis, A. L. Spek, *Acta Crystallogr*., 1990, A46, 194-201.

[17] H. Takemura, A. Takahashi, H. Suga, M. Fukuda, T. Iwanaga, *Eur. J. Org. Chem.*, 2011, 3171–3177.

[18] L. Wang, S. Fadlallah, C. Bellini, C. Orione, V. Dorcet, J.-F. Carpentier, Y. Sarazin, *Organometallics*, 2015, 34, 1321–1327.

[19] T. Heidemann, S. Mathur, *Eur. J. Inorg. Chem.*, 2014, 3, 506-510.

[20] S. C. Goel, M. Y. Chiang, W. E. Buhro, *Inorg. Chem.*, 1990, 29, 4640–4646.

Chapter 8

Appendix

1. Appendix for Chapter 2

Table 8-1. ROP of ε-CL using **1** – **8** and **I - IV** in the absence of BnOH.

Run	Cat.	CL: V: BnOH	T/°C	t/h	Conv[a] (%)	$M_{n,GPC}\times10^{-3}$[b]	$M_w\times10^{-3}$[b]	$M_{n,Cal}\times10^{-}$	PDI[d]	TON[e]	TOF (h^{-1})[f]
1	**1**	1000:1:0	130	24	98.5	7.13	10.57	112.43	1.48	985	41
2	**1**	500:1:0	130	24	99.7	8.21	11.64	56.90	1.41	499	21
3	**1**	250:1:0	130	24	97.5	5.14	6.51	27.78	1.27	244	10
4	**1**	100:1:0	130	24	98.1	2.69	3.14	11.18	1.16	98	4
5	**1**	50:1:0	130	24	90.4	0.97	1.66	5.13	1.71	452	19
6	**2**	500:1:0	130	24	64.1	2.65	3.91	36.48	1.47	321	13
7	**3**	500:1:0	130	24	99.1	2.84	3.20	56.56	1.12	496	21
8	**4**	500:1:0	130	24	97.9	1.37	2.22	55.80	1.61	490	20
9	**5**	500:1:0	130	24	99.4	6.08	8.88	56.66	1.46	497	21
10	**6**	500:1:0	130	24	99.0	5.67	8.11	56.43	1.43	495	21
11	**7**	500:1:0	130	24	96.3	5.35	8.76	54.89	1.63	482	20
12	**8**	500:1:0	130	24	99.7	5.52	8.76	56.90	1.59	499	21
13	**8**	500:1:0	100	24	77.1	2.91	4.38	43.94	1.50	386	16
14	**8**	500:1:0	80	24	nothing	-	-	-	-	-	-
15	**I**	500:1:0	130	24	46.3	2.51	3.60	32.63	1.41	232	10
16	**II**	500:1:0	130	24	65.1	3.54	4.32	32.71	1.21	326	14
17	**III**	500:1:0	130	24	57.6	3.96	5.20	41.36	1.31	288	12
18	**IV**	500:1:0	130	24	60.3	2.27	3.78	38.61	1.66	302	13

[a] Determined by ^{1}H NMR spectroscopy. [b] $M_{n/w}$, GPC values corrected considering Mark–Houwink method from polystyrene standards in THF, $M_{n/w}$ measured = 0.56 × $M_{n/w}$ GPC $\times10^3$. [c] Calculated from ([monomer]$_0$/[cat]$_0$) × conv (%) × monomer molecular weight (M_{CL}=114.14). [d] From GPC. [e] Turnover number (TON) = number of moles of ε-CL consumed/ number of moles V. [f] Turnover frequency (TOF) = TON/time (h).

Table 8-2. ROP of δ-VL using **1** – **8** and **I - IV** in the absence of BnOH.

Run	Cat.	VL: V: BnOH	T/°C	t/h	Conv[a] (%)	$M_{n,GPC}\times10^{-3}$[b]	$M_w\times10^{-3}$[b]	$M_{n,Cal}\times10^{-3}$[c]	PDI[d]	TON[e]	TOF (h^{-1})[f]
1	**1**	1000:1:0	130	24	93.5	2.51	3.75	93.61	1.44	935	39
2	**1**	500:1:0	130	24	90.7	3.46	5.48	45.40	1.59	454	19
3	**1**	250:1:0	130	24	95.1	2.36	3.21	23.77	1.36	238	10
4	**1**	100:1:0	130	24	92.4	1.56	2.95	9.24	1.89	92	4
5	**1**	50:1:0	130	24	93.0	0.53	1.36	4.65	2.56	465	19
6	**2**	500:1:0	130	24	60.2	2.41	3.88	43.20	1.61	301	13
7	**3**	500:1:0	130	24	77.3	1.37	2.22	38.69	1.62	387	16

8	**4**	500:1:0	130	24	99.5	3.06	4.93	56.54	1.61	498	21
9	**5**	500:1:0	130	24	99.1	7.64	12.65	56.67	1.65	496	21
10	**6**	500:1:0	130	24	99.6	3.97	5.08	56.33	1.28	498	21
11	**7**	500:1:0	130	24	93.4	4.29	6.23	46.77	1.45	467	19
12	**8**	500:1:0	130	24	99.4	9.08	12.86	49.76	1.42	497	21
13	**8**	500:1:0	100	24	90.4	5.44	6.36	45.25	1.16	452	19
14	**8**	500:1:0	80	24	nothing	-	-	-	-	-	-
15	**I**	500:1:0	130	24	83.1	1.89	2.43	41.55	1.33	416	17
16	**II**	500:1:0	130	24	92.1	3.27	4.14	46.60	1.26	461	19
17	**III**	500:1:0	130	24	79.2	2.53	4.12	33.12	1.63	396	17
18	**IV**	500:1:0	130	24	86.2	3.55	5.67	41.23	1.60	431	18

[a] Determined by ^{1}H NMR spectroscopy. [b] $M_{n/w}$, GPC values corrected considering Mark–Houwink method from polystyrene standards in THF, $M_{n/w}$ measured = 0.57 × $M_{n/w}$ GPC ×10^3. [c] Calculated from ([monomer]$_0$/[cat]$_0$) × conv (%) × monomer molecular weight (M_{VL}=100.16). [d] From GPC. [e] Turnover number (TON) = number of moles of δ-VL consumed/ number of moles V. [f] Turnover frequency (TOF) = TON/time (h).

Table 8-3. ROP of co-polymer (ε-CL +δ-VL) using **1 – 8** and **I – IV** in the absence of BnOH**.**

Run	Cat	CL:VL:V	T/^{o}C	CL:VL[a]	Conv[b] (%)	$M_{n,GPC}$×10^{-3}[c]	M_w×10^{-3}[c]	PDI[d]
1	**1**[e]	250:250:1	130	46:54	64.3	8.53	11.38	1.33
3	**2**[e]	250:250:1	130	-	-	-	-	-
4	**3**[e]	250:250:1	130	35:65	37.5	3.45	5.67	1.64
5	**4**[e]	250:250:1	130	34:66	43.9	4.74	7.36	1.55
6	**5**[e]	250:250:1	130	40:60	55.1	6.88	9.71	1.41
7	**5**[f]	250:250:1	130	62:38	60.6	8.92	24.9	2.79
8	**5**[g]	250:250:1	130	58:42	30.5	3.65	5.46	1.49
9	**6**[e]	250:250:1	130	42:58	54.2	4.56	6.15	1.34
10	**6**[f]	250:250:1	130	66:34	52.3	6.84	8.79	1.28
11	**6**[g]	250:250:1	130	45:55	33.5	4.05	6.88	1.69
12	**7**[e]	250:250:1	130	40:60	55.9	4.36	6.75	1.54
13	**8**[e]	250:250:1	130	59:41	46.3	4.91	6.48	1.32
15	**I**[e]	250:250:1	130	41:59	60.1	6.67	10.45	1.58
16	**I**[e]	250:250:1	130	38:62	54.2	2.15	3.52	1.63
17	**II**[e]	250:250:1	130	36:64	58.3	3.93	5.65	1.43
18	**III**[e]	250:250:1	130	35:65	43.3	2.38	4.36	1.84
19	**IV**[e]	250:250:1	130	36:64	36.2	3.63	5.75	1.58

[a] Ratio of ε-CL to δ-VL observed in the co-polymer by ^{1}H NMR spectroscopy. [b] Determined by ^{1}H NMR spectroscopy. [c] $M_{n/w}$, GPC values corrected considering Mark–Houwink

method from polystyrene standards in THF, $M_{n/w}$ measured = [0.56 × $M_{n/w}$ GPC × (1-%CL) + 0.57 × $M_{n/w}$ GPC ×(1-%VL)] × 10^3. [d] From GPC. [e] ε-Caprolactone was firstly added for 24 h, then δ-valerolactone was added and heating for 24 h. [f] δ-valerolactone was firstly added for 24 h, then ε-caprolactone was added and heating for 24 h. [g] ε-caprolactone and δ-valerolactone were added in the same time and heating for 24 h.

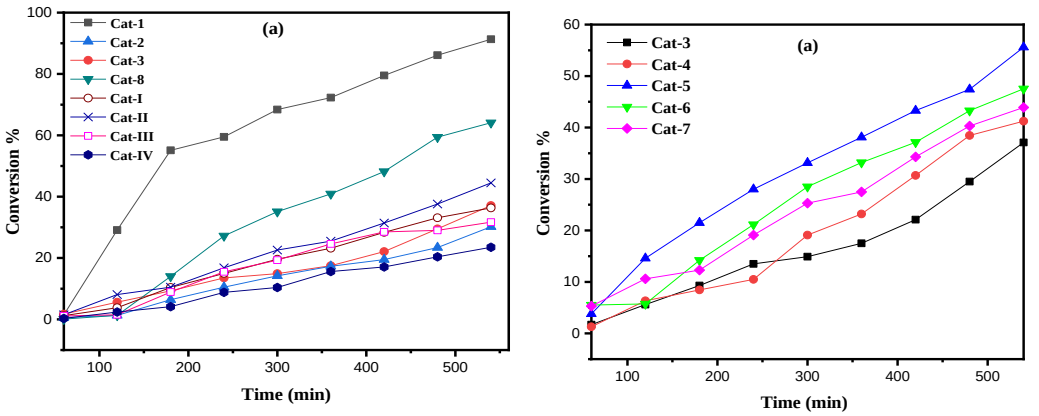

Figure 8-1. (a) Relationship between conversion and time for the polymerization of ε-CL by using complex **1-3**, **8**, and **I – IV;** (b) Relationship between conversion and time for the polymerization of ε-CL by using complexes **3-7**; Conditions: T=130 °C, $n_{Monomer}$: n_V: BnOH=500: 1: 1.

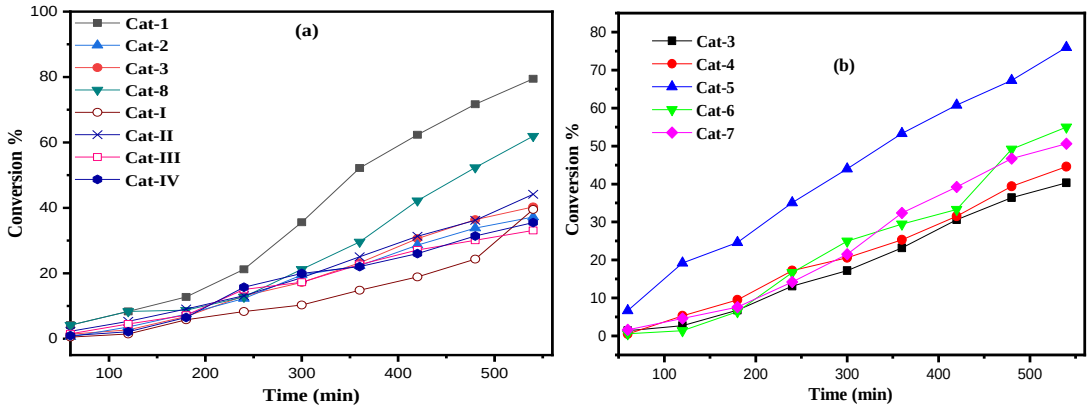

Figure 8-2. (a) Relationship between conversion and time for the polymerization of δ-VL by using complexes **1-3**, **8**, and **I** – **IV**; (b) Relationship between conversion and time for the polymerization of δ-VL by using complexes **3-7**; Condition: T=130 °C, $n_{Monomer}$: n_V: BnOH=500: 1: 0.

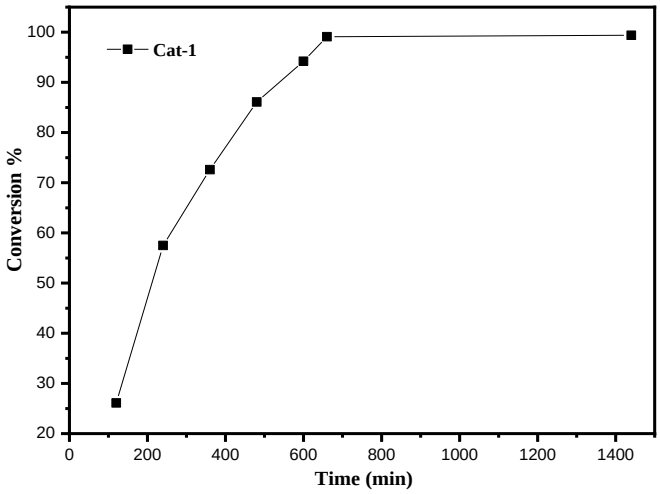

Figure 8-3. (a) Relationship between conversion and time for the saturation kinetics polymerization of CL by using complex **1**/BnOH; Condition: T=130 ^{o}C, $n_{Monomer}$: n_{V}: BnOH=500: 1: 1.

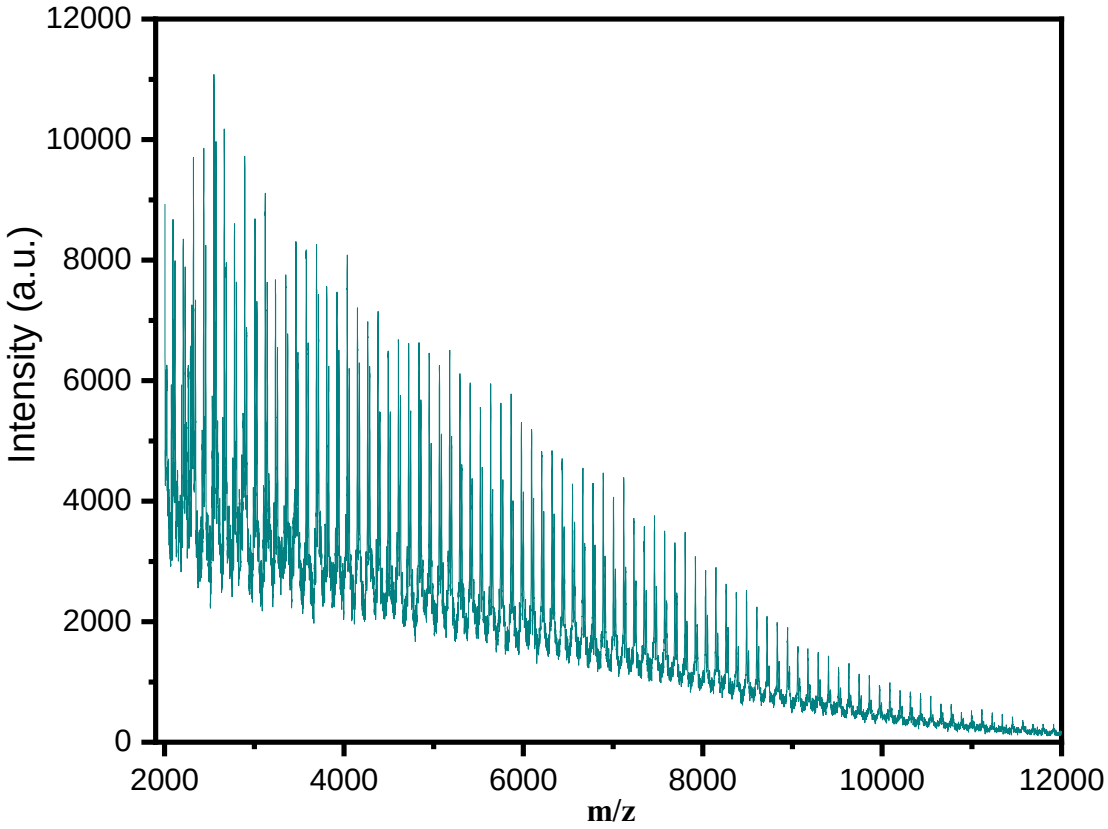

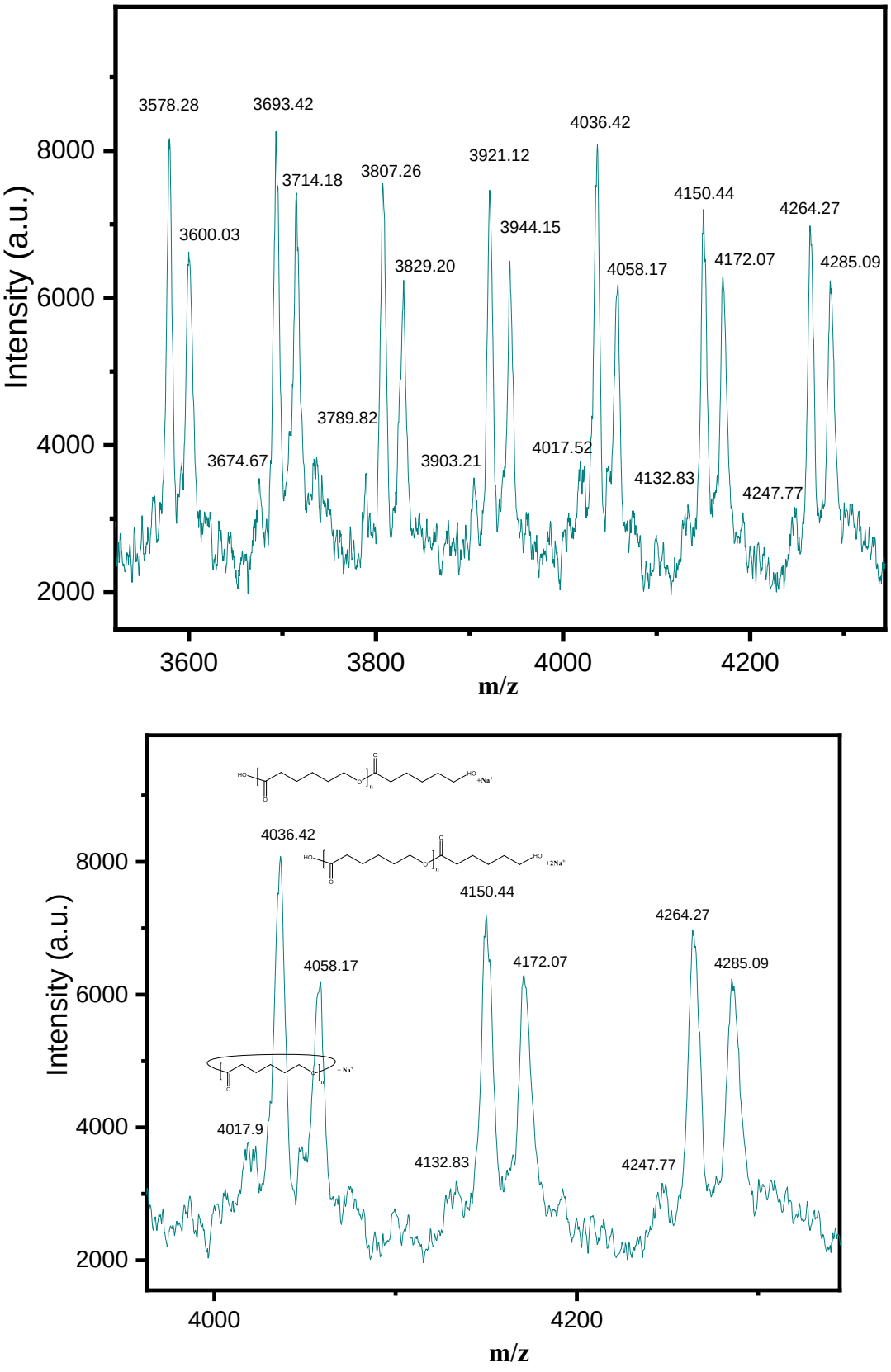

Figure 8-4. Mass spectrum of PCL by using **6** in the absence of BnOH (run 10, Table 8-1).

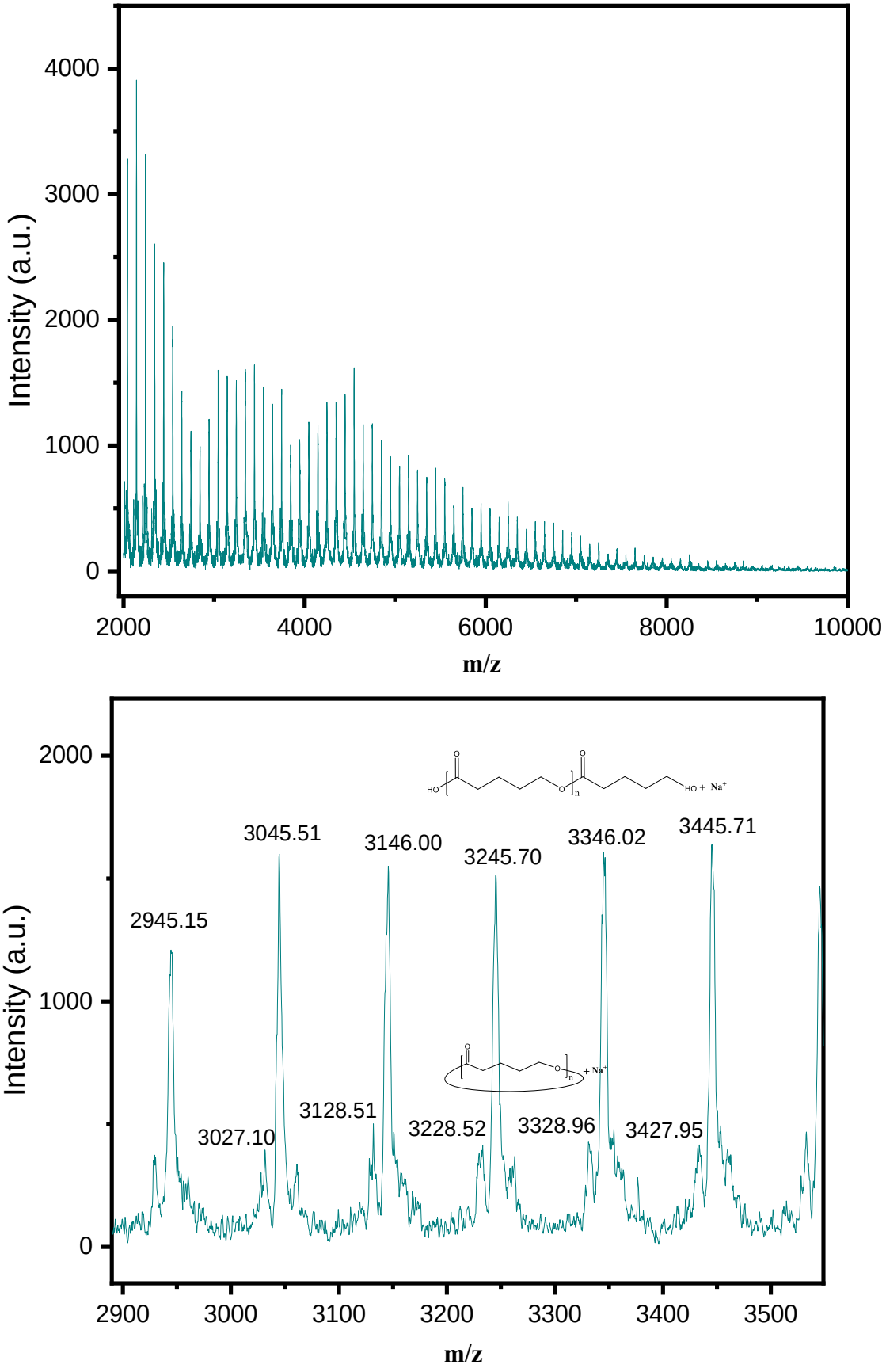

Figure 8-5. Mass spectrum of PVL by using **7** in the absence of BnOH (run 11, Table 8-2).

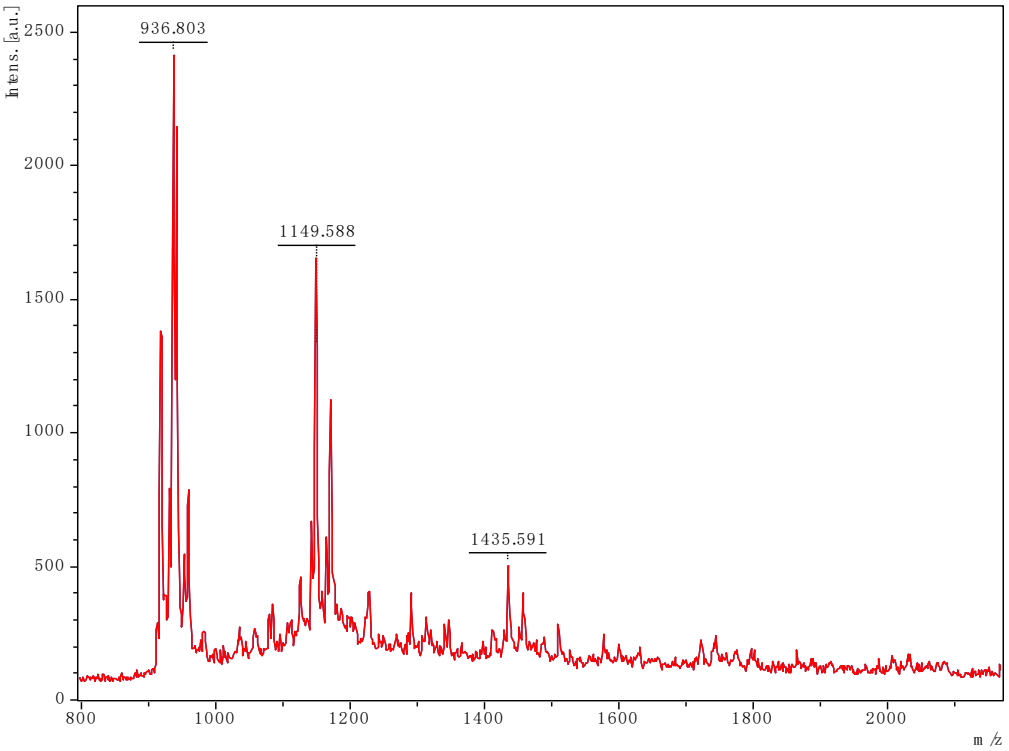

Figure 8-6. Mass spectrum of co-polymer (ε-CL +δ-VL) by using **I** in the absence of BnOH (run 15, Table 8-3).

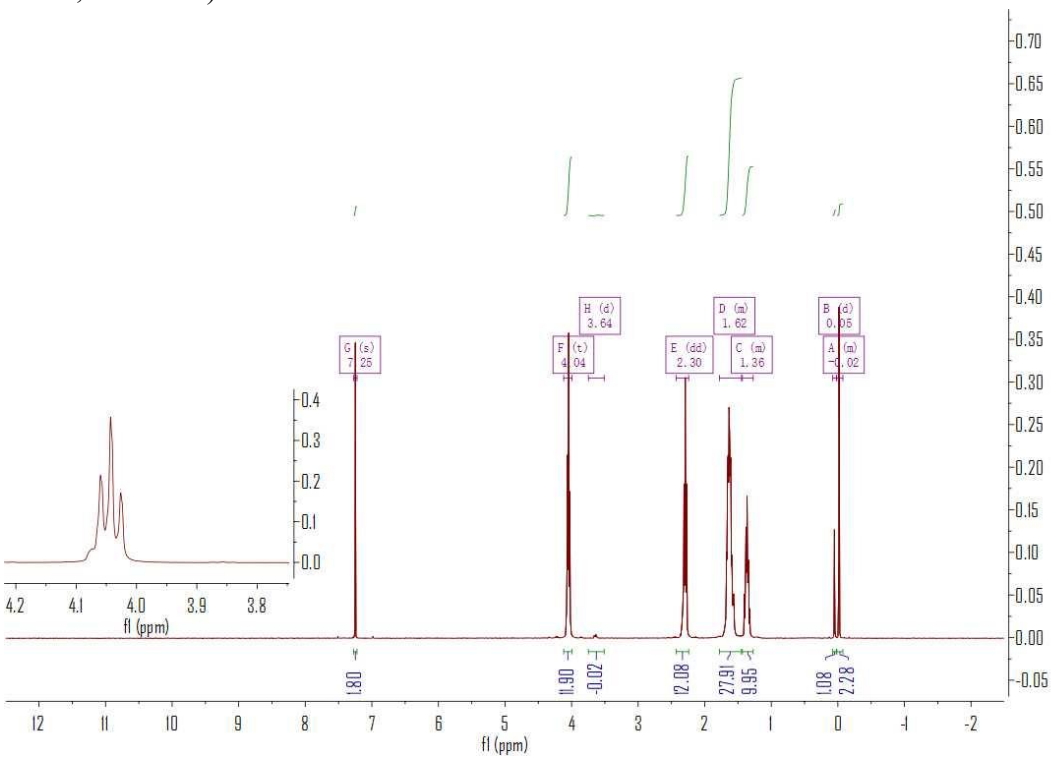

Figure 8-7. ^{1}H NMR spectrum ($CDCl_3$, 400 MHz, 298 K) of the PCL synthesized with **6** in the absence of BnOH (run 10, Table 8-1).

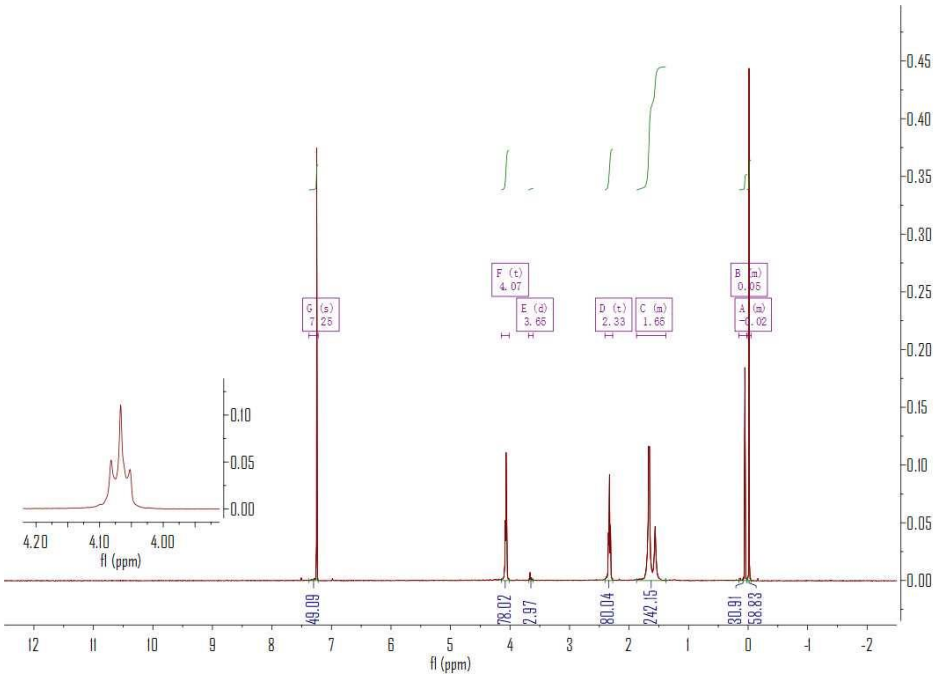

Figure 8-8. ^{1}H NMR spectrum ($CDCl_3$, 400 MHz, 298 K) of the PVL synthesized with **8** in the absence of BnOH (run 12, Table 8-2).

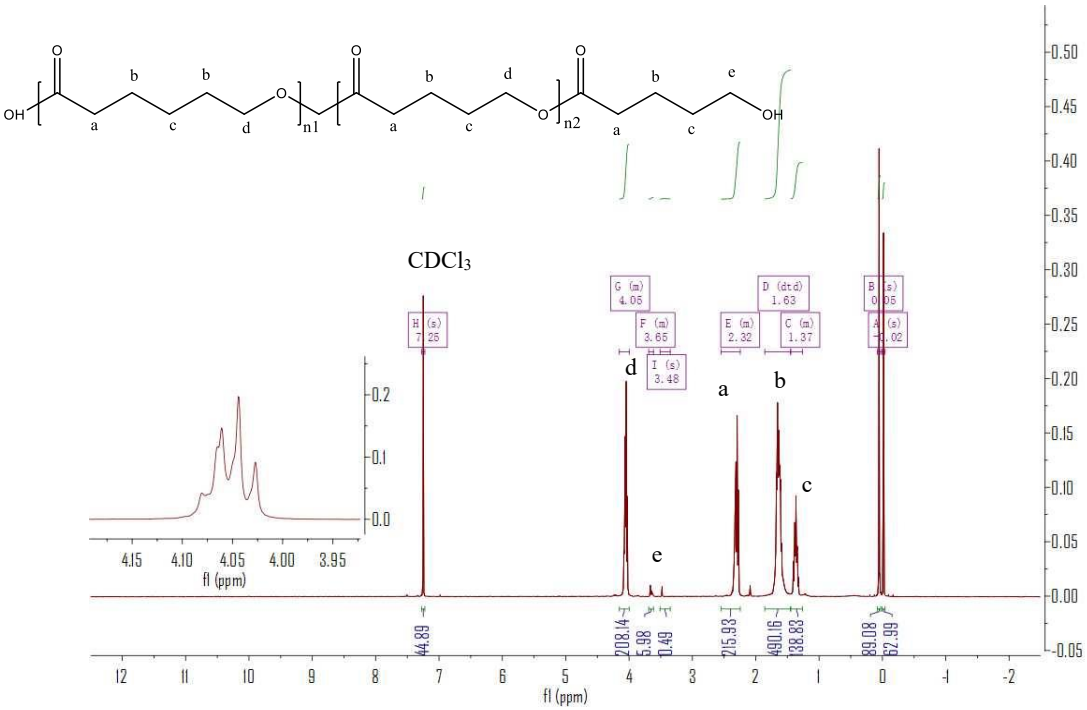

Figure 8-9. ^{1}H NMR spectrum ($CDCl_3$, 400 MHz, 298 K) of the CL-VL copolymer (1:1 ratio CL/VL) synthesized with **I** in the absence of BnOH (run 15, Table 8-3).

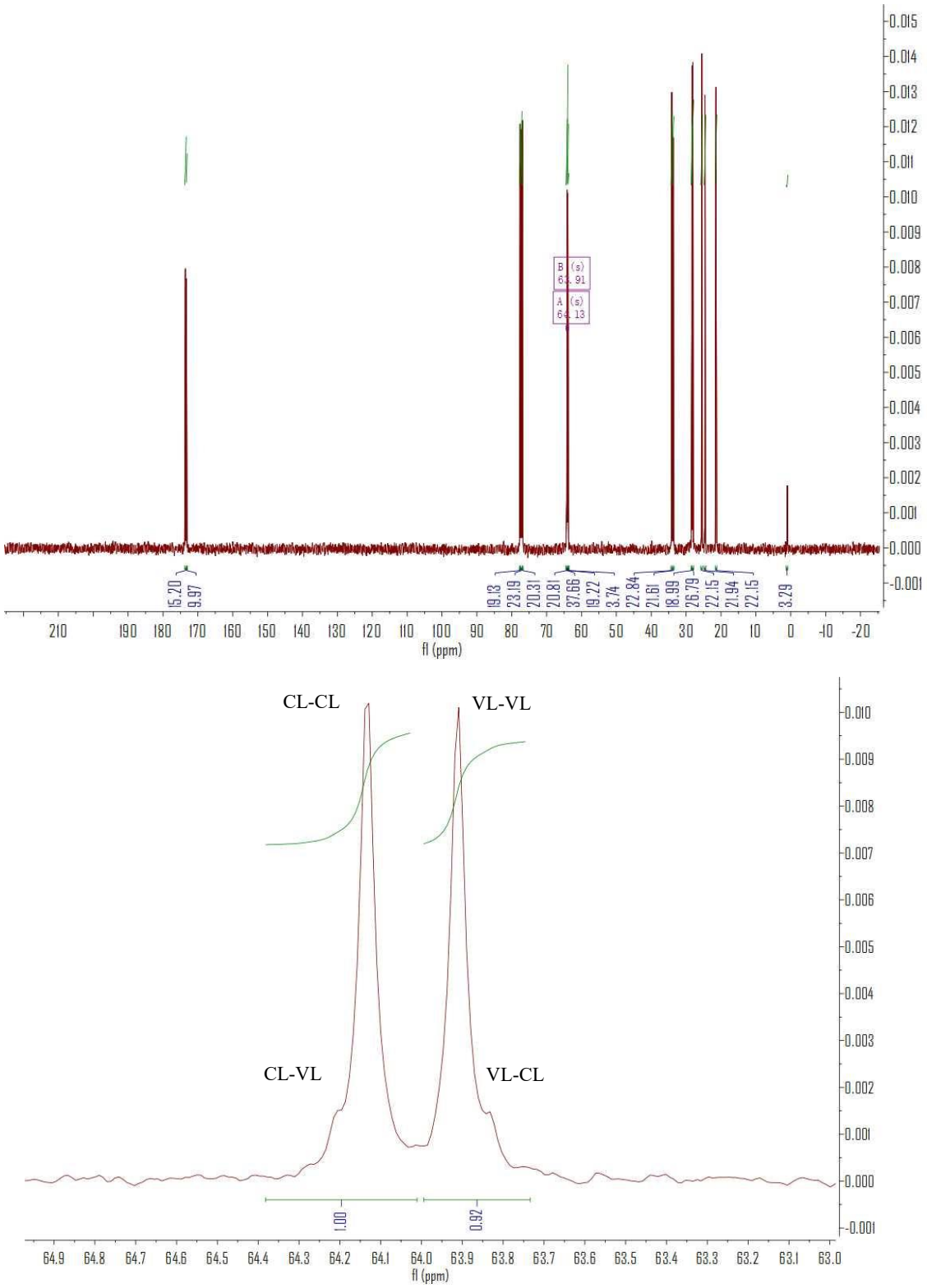

Figure 8-10. ^{13}C NMR spectrum ($CDCl_3$, 400 MHz, 298 K) of the CL-VL copolymer (run 1, Table 2-4).

Equation 8-1. Determination of number-average sequence length for CL[1]

$$L_{CL}=[(I_{CL-CL})/(I_{VL-CL})]+1$$

Where I_{CL-CL} and I_{VL-CL} is the area of the peak belonging to the CL-CL and VL-CL dyad, respectively.

Equation 8-2. Determination of number-average sequence length for VL. [1]

$$L_{VL}=[(I_{VL-VL})/(I_{CL-VL})]+1$$

Where I_{VL-VL} and I_{CL-VL} is the area of the peak belonging to the VL-VL and CL-VL dyad, respectively.

Equation 8-3. Determination of the Randomness Character (R). [1]

$$R=1/(L_{CL}) + 1/(L_{VL})$$

Completely block Copolymers: R = 0

Copolymers with a “blocking” tendency: R < 1

Completely random copolymers: R = 1

Copolymers with an alternating tendency: R >1

Completely alternating copolymers: R = 2

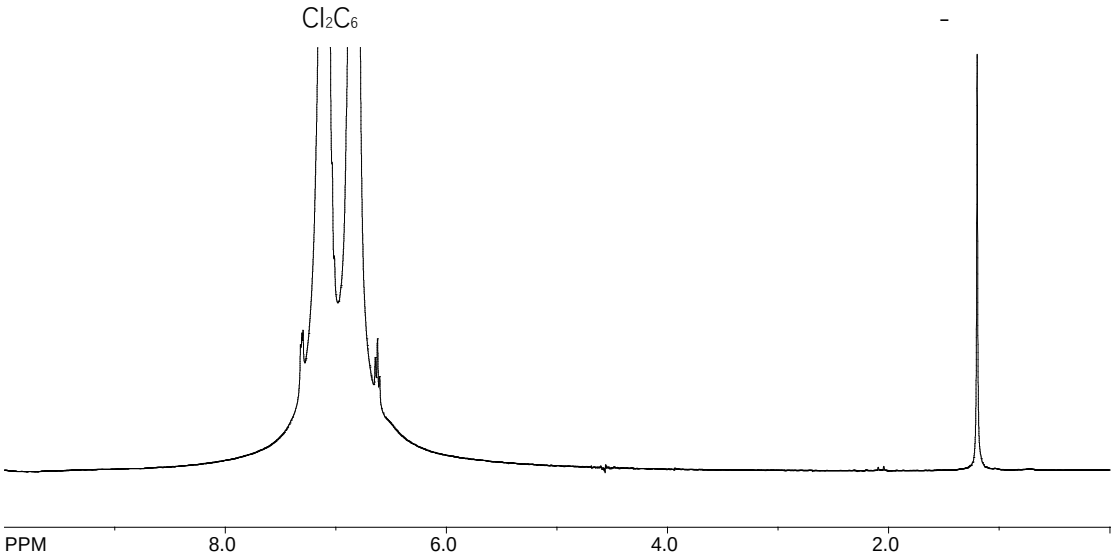

Figure 8-11. ^{1}H NMR spectrum ($Cl_2C_6H_4$, 100 °C) of polyethylene (run 6, Table 2-5).

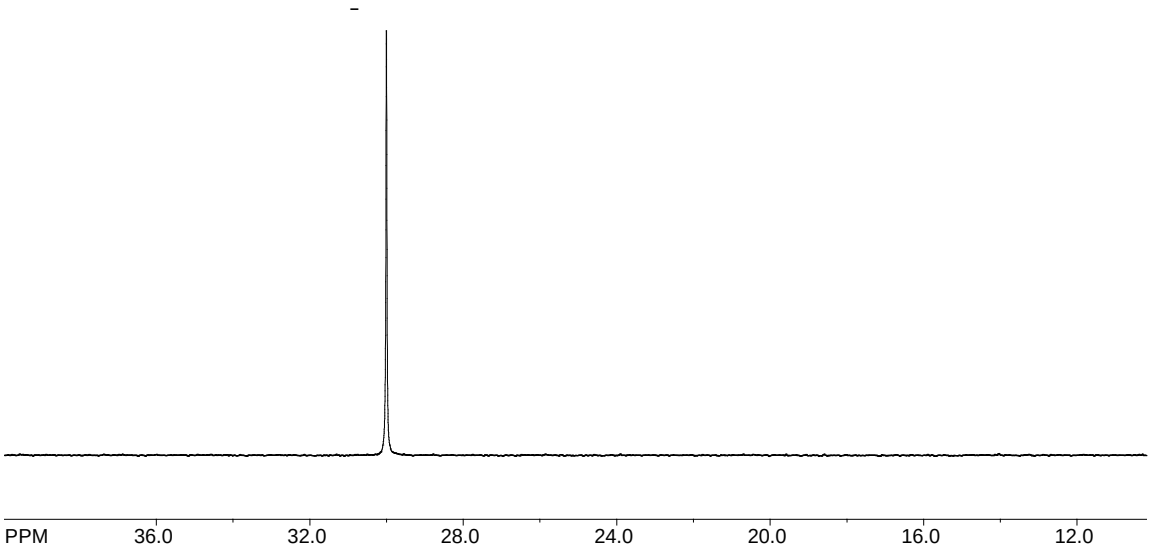

Figure 8-12. ^{13}C NMR spectrum ($Cl_2C_6H_4$, 100 °C) of polyethylene (run 6, Table 2-5).

Table 8-4. Crystal structure data for **1**·5MeCN, **2**·6MeCN, **3**·7MeCN·0.5CH_2Cl_2, **4**·4MeCN, **5**, **6**, **7**, **8**·4MeCN.[a,b]

Compound	**1**·5MeCN	**2**·6MeCN	**3**·7MeCN·0.5CH_2Cl_2	**4**·4MeCN
Formula	$C_{86}H_{109}N_9Na_2O_{11}V_2$	$C_{86}H_{114}N_6O_{16}V_4$	$C_{355}H_{421}Cl_2N_{21}O_{32}V_8$	$C_{90}H_{108}N_6O_{10}V_2$
Formula weight	1592.68	1691.59	5972.52	1535.77
Crystal system	Triclinic	Triclinic	Triclinic	Triclinic
Space group	$P\bar{1}$	$P\bar{1}$	$P\bar{1}$	$P\bar{1}$
Unit cell dimensions				
a (Å)	13.4214(3)	12.4983(4)	19.7899(3)	14.03540(10)
b (Å)	14.2596(5)	13.6976(2)	20.6775(3)	17.33960(10)
c (Å)	25.2549(7)	14.1554(3)	22.7696(5)	20.19060(10)
α (°)	85.709(3)	68.166(2)	69.271(2)	71.1680(10)
β (°)	78.946(2)	79.128(2)	76.567(2)	84.4590(10)
γ (°)	69.251(3)	75.546(2)	78.6270(10)	66.4560(10)
V (Å^3)	4435.9(2)	2165.92(10)	8407.9(3)	4260.59(6)
Z	2	1	1	1
Temperature (K)	100(2)	100(2)	100(2)	100(2)
Wavelength (Å)	0.71073	1.54178	0.71073	1.54178
Calculated density (g.cm^{-3})	1.192	1.297	1.180	1.181
Absorption coefficient (mm^{-1})	0.281	4.049	0.294	2.303
Transmission factors	0.674 and 1.000	0.711 and 1.000	0.744 and 1.000	0.285 and 1.000

(min./max.)				
Crystal size (mm^3)	0.14 × 0.07 × 0.01	0.16 × 0.07 ×0.035	0.06 × 0.06 × 0.02	0.18 × 0.08 × 0.035
θ(max) (°)	27.5	68.2	27.5	68.4
Reflections measured	80640	95054	110251	28571
Unique reflections	19896	7886	38753	28571
R_{int}	0.074	0.0519	0.062	0.057
Reflections with $F^2 > 2\sigma(F^2)$	13923	7406	24217	26256
Number of parameters	975	518	1863	970
R_1 [$F^2 > 2\sigma(F^2)$]	0.098	0.040	0.088	0.049
wR_2 (all data)	0.233	0.131	0.256	0.150
GOOF, S	1.127	1.11	1.03	1.04
Largest difference peak and hole (e $Å^{-3}$)	1.37 and –0.69	1.009 and -0.489	2.04 and –0.87	0.61 and -0.43
τ [c]	0.11	0.18	0.12	0.22

Compound	**5**	**6**	**8**·4MeCN[b]·
Formula	$C_{82}H_{90}F_6N_2O_8V_2$	$C_{80}H_{90}Cl_2N_2O_8V_2$	$C_{96}H_{108}N_8O_8V_2$
Formula weight	1447.43	1380.31	1711.96
Crystal system	Monoclinic	Monoclinic	Triclinic
Space group	$P2_1/c$	$P2_1/n$	$P\bar{1}$
Unit cell dimensions			
a (Å)	20.0005(13)	19.7039(9)	12.0966(2)
b (Å)	19.9315(8)	20.0862(7)	12.3373(2)
c (Å)	22.023(2)	20.6921(10)	17.8971(3)
α (º)	90	90	90.8728(8)
β (º)	116.080(10)	113.114(5)	107.9966(7)
γ (º)	90	90	99.2458(8)
V ($Å^3$)	7885.5(11)	7532.0(6)	2501.28(7)
Z	4	4	1
Temperature (K)	100(2)	100(2)	150(2)
Wavelength (Å)	0.71075	1.54184	0.71073
Calculated density ($g.cm^{-3}$)	1.219	1.217	1.137
Absorption coefficient (mm^{-1})	0.305	3.160	0.243

Transmission factors (min./max.)	0.555 and 1.000	0.738 and 1.000	0.974 and 0.990
Crystal size (mm^3)	0.12×0.02×0.01	0.150×0.030×0.005	0.11×0.06×0.04
θ(max) (°)	25.0	66.13	28.3
Reflections measured	86670	68213	29287
Unique reflections	13936	13175	12217
R_{int}	0.1918	0.1107	0.036
Reflections with $F^2 > 2\sigma(F^2)$	6929	5544	8563
Number of parameters	886	791	591
R_1 [$F^2 > 2\sigma(F^2)$]	0.096	0.085	0.059
wR_2 (all data)	0.192	0.247	0.185
GOOF, S	1.02	1.02	1.03
Largest difference peak and hole (e $Å^{-3}$)	1.14 and -0.71	0.420 and -0.378	0.87 and –0.28
τ [c]	0.43	0.38	0.28

[a] [2]

[b] For **8**: Data collected on a Bruker APEX 2 CCD diffractometer at Daresbury SRS station 9.8 (λ = 0.6710 Å).

[c] $\tau = (\beta - \alpha)/60$ [3]

2. Appendix for Chapter 3

Table 8-5. Crystallographic data for **9**·3CH_2Cl_2, **9′**·6CH_2Cl_2 and **10**·6.5MeCN.

Compound	**9**·3CH_2Cl_2	**9′**·6CH_2Cl_2	**10**·6.5MeCN
Formula	$C_{97}H_{136}Cl_6N_2O_{12}S_8V_2$	$C_{86}H_{106}Cl_{12}O_{13.09}S_8V_2$	$C_{92}H_{110}Cl_4N_2O_{10}Ti_4$·6.5($C_2H_3N$)
Formula weight	2093.13	2132.90	2004.06
Crystal system	Monoclinic	Triclinic	Monoclinic
Space group	$P2_1/n$	$P\ \bar{1}$	$P2_1/c$
a (Å)	15.5952(15)	11.8180(11)	29.8061(7)
b (Å)	14.9297(14)	12.0316(12)	18.5546(6)
c (Å)	24.581(2)	20.587(2)	40.3480(13)

α (º)	90	96.263(2)	90
β (º)	98.458(7)	103.581(2)	106.680(3)
γ (º)	90	93.263(2)	90
V (Å^3)	5661.0(9)	2818.3(5)	21374.1(11)
Z	2	1	8
Temperature (K)	150(2)	150(2)	100(2)
Wavelength (Å)	0.7749	0.71073	1.54178
Calculated density (g·cm^{-3})	1.228	1.257	1.246
Absorption coefficient (mm^{-1})	0.64	0.65	3.84
Transmission factors (min./max.)	0.937, 0.975	0.717, 0.860	0.553, 1.000
Crystal size (mm^3)	0.13 × 0.08 × 0.05	0.55 × 0.33 × 0.24	0.26 × 0.07 × 0.02
θ(max) (°)	27.5	28.3	68.3
Reflections measured	41136	53410	155537
Unique reflections	10028	13900	38456
R_{int}	0.119	0.042	0.204
Reflections with $F^2 > 2\sigma(F^2)$	5135	9834	22830
Number of parameters	662	632	2537
R_1 [$F^2 > 2\sigma(F^2)$]	0.082	0.070	0.142
wR_2 (all data)	0.281	0.222	0.426
GOOF, S	1.01	1.03	1.05
Largest difference peak and hole (e Å^{-3})	0.83 and –0.96	1.07 and –0.80	1.52 and –1.15

3. Appendix for Chapter 4

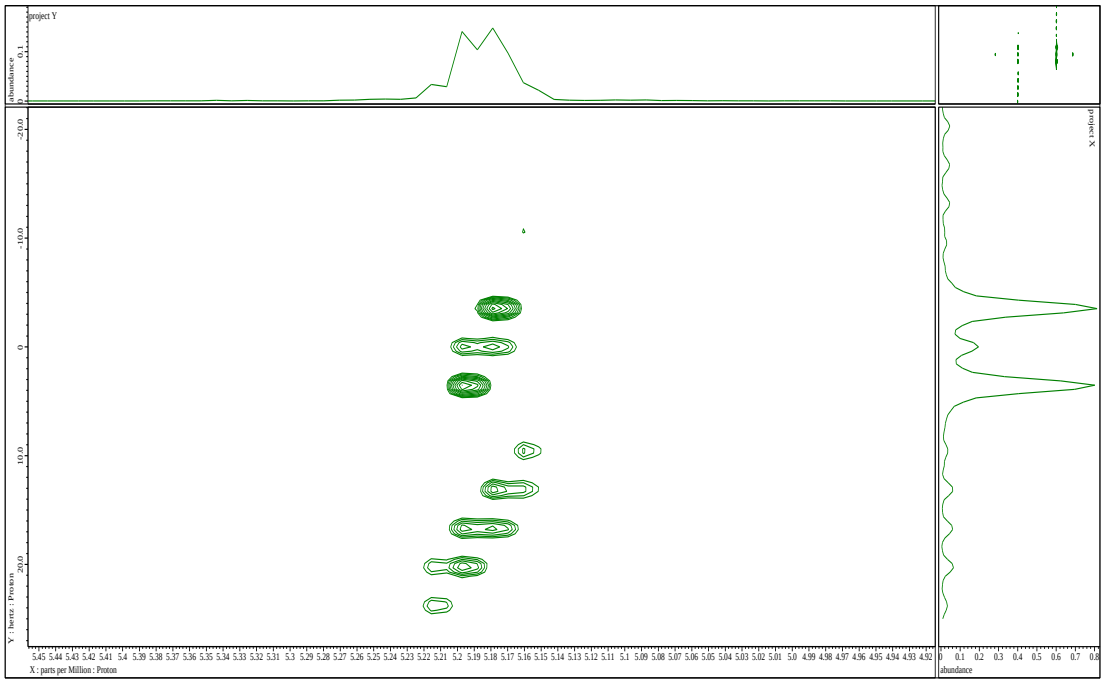

Figure 8-13. 2D *J*-resolved ^{1}H NMR spectrum ($CDCl_3$, 400 MHz, 298 K) of the PLA synthesized with **11**/BnOH (run 1, Table 4-3).

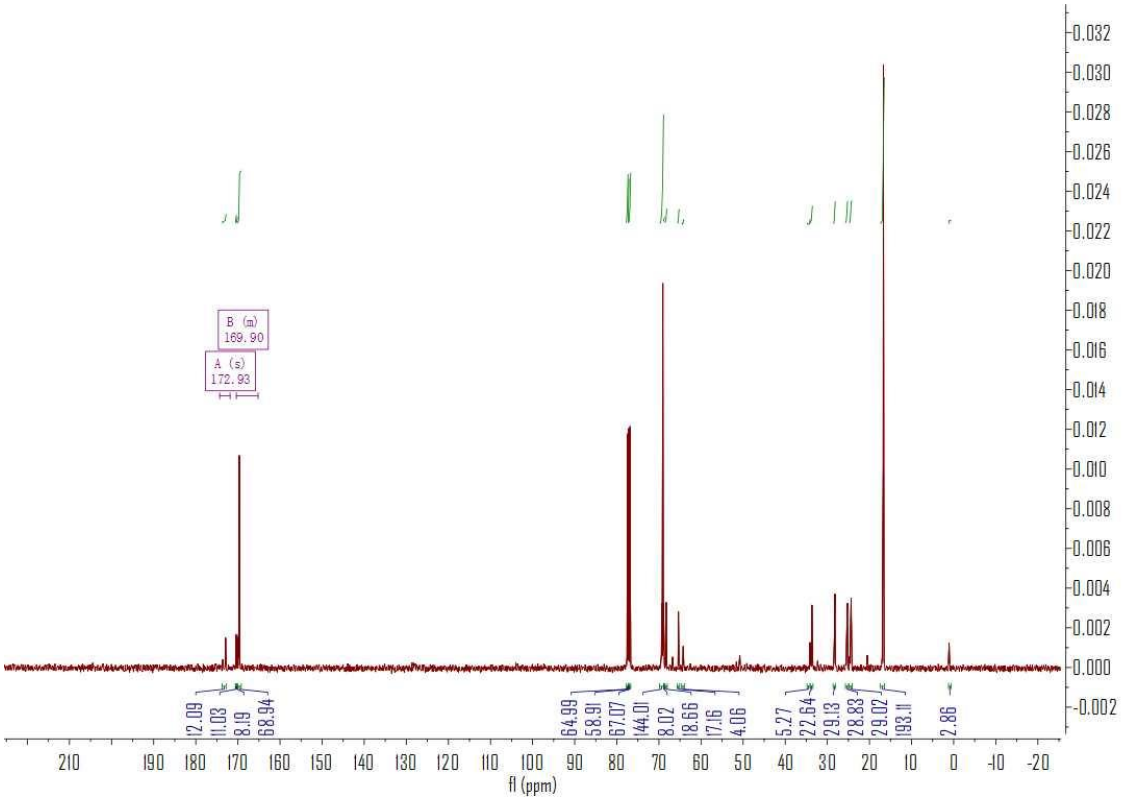

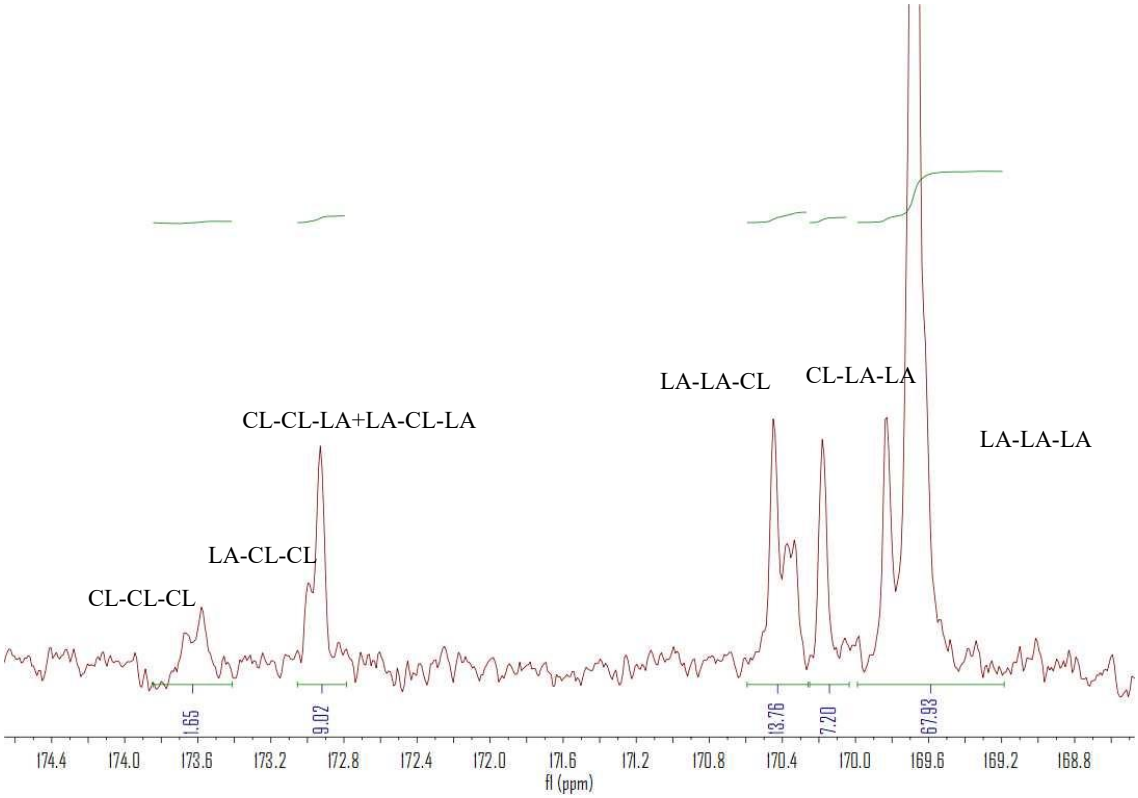

Figure 8-14. Carbonyl range of ^{13}C NMR spectrum ($CDCl_3$, 25 ºC) of PLA-PCL co-polymer. Triads have been assigned according to the literature.[4]

Equation 8-4. Determination of number-average sequence length for CL[4]

$$L_{CL}=[(I_{CL\text{-}CL\text{-}CL}+I_{LA\text{-}CL\text{-}CL})/(I_{CL\text{-}CL\text{-}LA}+I_{LA\text{-}CL\text{-}LA})]+1$$

Equation 8-5. Determination of number-average sequence length for LA. [4]

$$L_{LA}=\{[(I_{LA\text{-}LA\text{-}LA}+(I_{LA\text{-}LA\text{-}CL}+I_{CL\text{-}LA\text{-}LA})/2]/[I_{CL\text{-}LA\text{-}CL}+(I_{LA\text{-}LA\text{-}CL}+I_{CL\text{-}LA\text{-}LA})/2]+1\}/2$$

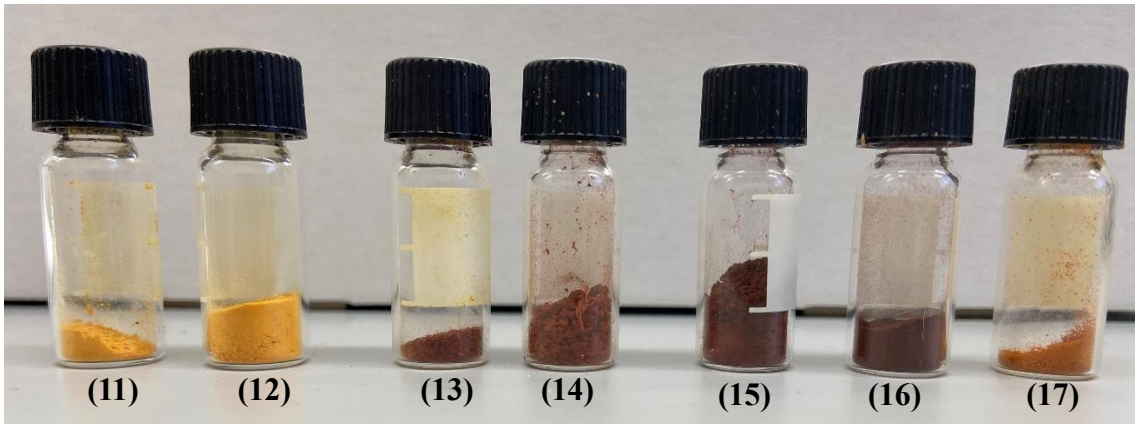

Figure 8-15. Picture of complexes **11-17**.

Table 8-6. Crystal structure data for **11**·3.5MeCN, **12**·MeCN, **13**·2.5MeCN, **14**·5MeCN, **15**·4.5MeCN, **16**·7MeCN, **17**·2MeCN.

Compound	**11**·3.5MeCN	**12**·MeCN	**13**·2.5MeCN	**14**·5MeCN
Formula	$C_{83}H_{109.5}N_{4.5}O_{10}Ti_2$	$C_{137}H_{167}NO_{18}Ti_4$	$C_{57}H_{63.5}F_{14}N_{4.5}O_6Ti_4$	$C_{62}H_{75}Cl_4N_7O_9Ti_2$
Formula weight	1426.04	2307.30	1365.14	1299.86
Crystal system	Monoclinic	Monoclinic	Monoclinic	Triclinic
Space group	P 2_1/c	C 2/c	P 2_1/c	$P\bar{1}$
Unit cell dimensions				
a (Å)	12.0347(2)	28.1243(7)	16.1213(2)	12.6749(8)
b (Å)	28.3198(4)	17.7721(4)	22.8130(2)	14.5410(8)
c (Å)	24.5367(3)	31.2326(9)	17.0185(2)	18.7696(10)
α (°)	90	90	90	111.979
β (°)	103.2370(10)	113.009(3)	102.381(10)	95.829
γ (°)	90	90	90	96.158
V (Å^3)	8140.4(2)	14369.0(7)	6113.42(12)	3151.55(3)
Z	4	4	4	2
Temperature (K)	100(2)	100(2)	100(2)	100(2)
Wavelength (Å)	1.54184	1.54178	1.54178	1.54178
Calculated density	1.147	1.061	1.416	1.240
Absorption coefficient	2.112	2.275	5.091	4.142
Transmission factors	0.69725 and 1.0000	0.52429 and 1.000	0.6143 and 1.0000	0.679 and 1.0000
Crystal size (mm^3)	0.200 × 0.120 × 0.040	0.160 × 0.030 × 0.010	0.150 × 0.080 × 0.050	0.090×0.060×0.020
θ(max) (°)	66.6	66.5	70.4	68.2
Reflections measured	75678	46013	55482	134309
Unique reflections	14383	12487	11396	11490
R_{int}	0.0521	0.0985	0.0415	0.0270
Reflections with $F^2 >$	12259	7981	9829	11030
Number of parameters	870	697	741	701

R_1 [$F^2 > 2\sigma(F^2)$]	0.117	0.085	0.063	0.031
wR_2 (all data)	0.368	0.234	0.178	0.091
GOOF, S	1.675	1.024	1.016	1.050
Largest difference	1.961 and -0.795	0.768 and -0.381	1.500 and -0.511	0.831 and -0.376

Compound	**15**·4.5MeCN	**16**·7MeCN	**17**·2MeCN
Formula	$C_{61}H_{73.5}Br_4N_{6.5}O_9Ti_2$	$C_{78}H_{93}Br_{12}N_{15}O_6Ti_4$	$C_{40}H_{46}F_{10}N_4O_4SiTi_2$
Formula weight	1457.15	2487.02	960.70
Crystal system	Triclinic	Triclinic	Triclinic
Space group	$P\bar{1}$	$P\bar{1}$	$P\bar{1}$
Unit cell dimensions			
a (Å)	12.8059(9)	17.7979(2)	8.8857(4)
b (Å)	14.7294(9)	18.1314(1)	13.0733(5)
c (Å)	18.6847(13)	18.4582(2)	18.4231(11)
α (°)	111.546(5)	71.110(1)	84.872(4)
β (°)	94.299(6)	74.116(1)	82.208(4)
γ (°)	96.876(5)	66.857(1)	73.277(4)
V (Å^3)	3227.4(4)	5108.21(10)	2027.83(18)
Z	2	1	2
Temperature (K)	150(2)	100(2)	100(2)
Wavelength (Å)	0.71073	1.54178	0.71075
Calculated density	1.394	1.549	1.573
Absorption coefficient	2.775	8.449	0.517
Transmission factors	0.825 and 0.625	1.0000 and 0.66859	1.0000 and 0.20966
Crystal size (mm^3)	0.360 x 0.260 x 0.200	0.120 x 0.080 x 0.050	0.100 × 0.060 × 0.020
θ(max) (°)	26.373	68.236	27.529
Reflections measured	25790	237393	14106
Unique reflections	13079	18616	14106
R_{int}	0.0792	0.0693	0.1992
Reflections with $F^2 > 2\sigma(F^2)$	8355	18616	10493
Number of parameters	699	986	547
R_1 [$F^2 > 2\sigma(F^2)$]	0.0458	0.0662	0.105
wR_2 (all data)	0.1066	0.1895	0.2964
GOOF, S	0.859	1.021	1.026
Largest difference	0.894 and -0.841	1.542 and -1.156	2.991 and -0.829

4. Appendix for Chapter 5

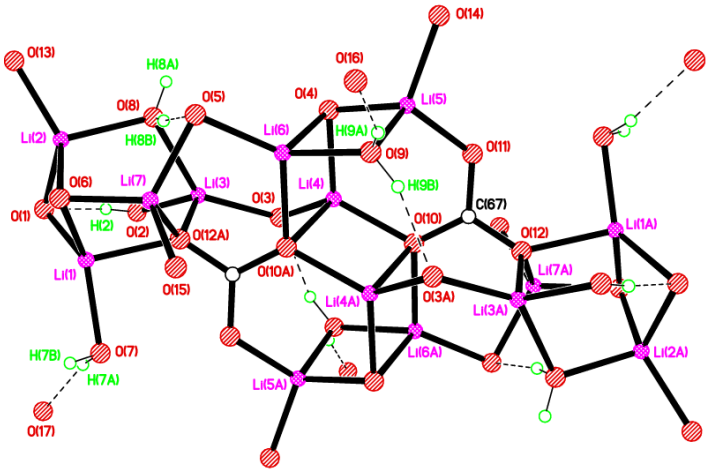

Figure 8-16. Core of the structure for $[Li_{14}(L^6H)_2(CO_3)(THF)_6(OH_2)_6]\cdot 14THF$ (**18**·14THF). Solvent molecules and hydrogen atoms omitted for clarity.

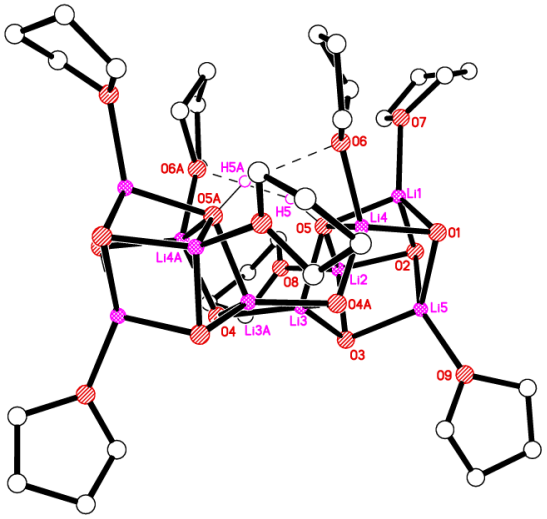

Figure 8-17. Alternative view of the core of the structure for $[Li_{10}(L^8)(OH)_2(THF)_8]\cdot 7THF$ (**19**·7THF). Unbound solvent molecules and hydrogen atoms omitted for clarity.

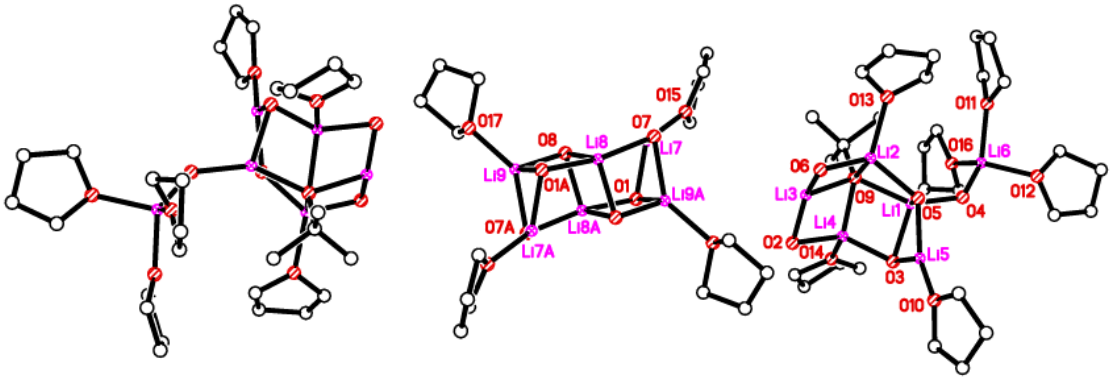

Figure 8-18. Alternative views of the core of the structure for $[Li_{18}(deBuL^8)_2(OtBu)_2(THF)_{14}]\cdot 4THF$ (**20**·4THF). Unbound solvent molecules and hydrogen atoms omitted for clarity.

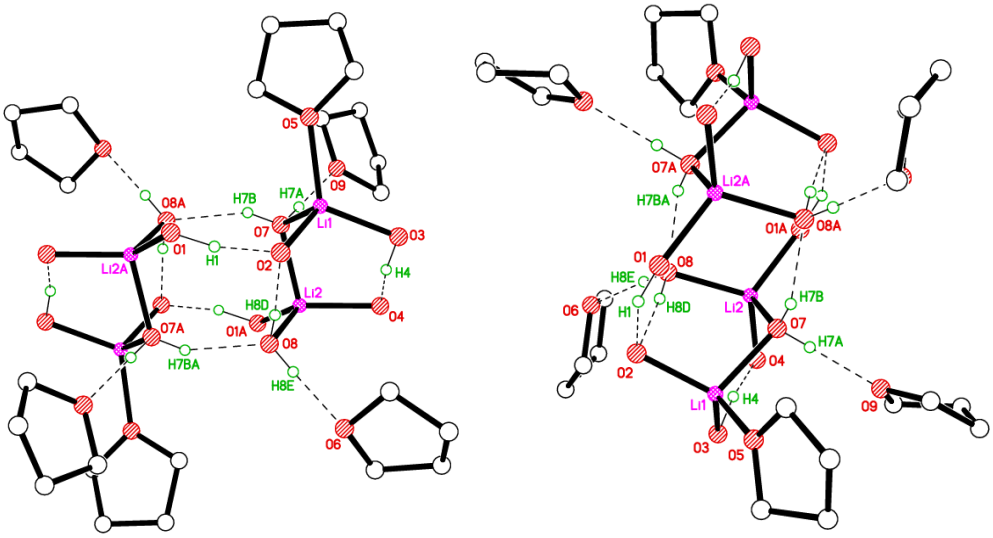

Figure 8-19. Two views of the core of the structure for $[Li_4(L^8H_4)(OH_2)_4(THF)_6]\cdot 5.5THF$ (**21**·5.5THF). Unbound solvent molecules and hydrogen atoms omitted for clarity.

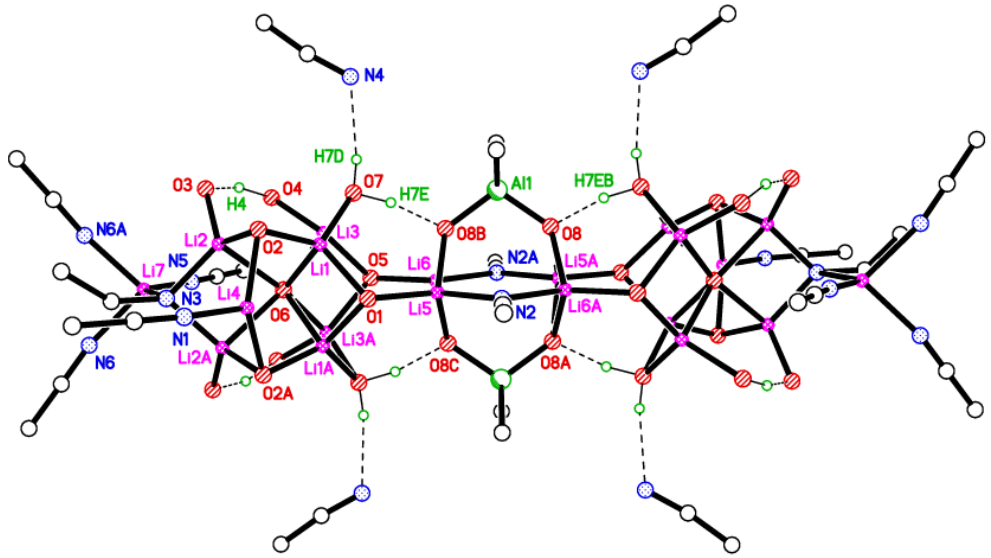

Figure 8-20. Core of the structure for $[(AlMe_2)_2Li_{20}(L^8H_2)_2(OH_2)_4(O^{2-})_4(OH)_2(NCMe)_{12}]\cdot 10MeCN$ (**22**·10MeCN). Unbound solvent molecules and hydrogen atoms omitted for clarity.

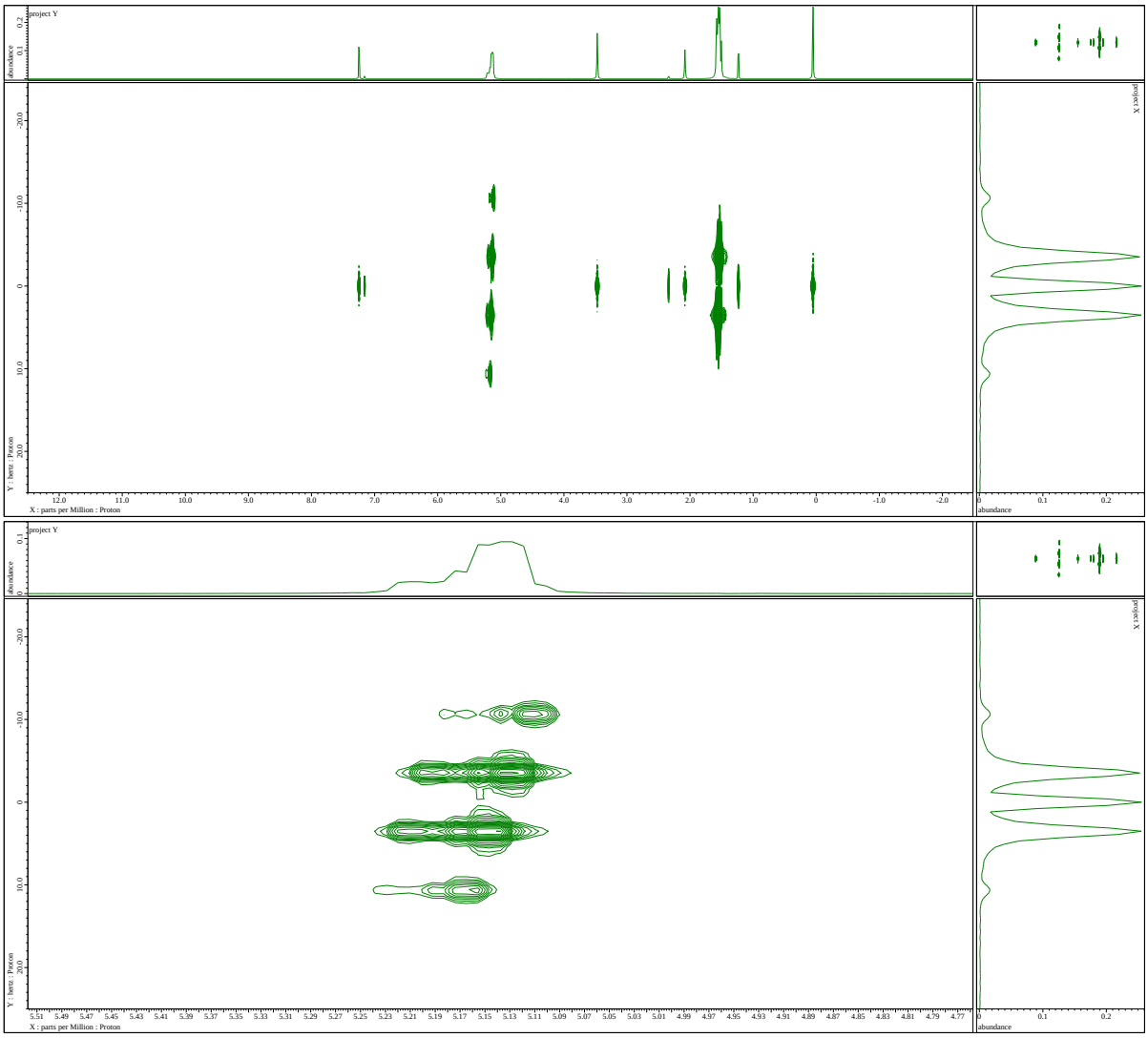

Figure 8-21. 2D *J*-resolved ^{1}H NMR spectrum ($CDCl_3$, 400 MHz, 298 K) of the PLA synthesized with with **20**/BnOH (run 3, Table 5-3).

Table 8-7. Crystal structure data for **18**·14THF, **19**·7THF, **20**·4THF, **21**·5.5THF, **22**·10MeCN.

Compound	**18**·14THF	**19**·7THF	**20**·4THF
Formula	$C_{214}H_{330}Li_{14}O_{44}$	$C_{148}H_{226}Li_{10}O_{25}$	$C_{200}H_{258}Li_{18}O_{38}$
Formula weight	3703.92	2474.67	3394.97
Crystal system	Triclinic	Monoclinic	Monoclinic
Space group	$P\bar{1}$	$I2/a$	$P2_1/n$
a (Å)	18.665(7)	21.884(5)	12.952(10)
b (Å)	18.967(7)	21.213(6)	33.08(2)
c (Å)	19.197(8)	33.174(9)	24.85(2)

α (º)	113.707(6)	90	90
β (º)	116.378(5)	105.105(19)	91.224(9)
γ (º)	90.897(6)	90	90
V (Å^3)	5416(4)	14868(7)	10645(14)
Z	1	4	2
Temperature (K)	150(2)	150(2)	100(2)
Wavelength (Å)	0.71073	0.71073	0.71073
Calculated density (g.cm^{-3})	1.136	1.106	1.059
Absorption coefficient (mm^{-1})	0.08	0.07	0.07
Transmission factors (min./max.)	0.926, 0.985	0.970, 0.972	0.990, 0.995
Crystal size (mm^3)	1.03 × 0.39 × 0.20	0.43 × 0.41 × 0.39	0.15 × 0.12 × 0.07
θ(max) (°)	22.5	27.5	22.5
Reflections measured	44841	101470	62490
Unique reflections	14152	16408	13868
R_{int}	0.113	0.081	0.071
Reflections with $F^2 > 2\sigma(F^2)$	7449	8972	4901
Number of parameters	1383	951	1066
R_1 [$F^2 > 2\sigma(F^2)$]	0.112	0.092	0.133
wR_2 (all data)	0.371	0.306	0.427
GOOF, S	1.06	1.07	0.92
Largest difference peak and hole (e Å^{-3})	0.72 and –0.49	1.42 and –0.55	0.49 and –0.32

Compound	**21**·5.5THF	**22**·10MeCN
Formula	$C_{134}H_{208}Li_4O_{23.5}$	$C_{224}H_{300}Al_2Li_{20}O_{26}N_{22}$
Formula weight	2222.75	3909.60
Crystal system	Triclinic	Orthorhombic
Space group	$P\ \bar{1}$	*Pnnm*
a (Å)	12.531(17)	23.5598(6)
b (Å)	17.16(3)	23.8191(7)
c (Å)	17.41(2)	24.2119(17)
α (º)	113.205(3)	90

β (º)	98.215(10)	90
γ (º)	101.44(2)	90
V (Å^3)	3269(8)	13587.1(11)
Z	1	2
Temperature (K)	100(2)	100(2)
Wavelength (Å)	0.6889	0.71073
Calculated density (g.cm^{-3})	1.129	0.956
Absorption coefficient (mm^{-1})	0.08	0.07
Transmission factors (min./max.)	0.933, 0.999	0.994, 0.997
Crystal size (mm^3)	0.09 x 0.02 x 0.02	0.09 × 0.05 × 0.04
θ(max) (°)	25.0	27.5
Reflections measured	25642	88207
Unique reflections	11133	15903
R_{int}	0.067	0.089
Reflections with $F^2 > 2\sigma(F^2)$	6853	8624
Number of parameters	771	931
R_1 [$F^2 > 2\sigma(F^2)$]	0.116	0.120
wR_2 (all data)	0.361	0.361
GOOF, S	1.05	1.05
Largest difference peak and hole (e Å^{-3})	0.66 and –0.63	1.00 and –0.93

5. Appendix for Chapter 6

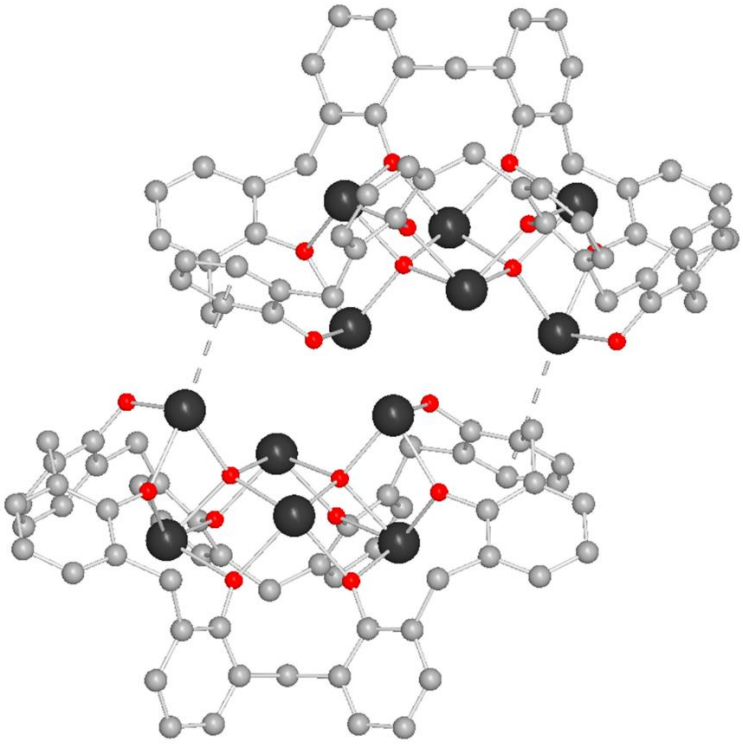

Figure 8-22. Two Pb-aryl interactions present result in the formation of the observed dimers for $[Pb_{12}(L^8)_2O_4]\cdot 8.7C_7H_8$ (**26**$\cdot 8.7C_7H_8$).

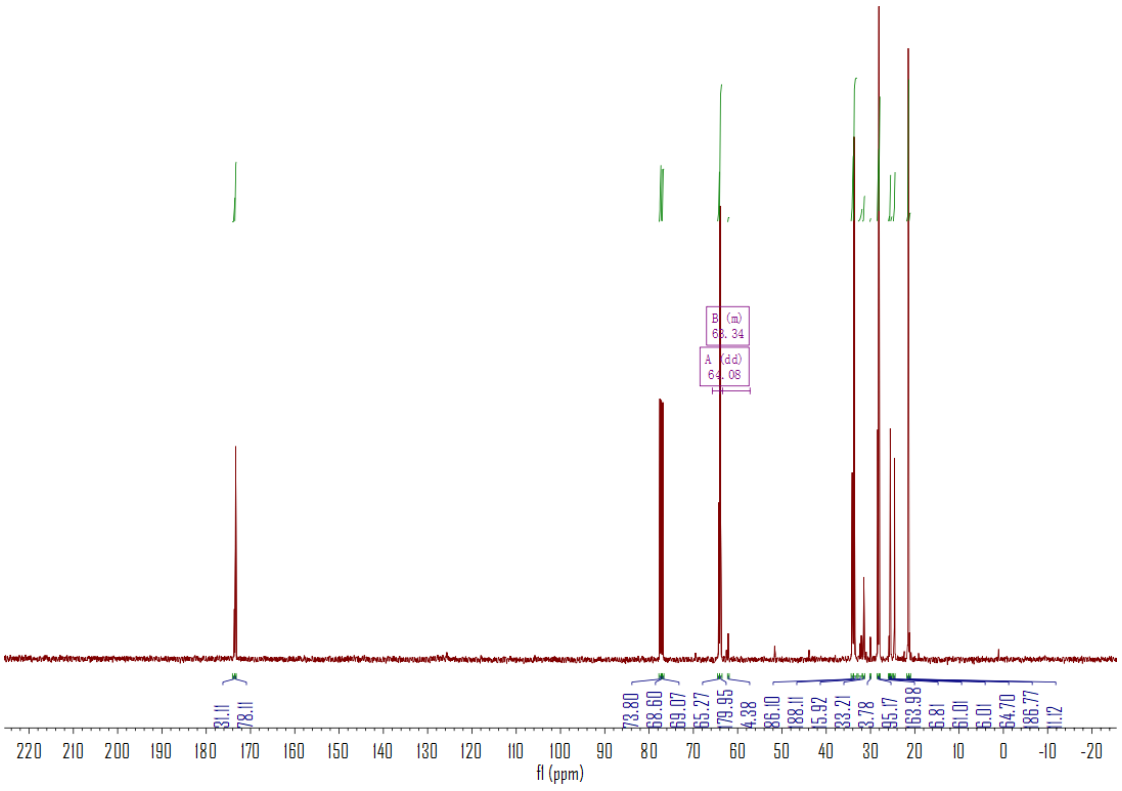

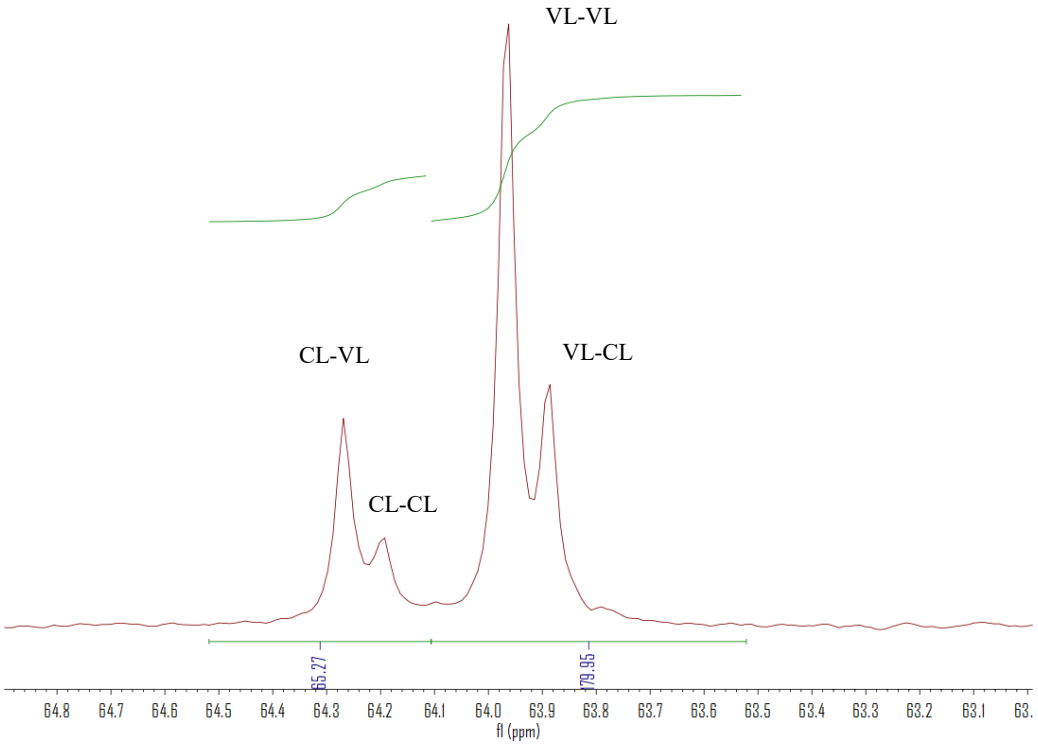

Figure 8-23. Carbonyl range of ^{13}C NMR spectrum ($CDCl_3$, 25 ºC) of PCL-PVL co-polymer synthesized with **25**/BnOH (run 4, Table 6-3).

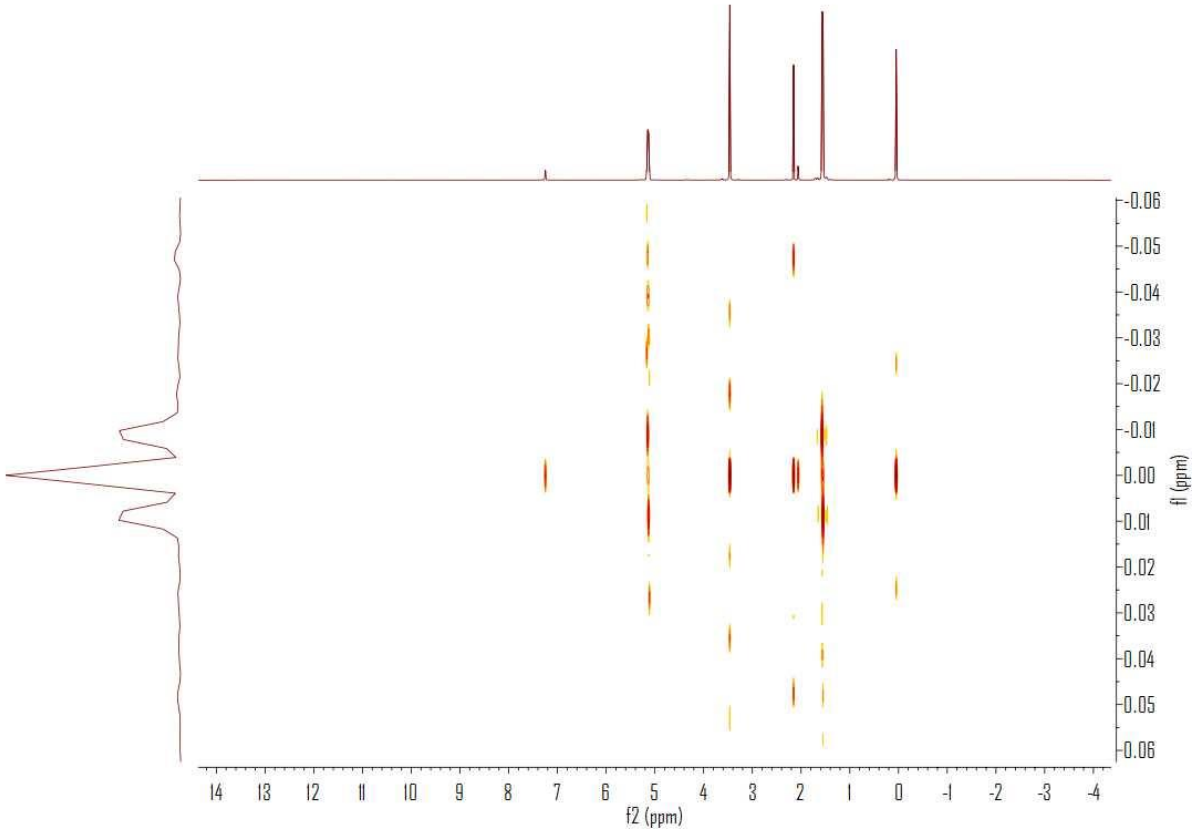

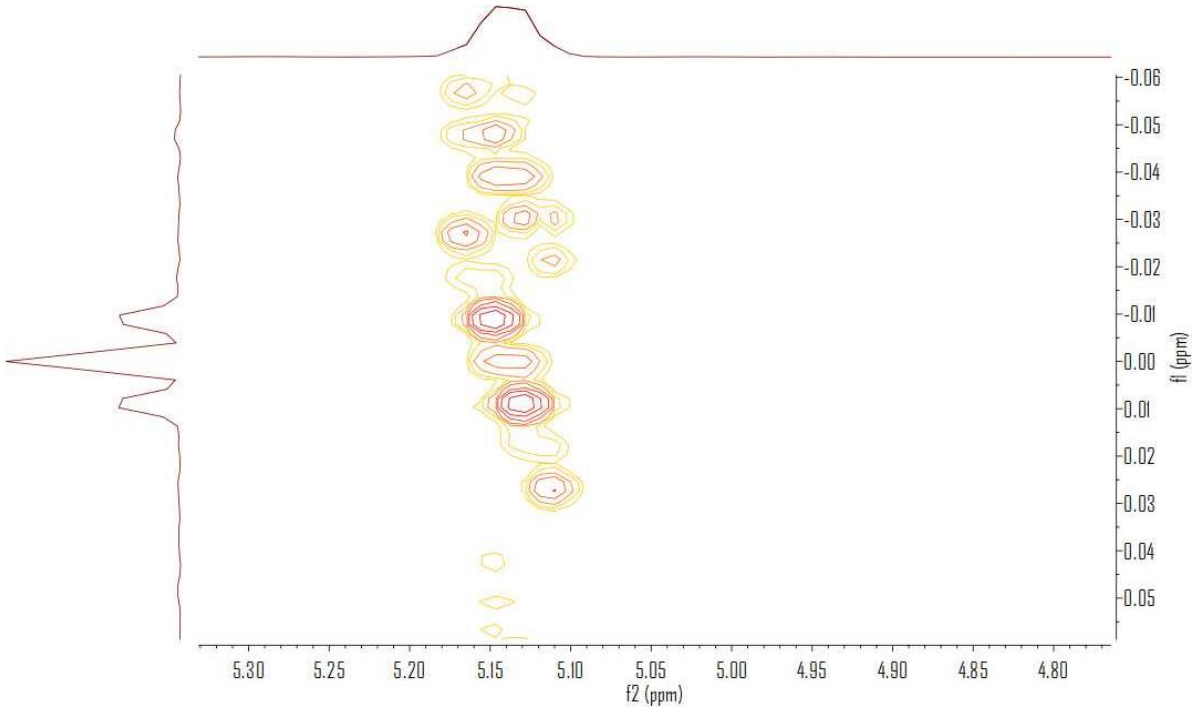

Figure 8-24. 2D J-resolved ^{1}H NMR spectrum ($CDCl_3$, 400 MHz, 298 K) of the PLA synthesized with **23**/BnOH (run 1, Table 6-4).

Equation 8-6. Determination of number-average sequence length for CL[1]

$$L_{CL}=[(I_{CL-CL})/(I_{VL-CL})]+1$$

Where I_{CL-CL} and I_{VL-CL} is the area of the peak belonging to the CL-CL and VL-CL dyad, respectively.

Equation 8-7. Determination of number-average sequence length for VL. [1]

$$L_{VL}=[(I_{VL-VL})/(I_{CL-VL})]+1$$

Where I_{VL-VL} and I_{CL-VL} is the area of the peak belonging to the VL-VL and CL-VL dyad,

respectively.

Equation 8-8. Determination of the Randomness Character (R). [1]

$$R=1/(L_{CL}) + 1/(L_{VL})$$

Completely block Copolymers: R = 0

Copolymers with a “blocking” tendency: R < 1

Completely random copolymers: R = 1

Copolymers with an alternating tendency: R >1

Completely alternating copolymers: R = 2

Table 8-8. Crystal structure data for **23**·2.5MeCN, **24**·14MeCN, **25**·11MeCN, **26**·8.7C_7H_8, **27**, **28**·4.75MeCN.

Compound	**23**·4.5MeCN	**24**·14MeCN	**25**·11MeCN
Formula	$C_{191}H_{236.5}Li_2N_{7.5}O_{17}Pb_4$	$C_{300}H_{371}Cl_2Li_{10}N_{18}O_{30}Pb_8$	$C_{229}H_{286}N_{11}O_{29}Pb_{13}$
Formula weight	3753.16	6509.72	6357.82
Crystal system	Triclinic	Triclinic	Triclinic
Space group	P–1	P–1	P–1
Unit cell dimensions			
a (Å)	13.7079(3)	23.1594(4)	19.2866(2)
b (Å)	15.0694(2)	25.7268(4)	23.0573(3)
c (Å)	22.7536(4)	28.7875(6)	29.8976(4)
α (º)	97.3001(15)	69.691(2)	72.2187(11)
β (º)	100.2859(17)	72.882(2)	82.1388(10)
γ (º)	102.8843(16)	85.7680(10)	67.9805(11)

V (Å^3)	4439.47(14)	15365.5(5)	11733.0(2)
Z	1	2	2
Temperature (K)	100(10)	100(2)	100(2)
Wavelength (Å)	0.71075	0.71075	0.71075
Calculated density	1.365	1.326	1.710
Absorption coefficient	7.706	4.441	9.349
Transmission factors	0.828 and 1.000	0.682 and 1.000	0.587 and 0.595
Crystal size (mm^3)	0.04 × 0.04 × 0.01	0.25 × 0.18 × 0.1	0.104 × 0.061 × 0.053
θ(max) (°)	70.4	26.3	28.3
Reflections measured	74814	327875	256697
Unique reflections	16536	62724	57728
R_{int}	0.0948	0.0644	0.0962
Reflections with $F^2 >$	14151	41423	37456
Number of parameters	961	3093	2358
R_1 [$F^2 > 2\sigma(F^2)$]	0.0795	0.0679	0.0756
wR_2 (all data)	0.1279	0.2025	0.1628
GOOF, S	1.228	1.014	1.027
Largest difference	1.90 and -2.42	3.92 and -1.58	5.05 and -1.88
Compound	**26**·8.7C_7H_8	**27**	**28**·4.75MeCN
Formula	$C_{236.9}H_{277.6}O_{20}Pb_{12}$	$C_{94}H_{122}Cl_2O_{10}Pb_6Si_2$	$C_{75.5}H_{89.25}N_{4.75}Cl_{0.5}LiNO_{8.5}Pb_5$
Formula weight	5931.25	2782.13	2303.70
Crystal system	Triclinic	Triclinic	monoclinic
Space group	Pbar1	P–1	I2/a
Unit cell dimensions			
a (Å)	17.5373(3)	14.3597(5)	19.7928(2)
b (Å)	17.9311(4)	15.8609(8)	33.7801(3)
c (Å)	21.0467(4)	15.8791(6)	24.5621(3)
α (º)	67.965(2)	66.795(5)	90
β (º)	86.0380(10)	67.082(4)	105.5489(10)
γ (º)	64.379(2)	88.389(3)	90

V (Å^3)	5497.3(2)	3027.9(2)	15821.3(3)
Z	1	1	8
Temperature (K)	100(2)	100(2)	100(2)
Wavelength (Å)	0.71075	0.71075	0.71075
Calculated density	1.792	1.532	1.771
Absorption coefficient	9.211	8.376	10.668
Transmission factors	0.809 and 1.000	0.628 and 1.000	0.733 and 1.000
Crystal size (mm^3)	0.04 × 0.01 × 0.01	0.090 × 0.060 × 0.025	0.09 × 0.08 × 0.07
θ(max) (°)	27.6	25.0	31.97
Reflections measured	194208	57186	211141
Unique reflections	25401	10657	24791
R_{int}	0.0809	0.0600	0.0591
Reflections with $F^2 >$	21078	6953	18155
Number of parameters	1159	582	774
R_1 [$F^2 > 2\sigma(F^2)$]	0.044	0.0816	0.0389
wR_2 (all data)	0.114	0.2366	0.0897
GOOF, S	1.02	1.035	1.059
Largest difference	3.57 and –2.30	4.36 and -2.20	2.79 and -1.34

6. References

[1] (a) Q. Hu, S.-Y. Jie, P. Braunstein and B.-G. Lia, *Chinese J. Polym. Sci*. 2020, 38, 240–247; (b) M. A. Woodruff and D. W. Hutmacher, *Prog. Polym. Sci.,* 2010, 35, 1217−1256; (c) T. Wu, Z. Wei, Y. Ren, Y. Yu, X. Leng and Y. Li, *Polym. Degrad. Stab.,* 2018, 155, 173−182; (d) M. T. Hunley, N. Sari, and K. L. Beers, *ACS Macro Lett*., 2013, 2, 375−379. (e) Z. Sun, Y. Zhao, O. Santoro, M. R. J. Elsegood, E. V. Bedwell, K. Zahra, A. Walton, and C. Redshaw, *Catal. Sci. Technol.*, 2020, 10, 1619−1639.

[2] SAINT and APEX 2 software for CCD diffractometers, Bruker AXS Inc., Madison, USA, 2006.

[3] A. W. Addison, T. N. Rao, J. Reedijk, J. van Rijn and G. C. Verschoor, J. Chem. Soc., *Dalton Trans*., 1984, 1349–1356.

[4] (a) F. Della Monica, E. Luciano, A. Buonerba, A. Grassi, S. Milione and Carmine Capacchione, *RSC Adv*. 2014, 4, 51262−51267; (b) P. Vanhoorne, P. Dubois, R. Jerome and P. Teyssie, *Macromolecules* 1992, 25, 37–44; (c) J. Kasperczyk and M. Bero, *Makromol. Chem*. 1991, 192, 1777–1787; (d) J. Kasperczyk and M. Bero, *Makromol. Chem*. 1993, 194, 913–925; (e) N. Nomura, A. Akita, R. Ishii and M. Mizuno, *J. Am. Chem. Soc*. 2010, 132, 1750–1751; (f) G. Li, M. Lamberti, D. Pappalardo and Claudio Pellecchia *Macromolecules*, 2012, 45, 8614−8620.